Functional characterization of new antimicrobial lead structures against *Mycobacterium tuberculosis*

Inaugural dissertation

for the attainment of the title of doctor

in the Faculty of Mathematics and Natural Sciences

at the Heinrich Heine University Düsseldorf

Presented by

Anna-Lene Ilse Rosemarie Kiffe-Delf

from Münster

Düsseldorf, October 2023

from the Institute of Pharmaceutical Biology and Biotechnology

at the Heinrich Heine University Düsseldorf

Published by permission of the

Faculty of Mathematics and Natural Sciences

at Heinrich Heine University Düsseldorf

Supervisor: Prof. Dr. Rainer Kalscheuer

Co-supervisor: Prof. Dr. Thomas Kurz

Date of the oral examination: 29.01.2024

Table of content

I. Summary

Annually, approx. 1.4 million people die from *Mycobacterium tuberculosis,* the causative agent of tuberculosis. Therefore, it is one of the most common causes of death worldwide. Drug resistance is a growing problem as the incidence of drug-resistant bacteria increase and nearly no new drug family enters the market. The development of extensive and total drug resistance leaves hardly any treatment options open. Therefore, it is crucial to find new agents with new mechanisms of action against these pathogens. In this context, screening of molecule libraries against *M. tuberculosis* plays an important role. This study investigates three lead structures in more detail concerning their antimycobacterial activity. The first part of the work deals with the flavonoid-derived substance chlorflavonin (CF), for which an anti-tubercular effect has already been described. Extensive structure-activity relationship (SAR) analyses revealed the similarly active derivative bromflavonin (BrF), which, like CF, shows no cytotoxicity *in vitro*. Both compounds are characterized by potent inhibition of the catalytic subunit of the acetohydroxy acid synthase IlvB1.

Further SAR analyses revealed that many CF derivatives could not hamper the growth of *M. tuberculosis*, while they strongly inhibited activity of the isolated enzyme IlvB1 *in vitro*. That indicates that uptake of many derivatives across the mycobacterial cell wall is probably a limiting factor, resulting in very few compounds exhibiting cellular activity. Thus, CF and BrF represent the most promising lead structures suitable for preclinical studies due to their chemical properties and antibacterial potency.

The alkoxy amide-based structures KSK-104 and KSK-106 have been identified previously in the research groups of Profs. Kalscheuer and Kurz with potent anti-tubercular activity, no cytotoxicity, and vigorous intracellular activity in infected macrophages (data not published). Enzymes potentially capable of cleaving KSKs were identified with the amidohydrolases AmiC and Rv0552, leading to the hypothesis that the KSKs are prodrugs that need to be hydrolyzed in the bacteria after uptake. A variety of methods demonstrated that the molecules, indeed, are cleaved within the cells. However, other more active substances were found during SAR analysis. One of these molecules, OMK-175, has also been analyzed in more detail and showed good properties similar to the KSKs. With their excellent *in vitro* characteristics, the KSKs are currently in preclinical testing, which will prove their effectiveness in a relevant animal infection model.

Ultimately, FFK-088 is a new thiazole-containing compound with anti-tubercular activity, no cytotoxicity but activity against extensively drug-resistant forms of *M. tuberculosis*. Further analysis showed a strong synergistic effect with delamanid, ethambutol, and rifampicin. Thus,

FFK-088 represents a substance that can be used as a basis for the development of new antitubercular antibiotics.

In summary, FFK-088, CF, and the KSKs were found to represent three new structural scaffolds that may provide a basis for curbing the global spread of tuberculosis.

II. Abreviations:

percent	%
volume percent	% (v/v)
mass percent	% (w/v)
degree Celsius	°C
microgram	µg
microliter	µL
micromolar	µM
16 S ribosomal ribonucleic acid	16SrRNA
peptidoglycan-arabinogalactan complex	AGP
acetohydroxyacid synthase	AHAS
antimicrobial resistance	AMR
anhydrotetracycline	Atc
adenosine triphosphate	ATP
branched-chain amino acid	BCAA
bedaquiline	BDQ
butyloxycarbonyl	BOC
bromflavonin	BrF
basepair	bp
chlorflavonin	CF
coronavirus disease	COVID-19
column volumes	CV
Dalton	Da
desoxyribonucleic acid	DNA
dormancy regulon	DosR
days post-infection	dpi
drug-resistant tuberculosis	DR-TB
dithiothreitol	DTT
Escherichia coli	*E. coli*
exempli gratia, for example	e.g.
exported repetitive protein	Erp
et alia	*et al.*
ethambutol	ETB
fractional inhibition concentration index	FICI
figure	fig.
gram	g
hydrochloric acid	HCl
human immunodeficiency virus	HIV
high-performance liquid chromatography	HPLC
Hertz	Hz
inosine monophosphate	IMP
isoniazid	INH
intravenously	IV

kilodalton	kDa
KSK-104 and KSK-106	KSKs
kilovolt	kV
KwaZulu Natal	KZN
liter	L
lysogeny broth	LB
liquid chromatography	LC
liquid chromatography mass spectroscopy	LC-MS
liquid chromatography tandem mass spectroscopy	LC-MS/MS
Mycobacterium abscessus	*M. abscessus*
*Mycobacterium b*ovis	*M. bovis*
Mycobacterium marinum	*M. marinum*
Mycobacterium smegmatis	M. smegmatis
Mycobacterium tuberculosis	M. tuberculosis
megabase pairs	Mb
multidrug-resistant	MDR
multidrug-resistant tuberculosis	MDR-TB
methanol	MeOH
milligram	mg
minimal inhibitory concentration	MIC
minutes	min
milliliter	mL
millimeter	mm
millimolar	mM
milliseconds	ms
mass spectrometry	MS
statistical sample size	*n*
sodium chloride	NaCl
nanoliter	nL
nanometer	nm
nanomolar	nM
optical density	OD
phosphate-buffered saline	PBS
polymerase chain reaction	PCR
phthiocerol dimycocerosate	PDIM
phorbol-12-myristate-13-acetate	PMA
perorally	PO
parts-per-million	ppm
pyrazinamide	PZA
pyrazinamidase	Pzase
genomic region of difference 1	RD1
research group	RG
working group of Prof. Dr. Thomas Kurz	RG Kurz
rifampicin	RIF
ribonucleic acid	RNA
resuscitation-promoting factors	Rpf

revolutions per minute	rpm
ribosomal protein S1	RpsA
ribosomal protein S12	rpsL
rifampicin resistance	RR
rifampicin-resistant tuberculosis	RR-TB
room temperature	RT
structure-activity-relationship	SAR
severe acute respiratory syndrome coronavirus 2	SARS-CoV-2
sodium dodecyl sulfate-polyacrylamide gel electrophoresis	SDS-PAGE
standard error of mean	SEM
selectivity index	SI
spontaneous resistant mutants	SRM
streptomycin	STREP
tuberculosis	TB
totally drug-resistant	TDR
Transposon insertion sequencing	Tn Seq
tumor necrosis factor α	TNFα
ultraviolet	UV
Volt	V
World Health Organization	WHO
wild type	WT
extensively drug-resistant	XDR
Ohm	Ω

1 Introduction

There are many human pathogens around the world including bacteria that can cause life-threatening infections. In 1929, a new era has begun through the accidental discovery of the staphylococci-inhibiting properties of the mold *Penicillium rubens*, which led to a decrease in the growth of a staphylococci culture [2]. Further studies led to the discovery of the first antibiotic penicillin, which saved millions of lives since its discovery and was furthermore the starting point for the era of antibiotics. Afterwards, many other antibiotics and antimicrobial chemotherapeutics were discovered which lowered the mortality and morbidity caused by bacterial pathogens [3]. Since this point, also the resistance of bacteria against these therapeutics has coevolved. Nowadays, antimicrobial resistance (AMR) costs many lives, and studies project that around 10 million people might die because of AMR globally in 2050, more than caused by cancer and diabetes [4]. According to the World Health Organisation (WHO), *Mycobacterium tuberculosis* (*M. tuberculosis*), the causative agent of tuberculosis (TB), is the 13th leading cause of death worldwide and the second leading single infectious killer after the severe acute respiratory syndrome-coronavirus-2 (SARS-CoV-2) [1]. Due to the rapidly increasing and already high amount of AMR-related death worldwide, it is important to find new effective therapeutics against this pathogen including resistant strains.

In the following, an overview of different mycobacterial pathogens including *M. tuberculosis* is provided, before the history and the current situation of antibiotics will be described. In the end, there is a short outline of the different highly-potent anti-tuberculosis substances that this work is focusing on.

1.1 Mycobacteria

Mycobacteria are rod-shaped bacteria with a size between 0.2 to 0.6 µm width and one to ten µm length. Currently, there are about 170 known mycobacterial species, all of which are non-motile, non-catalase positive, and non-spore-forming organisms [5]. Most of them are environmental. The colony morphology on solid media varies between smooth and rough, with a color development of white, pink, or yellow [6]. Most of these species are aerobic, but only some are microaerophilic [7]. In history, the genus *Mycobacterium* was first established in 1896 [8], when Armauer Hansen found the first illness-related mycobacteria in individuals with leprosy in 1873 [9]. The next big discovery

was *M. tuberculosis* by Robert Koch in 1882 [10]. Many other species were found in the following years, so we have a large number of different taxa nowadays.

A characteristic of mycobacteria is the cell wall, that will be explained in chapter 1.2. Because of this unique structure, the bacteria can be stained and verified by the Ziehl-Neelsen staining [11]. It is a staining method, which was further improved by Paul Ehrlich, Franz Ziehl, and eventually altered by Friedrich Neelsen. This method stains specific lipids, which are present in the mycobacterial cell wall and are called mycolic acids. For this staining procedure, methylene blue, carbol-fuchsin, and acid alcohol are used. In the presence of acid-fast lipids such as mycolic acids, the stained organisms retain a red color after acid alcohol treatment [3].

The mycobacteria can be divided into different groups. One way of distribution is the division between slow and rapid growers. Rapid growers are defined as having colonies visible on solid culture media after seven days, while slow growers require more time [12]. Some of the most popular species, which are frequently cultivated in the laboratory for research purposes, are *Mycobacterium b*ovis *(M. bovis), Mycobacterium smegmatis (M. smegmatis)*, and *M. tuberculosis*, which are briefly presented in the following. *M. smegmatis* is one of the rapidly growing environmental bacteria that Lustgarten first isolated in 1884 [13]. It mainly lives in aggregates of cells, which were attached to each other and form biofilms [13]. *M. smegmatis* is mostly found in water, plants and soil and has not been declared a human pathogen [14, 15]. Because of this fact and its typical mycobacterial characteristics, it is often used as a fast-growing surrogate for different slow-growing mycobacteria, such as *M. tuberculosis* [16]. Its cell surface morphology generally is smooth, shiny, coarsely collapsed, or wrinkled [17]. *M. smegmatis* has many conserved mycobacterial gene orthologues and almost the same cell physiology as other mycobacteria [18]. Interestingly, bedaquiline (BDQ), an anti-tuberculosis drug, was discovered through an *M. smegmatis* screening [19], which shows the relevance of this bacteria in research. Another way of grouping mycobacteria is to classify them into species belonging to the *Mycobacterium tuberculosis*-complex. This large group is defined as the mycobacteria, which can cause tuberculosis in animals and humans. It consists of 12 members of the *Mycobacterium* genus and includes *tuberculosis, bovis, canettii, africanum, microti, orygis, caprae, pinnipedii, mungi, suicattae,* and the Dassie and Chimpanzee bacilli [20]. One common feature of them is the formation of granuloma, which is an aggregation of immune cells [21]. Furthermore, they are, in general, virulent and can infect multiple hosts. Humans are only susceptible to eight of these members. *M. bovis* also infects numerous hosts, including several domestic animals, especially cattle and wildlife. Human primary infection by *M. bovis* is caused by consuming cattle

products or aerosol inhalation with infective body fluids or droplets from infected animals [22]. This study used non-virulent Bacillus Calmette Guérin (BCG) varieties: *M. bovis BCG* Pasteur and *M. bovis BCG* Danish 1331. These two are attenuated vaccine strains obtained from the virulent bacillus *M. bovis* by Jean-Marie Camille-Guérin and Léon Charles Albert Calmette [23]. According to Louis Pasteur`s strategy to affect the virulence of a bacterium, they began to passage a virulent isolate of *M. bovis* on different media in 1908. After 230 passages in 13 years, the bacterium has lost a genomic region spanning nine genes, which are coding for the proteins Rv3871, PE35, PPE68, ESAT-6, CFP-10, Rv3876, Rv3877, Rv3878, and Rv3879c, summarized as the region of difference 1 (RD1) as we now know by modern whole-genome sequencing studies [23]. In 1921, the first vaccine trial of infants was performed with this attenuated strain and was subsequently released as a vaccine [24]. In general, this vaccination has saved millions of lives over the last century by activating anti-mycobacterial immunity and, with this, the prevention of the most severe forms of TB [25]. Nowadays, the vaccine is still used in many countries but the efficacy is very weak, so that in many other countries it is no longer prescribed. This makes the development of new antibiotics particularly important. There are also some so-called non-tuberculous mycobacteria like *Mycobacterium marinum (M. marinum)* and *Mycobacterium abscessus (M. abscessus)* that also can cause diseases, such as skin infections, mainly in immunocompromised people [26].

M. tuberculosis is described in more detail in the following chapter, as it is the main focus of this work.

1.2 The bacterium *Mycobacterium tuberculosis*

M. tuberculosis, the causative agent of TB, is a human pathogen from the bacteria kingdom, the actinobacteria phylum, the suborder of the Corynebacterineae, and the family of the Mycobacteriaceae. The obligate aerobe, facultative intracellular bacteria are chemoorganotrophic and slow-growing with a generation time at optimal conditions of around 24 hours in liquid media, while colonies appear after three weeks on solid agar medium [27]. It has been postulated that the genus *Mycobacterium* evolved 150 million years ago [28]. However, *M. tuberculosis* was found by Robert Koch first in 1882 [29]. A significant step in tuberculosis research was the whole-genome sequencing of *M. tuberculosis* in 1998. It was found that the genome has a size of 4.4 Mbp, which encodes for 4018 genes with a very high GC content of 65.9% [30]. Further whole-genome mutagenesis studies have shown around 600 genes that were essential for the

in vitro growth of *M. tuberculosis* [31]. One of the main characteristics of *M. tuberculosis* is the cell's unique envelope (Figure 1). It is composed of four layers (I-IV): the external capsule (I), which consists of neutral polysaccharides [32]. Next, there is an asymmetrical outer membrane, also called “mycomembrane” (II). It is only weakly connected to the external capsule. The inner leaflet of the mycomembrane is based on long-chain fatty acids (C_{60}-C_{90}), and the outer leaflet mainly includes non-covalently attached lipoglycans and (glycol)lipids. Examples are sulfoglycolipids, trehalose mono- and dimycolates, lipomannan, lipoarabinomannan, and (lipo)proteins, and phosphatidylinositol mannosides [33, 34]. All are involved in various biological processes such as biofilm formation, pathogenicity, and persistence [35]. This membrane is covalently linked through the mycolic acids (III) to the peptidoglycan-arabinogalactan complex (AGP), which build the periplasmic space. Inside the cell is the inner membrane, which is also called the plasma membrane (IV) [32]. Because of this complex structure, the permeability across this barrier is very low, which makes it challenging to find new anti-TB drugs [36, 37].

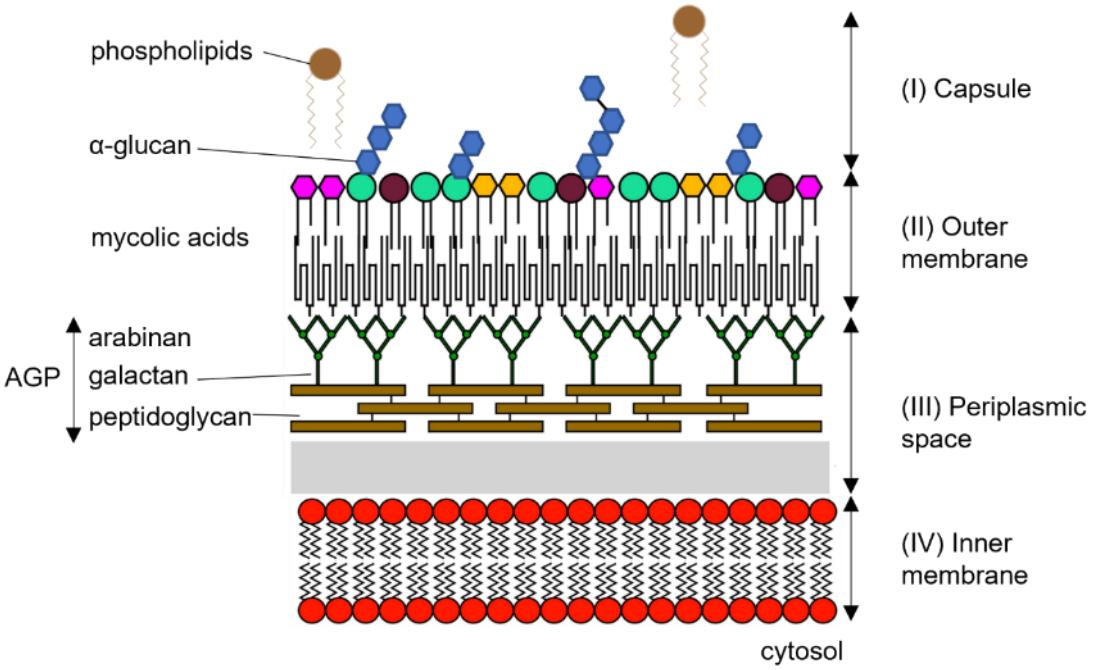

Figure 1: Schematic representation of the mycobacterial envelope. The cell envelope consists of four main layers: (I) the external capsule, (II) an asymmetrical outer membrane, that is covalently linked to (III) the periplasmic space with the peptidoglycan-arabinogalactan complex (AGP), and (IV) the inner membrane. Figure adapted from Vincent, A. et al., 2018 [38].

The primary host cells for *M. tuberculosis* are the macrophages, which firstly phagocytose the bacteria after infection of a human individual [39]. The internalization procedure is described in section 1.2.1 in more detail. A wide variety of resistance mechanisms have evolved through adaptations. One of these is the thick mycobacterial

cell wall, which grants mycobacteria resistance against some anti-bacterial effector mechanisms of the macrophages [40]. After the internalization and the switch to the latent state, they can persist for a long time. After this non-replicating phase, they can be reactivated to cause active disease [41].

Due to its ability to adapt to different stress situations, its unique cell wall structure, and its airborne transmission, *M. tuberculosis* became a global pathogen. Due to the high infection rate in humans, TB occurs worldwide and is particularly prevalent in Sub-Saharan Africa and Southeast Asia.

1.2.1 Tuberculosis: Epidemiology and Pathogenesis

TB, caused by *M. tuberculosis*, is one of the oldest diseases affecting humans and causes global morbidity and mortality [42, 43]. According to the WHO, 10.6 million people fell newly ill with TB in 2021 worldwide. The number of new infections increased in 2021 after a long steady period of infection numbers [1]. TB is known to be a poverty-related disease because of the need for access to diagnostic tools and long medication phases. Geographically, most of the TB cases occur in South-East Asia (45%), Africa (23%), and the Western Pacific (18%) (Figure 2A). The 30 countries with the highest TB burden accounted for 87% of all TB cases occurring worldwide. These countries are predominantly low-income and middle-income countries. In 2021, 1.6 million people died from TB [1] with drug-resistant tuberculosis (DR-TB) accounting for a large proportion of deaths. In 2021, there were 450,000 cases of DR-TB (Figure 2B). One predominant form of DR-TB exhibits resistance to rifampicin (RIF; RR-TB), which is one of the most effective first-line antibiotics. More detailed information on RIF is provided in chapter 1.3.2.3. On the other hand, multidrug-resistant TB (MDR-TB) is tuberculosis with resistance to RIF and isoniazid (INH), which is also a first-line antibiotic. Both forms (RR-TB and MDR-TB) need to be treated with a second-line antibiotic, e.g., pretomanid or delamanid. The countries with the highest numbers of MDR-TB and RR-TB are India (26%), the Russian Federation (8.5%), and Pakistan (7.9%). In parallel with the increasing number of infections, DR-TB cases have also increased compared to previous years. This is a dramatic development [1]. Mathematical analyses and simulation models predict that the number of TB cases will continue to increase due to the lack of rapid diagnosis and appropriate treatment options for RR-TB [44-46].

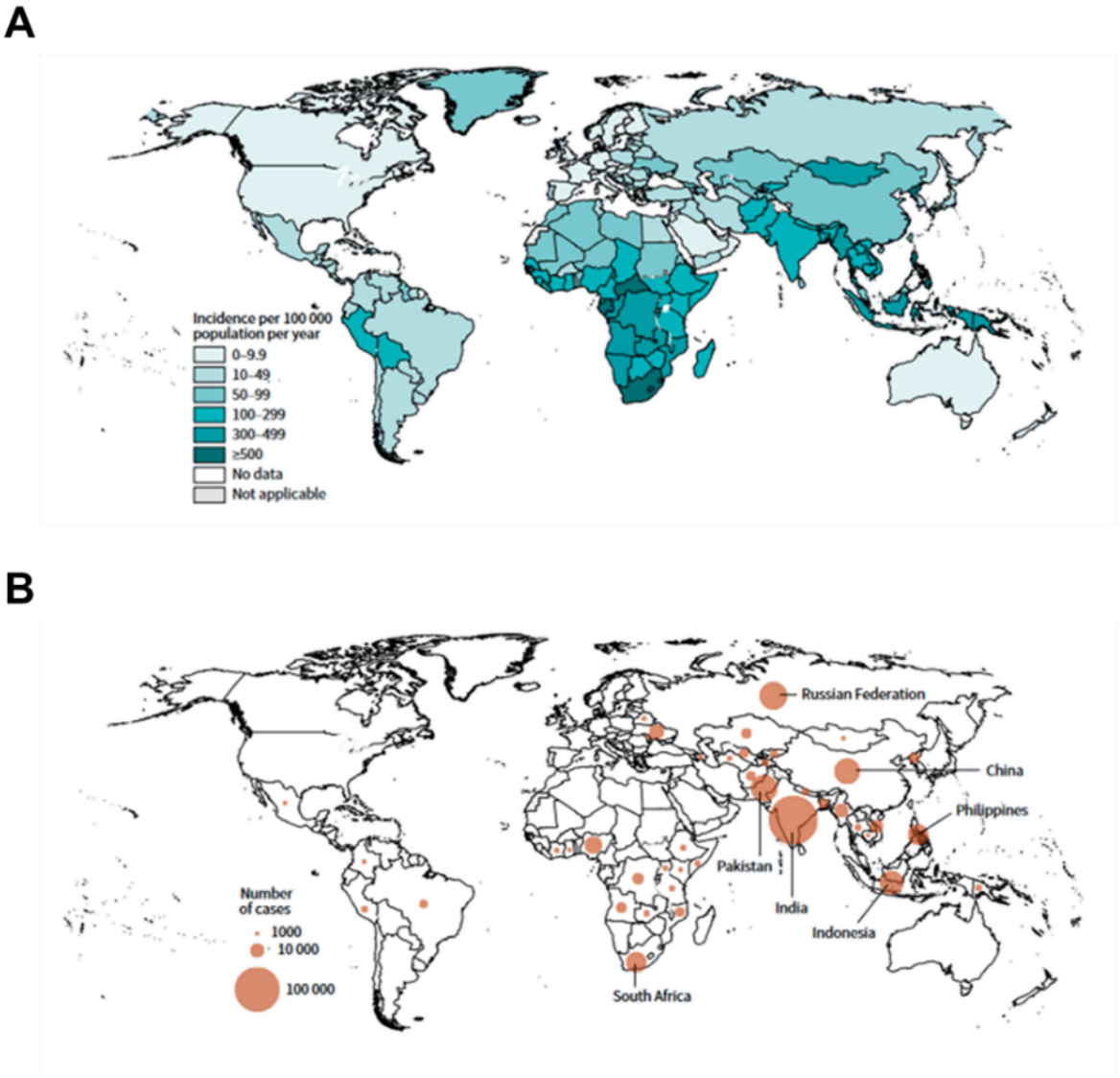

Figure 2: Estimated incidence rates of people infected with TB and drug-resistant TB in 2021. Estimated 10.6 million people fell ill with TB worldwide in 2021 with the highest cases in South-East Asia, Africa, and Western Pacific **(A)**. Globally, the estimated number of multidrug-resistant TB (MDR-TB) and rifampicin-resistant TB (RR-TB) grew to 450,000 incident cases. The highest proportions are in India, the Russian Federation, and Pakistan **(B)**. Figure and Data from WHO, Global Tuberculosis Report (2022) [1].

The only known environmental reservoir of *M. tuberculosis* is in humans. Due to this specificity, there has been a long history of host-pathogen adaptation during human evolution that started at least 6,000 – 9,000 years ago, but this process is not yet fully understood [47, 48]. *M. tuberculosis* is mainly a pulmonary pathogen. The bacteria are transmitted via aerosols and infect mainly the lung, but they can also spread throughout the whole body and affect different organs and tissues resulting in extrapulmonary TB. Even though there is a very large number of infections with *M. tuberculosis*, only a small proportion of approx. 10% of them develop an active TB disease [49, 50]. This is because there are different forms of TB infections: In latent TB infection, the bacteria are isolated in granulomas and are in a persistent form, in which the metabolism is reduced to a

minimum. It is an asymptomatic and non-transmissible state (Figure 3). Due to intracellular residence in the macrophages, the host immune system can hardly act against this form, and the bacteria can survive in a dormant state for weeks up to several decades [51]. However, if an active form develops, the bacteria leave the granulomas. The disease develops with symptoms such as cough, hemoptysis, fever, night sweats, fatigue, lack of appetite, and weight loss [48]. Recent findings have shown that in addition to the two forms, there are also mixed forms so that a spectrum emerges, e.g., some patients have an active, culture-positive disease but are asymptomatic. These forms are called subclinical TB [52-54].

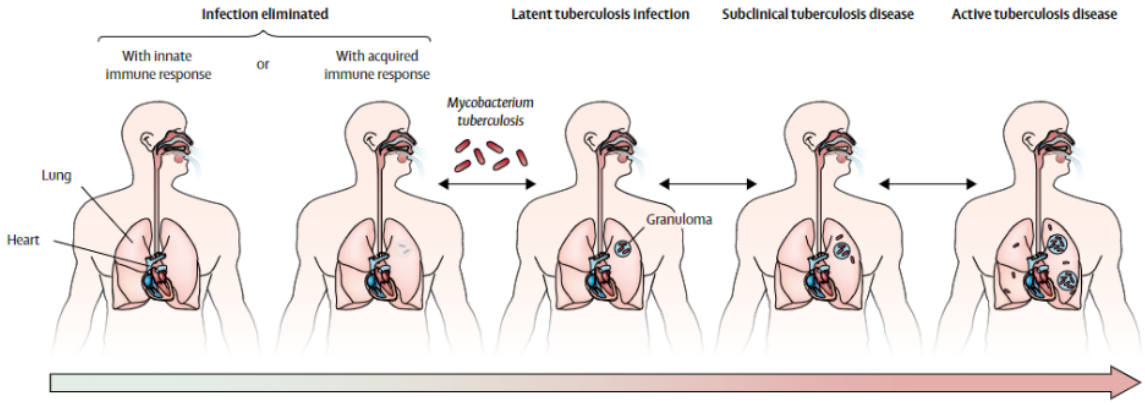

Figure 3: The tuberculosis infection and disease. Infection with *M. tuberculosis* and the categorization into active and latent TB and the mixed form, subclinical TB. Figure from Furin, J. *et al.*, 2019 [41].

The infection cycle of *M. tuberculosis* begins with the inhalation of the bacteria. After passing through the upper respiratory tract, they enter the lower respiratory tract, where the bacteria encounter alveolar macrophages. These macrophages are the main cell type that the bacteria infect [48, 55]. Macrophages perceive bacteria by recognizing pathogen-associated molecular patterns via host cell pattern recognition receptors, leading to pathogen phagocytosis [56]. After internalization, *M. tuberculosis* blocks the fusion of phagosomes with lysosomes, normally resulting in a decreased pH inside the phagosomes, to ensure bacterial survival [56]. In addition, *M. tuberculosis* utilizes the secretion system ESX-1 to secrete proteins into the cytosol of the macrophages promoting the disruption of the phagosomal membrane. This step is essential for the bacteria and has been linked to the surveillance pathway that facilitates bacterial survival [57, 58]. From then on, the bacteria have overcome the first defence mechanisms of alveolar macrophages, monocytes, or dendritic cells, which were supposed to eliminate the bacteria. Thus, *M. tuberculosis* gains access to the pulmonary interstitium, e.g., by transmigration of infected macrophages through the alveolar epithelium to the lung parenchyma. Another possibility is a direct infection of the alveolar epithelial cells. In the

next step, *M. tuberculosis* is transported by monocytes or dendritic cells to pulmonary lymph nodes to induce T-cell priming. This subsequently leads to granuloma formation [48]. A granuloma is a compact and organized aggregate of mature uninfected macrophages, T-cells, fibroblasts, and neutrophils, which surround infected macrophages that arise in response to a persistent stimulus [56, 59-61]. With these granulomas, the host tries to encapsulate the bacteria from the rest of the body [48]. The surrounding immune cells are secreting cytokines, like tumor necrosis factor α (TNF- α) or interferon γ, which activate the macrophages to produce reactive nitrogen and oxygen species. The bacteria can survive in this toxic environment in a latent state for up to decades [58]. Various stimuli can reactivate *M. tuberculosis*, e.g., diabetes, weakening of the immune system due to immunosenescence, malnutrition, or co-infection with other pathogens (e.g., HIV, COVID-19) [62]. Subsequently, the bacteria begin to multiply in the macrophages. At a certain point, the bacterial load is too high, and the macrophages will be lysed or ruptured. As a result, the bacteria are released and enter the respiratory tract to be further disseminated or reach the bloodstream. These steps turn the latent form into an active form, and the patient begins to show symptoms and becomes infectious [51]. This leads to the infection of other individuals because no proven immunization is established. A century ago, the *M. bovis* BCG strain (seeChapter 1.1) was used as a vaccine routine for newborns and young children [25]. However, the vaccination does not show effective preventive immunization, especially in adults, which is why the vaccination is no longer recommended in Germany today [63]. So, there is only the possibility of treatment with effective drugs after infection. The first anti-tuberculosis drugs were developed in 1940. Today, according to WHO, the four first-line antibiotics RIF, INH, ethambutol (ETB), and pyrazinamide (PZA) in combination serve as an effective treatment against sensitive TB. This is given for up to six months (see Chapter 1.3.2). In addition to antibiotic resistance, dormancy of *M. tuberculosis* plays a role in the treatment. Many antibiotics are only effective against actively growing cells of *M. tuberculosis*. It would be important to have an effective agent against latent TB, thereby also indirectly preventing development of active TB. However, this is still very difficult, since the mechanisms of persistence and dormancy of *M. tuberculosis* are not yet fully understood. The phagocytosis of the bacteria leads to changes in environmental conditions, like acidification, starvation, and oxidative and nitrosative stress [64]. *M. tuberculosis* secretes ureases to neutralize the pH, and its unique cell wall helps to tolerate low pH [65]. However, the harsh environment causes cell stress and the bacteria enter into a dormant state. This is characterized by slower or no replication and extremely reduced metabolism. However, an important factor in the switch from active to dormant state is the dormancy survival regulator DosR. It controls 48 genes in *M. tuberculosis*,

which are colocalized in the genome and are clustered into nine blocks [66]. This regulon is controlled by DosS and DosT, a two-kinase system, which activate the response regulator [67, 68]. DosR can be induced by different stress conditions, such as hypoxia, which is triggered by phagocytosis for instance [67]. DosS is associated with the maintenance of DosR and DosT and interacts mainly in the early phase of hypoxia by activating DosR [69]. This leads to a reduction in metabolism and energy levels. This strategy allows long-term survival in the absence of oxygen [70].

The reactivation to the active state is also not fully understood. It is known that autoimmune diseases and secondary infections increase the risk of developing active disease. The reactivation of the metabolism and the replication are linked to resuscitation-promoting factors (Rpf). There are five in *M. tuberculosis* (RpfA-RpfE) [71]. Also, the DosR system is associated with reactivation [72]. The term dormancy indicates a metabolic state. Persistence, on the other hand, means the ability of bacteria to survive in the presence of drugs without changing genetically (phenotypical resistance or drug tolerance) [73]. It was reported that during conditions inducing persistence, the genes of the DosR regulon are not activated and thus do not play a role in the drug tolerance of *M. tuberculosis* [70]. It is important to understand the processes in more detail to find drugs against the dormant state, as most drugs are only effective against replicating bacteria.

1.2.2 Tuberculosis and COVID-19

The coronavirus disease (COVID-19) is caused by the severe acute respiratory syndrome coronavirus 2 (SARS-CoV-2) and is infectious. It was declared a global pandemic by the WHO in March 2020 [74, 75]. During the pandemic, there was a decrease in the reported number of people who were newly diagnosed with TB [1, 50]. According to WHO, this could indicate a greater number of people who have undetected TB and are not receiving treatment, as TB diagnosis was greatly reduced during the Corona pandemic. This could then subsequently lead to a wider spread of TB. In 2021, the number of new TB infections and also DR-TB cases increased for the first time after a long period of stagnation [1]. The higher the number of TB cases, the higher the number of deaths from TB. This makes the COVID-19 pandemic a challenge also for other diseases, such as TB. However, it did not only have negative effects regarding the transmission of TB. The lockdown and the use of masks in public may have minimized the spread, according to the WHO. Nevertheless, malnutrition, poverty, and the lack of diagnosis and treatment have negatively impacted the national TB programs [1, 76].

1.3 Antibiotics and anti-tuberculosis therapy

Antimicrobial substances play a major role in the control of bacterial infections. These can be divided into two main groups: antibiotics and antimicrobials. While antibiotics are natural substances produced by living microorganisms, antimicrobials are synthetically synthesized. Both inhibit the growth of other microorganisms [77]. These substances can be bactericidal, which causes cell death, or bacteriostatic, which inhibits cell proliferation. These bacteriostatic substances depend on the patient's immune system, which continues to fight against the infection. Antibacterial drugs used in TB treatment have different modes of action as described in the following chapters, following a brief description of the history of antibiotics.

1.3.1 History of antibiotics

In 1929, a new era began with the accidental discovery of penicillin by Alexander Fleming, which slowed the growth of bacteria [78]. This was the first antibiotic that could be used to treat infectious diseases. Before, there were only some antimicrobial substances, like salvarsan, which was developed mainly by Paul Ehrlich in 1910, that changed modern medicine. It prolonged the average life of people infected with syphilis by 23 years [79]. However, it turned out to be toxic because of the arsenic core structure and was replaced with penicillin, which was safer [80]. Penicillin is a β-lactam antibiotic, which consists of a central β-lactam ring [81]. From this time, penicillin and other antibiotics were discovered, industrially produced, and introduced as promising treatment options against otherwise fatal infections. Other classes of antimicrobials, including sulfonamides, aminoglycosides, and quinolones, were mainly found between the years 1940 and 1970. Therefore, this period is also known as the golden era of antibiotics [82]. Louis Pasteur laid the foundation for this idea with his statement that microbes can secrete substances to kill other bacteria. [79]. In the late 1930s, Selman Walksman was the first person to start a systematic study of antimicrobial compounds produced by microbes. This was the starting point of the early mentioned golden era. For that purpose, filamentous Actinomycetales were employed to produce these compounds [83, 84]. In this screening, many antibiotics were discovered, including neomycin and streptomycin (STREP). With STREP, the first active anti-tuberculosis agent was found. Members of the genus *Streptomyces* were identified as a rich source of natural products representing secondary metabolites with anti-microbial effects [83, 85]. Most antibiotics found in the golden era are still in clinical use, but their efficiency has been reduced due to the rise of AMR [86]. Since many antibiotics were found within a short period, their scarcity was not foreseeable, and they were used very frequently, especially during

World War II. This led to the increased development of resistance to the antibiotics used. Today, AMR is one of the biggest threats and can affect anyone and occurs when bacteria develop the ability to resist the effects of the antibiotics, that were once effective. This happens when bacteria spontaneously mutate or acquire genes that allow them to defend against the antibiotic [87]. As a result, the disease gets harder and sometimes impossible to treat and leads to prolonged hospital stays, higher costs, and increased mortality [88]. There are three main reasons for the emergence of antibiotic resistance. These are the overuse of chemotherapy, the extensive use in agriculture, and the improper prescription of antibiotics [89, 90]. Drug resistance is not only known for many bacteria, but also for parasites like the malaria parasite *P. falciparum*, and viruses, like the human immunodeficiency virus (HIV) [91]. Because of this dramatic progress, it holds great significance to diminish the emergence of resistance through improved patient education, reduced prescription practices, and prevention of infection transmission. In addition, new antibiotics need to be found [91]. After World War II, research has focused on new β-lactam structural variations, such as methicillin, to combat AMR [92]. Resistance to this antibiotic also developed shortly after its introduction to the market. There are different ways of resistance development. One way is the direct modification of the target gene. The other is the inactivation of the drug, which can be due to modifications like conjugation of chemical groups, like acetylation, phosphorylation, or hydrolysis [93]. Another variant is the reduction of the intracellular concentration of the antibiotic, which can be generated by increased efflux or reduced permeability [93]. A multidrug efflux pump inhibitor is a new target for resistant bacteria [94].

A priority list for the development of new antimicrobial substances for resistant bacteria has been published by the WHO [95]. The WHO suggests focusing on Gram-negative bacteria like carbapenem-resistant *Acinetobacter baumannii, Pseudomonas aeruginosa*, and carbapenem and third-generation cephalosporin-resistant Enterobacteriaceae, which all have a critical priority. In the second group, with a high priority, there are Gram-positive bacteria, such as vancomycin-resistant *Enterococcus faecium* and methicillin-resistant *Staphylococcus aureus* [95]. *M. tuberculosis* is not listed on the WHO priority list because it has already been independently prioritized with the “END TB STRATEGY” [96]. Fernandez concluded this resistances could lead to a pre-antimicrobial drug era [90]. Nowadays, there are also approaches being pursued of target- and structure based drug design that precisely focus on an isolated target that is essential for viability of pathogenic bacteria. However, this often does not work because, e.g., the charge or permeability is not considered so that many of the designed inhibitors cannot penetrate the cells to reach their intracellular target [97]. As many routes to drug discovery have

proven very difficult, many pharmaceutical companies have turned their focus elsewhere, which means that finding new compounds continues to stagnate [98]. Due to globalization and modern lifestyle, antibiotic-resistant bacteria are rapidly distributed globally and can be found in other communities and hospitals. Due to their resistance, the bacteria are also a threat to all groups of society [90]. *M. tuberculosis* has also developed many resistances to different antibiotics, described below [1].

1.3.2 Treatment against tuberculosis

The mortality of TB is very high if this disease is not recognized and treated. The first anti-TB drug, STREP, was discovered by Selman Walksman in 1944, and in the following 20 years, other drugs have been developed [84]. Before that time, the standard TB therapy consisted only of fresh air, exposure to sunlight, and bed rest. Nowadays, the treatment against *M. tuberculosis* consists of combination therapy to prevent the development of resistance. Due to the chronic progression, the infectious nature, and the complex immunological response, there is a need for long-term treatment. In most cases of drug-susceptible TB, a combination of isoniazid (INH), RIF, ethambutol (ETB), and pyrazinamide (PZA) is taken every day for two months in the “intensive phase”. In the “continuation phase”, the treatment is carried out with only RIF and INH [99]. However, there are known cases where the treatment needs to be continued for up to two years [100]. Finding new active agents against TB is a major challenge. This is partly because *M. tuberculosis* has a very high intrinsic resistance due to its complex cell wall that serves as a permeability barrier and thus prevents the entry of most drugs [37]. Another reason could be that mycobacteria and streptomycetes, which produce many natural products with antibacterial activity, as described above, both belong to the phylum Actinomycetota. Therefore, it is suspected that *M. tuberculosis* has also evolved intrinsic mechanisms to block their mode of action [101]. The WHO recognizes that TB is still a significant health problem and has therefore established strategies consisting of improved diagnostic tools, drug delivery, and prevention strategies to eradicate *M. tuberculosis* by 2050 [102]. The following chapter will focus on the four first-line anti-TB drugs and STREP

1.3.2.1 Streptomycin

The first antibiotic found against *M. tuberculosis*, thus representing a new era of treatment, is STREP (Figure 4A), which was discovered by Walksman in 1944 [84]. A comparative study between the traditional treatment option consisting of sunlight and bed rest, and the new treatment with STREP showed the success of the antibiotic, as there was an improved survival rate of up to 50%. Because the research was not far

advanced and there were many errors in the treatment with STREP, resistance developed almost simultaneously [103]. STREP is a member of the aminoglycoside antibiotics. These drugs inhibit protein biosynthesis by binding to the 30S ribosomal subunit through the 16S ribosomal ribonucleic acid (16S rRNA) [104]. Resistance in *M. tuberculosis* is mainly caused by a mutation in the genes encoding ribosomal protein S12 (*rpsL)* or 16S rRNA. RpsL stabilizes the pseudoknot structure, which is formed by 16S rRNA [105]. The alteration of this structure disrupts the interaction between STREP and 16S rRNA, which causes resistance [106, 107].

1.3.2.2 Isoniazid

The first synthetically produced drug against *M. tuberculosis* is INH (Figure 4B). This drug, previously known as a cancer drug, was first used in the early 1950s for treatment against *M. tuberculosis*. As with STREP, monotherapy led to the rapid emergence of resistance. In the case of INH, the mechanism of action was unknown for a long time and was only clarified in some detail in the first decade of the 21st century [108]. Nowadays, it is known that this bactericidal drug is a prodrug. The active form is generated after passive diffusion through the mycobacterial cell wall. The active form is an isonicotinoyl radical, which is produced by the cytoplasmic multifunctional catalase/peroxidase KatG. These isonicotinoyl radical binds covalently to $NAD^{+,}$ leading to the formation of isonicotinoyl-NAD^{+} adducts [109]. They can inhibit the formation of the mycobacterial cell wall by inhibiting InhA, the enoyl-ACP reductase. Enoyl-ACP reductase is an essential part of the bacterial fatty acid synthase complex II and is responsible for the final step of fatty acid biosynthesis. Due to this inhibition, long-chain fatty acids such as mycolic acids can no longer be synthesized [110, 111].

1.3.2.3 Rifampicin

RIF is a semisynthetic drug initially derived from rifamycins obtained from *Amyxolatopsis rifamycinica* in 1957. Structural changes allowed the drug to be absorbed into the gastrointestinal tract and led to the development of RIF as it is used today (Figure 4C) [112]. Because of its lipophilic structure, rifampicin can act on both extracellular and intracellular organisms. This property allows it to pass through the lipid-rich cell wall of mycobacteria. It has a broad spectrum of activity and is active against gram-positive and gram-negative bacteria [113]. RIF is an inhibitor of bacterial desoxyribonucleic acid (DNA)-dependent ribonucleic acid (RNA) polymerase [114]. It binds to the β-subunit of the enzyme, which induces a conformational change that leads to the blockade of the elongation of messenger RNA (mRNA). Spontaneous dissociation of short, unstable DNA-RNA hybrids occurs, leading to transcription termination [115]. This upstream inhibition of protein biosynthesis during the growth phase of bacteria leads to a

bactericidal effect. However, because mycobacteria grow very slowly, prolonged therapy is required, and the risk of recurrence is increased with monotherapy [116]. Mutations in the target gene *rpoB* confer resistance towards RIF. This gene comprises 81 base pairs known as rifampicin resistance determining region [116, 117].

1.3.2.4 Ethambutol

ETB (Figure 4D) is one of the most popular front-line drugs. It was found in a synthetic compound screening against *M. tuberculosis* and was first discovered in 1961 [118]. The mode of action and resistance of this bacteriostatic agent is not entirely proven yet, but it was reported that it primarily hampers mycobacterial cell wall synthesis. In more detail, it inhibits the arabinogalactan polymerization, in which the two membrane-associated arabinosyl transferases EmbA and EmbB are involved [119-121].

Further analysis shows that it interferes with cell wall synthesis and plasma membrane integrity by inhibiting the enzyme MruI and affecting peptidoglycan biosynthesis [122]. Recently, a proteomic approach showed that energy metabolism and respiration genes are upregulated by ETB [123]. Therefore, it is speculated that ETB influences various enzymes.

1.3.2.5 Pyrazinamide

PZN (Figure 4E) is structurally related to nicotinamide and was discovered in 1952. It was the first drug that reduced the TB treatment by several months and had a sterilizing effect not only on actively replicating but also on dormant bacteria [124, 125]. PZN is known to be a prodrug that needs to be activated to pyrazinoic acid. This conversion is performed by the mycobacterial enzyme pyrazinamidase (PZase) [126]. Mutations in the gene *pncA*, which encodes for the enzyme PZase, lead to resistance toward PZN [126]. The mode of action of the active form is still under discussion. It is assumed that PZN targets different processes, e.g., translation. A protein involved in translation, ribosomal protein S1, was described as a putative target of pyrazinoic acid [127]. Further studies revealed that PZN inhibits RNA and protein synthesis and serine uptake. Another effect is that PZN destroys the membrane potential at low pH and by this, it is inhibiting growth. Furthermore, recent nuclear magnetic resonance spectroscopy methods showed that PZN binds competitively to mycobacterial fatty acid synthase I (FAS-I) [128]. It is postulated that in this case PZN, rather than pyrazinoic acid, binds directly to FAS-I [129]. However, no correlation between FAS-I inhibition and PZN has been established in other studies [130, 131].

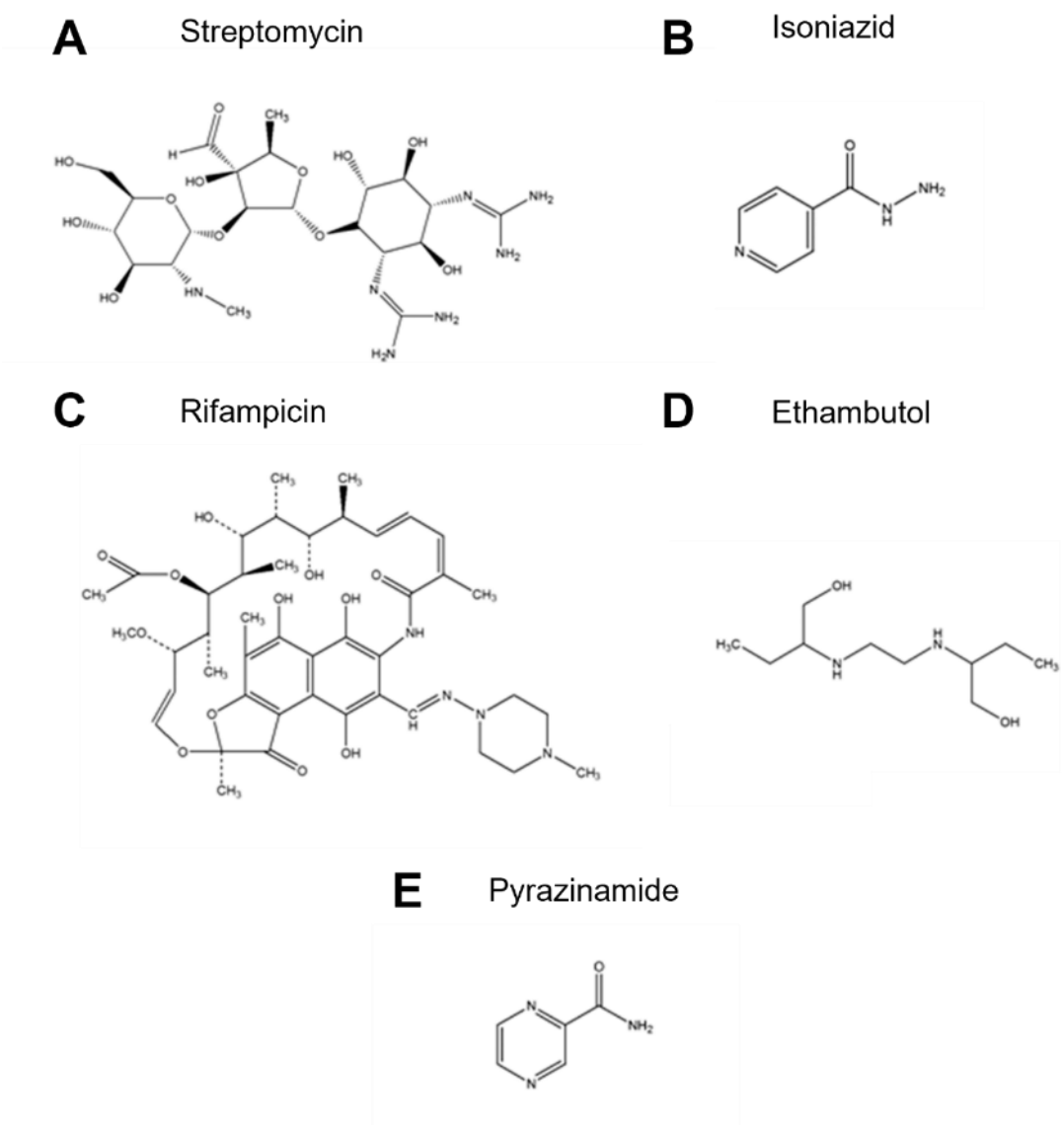

Figure 4: The first-line drugs and STREP used in TB therapy. The structure of the first identified antibiotic with anti-TB activity streptomycin **(A)** and the antibiotics used in first-line therapy for TB isoniazid **(B)**, rifampicin **(C),** ethambutol **(D)**, and pyrazinamide **(E)**. Figure adapted from Grotz et al. (2018) [132].

1.3.3 Drug-resistant *M. tuberculosis*

As described previously (in Chapter 1.2), *M. tuberculosis* can mutate rapidly, leading to the development of resistance to antitubercular drugs. These resistant bacilli are challenging to treat because only a few approved anti-TB drugs are active against DR-TB. These will be discussed in more detail in the next chapter. The mutations develop particularly quickly if the drugs are not used properly. Correct use includes, among other things, taking the medication daily over a long period and monitoring the patients [133]. In 2021, there were 450,000 incident cases of MDR-TB or RR-TB, which is 3.1% more

than in 2020. The countries with the highest percentage are the Russian Federation and several countries in Central Asia and Eastern Europe (Figure 2). Nowadays TB is not only a “poverty-related” disease, but there are an increasing number of cases also in Europe [1]. Drug resistance can be divided into RR-TB, MDR-TB, extensively drug-resistant (XDR), pre-XDR-TB, and totally drug-resistant (TDR) TB [134]. RR-TB is characterized by monoresistance against RIF, while MDR-TB includes resistance against both first-line antibiotics RIF and INH [1]. The previous chapter described the resistance obtained in more detail. The Center for Disease Control and Prevention (CDC) and WHO declared pre-XDR-TB as resistance to INH and RIF, and at least one fluoroquinolone like levofloxacin (LFX), moxifloxacin and ciprofloxacin or one injectable drug such as kanamycin, capreomycin, or amikacin [135]. XDR-TB is defined as resistance to INH and RIF and at least one fluoroquinolone, or one injectable drug, and to bedaquiline or linezolid. XDR-TB is associated with a high mortality rate, especially in combination with HIV-coinfection [136]. Recently, cases of total drug resistance (TDR-TB) have also occurred. In this case, the bacteria are resistant to all standard antibiotics [134]. The pre-XDR clinical isolates from KwaZulu-Natal (KZN), used in this study, were responsible for an outbreak of XDR-TB in South Africa between 2005-2007. These were further investigated and showed resistance against the antibiotics INH, RIF, ETB, STREP, PZA, ethionamide, kanamycin, amikacin, capreomycin, and ofloxacin [137].

Recently, only a small number of new drugs have entered the market. Some of them will be described in more detail in the following chapter, particularly concerning their mode of action and effect on DR-TB which poses a major challenge. To address this, the WHO has postulated strategies to end the TB epidemic by 2050. The main focus is on improving access to drugs and testing. One way to reduce the large proportion of DR-TB is to find new drugs. This can be done in different ways, e.g., screening of natural products or target-directed design of new lead structures [102].

1.3.3.1 Second-line anti-tuberculars

Second-line drugs are used only for the treatment of DR-TB. They include, among others, moxifloxacin, LFX, BDQ, linezolid, clofazimine, cycloserine, terizidone, DELA, PZA, and pretomanid. These drugs must be taken under the supervision of an experienced doctor because some of them have strong side effects [131]. These antibiotics must be only used against DR-TB, otherwise, resistance to these antibiotics would also develop more and more, reducing treatment options. In the following, the most important ones are described in more detail.

Bedaquiline

Upon its introduction in 2012, the diarylquinoline bedaquilline (Figure 5A) was found to have a novel mode of action. It exhibits potent antimicrobial activity by inhibiting the adenosine triphosphate (ATP) synthase, specifically by blocking the proton pumping mechanism in *M. tuberculosis* [138]. The ATP synthase is located in the inner membrane and generates energy in the form of ATP through a proton gradient called proton motive force created by electron transport chain [139-141]. The ATP synthase consists of two units: a cytoplasmic sector F_1 and a membrane sector F_0. The c units of F_0 have the function of an ion-conducting pathway and are arranged in a form like a disk. It has been demonstrated that the proton motive force through F_0 enhances the rotation of the cylindrical ring of subunit c and leads to coupled rotation of the catalytic subunit b of the F_1 domain, resulting in ATP synthesis from ADP and inorganic phosphate [139, 142, 143]. It could be shown that BDQ binds to subunit c and prevents the ATP synthase function [139, 140, 142]. The inhibitory effect of BDQ is specific to mycobacteria [142]. Clinical trials showed that it is safe and useful for treating MDR-TB resulting in 70.9% of sputum culture conversion within 119 days [144, 145]. Resistance to BDQ has been associated with mutations in two genes, namely *atpE* and *mmpR* [146, 147]. The *atpE* gene encodes the F_1/F_0-ATP synthase subunit c [146, 148], while the *mmpR* gene encodes the repressor of the MmpS5-MmpL5 efflux pump [149].

Delamanid

In 2006, a nitro-dihydro-imidazole derivative called delamanid (DELA) was discovered (Figure 5B) as a cell wall synthesis inhibitor, specifically targeting mycolic acids. DELA is a prodrug that requires activation by the enzyme deazaflavin-dependent nitroreductase (Rv3547, *ddn*). A reactive intermediate metabolite formed between delamanid and the desnitroimidazooxazole derivative is crucial in inhibiting the synthesis of keto and methoxy mycolic acids through the F420 coenzyme system [150]. This system generates and recycles cofactor F420 and produces nitrous oxide [151, 152]. In 2014, the WHO recommended the use of DELA as a drug against DR-TB [153]. However, resistant pathogens have already emerged, with the most frequent mutation being detected in *ddn* [154], whose product is involved in the F420 system. Other mutations, such as those in *fbiA, fbiB, fbiC*, and *fgd1*, whose products are also involved in the F420 system, can also induce resistance to DELA [155].

Pretomanid

In 2000, pretomanid (Figure 5C) was found as PA-824, which is also a nitroimidazole. It has shown promising results against dormant TB, but it also has several known side effects such as vomiting, low blood sugar, diarrhea, nerve damage, headache, and liver inflammation [156, 157]. When it reached phase III clinical trials, it received limited approval to be used against XDR-TB in combination with linezolid and BDQ, but in 2019 it was approved by FDA and in 2020 by EMA. This prodrug is considered to have a very broad target spectrum in *M. tuberculosis* and, like DELA, is activated by Ddn, which produces different active metabolites including nitric oxide. The molecular mechanism behind pretomanid's effect is not well understood, but it is known to impact the cell wall [158]. According to proteome analysis, there is an upregulation of genes such as *fasI* and *fasII*, both encoding for proteins involved in the eukaryotic-like fatty acid synthesis, *efpA* that encodes for an efflux pump, and three isoniazid-induced genes in the *iniBAC* operons associated with cell wall biosynthesis. Additionally, the *cyd* operon, which encodes subunits of the cytochrome bd oxidase, is also upregulated [159-161]. This cytochrome bd oxidase plays a role in energy-transducing respiration [162]. Research has shown that pretomanid can be effective against actively growing and dormant TB. In actively dividing bacteria, the drug interferes with mycolic acid biosynthesis, resulting in hydroxylate accumulation. In dormant bacteria, pretomanid's metabolite des-nitroimidazole generates reactive nitrogen species, leading to reduced ATP levels as observed in *M. smegmatis* [159]. Whole-genome sequencing of pretomanid-resistant clones revealed mutations in genes for the synthesis of cofactor F420, including *fbiC, fbiA, ddn, fgd, fbiB*, and *fbiD* [163].

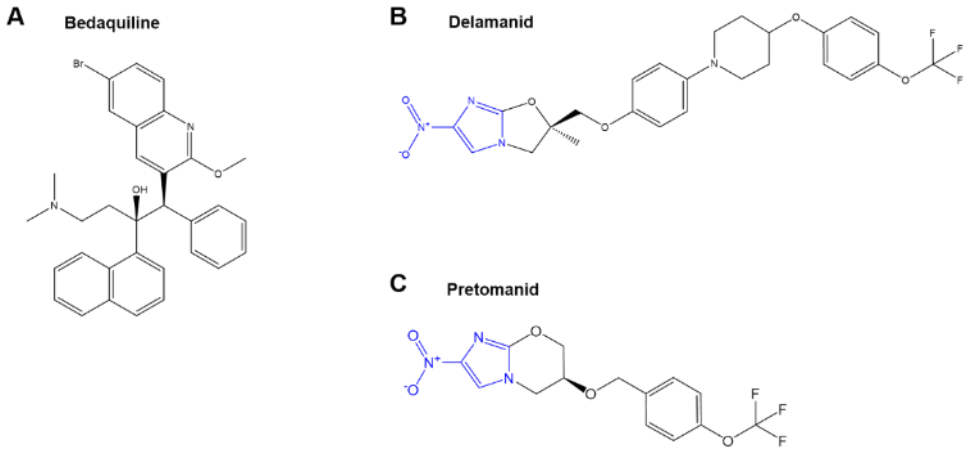

Figure 5: Chemical structure of bedaquiline (A), delamanid (B) and pretomanid (C). The nitroimidazole core structures of DELA and pretomanid are highlighted in blue. Figure adapted from Venugopala *et al.* (2021) [164].

Second-line drugs

There are several other second-line anti-tuberculosis agents. This chapter provides a brief summary of some of these agents. One group of anti-TB drugs is the fluoroquinolones, including ciprofloxacin, moxifloxacin, ofloxacin, levofloxacin, and sparfloxacin (Figure 6A) [165]. They all affect mycobacterial DNA replication and increase the level of DNA strand breaks generated by topoisomerase II, which subsequently leads to cell death [166-169]. In many bacterial species, there are two type II enzymes, the DNA gyrase and topoisomerase IV. However, in *M.* tuberculosis, there is only the DNA gyrase, which has functional properties of both. It untangles and unknots DNA and regulates the superhelical density of the chromosome and removes torsional stress, generated ahead of the DNA replication forks and the transcription complexes [170-173]. This DNA gyrase comprises a tetramer of two A and two B subunits [174]. Mutations in *gyrA* and *gyrB* are associated with resistance to fluoroquinolones [175]. In addition, there is a second group of second-line agents belonging to the aminoglycosides that interfere with protein synthesis and alter the 16S rRNA level (Figure 6B). Representatives of this group are kanamycin, amikacin, capreomycin, and viomycin. Drug resistance mainly results from mutations in the *tylA* gene that codes a putative rRNA methyltransferase affecting the ribosomes. These mutations change the structure of the ribosome and alter the binding to the antibiotic [176-178]. Another mutation is found in the 16S rRNA of the *rrs* gene*,* which encodes the ribosomal protein S12, which stabilizes the highly conserved pseudoknot structure formed by 16S rRNA [176]. Alterations in this structure can disrupt the interaction between the drug and 16S rRNA [179].

Cycloserine is an alanine analog that has a cyclic structure and shows no cross-resistance with other agents (Figure 6C) [180]. It affects the biosynthesis of the mycobacterial cell wall, particularly in the peptidoglycan biosynthesis process by targeting two enzymes, D-alanine ligase and alanine racemase [181, 182]. Resistance to cycloserine is associated with *alr*, which encodes the alanine racemase. However, mutations in 13 other genes were linked to cycloserine resistance that are involved in different mechanisms such as methyltransferase, transport system, stress response, and lipid metabolism. This indicates a complex mechanism of resistance [183].

Ethionamide is another antibiotic used as a second-line treatment (Figure 6D). It interferes with mycolic acid biosynthesis, forming adducts with NAD. This antibiotic targets the same molecular structure as INH, and it inhibits the NADH-dependent enoyl-acyl carrier protein reductase InhA [184]. Ethionamide is a prodrug, that requires

activation by a NADPH-specific flavin adenosine dinucleotide containing mono-oxygenase, which is encoded by *ethA* [185]. Mutations in *ethA* and *ethR* have been linked to resistance to this antibiotic. The *ethR* gene encodes a negative regulator of EthA. Additionally, mutations in the *inhA* gene have also been linked to resistance to ethionamide [185-187].

Furthermore, linezolid, an oxazolidinone antibiotic, binds to a specific location on the bacterial 23S rRNA of the 50S ribosomal subunit, hindering the formation of the 70S complex, which is critical for bacterial replication and division (Figure 6E) [188]. Its efficacy against DR-TB has been shown [189-191] and resistance to linezolid has been associated with mutations in 23S rRNA gene [192, 193]. The final antibiotic presented here is *para*-Aminosalicylic acid, which was first clinically used in 1946, initially as a first-line antibiotic (Figure 6F). However, with the discovery of more effective anti-tubercular agents, it was reclassified as a second-line antibiotic. The p*ara*-Aminosalicylic acid is a structural analog of *para*-aminobenzoic acid and is synthesized from chorismate by aminodeoxychorismate lysate and aminodeoxychorismate synthase [194, 195]. In the folate metabolic pathway, enzymes transform *para*-Aminosalicylic acid into 2´-hydroxy-7,8-dihydrofolate and 2´-hydroxy-7,8-dihydropteroate, which inhibit dihydrofolate reductase by competing for binding sites, thus hindering the synthesis of folic acid [196, 197]. This is an effective target because bacteria are incapable of using external sources of folic acid and by this cell growth is slowed down [198, 199]. The p*ara*-Aminosalicylic acid resistance is associated with mutations in *thyA*, which encodes folate-dependent thymidylate synthase, and *folC*, which encodes a dihydrofolate synthase [197, 200].

To summarize, very few new agents have recently been approved against *M. tuberculosis*. Resistance to nearly all of the described antibiotics developed shortly after approval. Therefore, it is crucial to find new agents against TB.

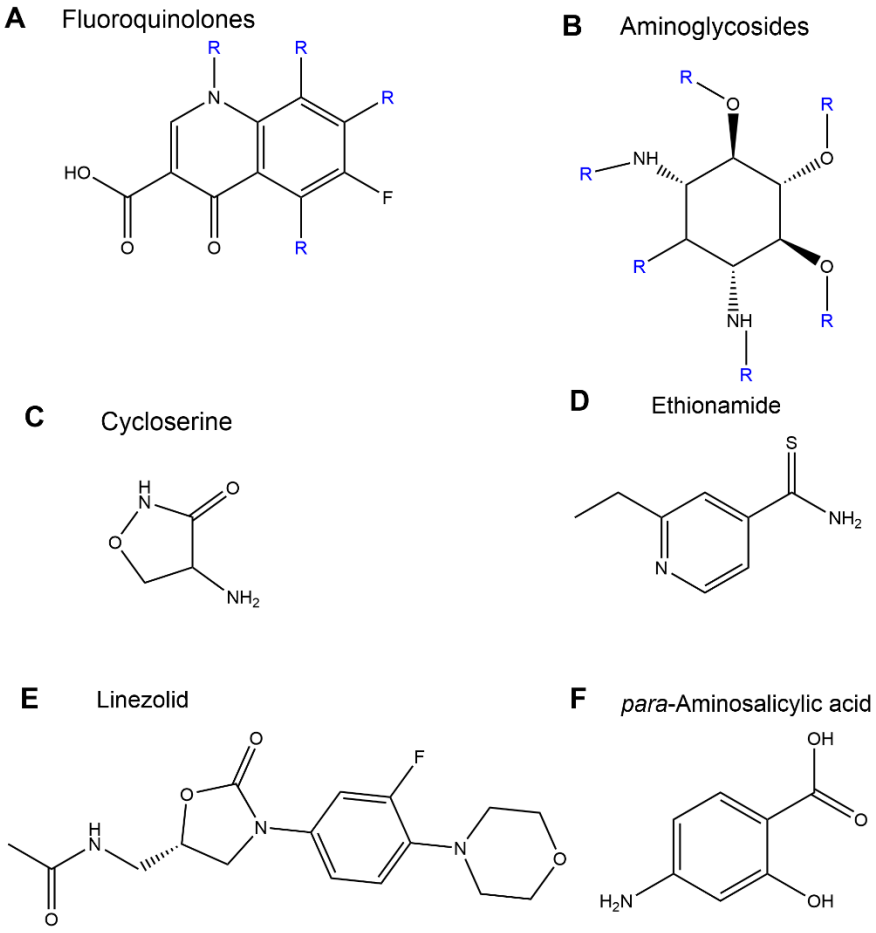

Figure 6: Core structure of fluoroquinolone (A), and aminoglycoside antibiotics (B), and the chemical structure of cycloserine (C), ethionamide(D), linezolid (E), and *para*-Aminosalicylic acid (F).

1.4 Approaches for developing new antibiotics

As mentioned in the last chapters, it is especially important due to the antibiotic-resistant mutants among all bacteria to introduce new antibiotics that have activity against the resistant mutants. After the golden era of antibiotics, the pharmaceutical industry has developed very few antibiotics that have completed clinical trials and can be used. Thus, it is necessary to discover novel active compounds [201]. One approach involves the broad screening of available molecule libraries against a specific pathogen, without any prior directional selection, which necessitates testing numerous molecules. This process has evolved into a directed variant driven by the whole genome sequencing of a wide variety of pathogenic bacteria. This makes it possible to develop an active compound that binds directly to a specific desired target. The target should be present only in the bacterium and not in mammals so that there is no cross-reaction [202]. For that purpose, computational programs have been used to predict effective compounds. Fine-tuning is then done by co-crystallization of the protein [203]. However, no antibiotic found by this

route has yet been marketed [204]. One explanation for the poor effectiveness of this method could be attributed to the poor penetration into the cell or efflux of the substance, resulting in a worsened efficacy [205]. Another modern method is the revert to natural products which involves extracting and purifying active compounds from a natural product. These are diverse molecules, that are originated from different sources, like plants, fungi, marine organisms, and bacteria. They all have developed many substances, that gave them an evolutionary advantage over others because they can protect them from stressful situations and enemies [206]. Natural products are an endless source of compounds for drug development. The isolation and identification method includes technologies like mass spectrometry (MS), high-performance liquid chromatography (HPLC), microfluidics, nuclear magnetic resonance spectroscopy, and for the improvement of the outcome, computational algorithms [207]. For high throughput assays, microfluidics systems and bioreactors were used and different approaches can vary the outcome, like bacterial co-cultivation or a variation in the cultivation parameters, like the medium composition, cultivation temperature, and cultivation time. But there are also disadvantages of these methods, including the complexities of the chemistry, the slowness of working with natural products, the small yield, and difficulties in supply and access [208-210]. The need for high-throughput processes has spurred the creation of several innovative solutions, one of which is the Ichip. This platform enables the cultivation and isolation of microbial species that were previously unculturable. The Ichip functions as an isolation chip, with hundreds of diffusion chambers that allow naturally occurring growth factors to permeate from neighboring cells. To each chamber only one cell is added, which results in pure cultures that can be directly isolated and used for drug discovery [211].

There are also further approaches, such as drug repurposing, in which drugs that are already approved by FDA and clinically used, are bioinformatically or empirically investigated to see if they also have other effects. The methodologies can be grouped as target-oriented, drug-oriented, and disease or therapy-oriented, which depends on the available information like pharmacokinetic and toxicological properties of drug molecules, and the quality and quantity of the molecule [212]. The big advantages are the short development timelines, and lower development costs because they already have been pharmacologically investigated [212]. A disadvantage of this method is that a new application may need different formulations and concentrations, which increase the risk of side effects. Because of that, the repurposed drugs also need clinical trials before usage [213]. Bacteriophages are another starting point. These are capable of killing bacteria [214]. In some countries, they have already been used in humans against

bacterial infections [215]. An advantage is that they probably have a new mechanism of action. The disadvantages are that standardization is difficult, and when used systematically in humans, they are immunogenic, and, in addition, lysis of the bacteria can lead to a toxic shock [216, 217]. Several methods already exist to address these drawbacks, such as utilizing bacteriophages solely as a carrier of antibiotics or using only their gene products as therapeutic agents [215, 218, 219]. Another genetic approach to discovering new drugs involves cloning large fragments of non-culturable bacterial genomes into a culturable bacterium and expressing them using recombinant DNA technology [220-223]. For this purpose, DNA is extracted from bacteria, e.g., from environmental samples, and it is cloned into artificial chromosomes [224]. The open reading frames can then be expressed and analysed for antibacterial activity. In case of a positive finding, various molecular DNA techniques are applied to increase the production of the active substance [202].

At the moment, the majority of new compounds are analogues of existing antibiotics. Due to the resistance of many bacteria against antibiotics, it is necessary to discover new families of antibiotics. In the following, three new groups of anti-mycobacterial substances will be introduced.

1.4.1 The natural compound chlorflavonin

In prior studies, the flavonoid natural compound chlorflavonin (CF) was isolated from the endophytic fungus *Mucor irregularis*, which was isolated from the medicinal plant *Moringa stenopetala* [225]. This natural product showed potent activity against *M. tuberculosis* H37Rv with an MIC_{90} of 1.56 µM and activity against *M. tuberculosis* XDR clinical isolates. Further analysis showed no cytotoxic effects against the monocyte cell line THP-1 and lung fibroblast cell line MRC-5 [225]. CF was first isolated from *Aspergillus candidus* in 1969, and one year later, the structure was elucidated [226]. This 3´-chloro-5,2´-dihydroxy-3,7,8-trimethoxy flavone (see Figure 7A) showed antifungal activity against *Aspergillus amstelodami, Aspergillus fumigatus, Aspergillus ochraceous* (MIC_{90} of 0.08 mg/mL) and slight activity against the plant pathogen *Botrytis cinerea* and the mold *Paecilomyces variotii* (MIC_{90} of 2.5-5.0 mg/mL) [227]. In *M. tuberculosis,* it has a bacteriostatic effect. Combined with RIF, ETB, and BDQ, it exhibits an additive effect, while with INH and DELA, it leads to a synergistic killing effect. Furthermore, it has intracellular activity against *M. tuberculosis* within infected macrophages *in vitro*. Analysis of spontaneous resistant mutants and confirmation by enzyme assay showed that CF inhibits the large catalytic subunit IlvB1 of the acetohydroxyacid synthase (AHAS) [225]. It is known that IlvB1, in combination with the regulatory subunit IlvN is

mediating the first step of the *de novo* branched-chain amino acid (BCAA) and pantothenic acid biosynthesis [228-234]. This enzyme catalyzes the condensation of two pyruvate molecules to acetolactate, or the condensation of pyruvate and α-ketobutyrate to acetohydroxybutyrate with the release of CO_2 (see Figure 7B), after further conversion steps resulting in leucine, valine, isoleucine, and pantothenic acid [235]. The incubation of *M. tuberculosis* with CF leads to auxotrophies of these amino acids [225]. The fact that AHAS is present in archaea, algae, bacteria, plants, and fungi but not in mammals makes it an attractive target for developing new antibiotics, antifungals, and herbicides [236-238]. The lack of AHAS in humans explains the absence of cytotoxicity and makes CF a promising and novel antibiotic for anti-tuberculosis therapy.

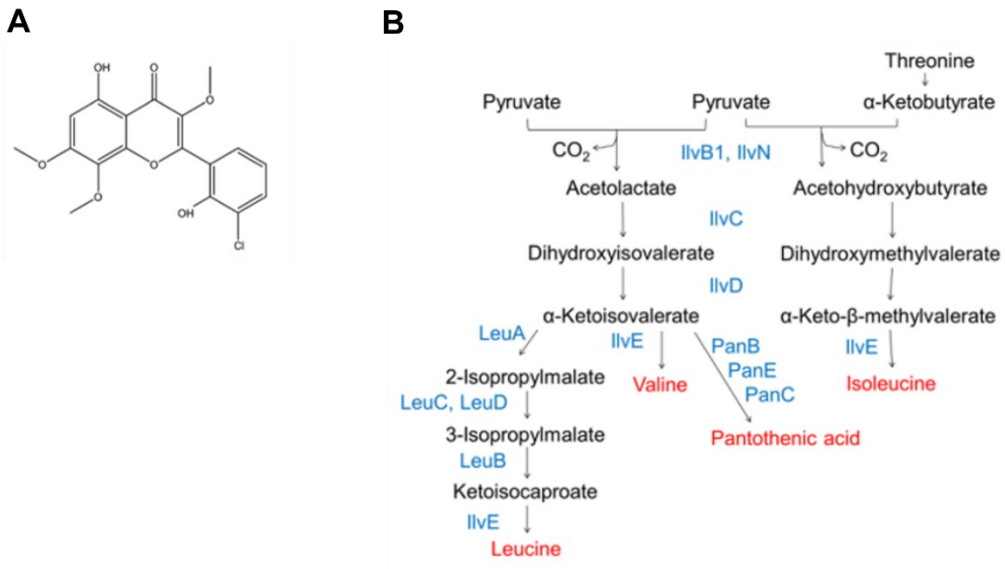

Figure 7: CF blocks the biosynthesis of branched-chain amino acids. (A) Chemical structure of CF. **(B)** Role of the acetohydroxyacid synthase IlvB1 and regulatory subunit IlvN in the pathway for the biosynthesis of branched-chain amino acids and pantothenic acid in *M. tuberculosis.* Figure adapted from Rehberg *et al.* (2018) [225].

1.4.2 Hydroxamic acid-based molecules with an anti-tuberculosis activity

The antimycobacterial effect of hydroxamic acid derivatives was first described in a patent with α-aminooxyhydroxamic acid derivatives in 1971 [239]. However, a publication with follow-up results on these derivatives was never published. In the following years, other derivatives were published by the same working group. A hybrid of isoniazid and aminoxyacetic acid showed the best activity against *M. tuberculosis* (MIC_{90} of 0.07 µg/mL) and low cytotoxicity [239]. *In vivo*, the compound showed activity against *M. tuberculosis* in a 3-month infection model with guinea pigs and mice [239]. Subsequently, other derivatives were patented. These include α-aminooxyamides and α-aminooxyhydrazides derivatives, both with a terminal aldoxime. The lead structures

KSK-104 and KSK-106 (KSKs) used in this work have been previously established in cooperation between the research groups of Profs. Kalscheuer and Kurz and differ from the previously described compounds (Figure 8). The molecules can be divided into three regions – A, B, and C. Both have an alkoxyamide backbone (region B) and a benzyl group in region C. Region A distinguishes the two molecules. KSK-104 has a *para*-substituted biphenyl group in this region, whereas KSK-106 has a phenyl group substituted with a phenyl ether in *para*-position. Both molecules have excellent activity against *M. tuberculosis* and no cytotoxic effects against the tested cell lines, like the monocyte cell line THP-1 or liver cell line HEPG2 [240]. Furthermore, both substances have a bactericidal activity and show an additive effect in combination with INH, RIF, ETB, and DEL [240]. The analysis of spontaneous resistant mutants (SRM) raised against the KSKs revealed mutations in two different amidohydrolases. For KSK-104, two different mutations in the gene *rv0552,* encoding a non-essential, conserved hypothetical protein predicted to have amidohydrolase activity, were found in five randomly chosen SRMs [240, 241]. According to the annotated hypothetical function, the enzyme can cleave carbon-nitrogen bonds, but not peptide bonds. For spontaneously KSK-106-resistant mutants, four different mutations in the gene *amiC* were found for all but one SRM [240]. The gene *amiC* also encodes for an amidohydrolase that likely has the capability to hydrolyze C-N bonds. In a recent publication, resistance to different amide-containing compounds, indole 4-carboxamides, was also reported to be mediated through mutations in *amiC*. The authors were able to show that in the presence of the mutated amidohydrolase, the hydrolysis of the indole 4-carboxamides decreases, and thereby the activation of these compounds is blocked [242]. With all this information, KSKs are thought to be prodrugs that are cleaved by the amidohydrolases and thereby activated. This hypothesis is analyzed in this work.

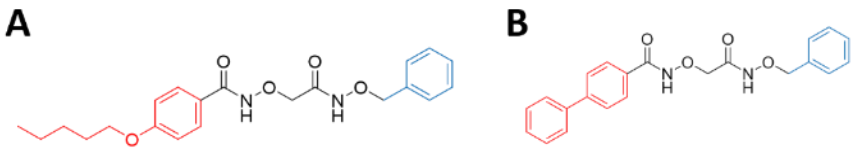

Figure 8: Chemical structures of KSK-106 (A) and KSK-104 (B). The core region (region B) is shown in black, whereas region A is highlighted in red and region C in blue.

1.4.3 Thiazoles as a basic scaffold for the development of new antimycobacterial agents

Thiazoles are found in many compounds. It is a heterocyclic molecule containing sulfur and nitrogen (see Figure 9). Molecules containing thiazoles have different activities, including antiparkinson, anti-inflammatory, antiviral, anticonvulsant, and antibacterial activities [243-245]. Naturally, thiazoles occur in vitamin B1, also known as thiamine. Besides this natural resource, various thiazole-containing molecules have also been found in many empiric compound screening campaigns, e.g., as a thiazole-based inhibitor of an epigenetic reader module of post-translational modifications called bromodomain, especially for the protein ATAD2, which is a nuclear coregulator cancer-associated protein [246]. Furthermore, lead structures with activity against *M. tuberculosis* have also been found with phenylthiazoles, which target the ribosomal peptidyl transferase center [247], or methylthiazoles, which inhibit InhA [248]. There are a lot of other examples of thiazole derivatives, like 2-arylthiazolidin-4-one-thiazole hybrids, that also have potent activity against *M. tuberculosis.*

In summary, this highlights the strong activity of thiazoles against *M. tuberculosis* and shows the possibility of finding new antitubercular thiazole-containing substances.

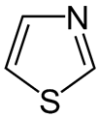

Figure 9: Chemical structure of a thiazole.

1.5 Aim of the study

Today, the formation of resistance in bacteria is caused, among other things, by the incorrect use of medicines and the frequent administration of antibiotics in animal breeding. Resistance in pathogenic bacteria is a significant challenge. New active substances against bacteria should be found and analyzed to combat this problem. In the present work, the main focus has been set on the bacterium *M. tuberculosis*, which is the causative agent of tuberculosis.

Part of the work deals with the previously identified natural active substance chlorflavonin. With its antimycobacterial property, no cytotoxicity, and a new mode of action, this represents a potentially suitable compound against *M. tuberculosis*. A more detailed characterization of the mode of action, the elucidation of structure-activity relationships, and the discovery of putatively more potent derivatives were particularly relevant in this part of the work.

The analysis of KSK-104 and KSK-106, previously found to be active against *M. tuberculosis* in the research groups of Profs. Kalscheuer and Kurz, should also be further investigated. In particular, since it was hypothesized that these substances are prodrugs, the cleavage products, and thus, the active substance should be identified. Methods such as detecting putative cleavage products in culture supernatants by HPLC and LC-MS/MS were to be established and applied. Since previous analyses have shown that the amidohydrolases AmiC and Rv0552 play a role in developing resistance, a closer focus should also be placed on this aspect.

In addition, screening of a compound library consisting of synthetically produced thiazole derivatives was performed to find a new agent against *M. tuberculosis*. Various methods should be used to determine the effect, mode of action, and drug target of the most active compound FFK-088.

2 Material and Methods

2.1 Chemicals

Name (purity)	CAS Number	Producer
(+)-Maltose monohydrate	6363-53-7	Roth
1,4 Dithiotreitol (>99%)		Roth
3,3'-Diaminobenzidine tetrahydrochloride hydrate (>=96%)	868272-85-9	Sigma
Acetoin (>98%)	CAS 513-86-0	TCI
Adenosine-5'-monophosphate monohydrate [ATP disodium salt]	18422-05-4	fluorochem
Agar noble		BD Difco
Ammonium acetate (>98%)	631-61-8	Sigma
Ammoniumchloride (p.a.)	12125-02-9	Applichem
Ampicillin sodium salt		Sigma-Aldrich
Bedaquiline (99.97%)	843663-66-1	MEC
Bromphenol Blue	115-39-9	Fisher
Calciumchloride x2 H2O (99.50%)	10035-04-8	Grüssing
Caliumchlorid-dihydrate (p.a.)	10035-04-8	Merck
Casein hydrolysate (Peptone from casein)	91079-40-2	Sigma
Cetyltrimethylammonium bromide (99%)	57-09-0	Applichem
Chlorflavonin		Sigma
Colistin	1264-72-8	Serva
Coomassie® Brillantblau G-250 (C.I. 42655)	6104-58-1	PanReac AppliChem
Copper(II) sulfate	029-004-00-0	Honeywell
Creatine, anhydrous (98%)	57-00-1	Alta Aesar
D-(-) Arabinose (>=99%)	10323-20-3	Fluka
D-(-) Arabinose (>=99%)	10323-20-3	Roth
D(-) Mannitol	69-65-8	VWR
D(+) Saccharose (>=99.5%)	57-50-1	Roth
D-(+)-Glucose monohydrate	14431-43-7	lagerhaltig im ZCL
D-(+)-Mannose (>=99%)	3458-29-4	Fluka

Delamanid (>=97%)	843663-66-1	cayman
Difco Agar Noble		BD
Difco Yeast Nitrogen Base w/o Amino Acids		Difco
di-Potassium hydrogenphosphate xH2O	16788-57-1	Grüssing
Dodecyl sulfate sodium salt (SDS)	151-21-3	Serva
D-Pantothenic acid hemicalcium salt		Sigma
DTT		Thermo Fisher
EDTA disodium salt 2-hydrate (p.a.)	6381-92-6	Applichem Panreac
Ethambutol dihydrochloride	1070-11-7	Sigma
Glass beads acid-washed <=106 µm		Sigma
Glass beads acid-washed 453-600 µm		Sigma
Glucose Oxidase/Peroxidase reagent		SIGMA
Glycerol phosphate disodium salt hydrate	55073-41-1	Sigma
Glycine (p.a.)	56-40-6	Sigma Aldrich
Hefeextrakt mikro-granuliert		Roth
HEPES sodium salt for buffer solutions	75277-39-3	Applichem Panreac
Hygromycin B		
Imidazole (p.a.)	288-32-4	Sigma Aldrich
Iron(II)chloride tetrahydrate	13478-10-9	in 15ml Falkon
Iron(II)sulfate heptahydrate (>99%)	7782-63-0	Sigma Aldrich
Isoniazid	54-85-3	Fluka
Isopropyl-β-D-thiogalactopyranoside (IPTG), dioxanfree, for biochemistry	367-93-1	
Potassium chloride (p.a.)	7447-40-7	Merck
Kanamycin sulfate	25389-94-0	Applichem
Magnesium chloride hexahydrate	7791-18-6	VWR
Magnesium sulfate heptahydrate	10034-99-8	Acros Organics
Moxifloxacin 98.87%	151096-09-2	BLDpharm
NI-NTA Agarose Protino		MN
Paraformaldehyde DAC (reinst)	30525-89-4	Roth
Pepton from casein	919079-40-2	ROTH
Peptone from soyabean, enzymatic digest	91079-46-8	Sigma-Aldrich
Potassium acetate for molecular biology	127-08-2	Applichem Panreac
Potassium phosphate hydrate (98%)	7778-53-2	chemPUR

Proteinase K		Roth
Resazurin sodium salt	62758-13-8	Sigma
SKIM milk powder		OXOID
Sodium pyruvate	113-24-6	Fisher
Sodium acetate	127-09-3	Sigma-Aldrich
Sodium acetate	127-09-3	VWR
Sodiumhydroxid mikrogranulate	1310-73-2	CHEMSOLUTE
Sodium phosphate dibasic Na_2HPO_4 (for analysis)	7558-79-4	Acros Organics
Sodium phosphate monobasic monohydrate (p.a.)	10049-21-5	Sigma-Aldrich
Sucrose, Saccharose	57-50-1	Serva
Thiamine hydrochloride (>=99%)	67-03-8	Sigma-Aldrich
Thiamine pyrophosphate	CAS 154-87-0	AppliChem
Tris(2-carboxyethyl)phosphine hydrochloride solution	51805-45-9	BLD Pharmatech
Trisodium phophate anhydrous	7601-54-9	fuorochem
tris-Sodium citrate dihydrate (>=99.5%)	6132-04-3	Fisher
Triton X100	9036-19-5	Applichem Panreac
TRIzol Reagent		
Tylaxopol	25301-02-4	Sigma
Urea	57-13-6	VWR Chemicals
Zinc sulfate-7-hydrate (analysis)	7446-20-0	Applichem Panreac
α - Naphthol (>=99.5%)	90-15-3	Roth / Sigma-Aldrich
α-D-Glucose (>=96%)	158968-500G	Sigma

2.2 Kits and Solutions

Kit	Producer
BacTiter-Glo™ Microbial Cell Viability Assay	Promega
BCA Protein Assay Kit	Merck Millipore
Bradford Reagent	Sigma
Failsafe™ PCR Premix Buffers	epicentreR/ lucigen via Biozym
GoTaqR qPCR Master Mix	Promega
NucleoSpinR Gel and PCR Clean-up Kit	Macherey-Nagel
NucleoSpinR Plasmid Mini Kit	Macherey-Nagel
PD midiTrap™ G-25	GE Healthcare Life Sciences
RNase-Free DNase Set	Qiagen
RNeasy Mini Kit	Qiagen
SuperScript™ III First-Strand Synthesis SuperMix	Invitrogen

All kits were used following the manufacturer's protocols.

2.3 Enzymes

Enzyme	Producer
Phusion High-Fidelity DNA Polymerase	New England Biolabs
Taq polymerase	New England Biolabs

The DNA polymerases were used for the polymerase chain reaction following the specified protocol for the Failsafe™ PCR Premix buffers or Taq polymerase (REDTaq ReadyMix PCR Reaction Mix, Sigma).

2.4 Oligonucleotides

Primer Name	Sequence
5' amiC (PCR)	GGCTCGTGTGGCGATTTTCGAC
3' amiC (PCR)	TTAATGACGCCCCGCTGGGCTATC
5'rv0552 (PCR)	ATAGCACCGTTGGCGTCCACCCGCACCAT
3'rv0552 (PCR)	GGCGCATCAAAACTTCAGGACGGTTGAG
5' amiC (seq)	AATTATGTCGAGGCCGCCATCGCCCG
3' amiC (seq)	GAGAGCATCATGCCCACGG
5' rv0552 (seq)	TTATCGTCAGGCGCTCCTCCGGTG
3' rv0552 (seq)	TTATTGGAGGCGGTCGTGCTGTCGG

The PCR was performed according to the polymerase used (see chapter 2.3). The PCR products were separated on a 1% agarose gel and isolated and purified using NucleoSpinR Gel and PCR Clean-up Kit.

2.5 Devices

Device	Producer
Bio-Rad Gene Pulser Xcell™	Bio-Rad
Mx3005P QPCR System	Agilent Technologies
Nanodrop	Thermo Fisher
Nikon Eclipse TS100	Nikon
PrecellysR 24 Homogenisator	BERTIN/ peqlab
Sonoplus mini20	Bandelin electronic GmbH & Co.KG
Tecan infinite F200 Pro	Tecan
Thermal cycler FlexCycler	Analytic Jena AG
TissueLyser LT	Qiagen
UVP Gel Studio	Analytic Jena AG

2.6 Software

Software	Producer
ChemDraw 19	PerkinElmer Informatics
Clone Manager 9	Scientific and Educational Software
Fiji (is just ImageJ)	National Institute of Health, USA
GraphPad Prism 7.02	GraphPad Software Inc
i-control™ 1.1	Tecan Trading AG
MxPro – Mx3005P	Stratagene
NIS-Elements	Nikon
Office 2016	Microsoft
VisionWorks 8.19	Analytik Jena AG

The Figures were partly generated using Servier Medical Art, provided by Servier, licensed under a Creative Commons Attribution 3.0 unported license.

2.7 Bacterial growth conditions and determination of the minimal inhibitory concentration

2.7.1 Bacterial growth conditions

Middlebrook 7H9 liquid media (BD Diagnostics) was used to grow different mycobacterial strains. The cells were incubated aerobically at 37 °C and 80 rpm. 7H10 media (BD Diagnostics) was used for solid media, and the plates were incubated at 37 °C until the grown colonies were visible. Supplements were utilized according to the table.

For specific approaches, protein medium, Sauton´s medium, and reduced minimal medium were chosen for mycobacteria. If not mentioned differently, 7H9 was used.

Liquid cultures of several *Escherichia coli (E. coli)* strains were grown in lysogeny broth (LB medium, see below) at 37 °C and 180 rpm. 2% (w/v) agarose was added to the solution for solid LB media. *E. coli* cultures were incubated overnight at 37 °C. The supplements for selectivity are listed in the table below.

7H9 medium

10% (v/v)	Albumin dextrose salt (ADS)
0.5% (v/v)	Glycerol
0.05% (v/v)	tyloxapol
0.47% (w/v)	7H9 powder (Middlebrook)

7H10 medium

10% (v/v)	ADS
0.5% (v/v)	glycerol
	7H10 powder (Middlebrook)

ADS

5% (w/v)	Bovine serum albumin
2% (w/v)	Glucose
0.85% (w/v)	Sodium chloride

Protein medium

0.5% (v/v)	Glycerol
0.2% (w/v)	Glucose
0.085% (w/v)	Sodium chloride
0.47% (w/v)	7H9 powder (Middlebrook)

Reduced minimal medium (RMM)

0.015% (w/v)	L-asparagine x 1 H_2O
0.005% (w/v)	$(NH_4)_2SO_4$
0.1% (w/v)	KH_2PO_4
0.25% (w/v)	Na_2HPO_4
0.005% (w/v)	Ferric ammoniumcitrate
0.05% (w/v)	$MgSO_4$ x 7 H_2O
0.00005% (w/v)	$CaCl_2$
0.00001% (w/v)	$ZnSO_4$
0.05% (v/v)	tyloxapol
Adjust pH to 7,0.	
Addition of: 0.5% (v/v) glycerol; 0.1% (v/v) cholesterol; or 1% (v/v) glucose.	

Sauton´s medium

0.05% (w/v)	KH_2PO_4
0.05% (w/v)	$MgSO_4$ x 7 H_2O
0.2% (w/v)	Citric acid
0.005% (w/v)	Ferric ammoniumcitrate
0.4% (w/v)	L-asparagine x 1 H_2O
Adjust pH to 7,4	
Addition of: 0.5% (v/v) glycerol; 0.1% (v/v) cholesterol; or 1% (v/v) glucose.	

LB medium

0.5% (w/v)	Yeast extract
1% (w/v)	Bacto tryptone
0.5% (w/v)	Sodium chloride

2.7.2 Bacterial strains

Table 1: *M. tuberculosis* strains used in this study.

Strain	Biosafety level	Media complementation	Source/ reference
H37Rv	3		obtained from William R. Jacobs Jr., PhD, Albert Einstein College of Medicine, Bronx, USA
XDR KZN06 XDR KZN07 XDR KZN13 XDR KZN14 XDR KZN15	3		clinical isolates from KZN, South Africa, obtained from William R. Jacobs Jr., PhD, Albert Einstein College of Medicine, Bronx, USA
H37Rv pBEN::mCherry (Hsp60)/GFP (Atc)	3	50 µg/mL hygromycin	RG of Prof. Dr. Kalscheuer, University of Duesseldorf, Germany
spontaneously resistant mutant KSK-106 #5	3		RG of Prof. Dr. Kalscheuer, University of Duesseldorf, Germany
spontaneously resistant mutant KSK-104 #1	3		RG of Prof. Dr. Kalscheuer, University of Duesseldorf, Germany
double spontaneous resistant mutant KSK-104_KSK-106 (first against KSK-104; than against KSK-106)	3		This study

double spontaneous resistant mutant KSK-106_KSK-104 (first against KSK-106; than against KSK-104)	3		This study
spontaneously resistant mutant OMK-117	3		This study
spontaneously resistant mutant OMK-175	3		This study
spontaneously resistant mutant ABK-334	3		This study
spontaneously resistant mutant FFK-088	3		This study
$mc^2$6230 Δ*panCD* Δ*RD1*	2	100 mg/L pantothenic acid	obtained from William, R. Jacobs Jr., PhD, Albert Einstein College of Medicine, Bronx, USA

Table 2: *M. smegmatis* strain used in this study.

Strain	Biosafety level	Media complementation	Source/ reference
$mc^2$155	2		obtained from William R. Jacobs Jr., PhD, Albert Einstein College of Medicine, Bronx, USA

Table 3: *M. marinum* strain used in this study.

Strain	Biosafety level	Media complementation	Source/ reference
DSM No.: 44344= ATCC 927	2		DSMZ-German Collection of Microorganisms and Cell Cultures GmbH

Table 4: *M. bovis* BCG Pasteur and *M. bovis* BCG Danish 1331 strain used in this study.

Strain	Biosafety level	Media complementation	Source/ reference
BCG Pasteur	2		obtained from William R. Jacobs Jr., PhD, Albert Einstein College of Medicine, Bronx, USA
BCG Danish 1331	2		obtained from William R. Jacobs Jr., PhD, Albert Einstein College of Medicine, Bronx, USA

Table 5: *E. coli* strain used in this study.

Strain	Biosafety level	Media complementation	Source/ reference
Rosetta(DE3)pLysS pET30a::*ilvN*	1	40 µg/mL kanamycin	RG of Prof. Dr. Kalscheuer, University of Duesseldorf, Germany
Rosetta(DE3)pLysS pET30a::*ilvB1*	1	40 µg/mL kanamycin	RG of Prof. Dr. Kalscheuer, University of Duesseldorf, Germany

Table 6: Human cell lines used in this study.

Strain	origin	Biosafety level	Source/ reference
THP-1	monocytes	1	Deutsche Sammlung von Mikroogranismen und Zellkulturen GmbH
HuH7	hepatocyte-derived carcinoma cell line	1	Cell Line Service GmbH
MRC-5	fetal lung fibroblast	1	American Type Culture Collection
HEK293	embryonic kidney	1	CLS Cell Lines Service GmbH
H4	epithelial cell line	1	Cell Line Service GmbH
SH-SY5Y	brain neuroblast	1	Cell Line Service GmbH

Unless otherwise stated, *M. tuberculosis* wild type H37Rv is always used in the following.

2.7.3 Determination of minimal inhibitory concentration (MIC_{90})

Cells were precultured in 7H9 medium to an OD_{600} between 0.5 and 1 unless otherwise indicated to determine the MIC_{90} for slow-growing mycobacteria. The MIC assay was performed in a round-bottom-96-well format. The compounds were two-fold serially diluted starting with 100 µM in 50 µL. $1x10^5$ of these pre-cultured cells were seeded into each well, resulting in a total volume of 100 µL. These plates were incubated at 37 °C for five days. Next, 10 µL of a 100 µg/mL resazurin solution was added to each well and incubated overnight at room temperature. After the incubation, a final concentration of 5% (v/v) formalin was added to each well and incubated for an additional 30 min until the cells were fixed.

Fluorescence (excitation 540 nm, emission 590 nm) was measured using the Tecan infinite F200 pro reader, and the MIC_{90} values were calculated using DMSO samples as 100% and sterile medium as 0% growth.

For fluorophore-labeled samples, the BacTiter-Glo™ Microbial Cell Viability Assay (Promega) was used according to the manufacturer instructions: After five days of incubation in the 96-well plate, 50 µL of the cell suspension was mixed with 50 µL BacTiter-Glo™ solution in a Nuclon 96-well flat bottom white polystyrene plate (Thermo Fisher Scientific). The luminescence was measured using the Tecan infinite F200 pro reader. The calculation is identical to that for the resazurin dye.

For the determination of MIC_{90} for fast-growing mycobacteria, cells were precultured in 7H9 medium, if not mentioned differently, to an OD_{600} between 0.5 and 1. The MIC assay was performed in a round-bottom-96-well format. The compounds were two-fold serially diluted starting with 100 µM. $1x10^5$ of the pre-cultured cells were seeded in each well, resulting in a total volume of 100 µL. These plates were incubated overnight at 37 °C. Subsequently, 10 µL of a 100 µg/mL resazurin solution was added to each well and incubated at 37 °C until a color development from blue to pink was detectable in the DMSO samples. A final concentration of 5% (v/v) formalin was added to each well and incubated for 30 min until the cells were fixed.

Fluorescence (excitation 540 nm, emission 590 nm) was measured using the Tecan infinite F200 pro reader. MIC_{90} values were calculated using DMSO samples as 100% and sterile medium as 0% growth.

2.7.4 Checkerboard Synergy Assay

To determine the fractional inhibitory concentration index (FICI) of FFK-088 with bedaquiline (BDQ), rifampicin (RIF), and delamanid (DELA), a two-dimensional dilution of the compounds was prepared in round-bottom-96-well plates. In a total volume of 100 µL, $1x10^5$ cells were

seeded in each well and incubated at 37 °C for five days. Next, 10 µL of a 100 µg/mL resazurin solution was added to each well and incubated overnight at room temperature. A final concentration of 5% (v/v) formalin was added to each well and incubated for 30 min until the cells were fixed.

Fluorescence (excitation 540 nm, emission 590 nm) was measured using the Tecan infinite F200 pro reader. The FICI was calculated as the sum of the quotients of the lowest inhibitory concentration in a row (A and B) divided by the MIC_{90} of the compound itself (MIC_A and MIC_B). The resulting value indicates the behavior of the tested drug in the presence of another antibiotic: total synergism is ≤0.5, while partial synergism is between 0.5 and 0.75. No effect is in the range of 0.75 and 2; a value >2 means that the substances are antagonistic.

$$\mathrm{FICI} = \frac{\mathrm{A}}{\mathrm{MIC_A}} + \frac{\mathrm{B}}{\mathrm{MIC_B}}$$

2.7.5 Time killing kinetic

As described above*, M. tuberculosis* H37Rv cells were pre-cultured to the exponential phase. A culture of $1x10^6$ CFU/mL was prepared and distributed to 10 mL approaches containing various anti-tuberculosis agents: 3.9 µM FFK-088,10 µM isoniazid, 0.5 µM rifampicin, 0.5 µM bedaquiline, 2.5 µM delamanid or 5 µM ethambutol were added to a square bottle individually or in combination with 3.9 µM FFK-088. A sterile medium control and a DMSO control were prepared as controls.

The cultures were incubated at 37 °C and 80 rpm for 35 days. At different time points, samples were collected and diluted. The different dilutions were plated on Middlebrook 7H10 agar plates supplemented with 10% ADS and 0.5% glycerol and incubated for 14-17 days at 37 °C, and the grown colonies were counted. All experiments were performed in triplicates.

2.8 Growth conditions of human cell lines and determination of therapeutic indices

2.8.1 Growth conditions of human cell lines

All human cell lines were cultivated at 37 °C in a humidified atmosphere of 5% CO_2.

The monocytic cell line THP-1 (Deutsche Sammlung von Mikroorganismen und Zellkulturen GmbH) was grown in RPMI 1640 (PAN, P-18500) medium containing 10% (v/v) fetal bovine serum (FBS; 10438026 FBS, HI 500 mL GIBCO via ThermoFisher). For splitting and

cytotoxicity assay, cells were harvested using centrifugation (150 x g, 5 min) and resuspended into fresh media.

All adherent cell lines were washed with phosphate-buffered saline buffer (PBS) and incubated with 0.25% trypsin-ethylenediaminetetraacetic acid (Gibco®) for 5 min at 37 °C to detach them from the bottom of the cell culture flask (Greiner). To stop the process, fresh 10% FBS-containing medium was added. Cells were transferred to a 50 mL centrifugation tube (SARSTEDT) and centrifugated (150 x g, 5 min), resuspended in fresh media, seeded into 96-well plates for cytotoxicity assay or induction assay, or split into fresh cell culture flasks.

To adjust the correct cell density, cells were counted using the Neubauer hemocytometer with a chamber index of 10,000.

Different media are used for the different cell lines for optimal growth conditions: the human hepatocyte-derived carcinoma cell line HuH7 (Cell Line Service GmbH) was cultured in RPMI 1640 medium containing 10% (v/v) FBS, whereas the human fetal lung fibroblast cell line MRC-5 (American Type Culture Collection) was incubated in Eagle´s Minimum Essential Medium (EMEM biowest, MS00VF1007) containing 1% (v/v) Na-pyruvate and 10% (v/v) FBS. The human embryonic kidney cell line HEK293 (CLS Cell Lines Service GmbH) was cultivated in EMEM supplemented with 2 mM L-glutamine, 1% (v/v) non-essential amino acids, 1 mM sodium pyruvate, and 10% (v/v) FBS. Whereas the brain epithelial cell line H4 (Cell Line Service GmbH) and the brain neuroblast cell line SH-SY5Y (Cell Line Service GmbH) were cultivated in Dulbeccos´s Modified Eagles Medium (DMEM PAN, P04-04510) containing 10% (v/v) FBS.

2.8.2 Determination of cytotoxicity

To assess the cytotoxicity, $5x10^4$ cells were seeded in a 96-well-flat-bottom microtiter plate with a total volume of 100 µL. Twofold dilutions of the compounds of interest were prepared in appropriate media for the selected cell line. Cells were incubated for 48 h at 37 °C, with 5% CO_2. Subsequently, 10 µL of a 100 µg/mL resazurin solution was added to each well. Cells were incubated for at least two hours until color development was visible in the DMSO control samples. Fluorescence (excitation 540 nm, emission 590 nm) was measured using the Tecan infinite F200 pro reader. IC_{50} values were calculated using DMSO-treated cells as 100% and sterile with 0% growth.

The selectivity index (SI) is the ratio between IC_{50} and MIC_{90} values.

2.8.3 Macrophage infection assay

THP-1 cells were grown as described in Chapter 2.8.1. Initially, cells were counted using the Neubauer hemocytometer as described above. $1x10^5$ cells in a total volume of 100 µL were seeded into each well of a sterile 96-well flat-bottom polystyrene microtiter plate (Greiner). 50 nM phorbol-12-myristate-13-acetate (PMA) was added to the medium to differentiate the cells into adherent macrophage-like cells. The cells were incubated overnight at 37 °C, 5% CO2 in a humid atmosphere for differentiation. Afterward, the cells were washed twice with PBS. The *M. tuberculosis* H37Rv mCherry reporter strain was used for infection, which was cultivated in Middlebrook 7H9 broth supplemented with 150 µg/mL hygromycin. Before infection, the *M. tuberculosis* cells were harvested, washed, and resuspended in RPMI supplemented with 10% FBS. The cell density was adjusted to $3x10^6$ CFU/mL, and 100 µL of this solution was added to each well. After 3 h of infection, the supernatant was removed, and the cells were washed twice with PBS so that no non-phagocytized bacteria remained. In each well 100 µL RPMI supplemented with 10% (v/v) FBS, mixed with the antibiotics (3.9 µM and 7.8 µM FFK-088, 3 µM RIF, 20 µM STREP, DMSO) were added. The cells were incubated for 5 days at 37 °C, 5% CO_2 in a humid atmosphere, and afterward, they were fixed with a final concentration of 5% formalin. The fluorescence signals were documented using the Nikon Eclipse TS100 fluorescence microscope and the bright field, and the red channel (excitation 585 nm, emission 610 nm).

The pictures were taken with the NIS-Element Software. Furthermore, the integrated density of red fluorescence was calculated in comparison to DMSO (100%) and uninfected (0%) using Fiji (ImageJ).

2.9 Molecular and microbiological methods

2.9.1 Extraction of mycobacterial genomic DNA using the CTAB method

The extraction of genomic DNA was performed according to current protocols in Microbiology [249]. A 10 mL culture was transferred to a 15 mL centrifugation tube (SARSTEDT) and centrifugated for 10 min at 2000 g. The cell pellet was resuspended in GTE solution and transferred in a 2 mL tube containing 50 µL of a 10 mg/mL lysozyme solution. After mixing the solution, it was incubated overnight at 37 °C. A 2:1 solution of 10% sodiumdodecylsulfate (SDS) and 10 mg/mL proteinase K solution was prepared, and 150 µL of this solution was added to the cells and incubated for 20 to 40 min at 55 °C. Then 200 µL of a 5 M NaCl solution was added and mixed, followed by 160 µL of preheated CTAB. After mixing, the solution was incubated for 10 min at 65 °C. Afterward, an equal amount of 24:1 (v/v) chloroform/isoamyl

alcohol was added, mixed, and centrifugated for 5 min at maximal speed in a microcentrifuge. 900 µL of the aqueous layer was transferred in a fresh tube, and 900 µL of 24:1 (v/v) chloroform/isoamyl alcohol was added, mixed, and centrifugated for 5 min at maximal speed in a microcentrifuge. Then 800 µL of the aqueous layer was transferred to a fresh tube and mixed by inversion with 560 µL isopropanol, followed by five min of incubation at room temperature. The samples were centrifugated for 10 min at maximal speed, the supernatant was aspirated, and 1000 µL of 70% ethanol was added, mixed, and centrifugated. The supernatant was carefully aspirated. The air-dried pellet was solved in 50 µL of TE buffer, and the DNA concentration was measured.

CTAB solution

4.1 g sodium chloride was dissolved in 90 mL water, and 10 g cetrimide was added while the solution was stirred on the magnetic stirrer. The solution is incubated in a 65 °C water bath for solving purposes.

TE buffer

1 mL of a 1 M Tris-Cl (pH 8.0) is mixed with 0.2 mL of a 0.5 M EDTA (pH 8.0) solution. The mixture was filled with 98.8 mL of distilled water.

2.9.2 Generation and analysis of spontaneous resistant mutants

Spontaneous resistant mutants (SRM) were generated by plating $1x10^7$ to $5x10^8$ *M. tuberculosis* H37Rv WT cells on agar plates containing six to 10-fold MIC_{90} of selected compounds. For double-spontaneous resistant mutants (DSRM) of KSK-104 and KSK-106, $5x10^7$ of SRM-KSK-104#5 (or SRM-KSK-106#1) were plated on 7H10 agar plates containing six to 8-fold MIC_{90} of KSK-106 or KSK-104. Resistant clones appeared after four to eight weeks of incubation at 37 °C. The resistance was ruled out by the MIC's determination (see chapter 2.7.3).

2.9.3 Whole genome sequencing

For the whole genome sequencing, the DNA concentration of the genomic DNA had to be measured using the Nanodrop and the AccuClear kit (Biotium) for the presence of single-stranded DNA. The kit is used following the manufacturer's protocol. The samples were measured in the Genomics & Transcriptomics Labor (GTL) using Illumina sequencer, and the raw data were analyzed by Kristin Schwechel using *Mycobacterium tuberculosis* H37RvMA genome as reference (NZ_CM002884.1).

2.9.4 Recombinant expression and purification of IlvB1

E. coli Rosetta pet30a::*ilvB1* was pregrown overnight in LB supplemented with 40 µg/mL kanamycin at 37 °C and 180 rpm. On the next day, the main culture was started with 1% of the overnight culture and incubated at 37 °C and 180 rpm until an OD_{600} of 0.6 to 0.8 was reached. By the addition of 0.5 mM isopropyl-ß-D-thiogalactopyranoside (IPTG), the cells start to express the protein. For that protein expression, the cells were incubated overnight at room temperature. Next, cells were harvested by 30 minutes of centrifugation at 3000 rpm and 4 °C. The cell pellet is resuspended in a lysis buffer and incubated for 30 minutes on ice. Afterward, the cells were sonified 6 times for 10 seconds on ice using Bandelin Sonoplus. The resulting cell extracts were centrifugated for 40 minutes at 4 °C and 14,000 rpm. The ÄKTA purifier (Cytiva) used the supernatant for protein isolation. Before applying the sample, a blank run was performed by washing the (HisTrap™ FF crude 1 mL from Cytiva) column with 5 column volumes (CV) of ddH_2O and 5 CV of elution buffer. The equilibration of the column was done by running 10 CVs of binding buffer.

The prepared samples were loaded with a syringe to the HisTrap column and washed with 15 CVs of the binding buffer until the absorbance reached the baseline. The proteins were eluted with 5 CV of elution buffer in the last step. Following the operating instructions, the samples were re-salted via centrifugation using a vivaspin®500 (sartorius) and changed against the storage buffer. The samples were stored at -80 °C by adding 0.5% (v/v) mannitol and 10% (v/v) glycerol.

After the day's last run, the ÄKTA was cleaned by washing 20 CVs of 1 M sodium chloride, followed by 10 CVs of ddH_2O and 5 CVs of 20% (v/v) ethanol.

Lysis buffer

0.2 M	AMPD
0.2 M	NaCl
1% (v/v)	Triton-X-100

Elution buffer

350 mM	Imidazole
0.2 M	AMPD
0.2 M	NaCl

Binding buffer

25 mM	Imidazole
0.2 M	AMPD
0.2 M	NaCl

Storage buffer

0.2 M	AMPD
0.2 M	NaCl

Samples were analyzed using sodium dodecyl sulfate-polyacrylamide gel electrophoresis (SDS-PAGE) [250]. The gel was stained with Coomassie solution. For that, 1 g/L Coomassie Brilliant Blue, 50% (v/v) methanol, 10% (v/v) glacial acid, and 40% (v/v) ddH_2O were mixed. The gel is placed in this solution and heated in the microwave for 30 sec at medium watts.

Afterward, it was washed with water several times until the protein bands became visible. The protein concentration was measured using the Bradford Reagent (Sigma).

2.9.5 AHAS assay

The AHAS assay was performed as described by Choi *et al.*, 2005 [233] with minor variations. In a 96-well plate, the compound was two-fold or ten-fold diluted, starting with 112.5 µL reaction buffer. The reaction was started by adding 12.5 µL of a 750 mM stock solution of pyruvate. For the formation of acetolactate, the 96-well plate was incubated at 37 °C for 60 min. To stop all processes, 18.75 µL of a 4 M H_2SO_4 solution was added and incubated at 65 °C for 15 min. 100 µL of this mixture was transferred into a new transparent 96-well-F-bottom plate, and 90 µL of 0.5% (w/v) creatine was added and mixed vigorously.

Color development began by adding and thoroughly mixing 90 µL of a 5% (w/v) α-naphthol solution prepared in 2.5 M NaOH. The formation of a red complex was measured with the Tecan infinite F200 pro reader. For this purpose, the Tecan reader, preheated to 37 °C, was used in a kinetic cycle at the wavelength of 492 nm.

Reaction buffer

100 mM	K_3PO_4
10 mM	$MgCl_2$
1 mM	Thiamine diphosphate
50 µM	Flavin adenine dinucleotide (FAD)
2.5 µg/mL	Enzyme (IlvB1)

2.9.6 CF stability assay

An exponentially growing *M. tuberculosis* H37Rv WT cell culture was used and washed twice in protein medium (see chapter 2.7.1) and finally resuspended in protein medium to an OD_{600} of 1. The culture was then divided into square bottles. A final concentration of 100 µM of ABK-531 (CF), TAKK-009, or the corresponding volume of DMSO was added to a square bottle. As a control, the same concentration of the substances was solved in protein medium without bacteria. Samples were taken directly (t_0), and 24 hours (t_1), 72 hours (t_2), and 196 hours (t_3) after the addition of the compounds. For each time point, a 2.5 mL aliquot was removed from each culture and lysed by bead beating at 50 Hz for 5x3 minutes using 100 µm and 500 µm silica-zirconium beads. The samples were mixed with equal amounts of methanol and incubated for at least one hour at room temperature, and then they were centrifugated for 10 minutes at 14,000 rpm. The supernatants were stored at 4 °C until further use. For the

evaporation of the methanol, the samples were dried in the speedVac, and the leftover medium was dried in a freeze-dryer. The remaining substances were solved in 250 µL methanol and measured using the Dionex P580 system in combination with a diode array detector (UVD340S) and a Eurospher 10C18 column (125 mm x 4 mm) (Knauer). 10 µL of the solution was directly loaded onto the column. Metabolites were separated by running a 60 min gradient program with solvent A (ddH_2O containing 0.1% formic acid) and solvent B (methanol) at a 1 mL/min flow rate. The program starts with 10% solvent B for 5 min, then a gradient of 10% to 100% of solvent B for 30 min, followed by 10 min of 100% solvent B, and at the end, there is a running time of 15 min with 10% solvent B.

2.9.7 Analysis of KSK cleavage products using the Dionex P580 system

The experiment was performed according to chapter 2.9.6. Changes made: A final concentration of 100 µM KSK-104 and KSK-106 were added to the prepared H37Rv WT and the SRM-KSK-104#1, and SRM-KSK-106#5 strain.

Samples were taken directly (t_0), and 24 hours (t_1), 36 hours (t_2), and 144 hours (t_3) after the addition of the compounds.

2.9.8 Analysis of KSK cleavage products using LC-MS

For this experiment, the samples were prepared according to chapters 2.9.6 and 2.9.7. These samples were sent to the Center of Molecular and Structural Analysis@Heinrich Heine University and analyzed with a maXis.

The acquisition parameter used was the source type of ESI with a scan between 50 m/z to 1500 m/z in a positive ion polarity with a set capillary of 4000 V. The nebulizer was set to 2.0 bar, the dry heater to 225 °C, and the dry gas to 9.0 l/min. The APCI heater was set to 0 °C. The resulting graphs were provided in paper form.

2.9.9 Analysis of KSK cleavage products using GC-MS

For this experiment, the samples were prepared according to chapters 2.9.6 and 2.9.7.

1 µL of the sample was injected with a split ratio of 10 into the Agilent 5977 GC/MSD, which is connected with Agilent 8890 GC system. The heater was set to 300 °C with a total flow of 16.2 mL/min. The column is an Agilent 19091S-433UI: 1567254H. The used flow rate in the column was set to 1.2 mL/min.

The running program has a ramp in the oven temperature included. It starts with 0.5 min at 100 °C followed by a ramp to 250 °C in 9.5 min.

2.9.10 KSK metabolite extraction and analysis

For the metabolite extraction, an exponentially growing culture was used. These cells were cultivated in RMM without tyloxapol (see Chapter 2.7.1). The OD_{600} of the samples was adjusted to 0.5 and divided into 5.0 mL approaches. 5 µL of a 1 mM solution of KSK-106, which was solved in methanol (or methanol only), was added and incubated with the WT or SRM-KSK-106#5 for two days at 37 °C. Medium, containing KSK-106 or methanol, was used as a control. A sample was taken 48 hours after the addition of KSK-106.

In collaboration with Dr. Björn Burckhardt, the samples were analyzed using the HPLC (Waters UPLC Acquity), which was coupled with the mass spectrometer (Waters Quattro Premier xe) and the Phenomenex Aqua 3u C18 125A (100 x 2,00 mm) with a 3 µm particles HPLC column. The source temperature was set to 135 °C and the desolvation temperature to 500 °C. The LC has two solvent phases: solvent A (water with 0.1% formic acid) and solvent B (acetonitrile with 0.1% formic acid). 10 µL of the samples were loaded into the column using a flow rate of 0.5 µL/min. The samples were separated on the column using a gradient (starting with 80% solvent A for one minute, 50% solvent A for 30 seconds, 30% solvent A for 30 seconds, 0% for 1.5 minutes, and 80% for 1.5 minutes). The results were referred to a control with a known concentration to obtain the unknown concentration from it.

2.9.11 Native Pulldown

For the native pulldown, a protein lysate was needed. For this purpose, a 1000 mL culture of *M. tuberculosis mc²6230* was prepared in roller bottles (Thermo Fisher) using a protein medium defined as 7H9 medium without BSA. When the cells reached an OD_{600} of 0.6 to 1, the cells were harvested by centrifugation in 50 mL centrifugation tubes (SARSTEDT) at 3000 rpm, washed three times with a totale volume of 100 mL 1x PBS, and afterward solved in 15 mL 1x PBS. The cells were mechanically destroyed by bead beating using 100 µm and 500 µm silica-zirconium beads at 50 Hz for 5x3 minutes using the Peqlab Precellys homogenisator. Afterward, the suspension was centrifugated for 40 min at 13,000 rpm. The supernatant was transferred to a fresh centrifugation tube (SARSTEDT), and the solution was filtered twice through a sterile cellulose acetate filter with a pore size of 0.2 µm. The resulting cell-free protein lysate was transferred to the ACE facility at the university Duisburg-Essen. The procedure was performed in collaboration with David Podlesainski.

After determining the protein concentration of the cell lysate using the Bradford reagent, the lysate was aliquoted into 24 samples with 400 µL of lysate each. The six conditions were: DMSO, 5 µM biotin-conjugate, 5 µM OMK-307, 5 µM OMK-312, 5 µM OMK-307 with 40 µM KSK-106 for bead washing, and 5 µM OMK-312 with 40 µM KSK-106 for bead washing. All

samples were performed in four replicates. Afterward, each sample was filled with 99 µL PBS and mixed with 1 µL of either DMSO or one of the biotin probes (10 mM DMSO stock) and shaken for 30 min at 4 °C and 100 rpm. In the meantime, Pierce Avidin Agarose beads were equilibrated with PBS by exchange of the supernatant and centrifugation for 3 min at RT and 800 g for three times. Then the beads were aliquoted into each sample (approx. 50 µL bead volume and 100 µL of PBS) and incubated for 60 min at RT and 1250 rpm. After that, the beads were washed thrice with 1 mL PBS or 1 mL of 40 µM KSK-106 in PBS. For this, the approach was shaken at 1200 rpm for 10 min, followed by 5 min of centrifugation at 600 g. To dilute the remaining KSK-106, all samples were washed twice with PBS. These samples were then on bead digested using the 6 M Urea protocol.

The beads were taken up in 100 µL 6 M Urea in 50 mM NH_4HCO_3 (ABC buffer) containing 20 mM DTT. After 60 min and 1500 rpm incubation at RT, a final concentration of 40 mM iodoacetamide were added to the sample and incubated for 60 min at 1500 rpm in the dark at RT. Subsequently, 8 µL of a 0.5 DTT stock solution in 50 mM ABC buffer was added and incubated for 5 min at RT and 1500 rpm. The samples were then diluted with 484 µL of 50 mM ABC buffer for a final urea concentration of 1 M. In the next step, 10 µL of a 100 ng/mL trypsin stock solution (in 50 mM acetic acid) was added to each sample and incubated for 15 h shaking at 1100 rpm at 37 °C.

After that, a final concentration of 1% formic acid (FA, Fisher Chemicals) was added to each sample and centrifugated at 600 g for 5 min. The supernatant was transferred to a fresh protein Lo-bind tube, and 50 µL 1% FA was added to the beads, which were incubated for 15 min, shaking at 1100 rpm, and RT. The beads were pelleted by centrifugation at 600 rpm for 5 min, and the supernatant was added to the remaining supernatant.

For the following steps, prepared glass microfiber 200 µL tips containing 2 disks of glass microfiber (GE-Healthcare, pore-size: 1.2 µM, thickness: 0.26 mm) were used to eliminate residual glass beads. These were equilibrated with 50 µL 0.5% FA (STSA solution for StageTipping) and spun down at 50 g for 2 min until liquid has flown through. The equilibrated glass microfiber tips were transferred to a fresh protein Lo-bind tube. Afterward, the acidified supernatant was loaded onto glass microfiber tips and centrifugated at 100 g for 5 min. Next, the stage tipping protocol has to be followed.

50 µL MeOH was transferred immediately on top of the white plug in the C18-StageTip (self-made or commercial (Thermo)) and was centrifuged at 400 g for 2 min to desalt the peptides. After the addition of 50 µL STSB (0.5% (v/v) FA in 80% (v/v) ACN/H_2O) and centrifugation at 400 g for 2 min, 50 µL STSA was added to each sample and centrifuged at 800 g for 1 min. In the meantime, the samples were acidified by adding formic acid up to 0.5% FA, briefly vortexed

and spun down 10 sec at 16000 g. Then the peptide solution is loaded on the equilibrated Stage Tip and centrifugated at 800 g for 3 min. The peptides were washed by adding 50 µL STSA to the Stage Tip and centrifugated at 800 g for 3 min. After a second step of washing with 20 µL STSA, the bounded peptides were eluted with 25 µL STSB by 2 min centrifugation at 800 rpm. This step was repeated. The elution is placed in a SpeedVac until it is completely dry.

In the last step, the samples were resuspended in 15 µL of 0.1% FA and dissolved at 37 °C with shaking at 1500 rpm for 15 min. The finished samples were measured with LC-MS/MS on an Orbitrap Fusion Lumos (Thermo) coupled to Easy-nLC 1200 system (Thermo). The analytical column was self-packed fused silica capillary with an integrated sintered frit emitter (CoAnn Technologies ICT36007515F-50-5). It was self-packed with an integrated stationary phase with Reprosil-Pur 120 C18-AQ (Dr. Maisch GmbH).

The column oven temperature was set to 50 °C during data acquisition. The LC uses two solvent phases: solvent A (0.2% FA, 2% acetonitrile, 98% H_2O) and solvent B (0.2% FA, 80% acetonitrile, 20% H_2O). Peptides were directly loaded onto the column and separated on it by running a 105 min gradient of solvent A and B at a flow rate of 300 nL/min. The program starts with 3% solvent B for 5 min, 5 min 5% of solvent B, a gradient of 5% to 25% of solvent B for 70 min, followed by 15 min a gradient of 25% to 35% solvent B, 5 min 35-100% solvent B and 10 min 100% solvent B. Peptides were ionized using a Nanospray Flex ion source (Thermo).

The data were analyzed using the Uniprot *Mycobacterium tuberculosis* (strain ATCC 25618/ H37Rv) as reference proteome (UP000001584), and all searches were performed using the MaxQuant v2.0.6.0 software to avoid contaminants [251]. Andromeda search allows static modifications, like carbamidomethylation, and dynamic modification, like oxidation of the Acetyl (N-term). The digestion mode was set to Trypsin/P.

Further analysis of the MaxQuant output was done in Perseus v1.5.5.3 [252]. MS/MS counts were loaded, and usual suspects (e.g., potential contaminants, reverse hits, and hits only identified by site) were removed. In the last step, the technical replicates were grouped and filtered. Only the protein groups with valid values were kept, and a t-test was performed for them.

2.9.12 Microscopic analysis of fluorophore probes in *M. tuberculosis*

1 mL of an exponentially growing *M. tuberculosis* pBEN-mcherry reporter strain culture was incubated for two days with the fluorophore-tagged compounds using 1-fold MIC_{90} MIC_{90} at 37 °C. Next, 500 µL of each approach was washed twice with 500 µL 4% paraformaldehyde

(PFA), and the pellet was solved in 200 µL PFA solution. 10 µL of each sample were incubated on coverslips, previously treated with 0.1 mg/mL poly-D-lysine. Samples were analysed using Nikon Eclipse TS100 fluorescence microscope and the bright field, the green channel (excitation 475 nm, emission 510 nm), and the red channel (excitation 585 nm, emission 610 nm).

2.9.13 Iron chelating assay

Assay was performed according to Kuo, *et al.,* 2011. In a round-bottom-96-well plate, a two-fold serial dilution of the compounds was prepared in water. The starting concentration is 1000 µg/mL with a total volume of 100 µL. In each well, 2 µL of a 2 mM $FeCl_2$ solution and 4 µL of a 5 mM Ferrozin solution were added and mixed. After 10 min of incubation in the dark, the absorbance of 562 nm was measured using a Tecan infinite F200 pro reader. The chelating ability was calculated using the aqueous solution without the referred compound as blank and the sample without any compound as the positive control.

2.9.14 Zinc chelating assay

This assay was performed according to Maria Carmen *et al.,* 2018. In a 96-well plate, a two-fold serial dilution of the compounds in DMSO was prepared. The starting concentration was 10 mM in a total volume of 100 µL. In a second round-bottom 96-well plate, 150 µL of a 15 mM HEPES buffer (pH 6.8) was added to each well. Afterward, 50 µL of a 60 µM zinc chloride solution was added to each well and mixed well. As a negative control, the zinc chloride was replaced with water. After that, 50 µL of DMSO or the compounds solved in DMSO were added. After 2 min of mixing in the Eppendorf Thermomix at 500 rpm, 50 µL of the 250 µM dithizone solution was added. The 96-well plates are measured in a kinetic cycle at 540 nm for 30 min every 2 min. The chelating ability was calculated using the aqueous solution without any compounds as 0% and the solution without zinc chloride as 100%.

2.10 Statistics

Absolute numbers were compared with the students t-test. Statistics were calculated using Graph Pad Prism or Microsoft Excel.

3 Results

This study aimed to investigate the activity, mode of action, and target of different substances against *M. tuberculosis.* The first part (chapter 3.1) deals with the results regarding the flavone-like structures, which are based on the lead structure chlorflavonin (CF). The synthesis of the derivatives and lead structure were performed by Dr. Alexander Berger, Talea Knak, and Beate Lungerich from the working group of Prof. Dr. Thomas Kurz (RG Kurz) [253]. The second part (chapter 3.2) is about identifying and characterizing the highly active compounds KSK-104, and KSK-106 (KSKs), that were found in a library screening of synthetic derivatives by Dr. Lasse van Geelen. The shown derivatives have been provided by Dr. Alexander Berger and Dr. Oliver Michel (RG Kurz). The last part of the results (chapter 3.3) evaluates a thiazole-based structure found in a library screening. All derivatives in this part were provided by Fabian Fischer (RG Kurz).

3.1 Evaluation of the anti-mycobacterial properties of chlorflavonin

In prior studies, a substantial anti-tuberculosis effect of the natural product CF was shown with an MIC_{90} of 1.56 µM [225]. The basic structure of CF consists of a dihydroflavone that is substituted by a chloro group in the flavone at position 5´ (Figure 11A and B). The A ring is defined as the fused benzene ring, the C ring as the bound pyran, and the B ring as the phenyl substituent at position 2. Of particular note are the hydroxy groups at positions 5 and 6´, and methoxy groups at positions 3, 7, and 8.

This study focuses on the synthetic compound CF and its derivatives, which were synthesized in RG Kurz. First, the activity of the synthetic CF against *M. tuberculosis* H37Rv was determined, as shown in Figure 10. A dose-dependent inhibition of the mycobacteria could be detected, resulting in an MIC_{90} value of 1.56 µM. This value is comparable to the one for the natural product chlorflavonin, which Dr. Nidja Rehberg has analyzed before [225].

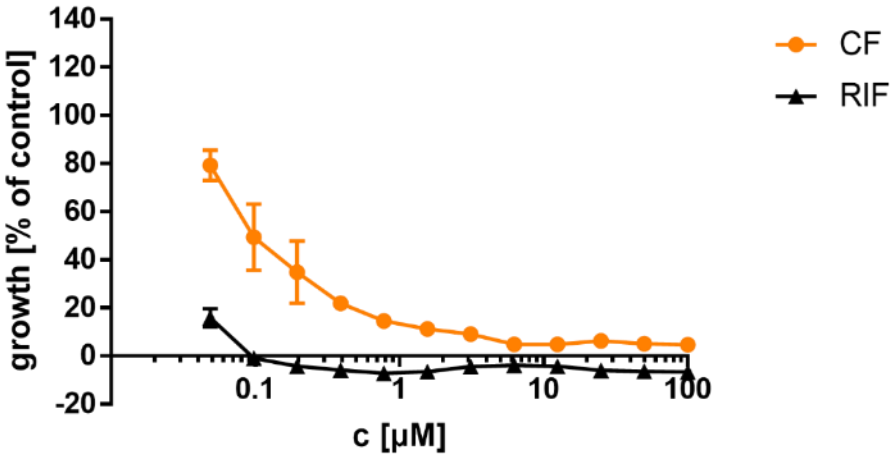

Figure 10: Activity of CF against *M. tuberculosis* H37Rv. Dose-response curve of *M. tuberculosis* H37Rv WT against CF. RIF was used as positive control, and DMSO as vehicle control. Data are shown as means of *n*=3 ±SEM.

3.1.1 Structure-activity relationship of chlorflavonin and its derivatives

To identify which regions, substituents, or substitution patterns are relevant for the activity of CF, Dr. Alexander Berger and Talea Knak designed, and synthesized various derivatives of CF. All compounds were screened against *M. tuberculosis* H37Rv, and the MIC_{90} value was calculated. Figure 11 shows only a fraction of the screened derivatives. In general, the results indicate that CF has very narrow structural requirements. That means that almost all variations at any position of the molecule lead to complete inactivity, as indicated by an MIC_{90} value of 100 µM or >100 µM. In the following paragraphs, there is a summary of some representative derivatives.

The brominated derivative bromflavonin (BrF, ABK-541) is the only derivative that shows a slightly increased activity compared to the lead structure, which is chlorinated at C5´. Since this substance has a similar anti-tubercular effect as CF, it is also used during the following experiments and structure-activity relationship (SAR) studies to clarify other essential structural elements. Nevertheless, neither a fluorinated derivative (ABK-550) nor an iodization (ABK-649) at C5' of the B-ring could improve the activity. Both molecules were inactive. Another derivative has a trifluoromethyl group at this position (ABK-657). This group is often used in medicinal chemistry for therapeutics because the fluorine atoms pull the electron density away from the carbon atoms and increase their chemical stability and by that, the resistance to metabolic degradation, and might enhances ligand-protein interaction [254, 255]. However, no activity was detected in the tested range for that derivative. This effect on the electron density was tested at the sixth position in the B-ring, where a difluoromethoxy group was added to the hydroxy group (TAKK-187). However, this substance had no activity either,

which shows that little variations are possible in these two positions. Some derivatives were designed, varying in the third position in the C-ring. The absence of the 3´-methoxy-substituent in comparison to CF results in a negative shift of the MIC_{90} to 6.25 µM (BLK-248). This result shows that there is a possibility to change the molecule within this position without a dramatic loss of activity. Because of this result, different changes in this position were created and tested. An example is an additional ethoxy group (TAKK-042 for the chlorinated form or TAKK-009 for the brominated form) or an ethylene glycol moiety (TAKK-100). All of these analyzed derivatives were inactive in the tested range. In another approach, derivatives were synthesized, which vary in the fifth position in the A-ring. The absence of the hydroxy group led to a decrease in the activity to 25 µM (ABK-516). This minimal activity is lost if the sixth position in the B ring is also varied by adding two methoxy groups (ABK-540) or an allyloxy group (ABK-512). The substitution at this position to an amino group decreases the activity to an MIC_{90} of 50 µM (TAKK-210). With another methoxy group at this position, the derivative is no longer active against *M. tuberculosis* (BLK-247). The substance is inactive when the ethoxy group is exchanged to a methyl group at the eighth position (TAKK-169).

In general, these findings indicate that the cellular killing effect is initiated in a highly structure specific manner by CF and BrF. Some positions allow minor variations leading only to small reductions in the MIC_{90}. Explanations for the loss of activity will be attempted throughout these chapters.

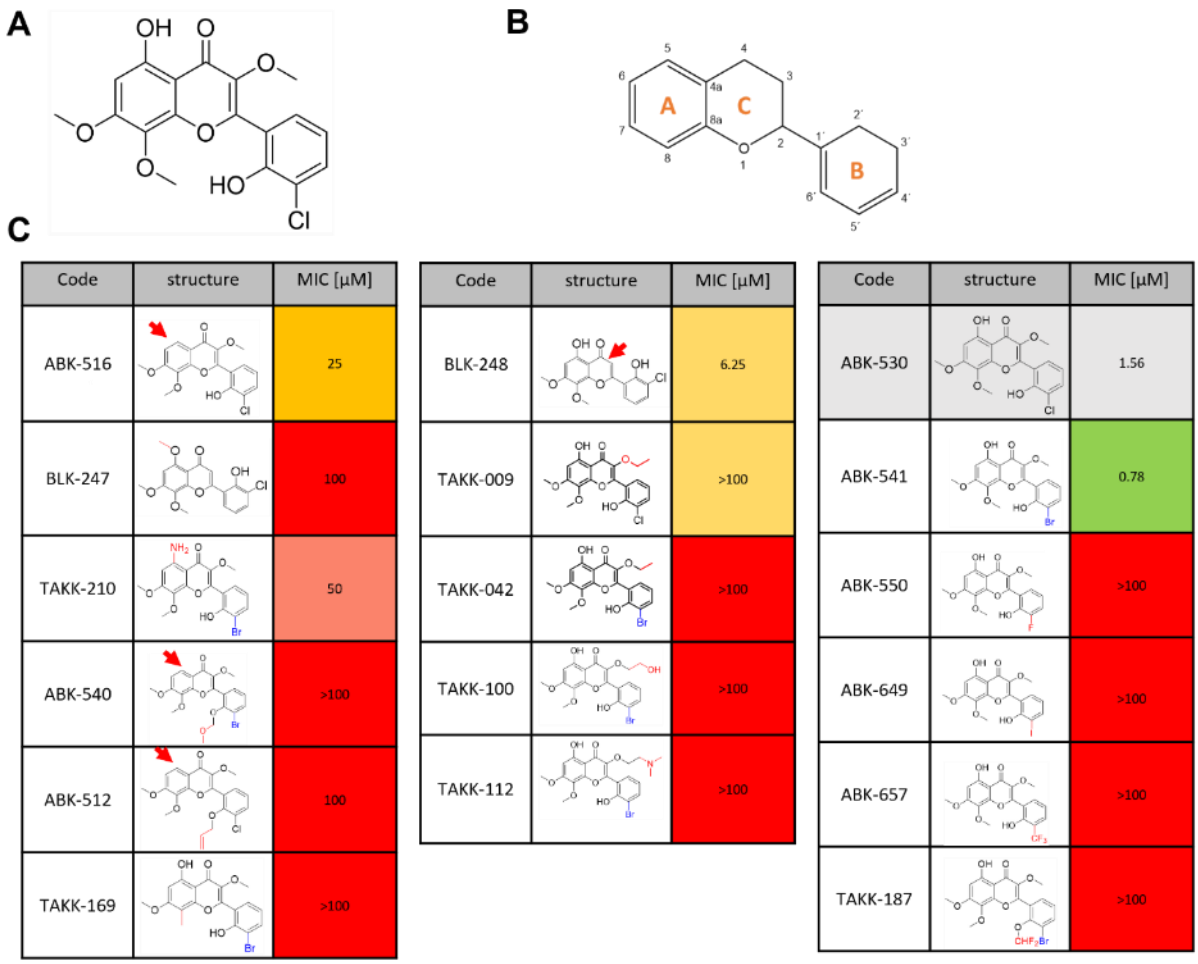

Figure 11: Heatmap representing MIC_{90} values of different CF derivatives. (A) Chemical structure of CF. **(B)** Numbering of the basic structure of CF. **(C)** Heatmap of antitubercular activity of CF derivatives. Structural variation as compared to the parent CF molecule are depicted in red or indicated with a red arrow. The table on the left shows changes in the A ring. The table in the middle illustrates changes in the B ring, while the right table illustrates the variations in ring C. CF (ABK-530) is highlighted in gray in the table on the right. Dr. Alexander Berger, and Talea Knak, University of Düsseldorf, Germany, have synthesized all derivatives. The heatmap shows a color code of the MIC_{90} values in µM, with active compounds shown in green, whereas inactive compounds are highlighted in red. The values were determined in triplicates.

3.1.2 The activity of chlorflavonin towards non-tuberculous mycobacteria

Given CF's known mode of action, that it inhibits AHAS activity [225], the question arose whether CF and BrF are active in various other mycobacteria. The results are illustrated in Figure 12, and corresponding MIC_{90} values are summarized in Table 7. It shows that not all mycobacteria are as sensitive as *M. tuberculosis* H37Rv to CF and BrF. At first, other slow-growing mycobacteria were analyzed. There was nearly the same dose-response curve progression for the virulent and attenuated *M. tuberculosis* strain. For the virulent H37Rv strain, it resulted in an MIC_{90} value of 1.56 µM for both substances, while higher activities were detectable for the attenuated $mc^{2}6230$ strain with an MIC_{90} of 0.39 µM. For *M. bovis BCG*

Pasteur, the dose-response profile was comparable with the one for *M. tuberculosis* H37Rv with just a little shift, resulting in an MIC_{90} of 3.13 µM for CF and BrF. Although *M. bovis BCG* Pasteur and *M. bovis BCG* Danish are closely related, both were tested to assess potential strain-dependent differences. As expected, *M. bovis* BCG Danish had comparable susceptibility resulting in an MIC_{90} of 3.13 µM for CF and 6.25 µM for BrF.

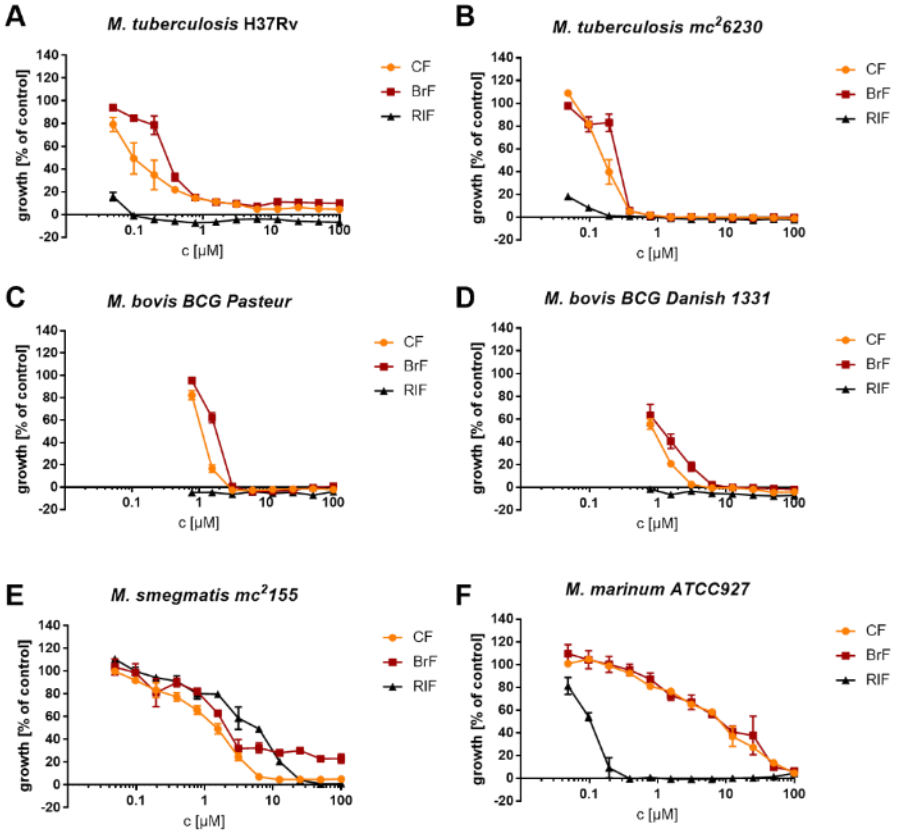

Figure 12: Activity of CF and BrF against various mycobacteria. Dose-response curve of CF, BrF, and RIF against **(A)** *M. tuberculosis* H37Rv, **(B)** *M. tuberculosis* mc²6230, **(C)** *M. bovis* BCG Pasteur, **(D)** *M. bovis* BCG Danish 1331, © *M. smegmatis* mc²155, and **(F)** *M. marinum* ATCC927. Data are shown as means of *n*=3 ±SEM.

Screens with *M. smegmatis* mc²155 (Figure 10E) and *M. marinum* ATCC927 (Figure 10F) were performed to evaluate the effect on fast-growing mycobacteria. In particular, *M. marinum* shows only minor growth inhibition for both compounds. However, it is evident that there is a concentration-dependent inhibition of growth, which results in an MIC_{90} of 100 µM. Only for *M. smegmatis* mc²155, a more significant difference between CF and BrF is detectable. For CF, the MIC_{90} value is comparable to all other mycobacteria with 6.25 µM, but BrF is inactive.

Table 7: Minimal inhibitory concentration of CF, BrF, and RIF against various mycobacterial species. CF, BrF, and RIF have been tested in microbroth dilution assays against various mycobacteria. All measurements were performed in triplicates.

	CF	BrF	RIF
M. tuberculosis H37Rv	1.56 µM	1.56 µM	0.09 µM
M. tuberculosis mc²6230	0.39 µM	0.39 µM	0.09 µM
M. bovis BCG Pasteur	3.13 µM	3.13 µM	≤0.05 µM
M. bovis BCG Danish	3.13 µM	6.25 µM	≤0.78 µM
M. marinum	100 µM	100 µM	0.19 µM
M. smegmatis	6.25 µM	>100 µM	25 µM

To gain further insight into the different activities against the mycobacteria, protein sequences of *M. tuberculosis* IlvB1 were analyzed using a BLAST procedure to identify orthologues between species [256]. Table S1 shows identical proteins in *M. bovis BCG, M. smegmatis,* and *M. marinum,* all with an identity of 100% compared to *M. tuberculosis*. That means the gene is present in all tested species, but it is unknown if the enzyme is expressed.

Summarizing the previous results, CF seems to inhibit all tested mycobacteria with the best activity in *M. tuberculosis* and *M. bovis* BCG Pasteur.

To further investigate the activity of CF and BrF, the substances were tested against various *M. tuberculosis* pre-XDR clinical isolates from KwaZulu-Natal (KZN), South Africa. These have developed resistance to INH, RIF, ethambutol (ETB), streptomycin (STREP), pyrazinamide, ethionamide, kanamycin, amikacin, capreomycin, and ofloxacin [137]. Figure 13 illustrates that CF and BrF are active against these pre-XDR-isolates with a loss of activity of just one or two dilution steps compared to the WT. That shows the relevance of these two compounds. The control antibiotics show the expected effect with all pre-XDR strains being resistant to RIF (MIC_{90} of >100 µM, Figure 13C) and still being sensitive to BDQ (MIC_{90} between 0.04 µM to 0.16 µM, Figure 13D).

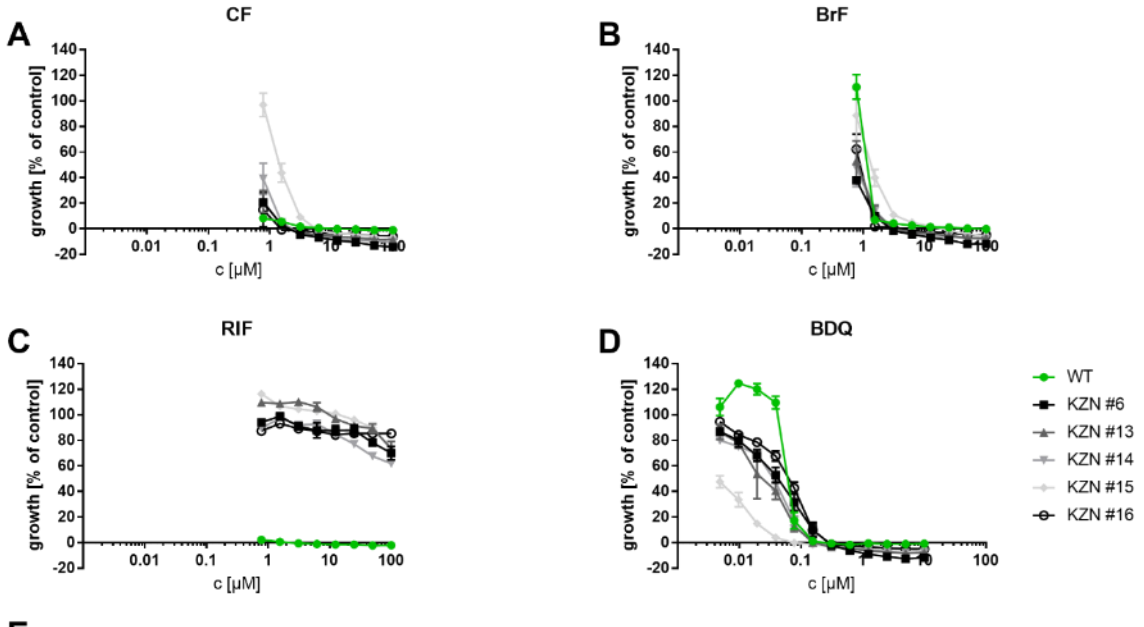

E

	CF	BrF	RIF	BDQ
	MIC_{90} [µM]			
H37Rv WT	0.78	1.56	0.78	0.16
KZN06	1.56	1.56	>100	0.16
KZN13	1.56	1.56	>100	0.16
KZN14	1.56	3.13	>100	0.16
KZN15	3.13	3.13	>100	0.04
KZN16	1.56	1.56	>100	0.16

Figure 13: Activity of CF and BrF against *M. tuberculosis* pre-XDR clinical isolates. Dose-response curves of several clinical isolates (KZN#6, KZN#13, KZN#14, KZN#15, KZN#16) in comparison to *M. tuberculosis* H37Rv WT, which were screened against **(A)** CF, **(B)** BrF, **(C)** RIF, and **(D)** BDQ. The resulting MIC_{90} values are given as micromolar concentrations summarized in table **(E)**. Data in **A**-**D** are shown as means of *n*=3 ±SEM.

3.1.3 Chlorflavonin and bromflavonin are not cytotoxic

To investigate the selectivity of CF and BrF, they were tested for potential cytotoxicity against different human cell lines. Figure 14 shows the results of the cytotoxicity analysis against the human fetal lung fibroblast cell line MRC-5, the monocytic cell line THP-1, and the embryonic kidney cell line HEK293. For THP-1 and MRC-5 cells, a weak concentration-dependent effect was evident, whereas no cytotoxic effect at all tested concentrations was measurable for HEK293 cells. Both compounds have an IC_{50} value between 100 µM and >100 µM. These results demonstrate that both compounds have almost no cytotoxic effect against various human cell lines originating from different tissues. Therefore, it is a promising indication that these compounds are unlikely to have strong side effects and harm the cells in the human

body. The selectivity index (SI) is used to get an overview of the therapeutic window of a substance, which is the quotient of the cytotoxicity and the antibacterial activity (IC_{50}/MIC_{90}). The result is shown in Figure 14D. Both compounds have a SI of 64, meaning there is a substantial therapeutic window, and it appears to be an excellent antibacterial compound.

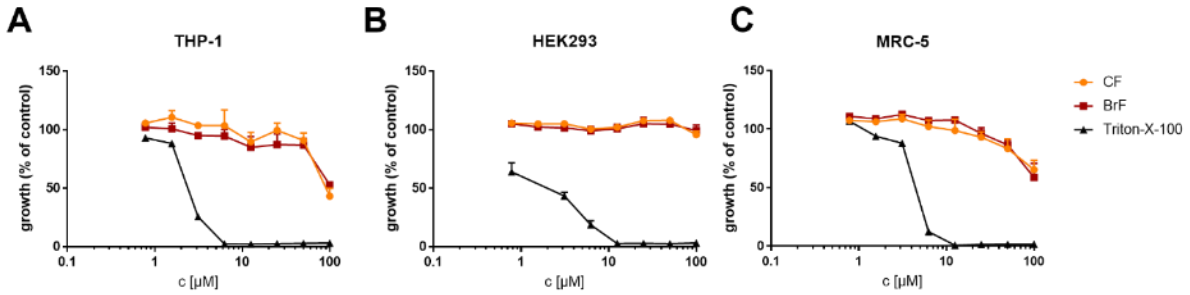

D

cell line	CF	BrF
THP1 (IC_{50})	100 µM	>100 µM
HEK293 (IC_{50})	>100 µM	>100 µM
MRC-5 (IC_{50})	100 µM	>100 µM
H37Rv (MIC_{90})	1.56 µM	1.56 µM
SI (IC_{50}/MIC_{90})	64	128

Figure 14: Cytotoxicity of CF and BrF. Dose-response curve of CF, BrF, and the positive control Triton-X-100 against the human cell lines **(A)** THP-1, **(B)** HEK293, and **(C)** MRC5. Data are shown as means of *n*=3 ±SEM. **(D)** Resulting MIC_{90} and IC_{50} values of CF and BrF screened against human cell lines and *M. tuberculosis* H37Rv. Values were determined in triplicates. The selectivity index (SI) was calculated as a ratio between IC_{50} and MIC_{90}.

3.1.4 Chlorflavonin derivatives can block the activity of IlvB1

The question remained unanswered as to why these minor structural deviations caused this drastic drop in activity, up to a complete loss in the tested range. To explore whether this loss is based on an internalization problem and the substances cannot enter the mycobacterial cell or on the inability to bind to the active site of IlvB1, an *in vitro* enzyme assay was performed. A C-terminal His-tagged IlvB1 protein was heterologously expressed in *E. coli* and purified using Ni-NTA agarose affinity chromatography. The result of the purification is shown in Figure S1. For further analysis, elution fractions E3 and E4 were pooled and chosen for further analyses. The AHAS assay was performed according to Choi *et al*. [233] as shown in Figure 15A (also see Chapters 2.9.5 and 3.1.5). For the assay, the educt of branched-chain amino acid biosynthesis, pyruvate, and the isolated enzyme IlvB1 were added to the reaction buffer and incubated at 37 °C. During this process, acetolactate is formed. By the addition of H_2SO_4, the reaction is stopped, and acetolactate gets carboxylated to acetoin. After adding creatine and α-naphthol, according to the method of Westerfeld, a red complex is formed with acetoin

[257]. To investigate whether this nonenzymatic complex formation is a linear process, the absorbance was measured in regular intervals for 45 min. Figure 15B demonstrates that this formation is not linear at any point, but looks more like a saturation curve. Since the negative control, in which no enzyme was present, also changed from yellow to a more brown color within that time, it was investigated whether the oxidation reaction that takes place during the time causes this curve progression. For that case, the negative control (background) was subtracted from the value obtained for the positive control. However, even in this case, the curve progression did not change; therefore, it cannot be attributed to the oxidation of α-naphthol. Without the addition of the substrate pyruvate, acetoin cannot be formed and thus no red complex can be created. In this case, the color change is linear, so the non-linear curve can only be associated with the formation of the red complex if acetoin is present. Next, the optimal wavelength was analyzed by detecting the absorbance between 400 nm and 700 nm every 5 nm after 30 min of red complex formation. The result is shown in Figure 15C. The most significant difference between the positive and negative control is at 525 nm. Due to technical limitation during detection, the red complex was measured at the wavelength of 492 nm, because some wells exceeded the detection limit after 45 minutes of complex formation. A wavelength of 492 nm was used during previous experiments with satisfying results. To decipher whether the concentration of pyruvate was appropriate for this assay, a Michaelis-Menten kinetic was measured. Following the standard protocol for Michaelis-Menten kinetics, pyruvate was added in different concentrations to the reaction. The result is shown in Figure 15D. It demonstrates that with all tested pyruvate concentrations, the absorbance (i.e., the acetoin concentration) increased linearly, meaning that no limitation occurred under these conditions. Based on this result, the assay was performed as previously described for further analysis.

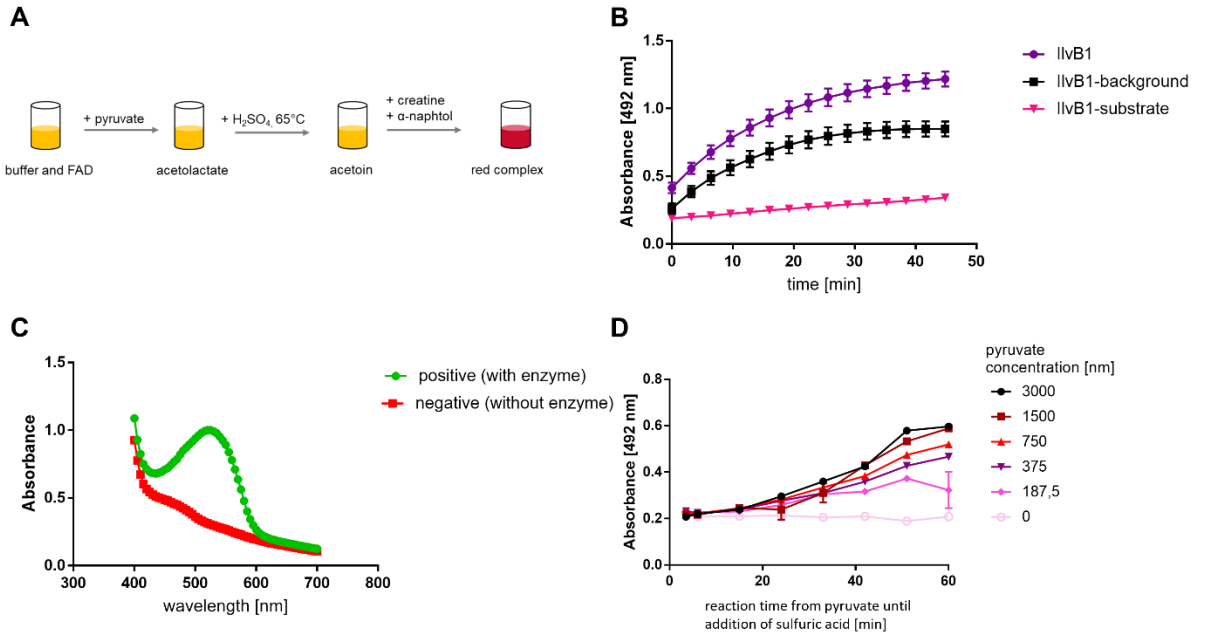

Figure 15: AHAS assay – general procedure and optimization. (A) Cartoon of the general procedure of the AHAS assay showing the educts, intermediates, and products. All experiments were performed according to Choi *et al*. [233] using pyruvate as substrate. **(B)** Comparison of absorbance of the uninhibited wells and these wells subtracted with the negative control. As a reference, the absorbance was measured without the addition of the substrate pyruvate. **(C)** Wavelength screening of the positive and negative control to determine the optimal wavelength for this assay. **(D)** Michaelis-Menten kinetics of IlvB1 and pyruvate using the AHAS assay. The time specification refers to the duration of the enzymatic reaction before the addition of sulfuric acid. Data are shown as means of at least *n*=3 ±SEM.

Next, these assay conditions were used to determine whether other CF derivatives could inhibit the enzyme activity of IlvB1 of the isolated protein *in vitro*. Initially, CF and BrF were tested. They showed a concentration-dependent inactivation of the enzyme activity for both derivatives with a similar effect. The comparison of the purchased natural CF (Sigma) and the one provided by RG Kurz did not show any differences, so further work was carried out only with the synthetically produced CF from RG Kurz. Next, the CF derivative library was tested with four different concentrations (100 µM, 10 µM, 1 µM, and 0.1 µM) to evaluate their potential to inactivate the enzymatic activity of IlvB1. The result of some derivatives is shown in Figure 16C-E. A heat map was created, in which the derivatives were categorized into four groups with respect to the level of their inhibitory effects (Figure 17).

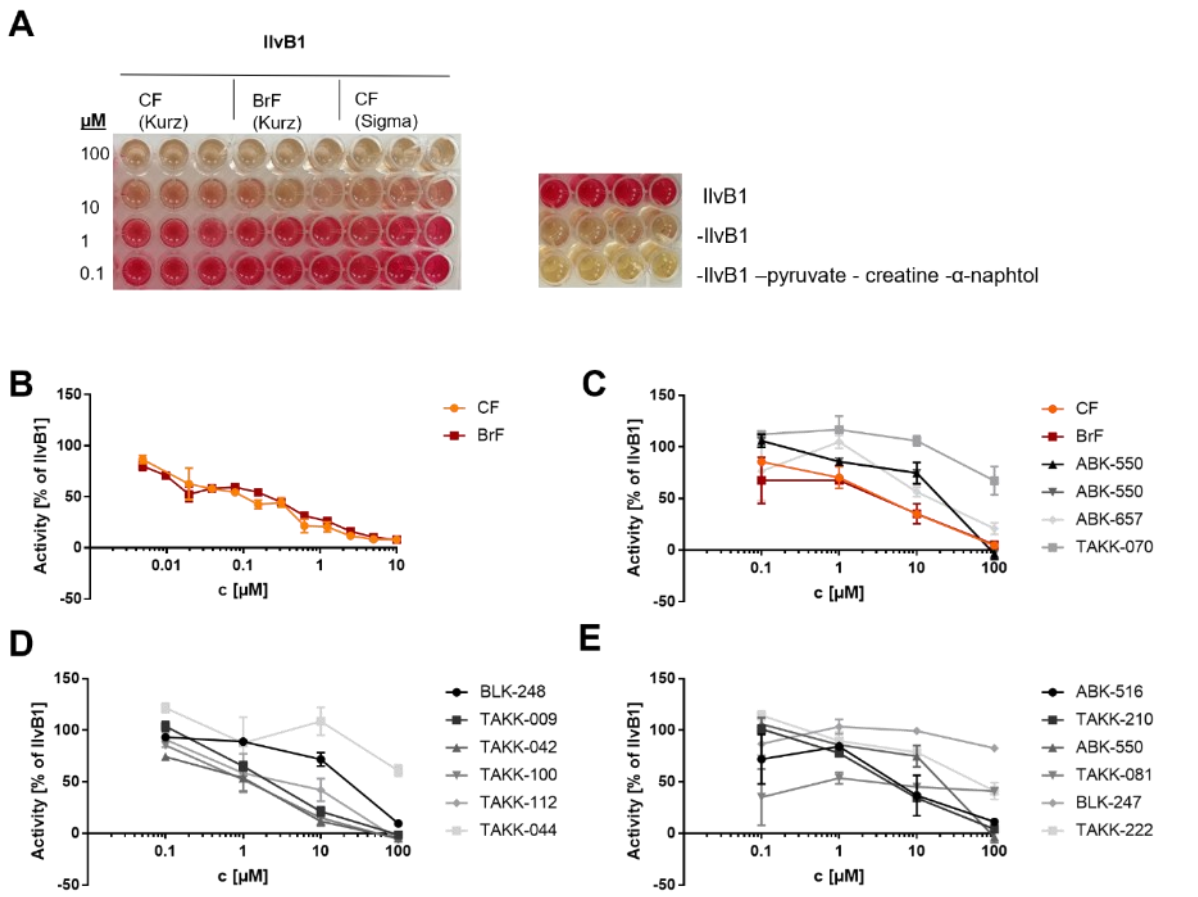

Figure 16: Activity assay with recombinant IlvB1. (A, B) Inhibition of the IlvB1 enzyme activity by different concentrations of CF and BrF. All experiments were performed according to Choi *et al.* [233] using reaction buffer and pyruvate as a substrate. **(A)** The activity of IlvB1 could be detected by the formation of a red complex and **(B)** measured by a microplate reader at an absorbance of 492 nm. **(B-E)** Activities were calculated as activity compared to uninhibited IlvB1**.** Data are shown as means of at least *n*=3 ±SEM.

Several substances allowed variation in different positions without a detectable significant change in the inhibition of IlvB1. In the B-ring at the fifth position, the brominated (ABK-541) and the fluorinated (ABK-550) forms were as active as the chlorinated (ABK-530) form. The trifluoromethyl group resulted in only a slight increase in IlvB1 activity at this position (ABK-657). A molecule, which harbors the chloride ion at the fourth position instead of the fifth (ABK-644), showed similar inhibitory activity. Further additions at the third position, for example, a methyl group (TAKK-070), prevent the inhibition of IlvB1 and show nearly no difference in IlvB1 activity compared to the DMSO control. In the C-ring, the substitution of the methoxy group at the third position with an ethoxy group either in the chlorinated (TAKK-009) or the brominated (TAKK-042) form had a comparable inhibitory effect compared to CF. Even the substitution of a hydroxy group with an ethoxy group did not lead to a substantial change in the activity (TAKK-100). Furthermore, substituting the dimethylamino group for an ethoxy group (TAKK-112) had

no significant influence. Only the complete removal of the methoxy group hampered blockade of IlvB1 enzyme activity (BLK-248). That could mean that the methoxy group or a structurally similar group at this position is needed to bind to the enzyme at the active site. One example of a completely inactive derivative is TAKK-044. In this case, the methoxy group is exchanged against an isopropoxy group. This example shows that there is a rigid structural requirement for this position. The A-ring has narrow structural requirements. There is a small number of substances that showed any inhibition of IlvB1. The only accepted change was replacing the hydroxy group at the fifth position with an amino group (TAKK-210). This group or the hydroxy group is needed in this position because the absence of any moiety in the chlorinated form (ABK-516) or the brominated form (TAKK-081) led to a weaker inhibition of IlvB1. Also, a methoxy group instead of the hydroxy group was not accepted for inhibiting IlvB1 (BLK-247), and also a more significant variation, e.g., an acetamide at this position, resulted in a reduction of activity (TAKK-222). Furthermore, the presence of one methoxy group each at the seventh and eighth position was needed for the inhibition (TAKK-123).

In summary, this experiment demonstrates that numerous derivatives can inhibit the enzyme IlvB1, thereby preventing the synthesis of acetoin in the assay and likely capable of impeding the production of branched-chain amino acids in the cell. However, these results do not match the *M. tuberculosis* MIC assay. There are only a few derivatives active against cells of *M. tuberculosis*. These findings raise the question of why there is such a big difference. The likely main explanation is that the substances have a poor internalization rate and cannot reach and inhibit the *M. tuberculosis* IlvB1 enzyme. Some experiments, shown in the next chapters, were performed to answer this question.

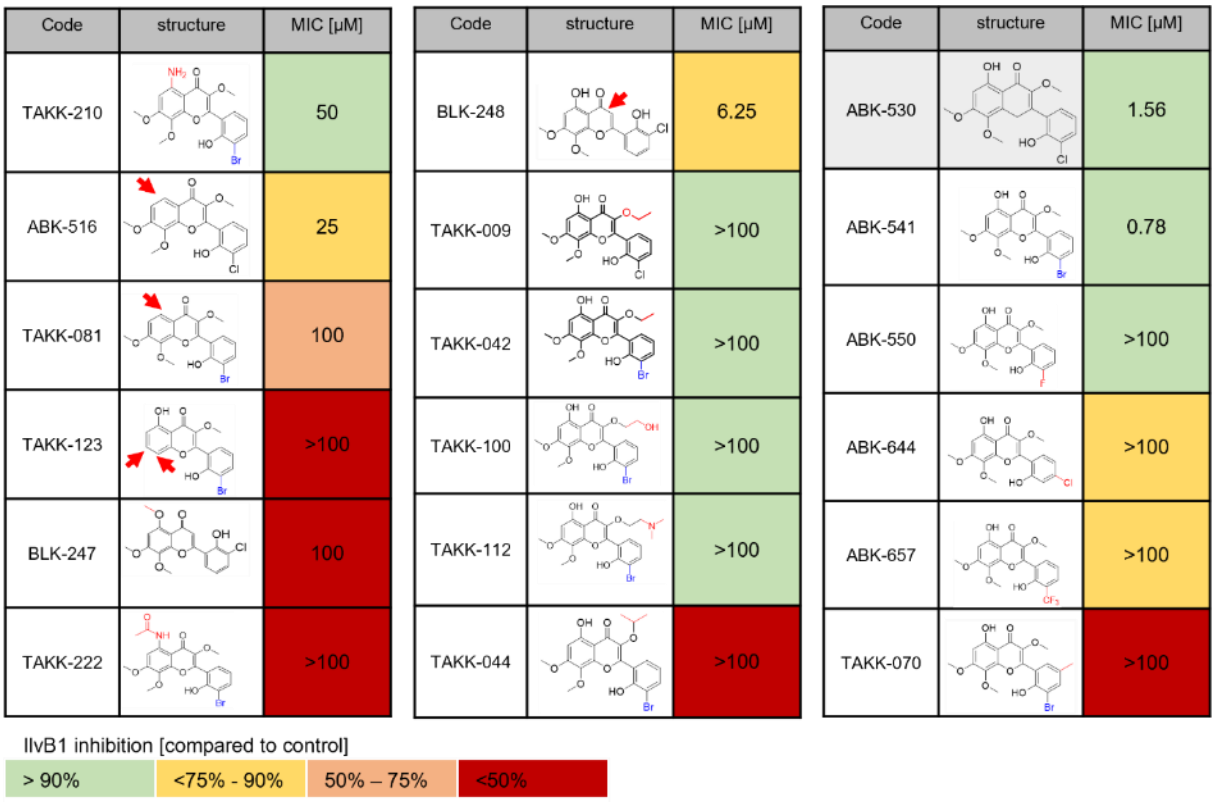

Figure 17: Inhibition of IlvB1 by various CF and BrF derivatives. Inhibition of the IlvB1 enzyme activity by different concentrations (100 µM, 10 µM, 1 µM, 0.1 µM) of CF derivatives. The main variation in the structure compared to the parent CF is highlighted in red, or indicated by an arrow if a substituent has been removed at this position. The shown derivatives have been divided into four groups. On the one hand, there is the green group. These are the substances that inactivate IlvB1 by more than 90% compared to the control. The second group has an inactivation between 75% and 90%, shown in yellow. This is followed by the derivatives with an inactivation between 75% and 50%, shown in orange. All others are highlighted in red. In addition, the MIC_{90} value (in µM) against *M. tuberculosis* cells obtained by the MIC assay is shown by the numbers to allow comparison of *in vitro* and whole-cell activity of compounds. Experiments have been performed in triplicates.

3.1.5 IlvN inhibits the IvB1 enzyme activity

Since IlvB1 and IlvN operate together, the question arose whether and to what extent IlvN regulates IlvB1. Therefore, both proteins were recombinantly expressed and purified as described above and shown in Figure S3. Next, AHAS activity of IlvB1 alone or in combination with IlvN was determined. Both were mixed in an equimolar ratio. Figure 18A shows that the activity of IlvB1 alone is much stronger than in combination with IlvN. That means that IlvN appears to be a negative regulator of IlvB1.

In contrast, as expected, the regulatory subunit IlvN alone has no AHAS activity at all. In this context, the inhibitory effect of CF is shown in Figure 18B. Since IlvN alone has no AHAS activity, it was excluded from this experiment. CF can block the AHAS activity of IlvB1 alone, as shown in the previous chapter, but also, in combination with IlvN, the AHAS activity is reduced. The reduction is, in both cases, concentration-dependent. This observation corroborates that CF directly interacts with the catalytic subunit IlvB1 and demonstrates that

the regulatory subunit IlvN under the tested conditions is not significantly altering the interaction between CF and its target structure IlvB1.

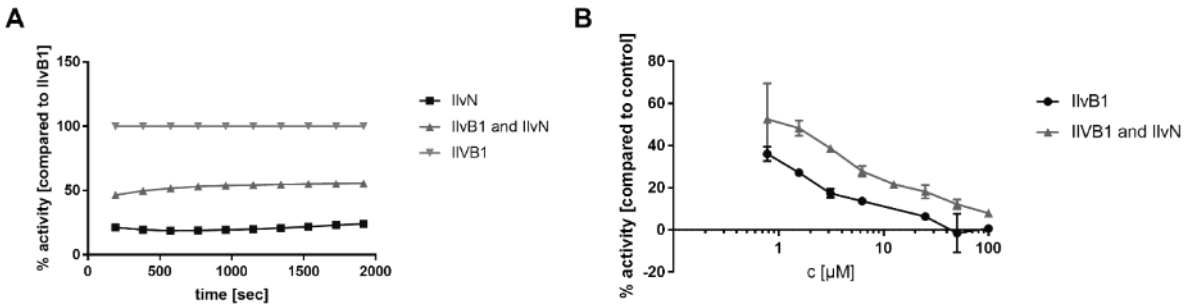

Figure 18: Activity assay of recombinant IlvB1 and IlvN. (A) shows the *in vitro a*ctivity of IlvB1, IlvN, and the combination of both in a equimolar ratio compared to the activity of IlvB1 (100%) itself over time. According to *Choi et al.* [233], all experiments used the reaction buffer and pyruvate as a substrate. The activity could be detected by the formation of a red complex and measured by a microplate reader at an absorbance of 492 nm. **(B)** illustrates activities of IlvB1 and the combination of IlvB1 and IlvN in the presence of different concentrations of CF. Data are shown as means of *n*=3 ±SEM.

3.1.6 Some chlorflavonin derivatives have activity against other mycobacteria

To investigate if some CF analogues have activity against other mycobacteria, they were tested against *M. smegmatis, M. bovis* BCG Danish*,* and *M. bovis* BCG Pasteur*.* In the first step, all derivatives were examined in a MIC assay at a single concentration of 100 µM, followed by a serial dilution MIC assay of all active compounds. To evaluate the effect of the compounds on fast-growing mycobacteria, a screening against *M. smegmatis* was performed. However, no activity of any compound was detected except for CF. Also, the three compounds active in *M. tuberculosis* (ABK-541, ABK-516, and TAKK-210, Figure 11 and Table 8) exert no activity in *M. smegmatis.* According to the BLAST search, IlvB1 is present and highly conserved in all tested mycobacteria. This difference in activity compared to *M. tuberculosis* should have another reason. One explanation could be that *M. smegmatis* has a different cell wall structure compared to *M. tuberculosis,* and thus the substances may not be internalized.

To evaluate if *M. bovis* is more susceptible to the derivatives, they were tested against *M. bovis* BCG Danish *and M. bovis* BCG Pasteur since minor differences were already present for BrF (see chapter 3.1.2). *M. bovis* BCG Pasteur was slightly more sensitive to some derivatives, such as TAKK-009 and TAKK-112.

Table 8: MIC_{90} values of CF derivatives against different mycobacteria. The table illustrates the activity of different CF derivatives against *M. tuberculosis* H37Rv, *M. smegmatis* mc²155, *M. bovis* BCG Pasteur, and *M. bovis* BCG Danish 1331. The red highlighted areas in the molecule represent the structural variation to CF, or if the substituent has been deleted it is indicated by an arrow. The exchange of chlorine against bromide is highlighted in blue. All MIC_{90} values are shown in µM and determined in triplicates.

	Code	ABK-530	ABK-541	ABK-516	ABK-550	TAKK-009	TAKK-100	TAKK-112	TAKK-210
MIC_{90} [µM]	Structure	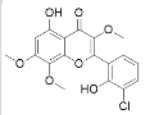	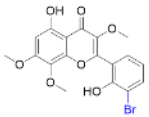	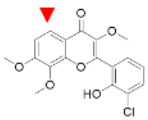	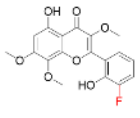	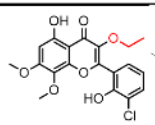	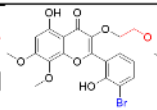	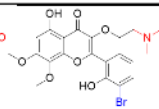	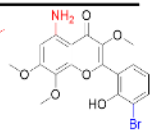
	M. tuberculosis H37Rv	1.56	0.78	25	>100	>100	>100	>100	50
	M. smegmatis mc²155	6.25	>100	>100	>100	>100	>100	>100	>100
	M. bovis BCG Pasteur	3.125	3.125	100	>100	50	100	50	100
	M. bovis BCG Danish 1331	3.125	6.25	50	12.5	50	50	100	100

Interestingly, there were different activities for *M. bovis* BCG Danish. Some derivatives had a concentration-dependent effect. The most active compounds were still CF and BrF, but there was also one compound with an MIC_{90} of 12.5 µM (ABK-550) and three with an MIC_{90} of 50 µM (ABK-516, TAKK-009, and TAKK-100). There is a high homology in the vaccination strains *M. bovis* BCG Danish and *M. bovis* BCG Pasteur [258]. That raises the question of why the antibacterial activity differs between these closely related strains. However, this question was not further pursued within the context of this dissertation.

3.1.7 Chlorflavonin is stable in mycobacterial cells

In addition to a poor penetration rate across the mycobacterial cell wall, the lack of cellular activity of some compounds could also be related by rapid metabolization by mycobacterial cells. To address this possibility, a CF-stability assay was performed to investigate the reduction of the activity of some derivatives, even if there is only a tiny structural variation compared to CF. For this purpose, the lead structure CF and one inactive compound were each added to an actively growing *M. tuberculosis* culture and incubated for up to 8 days. TAKK-009 was chosen as an inactive substance because it is one of the least modified substances with an ethoxy group instead of a methoxy group at position 3 in the C-ring. Furthermore, it is still active in the *in vitro* enzyme assay. These properties imply that the inactivity of this substance is probably caused by *M. tuberculosis*. To assess whether the substance might be subject of cleavage or conversion, samples of compound-treated cells were collected after different time points and prepared for measurement in a Dionex- High-Pressure Liquid Chromatography (HPLC) system (Figure 19).

The first samples were collected directly after the addition of the compounds (t_0). As a blank, a methanol control was initially measured. No significant peaks were measured, meaning the methanol was pure and the machine clean and operational. In the medium control, which means medium without any cells and compounds, some small peaks were detectable at a wavelength of 235 nm, which may have occurred through the medium's ingredients (Figure S5). Another control was inoculated medium just containing DMSO as a solvent control. Also, in this case, only some tiny peaks were measured, which might have occurred through the medium and the cells. For the subsequent time points, these controls have always been made and prepared in parallel to all other compound-treated samples and are shown in the supplementary Figure S5. They do not show strongly pronounced peaks, thus, no measurable contamination occurred during incubation and processing. Figure 19 and Figure 20 display the result of the experiment. The complete

graphs at 235 nm and 340 nm can be seen in Figure S6 and Figure S7. Immediately after adding the substances (t_o), a prominent peak (retention time: 28.033 minutes for CF and 29.450 minutes for TAKK-009) was found in the medium control and the cell suspension for both substances. In each case, a higher peak was detected in the medium control compared to the cell suspension. These peaks matched not completely the data of the CF calibration of the pure substances with a retention time of 28.297 minutes (Figure S4), but were perfectly congruent to the data of the extraction in the cell-free samples at t_0. Thus, CF and TAKK-009 could be detected well in the solution with this method after processing. After 8 days of incubation, there was only a minor change in the medium control for CF and TAKK-009. Both can be found in the medium control, although the peaks were not as high as they were at the beginning. This decreased peak height may be due to the purification process, and incipient degradation, which could begin in the medium at 37 °C. With this possibility of degradation, however, at least a second peak would be expected, but this was not seen here. It is therefore possible that CF is directly degraded into small fragments that are not detectable with this method, or that these have been lost during processing. When the two compounds were each incubated with *M. tuberculosis* for 8 days, the peaks also become smaller, but in this case, more than it was for the medium control. For both substances, another peak began to form, which eluted just before the main peak. That could be a degradation product or an altered form of each substance.

These results indicate that *M. tuberculosis* could have a slow working mechanism, which degrades CF and TAKK-009. However, this is too slow to prevent the effect of CF, which is also supported by the results of killing kinetics [225].

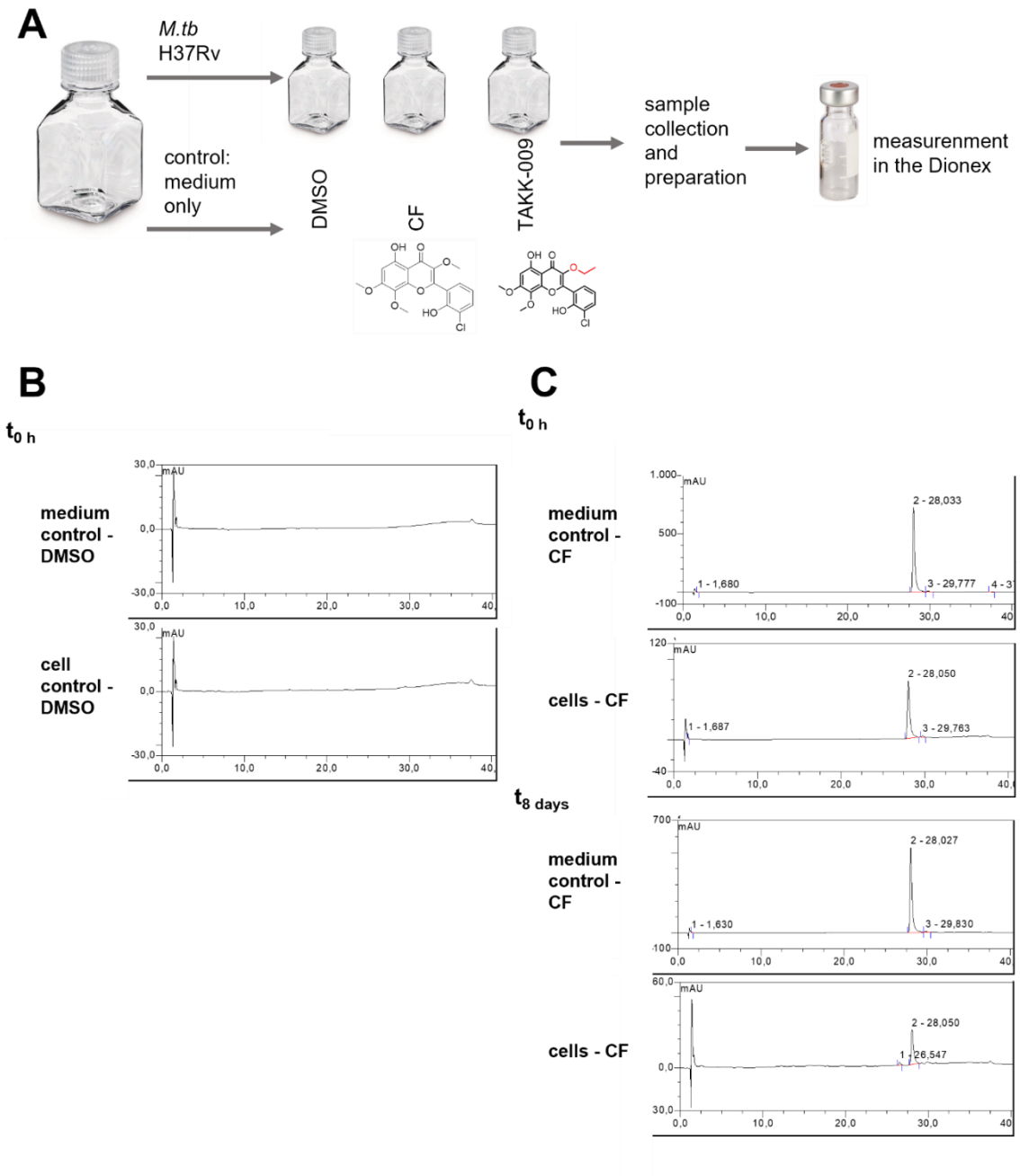

Figure 19: CF stability assay. (A) shows the schematic illustration of the assay with the basic steps. CF and TAKK-009 were incubated with *M. tuberculosis* H37Rv or medium only for several days, and samples were taken at different time points and analyzed using a HPLC with diode array detector (DAD) (Dionex). **(B-C)** shows the result of the screening, which was measured with the Dionex-HPLC at 340 nm. In **(B)** are the control samples, the medium control, and the cell control, which were incubated with DMSO. **(C)** demonstrates the result of the CF-treated medium and cell suspension directly and 8 days after adding the compounds. The signal intensity is displayed as mAU on the Y axis towards the retention time on the X axis.

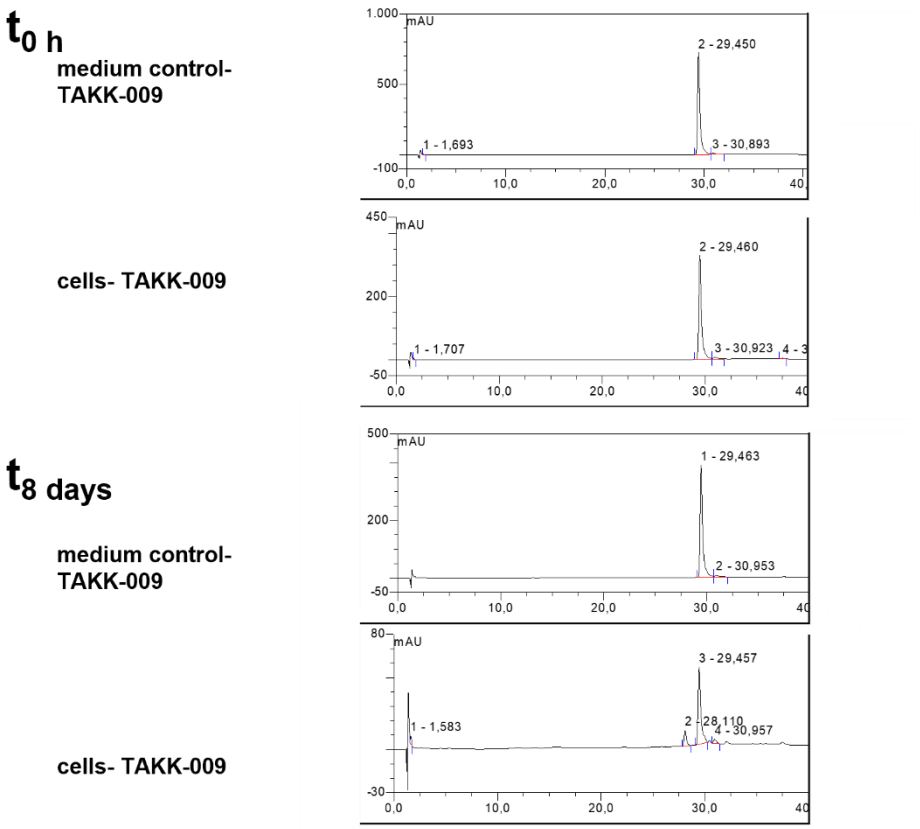

Figure 20: TAKK-009 stability assay. The result of the screening was measured with a HPLC with DAD (Dionex) at 340 nm. It shows the result of the TAKK-009-treated cell suspension and medium control at t_0 and 8 days after the addition of the compound. The signal intensity is displayed as mAU on the Y axis towards the retention time on the X axis.

3.2 KSKs – alkoxyamide-based molecules with anti-tuberculosis activity

As described in the introduction in chapter 1.4.2, KSK-104 and KSK-106 are substances with high anti-tuberculosis activity. The analysis of SRM revealed mutations in two amidohydrolases that confer resistance towards KSKs leading to the hypothesis that KSKs are prodrugs that need to be enzymatically hydrolyzed to their active form [240]. However, the exact mechanism of action, the target, and the activated structures formed by the amidohydrolases are unknown. Further analysis of these aspects will be described in this chapter.

3.2.1 Structure-Activity Relationship of the KSK derivatives

A broad-ranging structure-activity relationship analysis of over 200 derivatives was performed together with Dr. Lasse van Geelen. Here, only a small fraction is shown, but in the PhD theses of Dr. Alexander Berger and Dr. Oliver Michel, the totality of molecules is shown [253]. Some other selected derivatives will be presented in this thesis to address specific questions. The KSKs were tested in an MIC assay to obtain initial comparative values. KSK-104 showed a concentration-dependent activity resulting in an MIC_{90} of 0.78 µM. KSK-106, on the other hand, was slightly more active with an MIC_{90} of 0.39 µM (Figure 21).

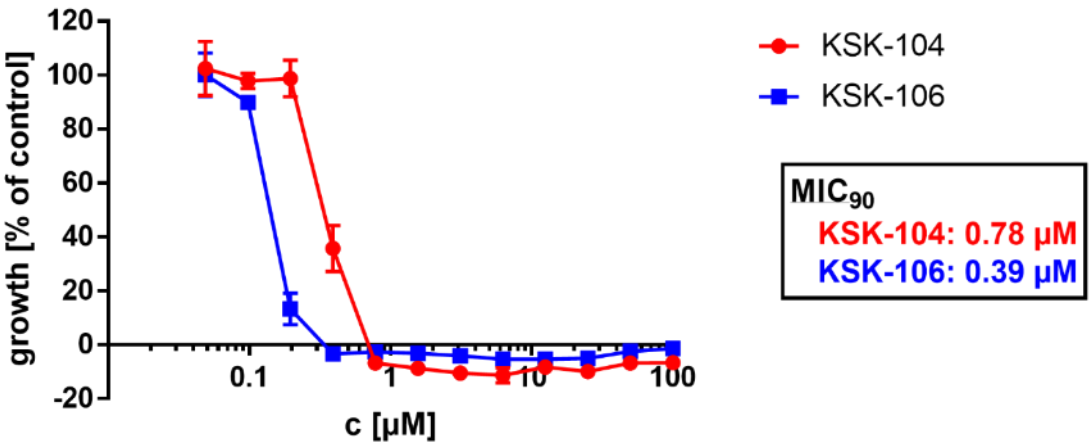

Figure 21: Activity of KSK-104 and KSK-106 against *M. tuberculosis* H37Rv. Dose-response curve of the KSKs and the resulting MIC_{90} values are illustrated. Data are shown as means of *n*=3 ±SEM.

The tested derivatives have been divided into three groups according to changes in regions A, B, or C (Figure 8). For changes in the left region, there are many examples of substances that did not lead to a substantial deterioration in activity against

M. tuberculosis (Figure 22). The KSK-104 and KSK-106 themselves also differ only in that region. KSK-104 has a *para*-substituted biphenyl moiety, whereas KSK-106 has a phenyl moiety substituted with a phenyl ether in *para*-position. Further examples of changes in region A are the exchange of the ether structure against a thioether (ABK-335) or the introduction of a terminal alkyne at the pentyl ether (OMK-077). More significant changes, such as the exchange of a benzyl ring for a pyrazine ring (ABK-334), were also relatively well tolerated and led to an MIC_{90} of 0.78 µM. The ether group in region A was of limited importance for activity, as omission led to only a slight decrease of activity to an MIC_{90} of 3.13 µM (ABK-201). A more profound negative impact on activity had the complete omission or exchange of the phenyl ring or the pentyl ether to an alkyne (ABK-380; MIC_{90}: 12.5 µM). Another example of an almost complete loss of activity is the exchange of the phenyl moiety (KSK-104 derivative) against naphthalene (KSK-118).

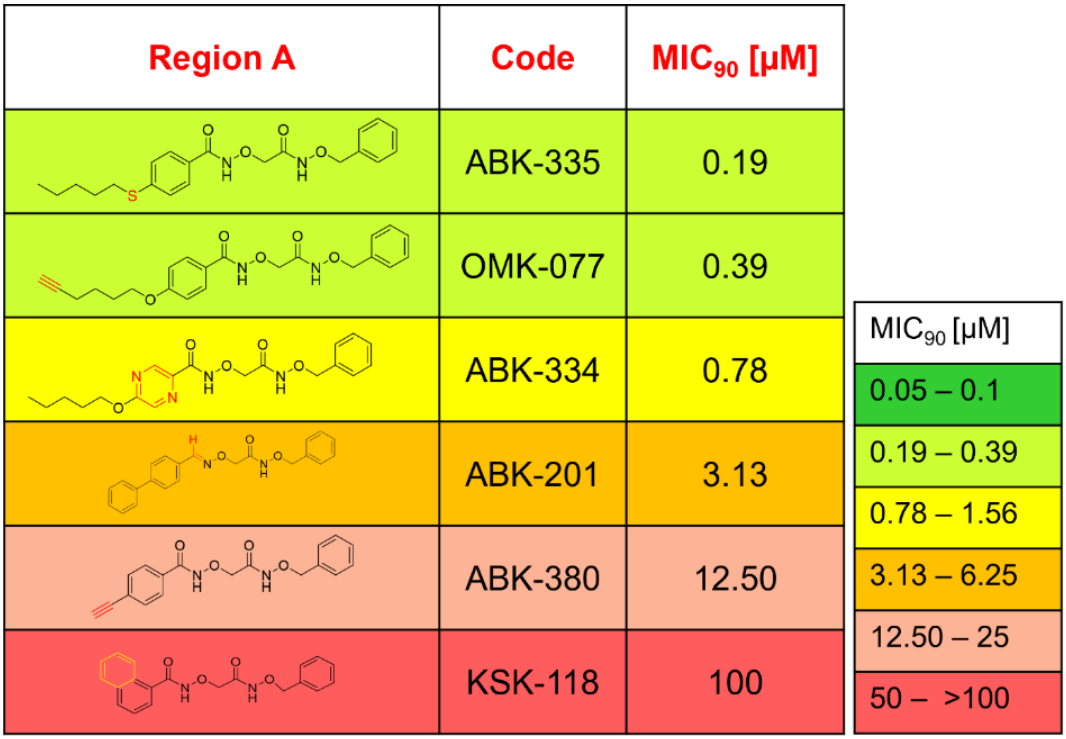

Figure 22: Heatmap representing MIC_{90} values of different KSK derivatives modified in region A. The red, or yellow highlighted areas in the molecule represent the structural variation of the KSKs. The table shows the MIC_{90} values. Dr. Alexander Berger, or Dr. Oliver Michel, University of Düsseldorf, Germany, have synthesized all derivatives. The heatmap shows a color code of the MIC_{90} values (in µM) determined in triplicates.

It should be emphasized that an increase in the number of C atoms in the ether side chain led to a deterioration of the activity (Figure 25). One carbon more led already to a decreased activity to a value of 1.56 µM. This remained up to an extension of three carbon atoms. With an extension of four, the MIC_{90} increased to 3.13 µM. This shows that the optimal chain length is as for KSK-106 with a phenyl unit. This analysis of region

A has shown that a wide variety of changes can be made with tolerable activities. Some derivatives with changes in region A have the same or slightly improved activity (OMK-077, ABK-335) but none with a substantial increase in activity compared to KSK-104 and KSK-106. The core region B, which consists of an alkoxyamide structure, represents the central group. Even small changes in that region led to a drastic reduction in activity (Figure 23). Examples are ABK-275 and ABK-130, in which only one methyl group has been added at different positions. A more dramatic decrease in activity occured when the two oxygen atoms attached to each amide group are omitted (BLK-106). These substances have no activity at all against *M. tuberculosis* in all tested concentrations. The same is true if the core structure consists of only one alkoxyamide group; thus, the entire core structure has been halved (OMK-199).

Region B	Code	MIC_{90} [µM]
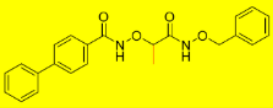	ABK-275	1.56
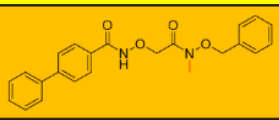	ABK-130	3.13
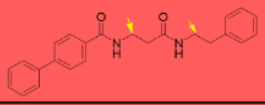	BLK-106	>100
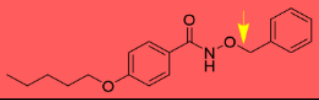	OMK-199	100
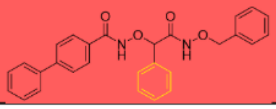	ABK-274	100

MIC_{90} [µM]
0.05 – 0.1
0.19 – 0.39
0.78 – 1.56
3.13 – 6.25
12.50 – 25
50 – >100

Figure 23: Heatmap representing MIC_{90} values of different KSK derivatives modified in region B. The red, or yellow highlighted areas in the molecule represent the structural variation, or if the substituent has been deleted it is indicated by an arrow. The table shows the MIC_{90} values. Dr. Alexander Berger, or Dr. Oliver Michel, University of Düsseldorf, Germany, have synthesized all derivatives. The heatmap shows a color code of the MIC_{90} values in µM, determined in triplicates.

Since the methyl group negatively influenced the activity (ABK-275), it is hardly surprising that a phenyl substitution at this position also led to a loss of activity, as can be seen for ABK-274. This shows that region B is essential for the activity of the KSKs, with almost no changes allowed to maintain strong activity. The KSKs are carrying a benzyl moiety in region C. The MIC_{90} remained unaltered if this group is replaced by a tetrahydropyranyl group (OMK-240) or a thiophene group (ABK-308), as shown in Figure 24. An alkyne, on the other hand, led to a marginal change in activity (ABK-267). On the contrary, the

conjugation of isoniazid to the KSK backbone harms the activity, resulting in an MIC_{90} of 50 µM (OMK-283). It was used because it has already been shown in previous publications that a hybrid of isoniazid and aminoxyacetic acid has high activity [239].

Region C	Code	MIC_{90} [µM]
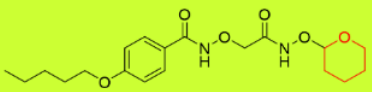	OMK-240	0.19
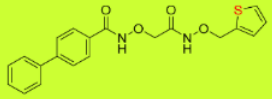	ABK-308	0.19
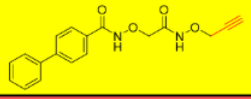	ABK-267	0.78
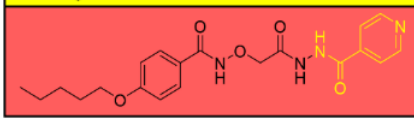	OMK-283	50

MIC_{90} [µM]
0.05 – 0.1
0.19 – 0.39
0.78 – 1.56
3.13 – 6.25
12.50 – 25
50 – >100

Figure 24: Heatmap representing MIC_{90} values of different KSK derivatives modified in region C. The red, or yellow highlighted areas in the molecule represent the structural variation. The table shows the MIC_{90} values in µM of the compounds that have been synthesized by Dr. Alexander Berger, or Dr. Oliver Michel, University of Düsseldorf, Germany. The heatmap shows a color code of the MIC_{90} values (in µM) determined in triplicates.

This analysis and the screening of the other derivatives revealed a compulsory structural requirement for core region B. In contrast, regions A and C are more tolerant of changes. Of particular note are the four derivatives shown in Figure 25A. These molecules have a much more potent activity than the parental KSKs. Here, OMK-76 and OMK-175 are examples with a phenylamide moiety in region C. As a result, the developed group becomes more labile and can be hydrolytically released more easily [259]. A fluoride is also attached to the benzyl ring in *ortho* (OMK-76) or *meta* (OMK-175) positions. Both molecules have an activity of 0.048 µM, which makes them remarkably potent and promising antitubercular lead structures considering their nanomolar cellular activity. OMK-366 is a KSK-106 derived derivative with a pentylester in region B. In summary, when analyzing the structure-activity relationship of region B, it becomes evident that alterations in this specific area are feasible but contingent upon complementary modifications in regions A or C. This is exemplified by OMK-366, which exhibits an activity of 0.048 µM. The activity also increases if region C is exchanged for a hexyloxy group (OMK-355).

A

C-Region	Code	MIC_{90} [µM]
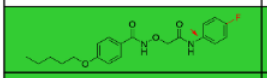	OMK-76	0.048
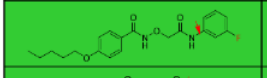	OMK-175	0.048
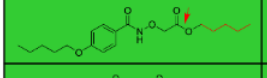	OMK-366	0.048
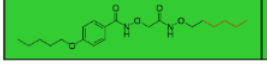	OMK-355	0.048

B

A-Region	Code	MIC_{90} [µM]
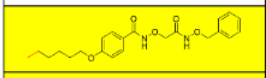	OMK-60	1.56
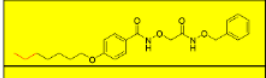	OMK-61	1.56
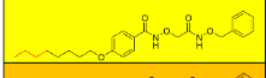	OMK-62	1.56
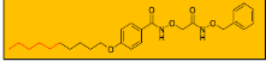	OMK-67	3.13

MIC_{90} [µM]
0.05 – 0.1
0.19 – 0.39
0.78 – 1.56
3.13 – 6.25
12.50 – 25
50 – >100

Figure 25: Heatmap representing MIC_{90} values of different highly-active KSK derivatives. Structure activity relationship of KSK derivatives. The red highlighted areas in the molecule represent the structural variation. If a substituent has been removed compared to the parent KSK compound, the corresponding position is indicated by an arrow. **(A)** represents derivatives with a higher activity than the KSKs, or **(B)** variations in region A with a gradual extension of the carbon chain. The table shows MIC_{90} values. Dr. Alexander Berger, or Dr. Oliver Michel, University of Düsseldorf, Germany, have synthesized all derivatives. The heatmap shows a color code of the MIC_{90} values in µM, determined in triplicates.

3.2.1.1 OMK-175 as a potential new lead structure

In the SAR screening, OMK-175 was particularly highlighted for its better activity than the parental KSKs (Figure 26A). Based on this, some experiments have been conducted to analyze whether this substance could offer itself as a potential new lead structure for further investigations. For this purpose, OMK-175 was first tested against different mycobacteria compared to the KSKs. A substantial activity could be seen especially against *M. bovis* BCG Danish with a MIC_{90} of ≤0.048 µM, while the potency against *M. bovis* BGG Pasteur was slightly lower with an MIC_{90} of 0.19 µM. Against *M. marinum,* there was hardly any activity with 50 µM, and against *M. smegmatis* no activity at all was observed in the tested concentration range. It should also be emphasized that OMK-175 had no cytotoxicity against the cell line THP-1 in the tested range. Thus, the compound with its potent antitubercular activity (MIC_{90} against *M. tuberculosis* H37Rv of 0.048 µM) and no cytotoxicity (IC_{50} >100 µM) exhibits a huge therapeutic window with a selectivity index of >2083 for *M. tuberculosis* H37Rv.

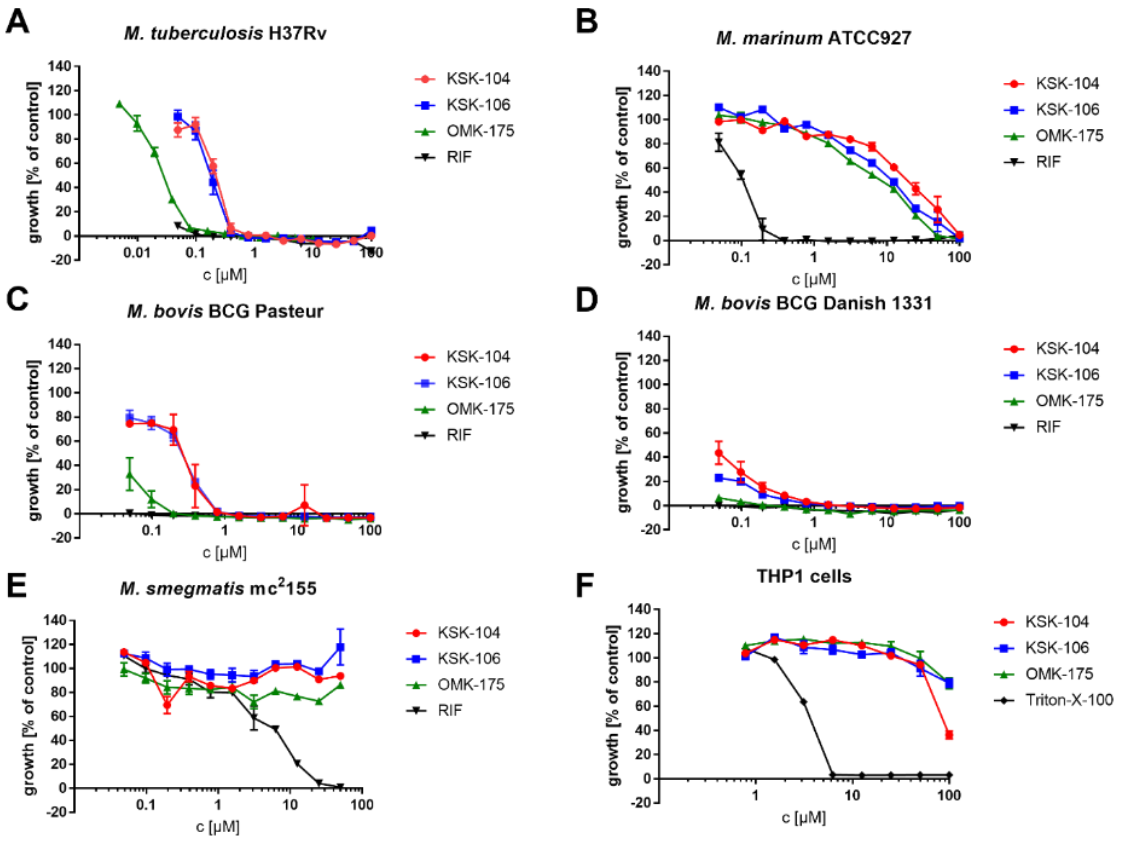

Figure 26: Selectivity of the KSKs and OMK-175. Dose-response curves of the KSKs and OMK-175 screened against different mycobacteria: **(A)** *M. tuberculosis* H37Rv, **(B)** *M. marinum*, **(C)** *M. bovis* BCG Pasteur, **(D)** *M. bovis* BCG Danish, © *M. smegmatis*, and **(F)** the human cell line THP-1. Data are shown as means of *n*=3 ±SEM.

In addition, the compound showed good activity against clinical pre-XDR isolates with MIC_{90} values ranging from 0.078 µM to 0.625 µM (Figure 27). These values represent very high activities indicating a new mechanism of action because of the acquired resistances of the pre-XDR isolates. In the case the clinical pre-XDR isolates were resistant towards OMK-175, one could conclude that the resistance mechanism was similar or the same as one of those against the ten antibiotics to which the pre-XDR isolates (see above) are resistant. However, lack of resistance suggests that the mode-of-action of OMK-175 substantially differs from clinical antitubercular drugs, corroborating the relevance of this new substance.

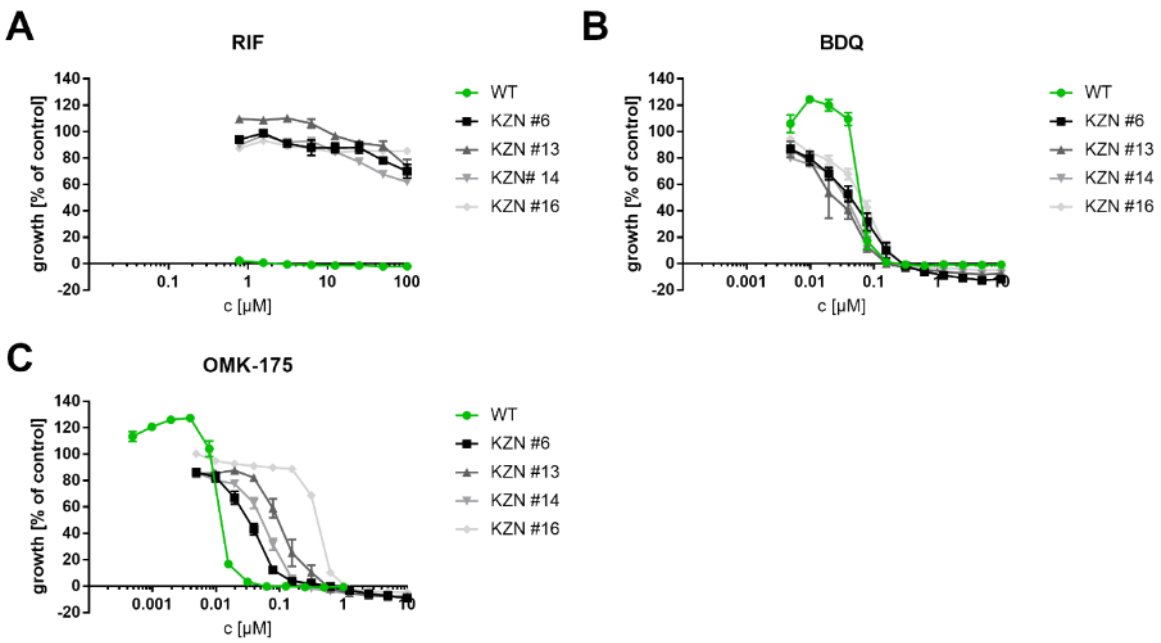

Figure 27: Activity of OMK-175 against *M. tuberculosis* pre-XDR clinical isolates. Dose-response curve of **(A)** RIF, **(B)** BDQ, and **(C)** OMK-175 against several clinical isolates (KZN#6, KZN#13, KZN#14, and KZN#16) in comparison to H37Rv WT. Data are shown as means of *n*=3 ±SEM.

To obtain more detailed information on the mechanism of action, SRMs to OMK-175 were generated by incubating *M. tuberculosis* H37Rv WT on agar medium containing a 10-fold MIC_{90} of this compound. Clones emerged with a frequency of 10^{-6} to 10^{-7} after seven weeks. Individual clones have been grown in a liquid medium and screened for resistance towards OMK-175 in a MIC assay. Figure 28 shows four individual clones with three different resistance patterns. With an accumulation of different resistance patterns, it is likely that different types of mutations, potentially also located in various genes, are underlying the resistance phenotype in those strains. To further analyze whether the mutations also affect KSK-106 activity, two of these mutants were tested against KSK-106. One mutant had almost the same concentration-dependent trend as the WT, but the other mutant also showed resistance to KSK-106. This suggests a new resistance mechanism in SRM-OMK-175 #3 and a similar or identical one in SRM-OMK-175 #2, e.g., a mutation in the amidohydrolase genes *amiC* or *Rv0552*.

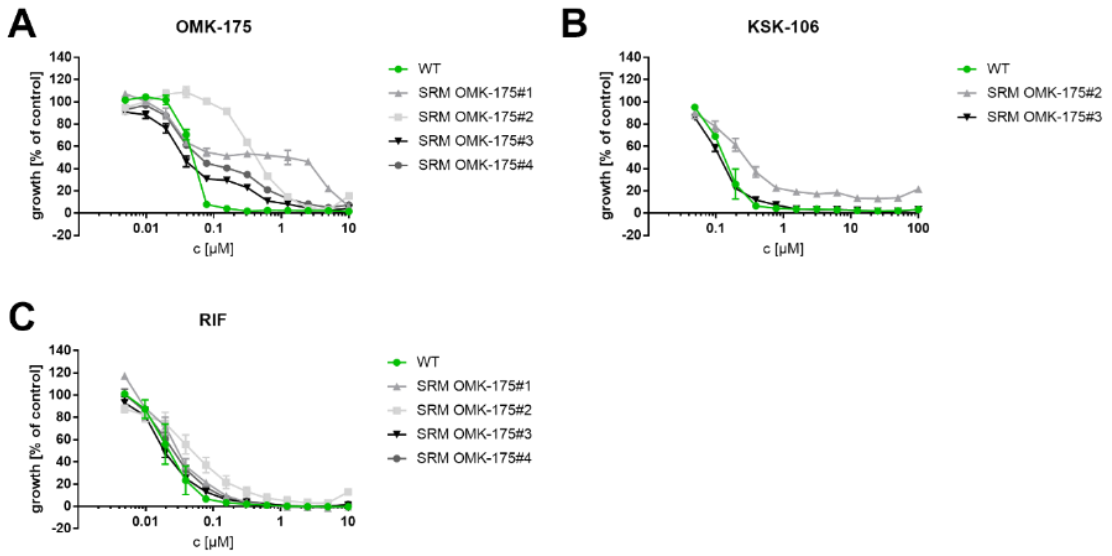

Figure 28: Resistance pattern of SRM-OMK-175. Dose-response curves of OMK-175 resistant clones of *M. tuberculosis* (#1, #2, #3, #4) against **(A)** OMK-175, **(B)** KSK-106, and **(C)** RIF. *M. tuberculosis* H37Rv WT is used as a control. Data are shown as means of *n*=3 ±SEM.

In summary, the presented results suggest that OMK-175 indeed might be used as a new lead structure for further analysis and SAR studies.

3.2.2 The KSKs are rapidly metabolized

In previous studies, by generating and analyzing SRMs raised against the parental KSKs, the amidohydrolases AmiC and Rv0552 were found [240]. These enzymes are supposed to be able to cleave carbon-nitrogen bonds [260]. To investigate if the amidohydrolases AmiC and Rv0552 can cleave the KSKs as potential prodrugs so that the putative active moiety is released, a KSK-metabolization assay was performed in cooperation with Dr. Björn Burckhardt. The first step was to prove this method and to investigate whether KSK-106 and ABK-227 could be found. If they were measurable, the following question was if they could be detected in the supernatant or the cell fraction of *M. tuberculoisis* cells treated with the compounds. ABK-227 is very likely one of the cleavage products that can be formed by the amidohydrolases (Figure 29). It is composed of regions A and B of KSK-106 and released in case hydrolysis occurs in region C. KSK-106 was incubated for 48 hours with *M. tuberculosis* H37Rv, and then samples were collected and prepared for measurement (Figure 29A). A large amount of the degradation product was detectable in the wild type with an average of 47.46 ng/mL. This amount was found in the supernatant fraction. Only 8.30 ng/mL of the parental KSK-106 was found, with a larger proportion of 5.40 ng/mL present in the pellet fraction.

The SRM of KSK-106 #5 has a non-sense mutation in the 129th amino acid in the gene of the amidohydrolase *amiC*. This mutation in the gene and the resulting probable non-

functional amidohydrolase could slow down the cleavage process. When KSK-106 was incubated with this SRM, KSK-106 was detected as the dominating peak with a total concentration of 85.29 ng/mL. A significantly higher proportion was found in the pellet fraction with 69.00 ng/mL. Only a minimal amount of ABK-227 was measured in the supernatant with 4.80 ng/mL. When the detected amount of KSK-106 and ABK-227 in the medium control is set as 100%, the overall recovery was 13.3% in WT, and 22.63% in SRM-KSK-106.

In comparison to the cell-free medium control with additional KSK-106, it is noticeable that a much higher concentration of KSK-106 was found in this control sample compared to the cell samples. Both were treated similarly. There is also a very low concentration of ABK-227 in the control samples, indicating a low self-degradation of the substance in the medium. This must be taken into account when considering the results. In the controls where no KSK-106 or ABK-227 was added to the cells, no KSK-106 or the metabolite was found either. The higher concentration of KSK-106 in the control indicates that KSK-106 is degraded into ABK-227 and other cleavage products when incubated with the cells.

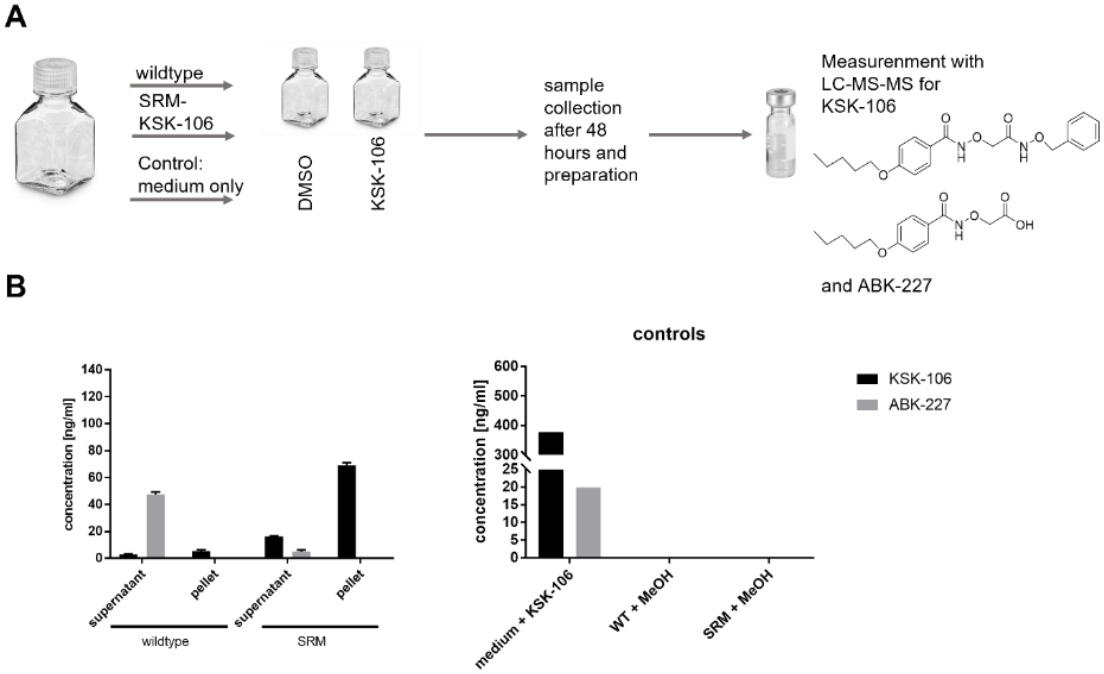

Figure 29: KSK-metabolization assay. (A) Cartoon of the general procedure of the metabolite screening showing the significant steps and the analyzed molecules. **(B)** The screening was measured employing LC-MS/MS by Dr. Björn Burckhardt. The diagram shows the measured concentration in ng/mL of KSK-106 and a putative cleavage product ABK-227 after incubation with the WT or SRM-KSK-106#5 (*amiC* E129*). The compounds were incubated for 48 hours with the cells or in the cell-free medium as a control.

3.2.2.1 The KSKs are cleaved by *M. tuberculosis* enzymes

So far, we have just considered specific metabolites that are formed after potential cleavage occurring between regions B and C. However, since the KSKs have another possible site of amidohydrolase attack between regions A and B, a broader metabolite screening was done next. To get an impression of the resulting KSK-cleavage products, the KSKs were incubated for 0 h (t_0), 24 h (t_1), 48 h (t_2), and 7 days (t_3) with the WT, SRM-KSK-104#1 (*rv0552* H67R), or SRM-KSK-106#5 (*amiC* E129*). The samples were further processed as shown in Figure 30B. SRM of KSK-106 #5 was chosen because it has a non-sense mutation in the 129th amino acid in the gene of the amidohydrolase *amiC*, which probably results in a non-functional amidohydrolase, which could slow down the cleavage process. To get an overview of which cleavage products were detectable, the individual pure substances were first measured with HPLC and DAD (Dionex), and retention times and UV spectra were added to the institute-internal compound library for later analysis.

Not all cleavage products were detectable by this method. The undetectable substances were regions B, C, and BC (Figure 30A; Figure S8, and Figure S9). The inability to detect region B can be explained by the absence of an aromatic ring and the very small molecular size. The explanation for why region C and BC are not easily detectable remains elusive. Perhaps these molecules either exhibit strong interactions with the column material, preventing their elution from the column within the time, or they were further degraded very rapidly after hydrolytic release. All other cleavage products shown were detectable by the DAD detector.

The result of the metabolite screening is shown in Figure 30C (signals and UV spectra are shown in Figure S10 – Figure S17). As a control, a sample was taken and processed directly after adding the substance to the bacteria or medium. It is visible that no KSK or KSK degradation product is found in the DMSO controls. A significant peak was detected in all other samples where KSK-106 was added. By comparison with our institute-internal library, this is supposed to be adenosine ribose. However, it is detectable (Figure S10) that the UV spectra of adenosine ribose and KSK-106 are not identical and only match with 98%. In the calibration of KSK-106 (Figure S8), this compound had a retention time of 31.097 min, which fits very well with the degradation data of KSK-106 with a retention time of 31.117 min (Figure S10). The small change in time could be caused by the different concentrations and purities of the sample. Since the samples were processed directly after the addition of KSK-106 and degradation is hardly possible in such a short time, it can be assumed that this peak is KSK-106. For this reason, the substance is referred to hereafter as KSK-106. In the medium control with additional KSK-106, only

KSK-106 can be detected at any time; thus, strong self-degradation in the medium can be excluded. In most cases, no KSK or KSK degradation product was detected in the DMSO controls. An exception was the WT-DMSO control at time point t_1 and SRM-KSK-106 at time point t_2. In both cases, AC-KSK-106 was detected. However, when looking at the graphs (Figure S11 and Figure S12), it is noticeable that the presumable AC-KSK-106 peaks were tiny. With such small peaks and thus low concentrations, erroneous results can quickly occur, which is why they are probably negligible. After 24 hours, many changes were observable. In the WT, AB-KSK-106-hydroxamic acid and A-KSK-106 were detected. However, the major peak here could be assigned to AB-KSK-106-hydroxamic acid. In SRM-KSK-104, two prominent peaks occurred. These were A-KSK-106 and AB-KSK-106. In contrast, in the SRM-KSK-106, the major peak was A-KSK-106, but small amounts of AB-KSK-106-hydroxamic acid were also detectable. After another 24 h (t_2), the main peak in the WT sample could be assigned to A-KSK-106. Interestingly, another peak appeared, which belonged to a substance eluted much earlier. According to automatic library assignment, this was supposed to be pestalotioprolide G, which is a macrocyclic lactone structure that cannot directly arise from KSK-106. This peak was also found in many other samples. To clarify the true identity of this molecule, further analyses have to be performed. By SRM-KSK-104, KSK-106 was degraded only to AB-KSK-106 and A-KSK-106 in approximately equal amounts. In contrast, almost only A-KSK-106 was still present in the SRM-KSK-106 preparation. All other components were not detectable. In the last batch of samples, after 7 days of incubation, only A-KSK-106 was detectable both in the WT and SRM-KSK-106 sample. With SRM-KSK-104, however, the degradation was much slower. AB-KSK-106 and A-KSK-106 were still detectable. The peak for A-KSK-106 was more pronounced than the one for AB-KSK-106.

In summary, KSK-106 is probably degraded by mycobacterial enzymes. This is not only induced by one amidohydrolase, as degradation also occurs in SRM-KSK-104 and SRM-KSK-106. However, the degradation is much slower for SRM-KSK-104. Since there is a mutation in *rv0552*, this could lead one to suspect that Rv0552 is the amidohydrolase, which is acting much faster than AmiC for KSK-106. Some of these approaches were measured with an LC-MS to support these results further. The result of this analysis is presented in the course of this chapter.

A

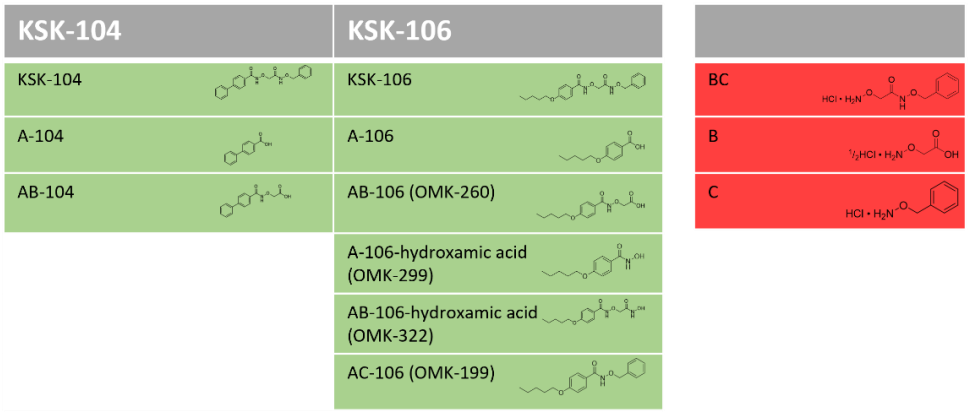

B

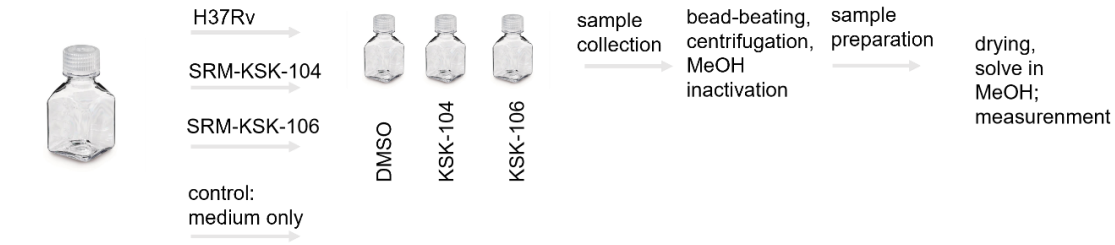

C

	t_0	t_1	t_2	t_3
MeOH				
Medium-DMSO				
Medium-KSK-106	KSK-106	KSK-106	KSK-106	KSK-106
WT-DMSO		(AC-106)		
WT-KSK-106	Adenosin Ribose	AB-106-hydroxamic acid; A-KSK-106;	A-KSK-106	A-KSK-106
SRM-104-DMSO				
SRM-104-KSK-106	Adenosin Ribose	AB-KSK-106; A-KSK-106;	AB-KSK-106; A-KSK-106	AB-106-hydroxamic acid; A-KSK-106;
SRM-106-DMSO			(AC-106)	
SRM-106-KSK-106	Adenosine Ribose	AB-106-hydroxamic acid; A-KSK-106	A-KSK-106	A-KSK-106

Figure 30: Qualitative assessment of KSK-106 metabolization during treatment of *M. tuberculosis* strains. **(A)** The measurement of the parent compound and of putative cleavage products was qualitatively determined employing HPLC with DAD (Dionex). The red color indicates the substances, which were not detectable, whereas the green ones were detectable. **(B)** Schematic representation of the treatment regime and the used strains. **(C)** Qualitative assessment of KSK-106 metabolization during incubation with *M. tuberculosis* cells as revealed by HPLC-DAD (Dionex). The table shows the detected KSK-106 parent compound and potential cleavage products for the wild type strain (WT), SRM-KSK-104#1 (r*v0552:* H67R), and SRM KSK-106#5 (*amiC* E129*). KSK-106 (100 µM initial concentration) was incubated for 0 h (t_0), 24 h (t_1), 48 h (t_2), and 7 days (t_3), before methanol extraction of metabolites and HPLC-DAD analysis. The substances enclosed in brackets have been detected with low intensity and cannot originate directly from KSK-106 due to the absence of region B. Instead, regions A and C must have reconnected subsequently for their formation.

The same experiment was performed with the other lead compound KSK-104. Only this compound was detectable in the medium control when KSK-104 was added. Also, only KSK-104 was detectable in all cell preparations at time point t_0. After 24 h, only KSK-104 was still measurable in both SRMs. However, in the presence of both functional amidohydrolases in the WT strain, the hydroxamic acid of region A of KSK-106 was detected, and no other cleavage product was found. This result is questionable because there is no KSK-106 in the approach and region A is different in KSK-104 and KSK-106. It can be assumed that a substance with a similar retention time and UV spectrum was detected at the time, or a ring-opening occurred. After another 24 h, at time point t_2, intact KSK-104 was still found in the WT, but the hydroxamic acid of region A of KSK-106 and region A of KSK-104 alone was also observed. In SRM-KSK-104, only KSK-104 was detectable, and in SRM-KSK-106, all regions were found comparable to the WT strain. In the final measurement, after 7 days, only the hydroxamic acid of region A of KSK-106 was detectable in the WT and SRM-KSK-106, while only KSK-104 continues to be measurable in SRM-KSK-104.

This result indicates that Rv0552 is required for the degradation of KSK-104. Degradation in presence of mutated AmiC is also slower than in the presence of both functional amidohydrolases in the WT strain.

	t_0	t_1	t_2	t_3
MeOH				
Medium-DMSO				
Medium-KSK-104	KSK-104	KSK-104	KSK-104	KSK-104
WT-DMSO		(AC-106)		
WT-KSK-104	KSK-104	KSK-104; A-106-hydroxamic acid	KSK-104; A-106-HA; A-104	A-106-hydroxamic acid
SRM-104-DMSO				
SRM-104-KSK-104	KSK-104	KSK-104	KSK-104	KSK-104
SRM-106-DMSO			(AC-106)	
SRM-106-KSK-104	KSK-104	KSK-104; A-106-hydroxamic acid	KSK-104; A-106-hydroxamic acid	A-106-hydroxamic acid

Figure 31: Qualitative assessment of KSK-104 metabolization during treatment of *M. tuberculosis* strains. Qualitative assessment of KSK-104 metabolization during incubation with *M. tuberculosis* cells was done by HPLC-DAD analysis (Dionex). The treatment and sampling scheme was similarly as shown in Figure 30B. The table shows the detected KSK-104 parent compound and potential cleavage products for the wild type strain (WT), SRM-KSK-104#1 (*rv0552* H67R), and SRM KSK-106#5 (*amiC* E129*). KSK-104 (100 µM initial concentration) was incubated for 0 h (t_0), 24 h (t_1), 48 h (t_2), and 7 days (t_3), before methanol extraction of metabolites and HPLC-DAD analysis.

To support these results and for more precise statements about the cleavage products, the experiment was repeated with samples, which were incubated for 48 h (t_2) with one of the KSK-compounds and measured in the CEMSA@HHU facility by LC-MS. The result is illustrated in Figure 32 and Figure S18 to Figure S25. After 48 h of incubation with KSK-104, a very high amount of KSK-104 was found in the medium control. A side peak with the molecular weight of AB-KSK-104 was also measurable. This could be due to the fact that small amounts of AB-KSK-104 were also formed during the incubation time in the medium and the processing of the samples. In the WT, small amounts of a substance with the molecular weight of AB-KSK-104 and a major peak with the molecular weight of A-KSK-104 were found. Thus, A-KSK-104 is probably formed in the batch after 48 h. In the presence of SRM-KSK-104, only one assignable peak with the molecular weight of AB-KSK-104 was detectable. In the presence of SRM-KSK-106, on the other hand, major peaks with molecular weights comparable to A-KSK-104, but also AB-KSK-104 were found. In all samples, there were furthers peaks with a molecular weight of 181 g/mol and 286 g/mol. However, these peaks were also found in the medium control and are thus probably not a degradation product but an impurity due to the medium or the purification itself. Since no A-KSK-104 was detectable in the approach with SRM-KSK-104, this could mean that KSK-104 is predominantly or more sufficiently cleaved by the amidohydrolase Rv0552 between regions A and B. After the addition of KSK-106 and incubation for 48 h, only a peak with a molecular weight comparable to KSK-106 was found in the medium control. The WT and SRM-KSK-104 had a prominent peak after 4.6 min. It fits to the molecular weight of A-KSK-106. Also, in the preparation with SRM-KSK-106, mainly this peak was identified. However, there is also a small peak with the molecular weight of KSK-106. Again, there were impurity peaks of 191 g/mol and 282 g/mol, respectively. This could also be seen in the medium sample and is therefore negligible and could be due to contamination found in the KSK starting substance or in the MeOH, with which the stock solutions of the compounds have been prepared. Another explanation is that it is an impurity resulting from the medium, purification, and/or measurement. KSK-106 could form A-KSK-106 in each case in WT and if either of the amidohydrolases AmiC or Rv0552 were mutated. That indicates that both amidohydrolases can cleave KSK-106, or another enzyme can take over their task.

A

KSK-104			KSK-106		
substance	mol. weight	structure	substance	mol. weight	structure
KSK-104	376.14	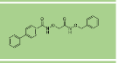	KSK-106	386.18	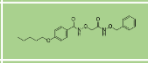
A-104	198.07		A-106	208.14	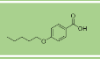
AB-104	271.09		AB-106 (OMK-260)	261.13	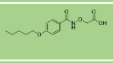
AB-104-HA	306.10		A-106-HA (OMK-299)	223.12	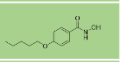
			AB-106-HA (OMK-322)	296.14	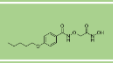
			AC-106 (OMK-199)	313.17	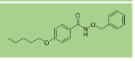

	mol. weight	structure
BC	232.06	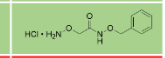
B	91.03	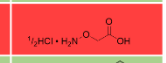
C	159.05	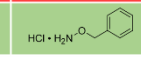

B

		t_2
KSK-104	Medium	KSK-104 ⊕ ; AB-104
	WT	AB-104; A-104 ⊕
	SRM-104	AB-104
	SRM-106	AB-104; A-104 ⊕
KSK-106	Medium	KSK-106
	WT	A-106
	SRM-104	A-106
	SRM-106	KSK-106; A-106 ⊕

Figure 32: Qualitative assessment of KSK-106 and KSK-104 metabolization during treatment of *M. tuberculosis* strains as revealed by LC-MS analysis. LC-MS analyses were performed in the CEMSA@HHU facility. Table **(A)** shows the structure of putative KSK-cleavage products and their molecular weight. The substances highlighted in green were detectable by the method, but those highlighted in red (region B) were not. **(B)** Summary of the detected KSK metabolites. Identification was done based on molecular weight. The respective chromatograms are shown in Figure S18 to Figure S25. (+) indicates the main peak. Results are shown for the incubation of KSK-104 or KSK-106 with the wild type strain (WT), SRM-KSK-104#1 (*rv0552*: H67R), and SRM KSK-106#5 (*amiC* E129*). The compounds were incubated for 48 h (t_2), then isolated and analyzed.

Taken together, these results suggest that KSK-106 is a substance that can be cleaved faster and more efficiently. The cleavage product A-KSK-106 is also measurable when a mutation in Rv0552 or AmiC is present. In the case of KSK-104, region A of KSK-104 can only be detected in WT and SRM-KSK-106. The mutation in *rv0552* leads to the detection of AB-KSK-104. Region C can probably be formed in all cases since this is the remaining part next to region AB of the molecule. However, there is no evidence that this

structure has been formed, as it has not been detected by this method. Furthermore, in addition to region C, also region BC could not be detected in free form, neither during incubation with KSK-104 nor KSK-106. Since the pure compounds have not been subjected to LC-MS analyses, it is unknown whether the compounds could principally be separated and detected by this method. Thus, to exclude measurement inaccuracies, a selection of samples was additionally measured by GC-MS. However, this method was also unable to detect region C (data not shown). In addition to technical limitations, there are further explanations conceivable for the inability to detect region C and BC in compound-treated cells. On the one hand, this phenomenon could be attributed to the rapid further metabolism or structural modifications of these regions after their hydrolytic release, so they are no longer detectable. On the other hand, it is also possible that region C is an active substance that binds, for example, covalently to a membrane molecule. The purification method with methanol and mechanical disruption by bead-beating is probably inefficient against a covalent binding; therefore, region C might not be present in the solution after the purification.

3.2.3 The putative metabolites have very low activity in *M. tuberculosis*

To obtain more information about the cellular effects of the possible cleavage products, they were first tested in a MIC assay. The cleavage products are the three individual regions: A, B, and C, which are linked by a carbon-nitrogen bond in the KSK molecules and can thus be cleaved by amidohydrolases. Furthermore, a compound containing a combination of regions A and B and regions B and C were also analyzed. In this experiment, the cleavage products of KSK-106 were initially investigated. The individual substances against *M. tuberculosis* had very low activity, as shown in Figure 33. However, a dose-dependent growth inhibitory effect is detectable for all tested variants. The most active compounds appeared to be regions B, BC, and AB. But all tested derivatives had only very weak activity resulting in a MIC_{90} between 100 µM and >100 µM.

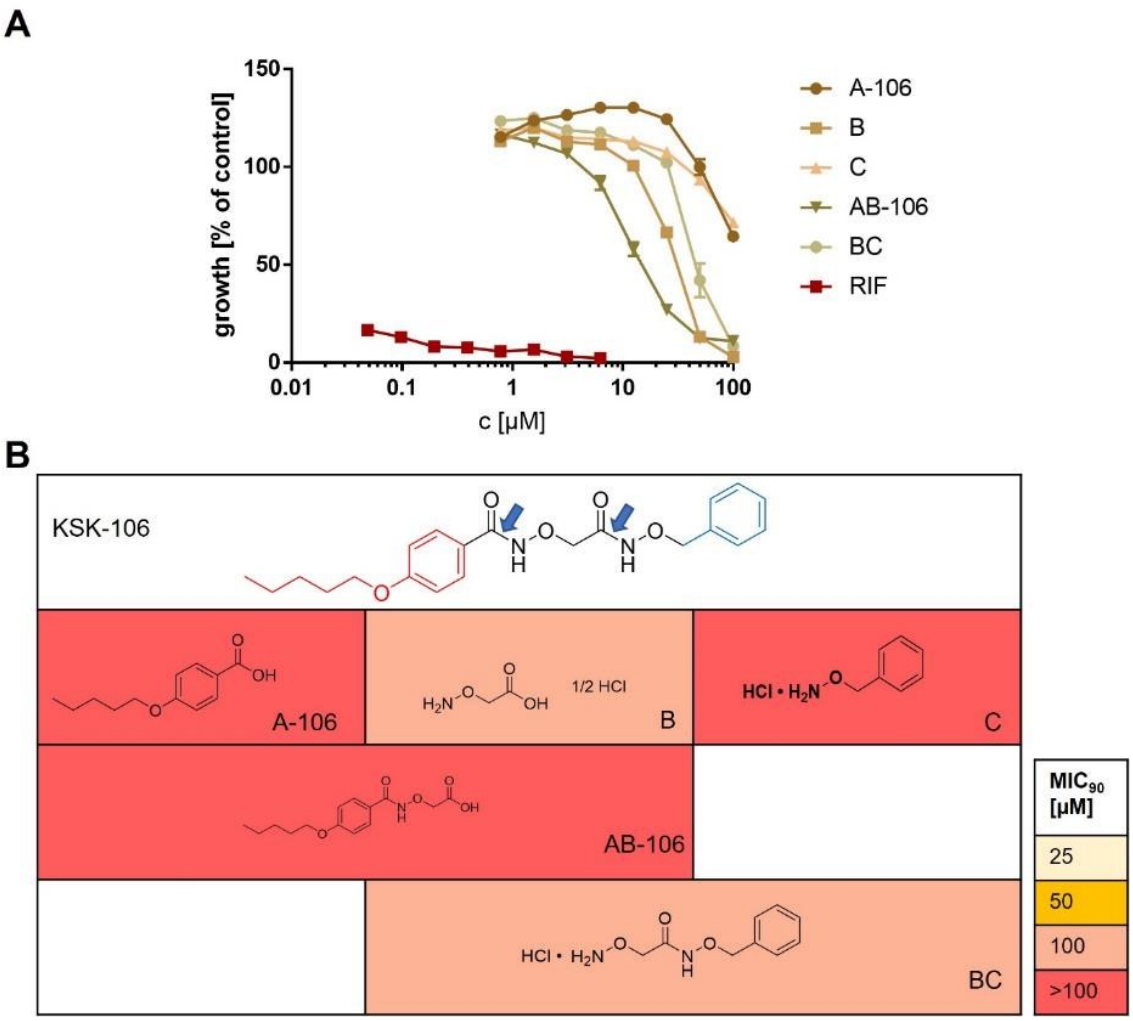

Figure 33: Activity of putative KSK-106 cleavage products against *M. tuberculosis* H37Rv. (A) Dose-response curve of the putative KSK-106 cleavage products. Data are shown as means of *n*=3 ±SEM. **(B)** The resulting MIC_{90} values are presented in a heatmap (from green = active to red = inactive). The arrows show the sites where amidohydrolases can potentially cleave the KSK-106 molecule.

The same experiment was performed with KSK-104 cleavage products. It shows comparable results with the one described above for KSK-106 (Figure 34).

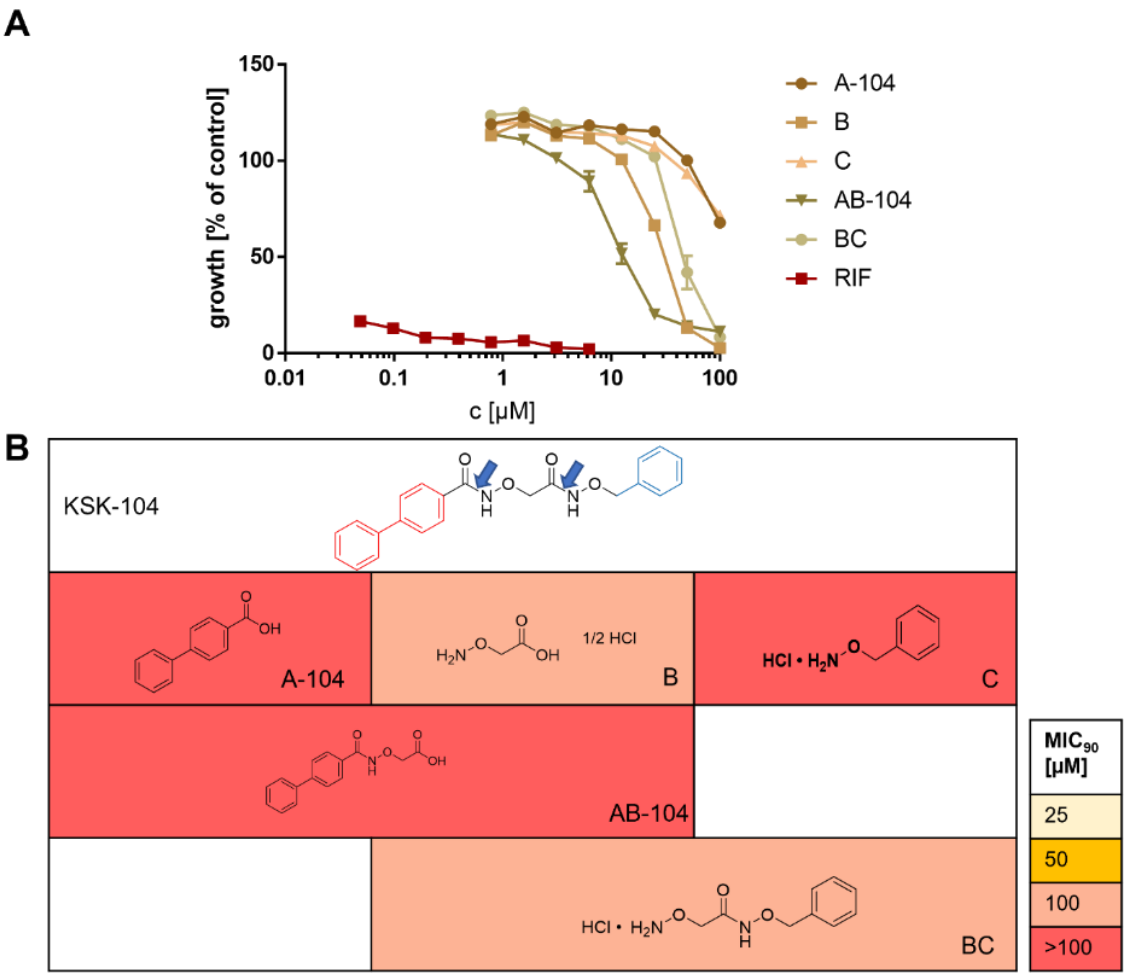

Figure 34: Activity of putative KSK-104 cleavage products against *M. tuberculosis* H37Rv. **(A)** Dose-response curve of the putative KSK-104 cleavage products. Data are shown as means of *n*=3 ±SEM. **(B)** The resulting MIC_{90} values are presented in a heatmap (from green = active to red = inactive). The arrows show the sites where amidohydrolases can potentially cleave the KSK-104 molecule.

This severe loss of activity compared to the parental KSKs could be due to several reasons. Firstly, it is conceivable that the individual components are largely devoid of activity, but their combination results in a synergistic effect that results in an antibacterial effect. Thus, the combinations of the individual regions were tested to determine whether the KSKs also act similarly. Figure 35 displays the result of this MIC assay. The starting concentration in the dilution series is also in combination 100 µM for each substance. There is a minimal shift in activity compared to the single compounds. The most active combinations for the KSK-106 cleavage products were the combination of regions A, B, and C; A and BC, A and B, and the mixture of B and C. All these combinations had a MIC_{90} of 50 µM, which is still very inefficient when the parental molecule KSK-106 has an activity in a nanomolar concentration. All other combinations were worse. The combination of AB and C had a MIC_{90} of 100 µM, and the combination of A and C showed nearly no anti-bacterial activity in this setup (>100 µM). The same results were received

for KSK-104, except for the combination of AB and C. It presents an MIC_{90} of 100 µM. These experiments indicate that region B is needed for the activity because regions A and C are the only combinations with significantly less activity than the others. But it also indicates that the combination of various potential cleavage products does not nearly reveal the same potency as the parental compounds. Therefore, there should be another reason for the decline in activity, which could be that the complete substance is required for internalization while the degradation products alone cannot enter the cell because of the complex *M. tuberculosis* cell wall structure. To investigate whether there is improved activity when the integrity of the cell wall is impaired, colistin was added to the assay to attack the cell wall, potentially resulting in enhanced uptake of cleavage products [261, 262].

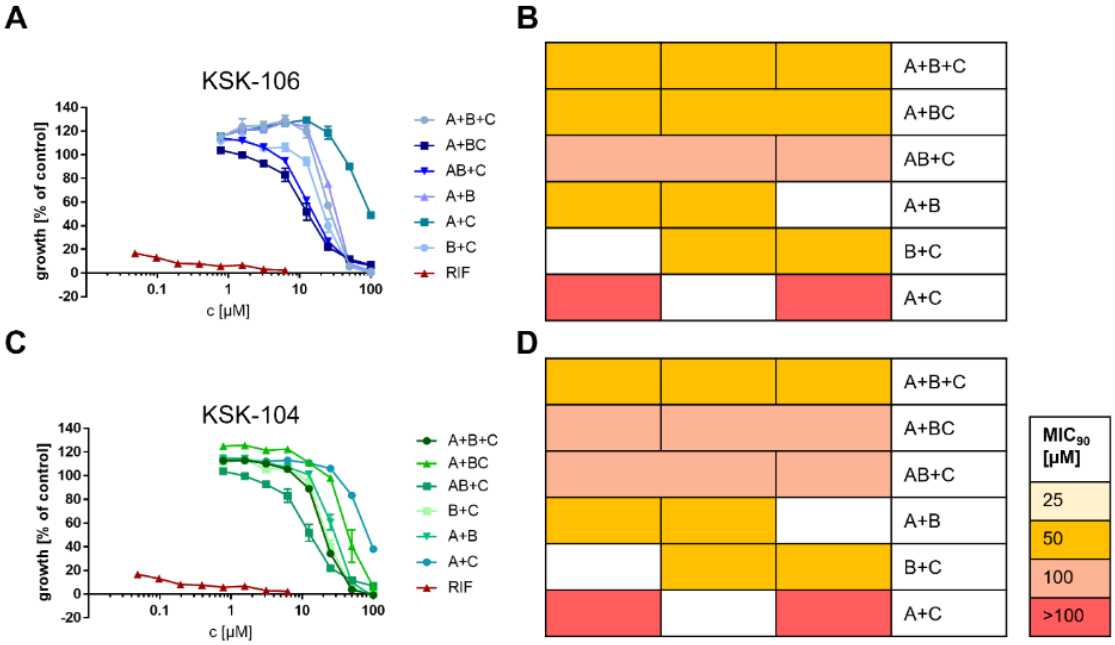

Figure 35: Activity of the combined putative KSK-106 or KSK-104 cleavage products against *M. tuberculosis* H37Rv. (A; C) Dose-response curve of the combination of the putative cleavage products. 100 µM means that every derivative has a starting concentration of 100 µM in that case. Data are shown as means of *n*=3 ±SEM. **(B; D)** The resulting MIC_{90} values in µM are shown in a heatmap (from green = active to red = inactive). **(A;B)** are the KSK-106 cleavage products, whereas **(C;D)** are KSK-104 cleavage products.

To analyze if colistin, a drug known to be active against gram-negative bacteria, also influences cell growth of *M. tuberculosis*, a dose-response curve was measured employing the resazurin dye reduction assay. A low but concentration-dependent decrease in fluorescence intensity, which is equivalent to cell viability, was observed, demonstrating that colistin can inhibit the growth of *M. tuberculosis* to a certain extent. For further experiments, a colistin concentration of 6.25 µM was chosen because this is

the value at which less than 50% of the cells grow compared to the control. An additional concentration was tested at which about 60% of the cells survive (Figure 36A and 36B).

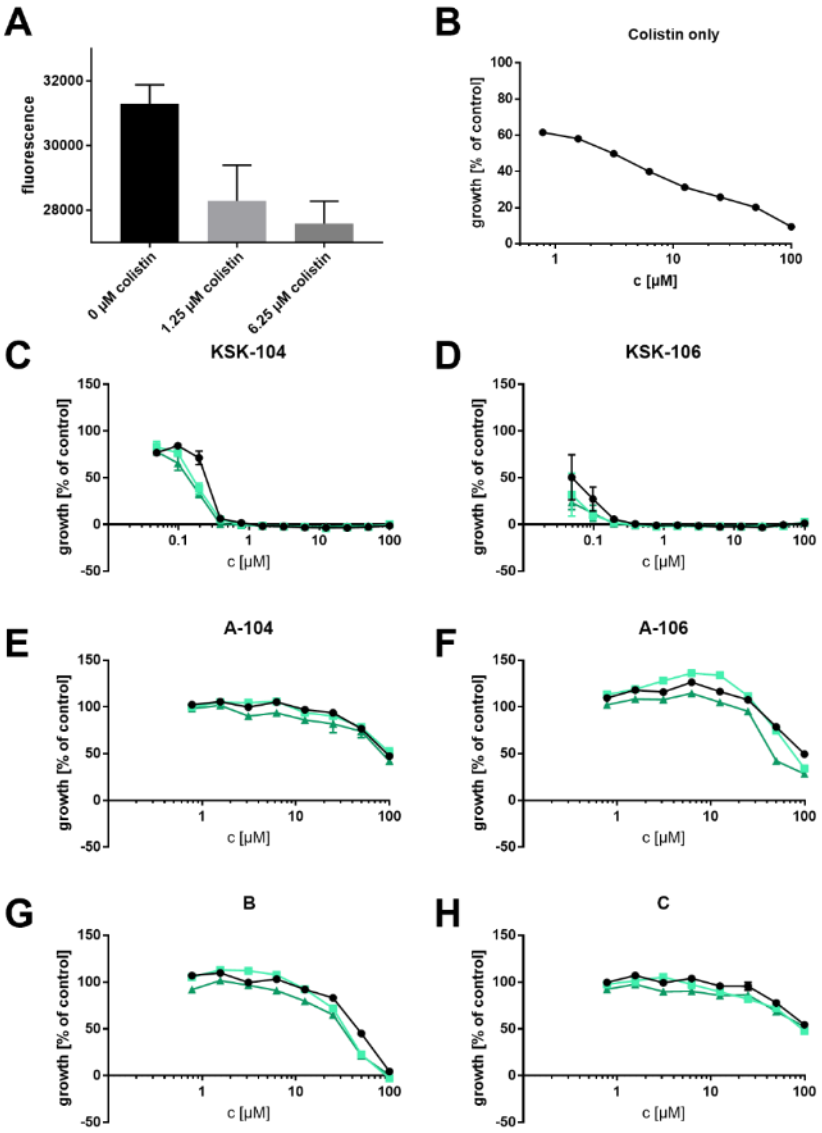

Figure 36: Activity of the putative KSK cleavage products in combination with colistin against *M. tuberculosis* H37Rv. (A) Fluorescence intensity of cells treated with 0 µM, 1.25 µM, or 6.25 µM colistin as a correlate of residual growth as determined by resazurin staining. **(B)** Dose-response curve of colistin alone. **(C-H)** Dose-response curve of the putative KSK cleavage products in combination with 0 µM, 1.25 µM, or 6.25 µM colistin. Data are shown as means of *n*=3 ±SEM.

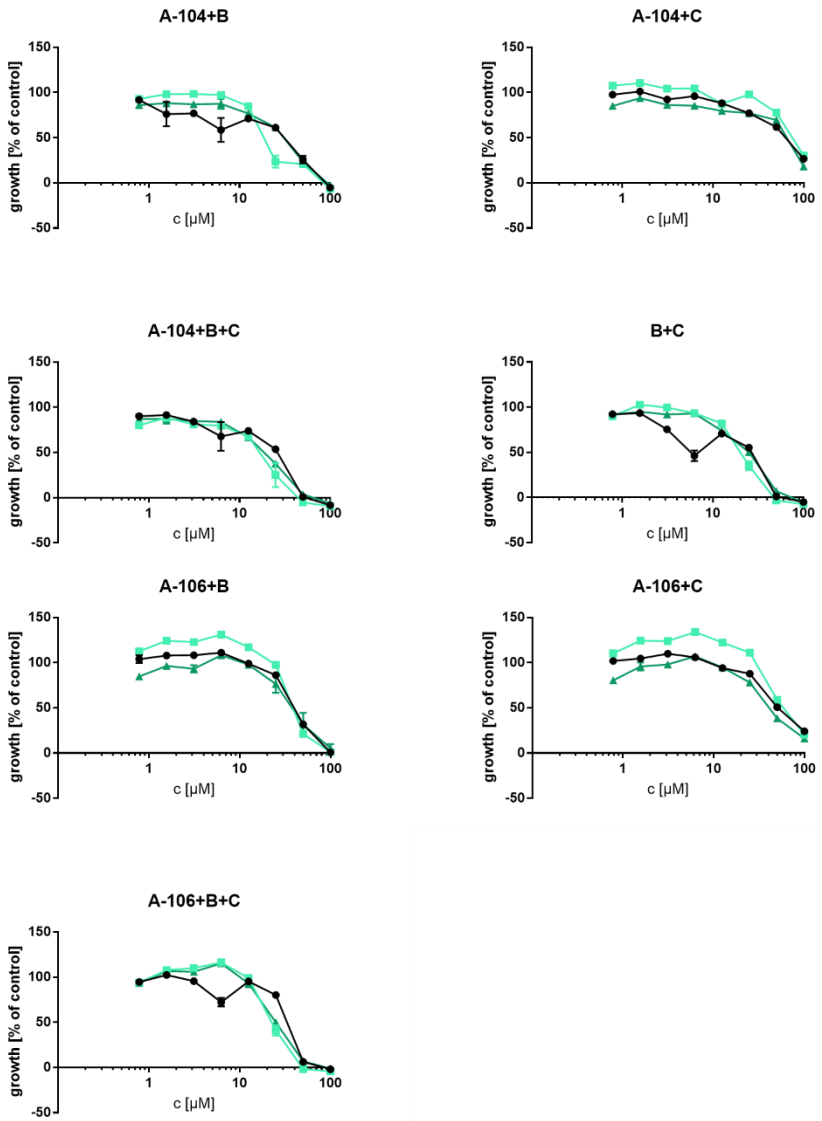

Figure 37: Activity of the combined putative KSK cleavage products in combination with colistin against *M. tuberculosis* H37Rv. Dose-response curve of the combined putative KSK cleavage products, each with a combination of 0 µM, 1.25 µM, or 6.25 µM colistin. 100 µM means that every individual derivative has a starting concentration of 100 µM. Growth was measured employing resazurin staining. Data are shown as means of *n*=3 ±SEM.

However, the addition of different concentrations of colistin did not substantially improve the activity of KSK-cleavage products against *M. tuberculosis* in combination treatment (Figure 36 and 37). Also, the combination of different putative cleavage products with colistin resulted in no significant improvement in activity against *M. tuberculosis*. That means that there is no synergism between the compounds and colistin. Due to their strong cellular activity, it is obvious that KSK-104 and KSK-106 can easily get internalized by *M. tuberculosis*, but the cleavage products might not have the required physicochemical properties to get inside the cell.

3.2.3.1 The KSK-spontaneous resistant mutants are not resistant against all other KSK derivates

In former studies, SRM-KSK-106 and SRM-KSK-104 were created and analyzed by Dr. Lasse van Geelen. Both SRMs have a mutation in an amidohydrolase (see Chapter 3.2.2.1). To obtain further information on the KSKs and their activation, the KSK library was tested against both SRMs compared to the WT. In this chapter, only a small representative section is shown. The compounds are divided into three groups. In the first group, many derivatives show a strong reduction in activity only to SRM-KSK-106 (Figure 38A). Nearly all represent KSK-106 derivatives, like OMK-119, OMK-170, or ABK-363. Also, OMK-175, which was previously described, belongs to this group. In the second group, there are molecules to which both SRMs are resistant. Most of them are KSK-104 derivatives (Figure 38B). All shown derivatives have a variation in region C. An example is ABK-191, which has an additional fluoride ion in the *para*-position. In ABK-267, there is an alkyne instead of the entire region C. Since SRM-KSK-104 has a mutation in *Rv0552* and SRM-KSK-106 in *amiC*, inferences can be made about the enzymes. The mutation in *Rv0552* probably results in impaired cleavage exclusively of KSK-104 derivatives, as shown in Chapter 3.2.2.1. With this, it is likely, that these molecules are not activated, and thus there is no or little activity in SRM-KSK-104. The mutation has very little or no influence on the activity of the KSK-106 derivatives compared to the activity in the WT. That means that AmiC can cleave some KSK-106 derivatives but no KSK-104 derivatives. In contrast, the mutation in AmiC in SRM-KSK-106 results in the inability to cleave KSK-104- and KSK-106 derivatives. That indicates that Rv0552 might have a narrower substrate specificity if it can be assumed that no other amidohydrolase is involved in the cleavage of the KSKs.

A

		parental strain	*Rv0552**	*amiC**
OMK-119	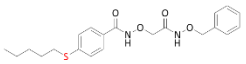	0.39	0.39	100
OMK-170	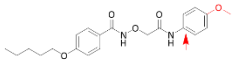	0.19	0.39	12.5
ABK-363	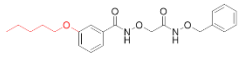	3.13	25	>100

B

		parental strain	*Rv0552**	*amiC**
ABK-191	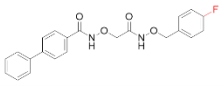	1.56	6.25	6.25
ABK-267	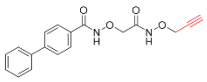	1.56	12.50	12.50
ABK-311	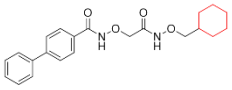	0.39	3.13	12.50
ABK-519	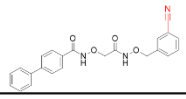	1.56	50	25

C

		parental strain	*Rv0552**	*amiC**
OMK-096	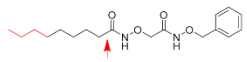	0.78	0.78	0.78
OMK-270	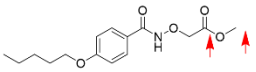	0.39	0.39	0.39
OMK-117	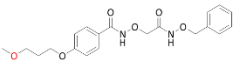	0.39	0.39	1.56
ABK-334	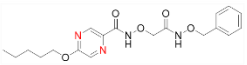	0.39	0.39	0.78
ABK-130	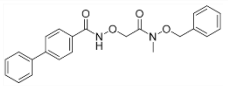	6.25	6.25	6.25

MIC_{90} [µM]
0.05 – 0.1
0.2 – 0.4
0.8 – 1.6
3.2 – 6.5
12.5 - 25
50 - >100

Figure 38: Heatmap representing MIC_{90} values of different KSK derivatives against *M. tuberculosis* H37Rv WT, SRM-KSK-104#1, and SRM-KSK-106#5 to illustrate structure-activity relationships. The tables show the MIC_{90} values in µM. The red highlighted areas in the molecule represent the structural variation compared to the parental compound. In case a substituent has been removed, the corresponding position is indicated by an arrow. **(A)** Examples of compounds showing a strong decrease of activity only in SRM-KSK-106. **(B)** Examples of compounds showing comparable cross-resistance for both SRMs. **(C)** Compounds for which no resistance was detected in both used SRMs compared to the WT. Dr. Alexander Berger, or Dr.

Oliver Michel, University of Düsseldorf, Germany, have synthesized all derivatives. The heatmap shows a color code of the MIC_{90} values determined in triplicates.

However, a third group of substances had nearly the same activity in both SRMs and the WT. Examples of this are shown in Figure 38C. All substances are KSK-106-derived molecules, like OMK-096 (= *N*-(2((benzyloxy)amino)-2-oxoethoxy)nonamide). It has a variation in region A, whereas OMK-270 has no benzyl ring in region C. Further examples are OMK-117 and ABK-334, both with a variation in region A, and ABK-130, with a change in region B. These molecules are all active derivatives with huge structural variations compared to KSK-106. This could indicate that these molecules can be cleaved with similar efficacy by Rv0552 and AmiC. It is further possible that yet one or more different other amidohydrolases or enzymes are involved in their cleavage or that they even rely on a different mechanism that does not require hydrolysis. To get more information about this mechanism, SRMs of some derivatives that were still active against both SRMs were created, which is described in the following chapter 3.2.4.

3.2.4 Generation of spontaneous resistant mutants of several KSK derivatives

To further investigate the resistance mechanism, SRMs were created against some of the compounds that did not result in any resistance phenotype in SRM-KSK-104 and SRM-KSK-106 (see Chapter 3.2.3.1). For this purpose, the WT was plated and incubated on 7H10 agar plates supplemented with 6- to 10-fold MIC_{90} of the respective substance and incubated for several weeks until single colonies appeared.

Here, the results of three derivatives, OMK-117, ABK-334, and ABK-130, are described in more detail. Even after three months, no colonies developed in the presence of ABK-130, which has an MIC_{90} of 12.5 µM. It indicates that this compound does not rapidly lead to mutations in *M. tuberculosis* and is, therefore, an interesting substance for further preclinical development with a low micromolar potency. However, it has to be emphasized that the antitubercular activity is much lower compared to the parental KSKs.

For the OMK-117 approach, colonies appeared after five weeks, which occurred with a frequency of approx. 10^{-6}. Single colonies were cultivated in liquid media and analyzed. The clones showed a high-level resistance with a 32-fold shift in MIC_{90} (Figure 39).

For ABK-334, colonies were formed with a frequency of approx. $2x10^{-6}$ and were detectable after five weeks of incubation. The isolated and analyzed mutants showed a

16-fold shift in MIC_{90} (Figure 39). For further investigations, whole-genome sequencing was performed for two of these mutants. The mutants examined were SRM-ABK-334#1 and SRM-ABK-334#2. Both have a mutation in *amiC* and *ppsA,* as shown in Table S2. The protein encoded by the gene *ppsA* plays a role in the biosynthesis of phthiocerol dimycocerosate (PDIM) and other lipids. In this context, *ppsA-ppsE* encode a type I modular polyketide synthase. Proteins involved in PDIM biosynthesis play a significant role in cell wall synthesis. PpsA-PpsC attach ketide units to long-chain fatty acids [263, 264]. In previous studies, mutations in *ppsA* have been associated with substance tolerance, e.g., in RIF-resistant mutants [263]. It does not explain why the substance ABK-334 does not exhibit resistance in SRM-KSK-104 and SRM-KSK-106. This compound may interact differently with AmiC with a different binding mode compared to the parental KSKs. To clarify this, further SRMs of this type of derivative should be generated and analyzed. Furthermore, the cross-resistance of SRM-ABK-334 against the KSKs has to be investigated.

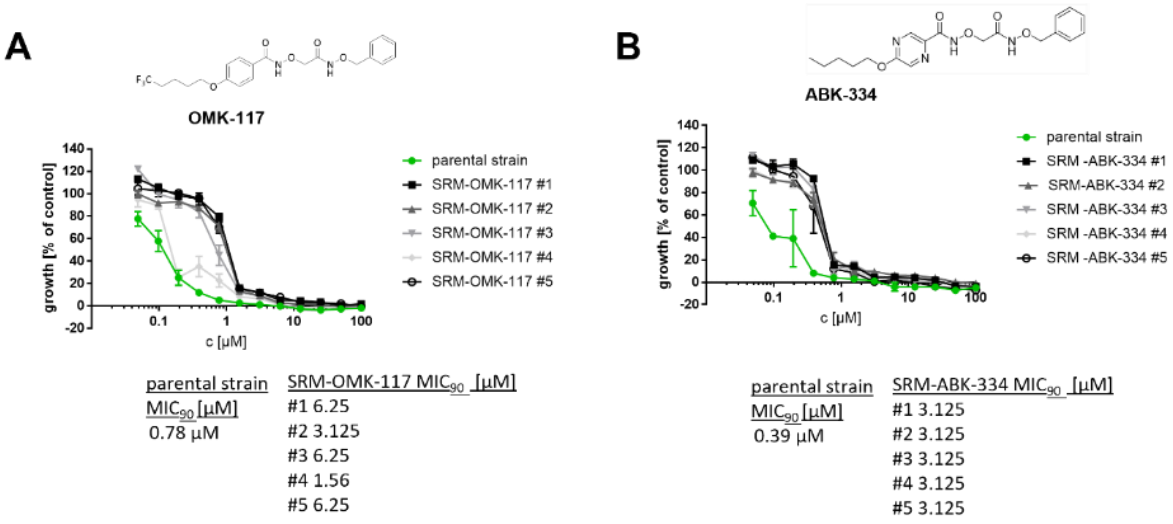

Figure 39: Resistance pattern of SRMs against OMK-117 and ABK-334. (A) Dose-response curve for OMK-117 of independent mutant clones raised against OMK-117 (SRM-OMK-117) and **(B)** dose-response curve for ABK-334 of independent mutant clones raised against ABK-334 **(**SRM-ABK-334). The parental strain *M. tuberculosis* H37Rv WT is shown as a control. The resulting MIC_{90} values are shown beneath the graph. The structure of the tested compound is displayed above each graph. Data are shown as means of *n*=3 ±SEM.

3.2.5 Double spontaneous resistant mutants against both KSKs behave differently regarding various KSK derivatives

To obtain more detailed information on the effect of KSK-104 and KSK-106, SRM-KSK-104#1 and SRM-KSK-106#5 have been plated on a medium containing the respectively

other KSK-compound to obtain double spontaneous resistant mutants (DSRM) against KSK-104 and KSK-106. After about 6 weeks, colonies appeared on the plates at a frequency of about 10^{-7}. These independent clones were grown in a liquid medium, and the resistance was tested by MIC assay. In the variant with SRM-KSK-106 as the parental strain, which has been incubated on a medium with KSK-104 (DSRM-KSK-106-KSK-104), many clones with enhanced resistance emerged. As expected, they were each more resistant than both SRMs. Moreover, the same was detectable for the opposed order (for DSRM-KSK-104-KSK-106). But it became clear that these two DSRMs behave differently. Especially the incubation with KSK-106 showed a shift in resistance in the DSRM-KSK-104-KSK-106. It indicated different mutations in the respective approaches.

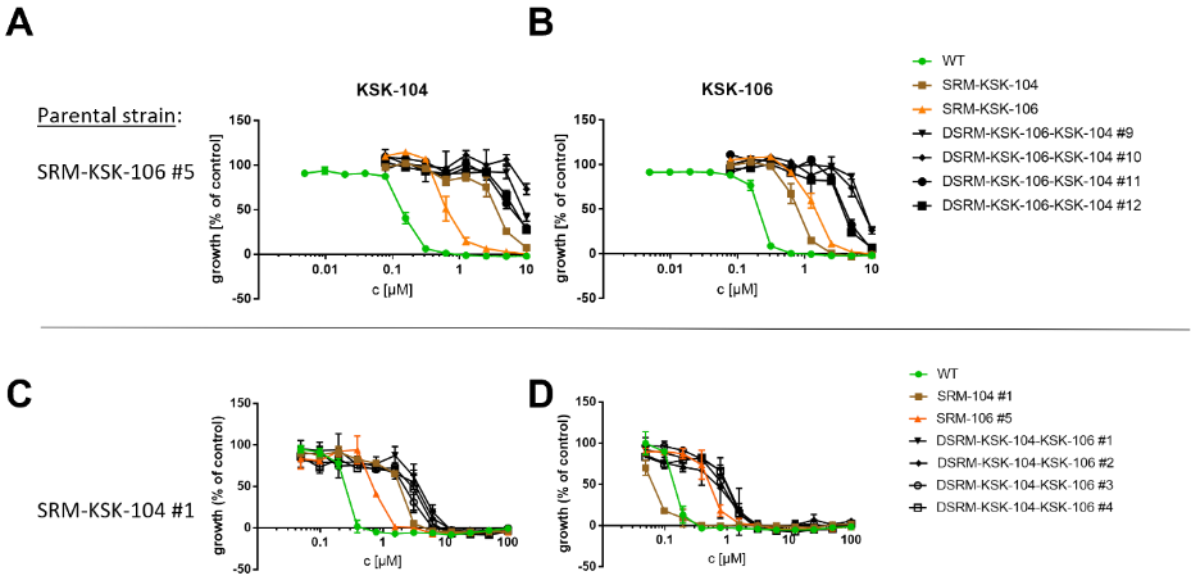

Figure 40: Resistance pattern of DSRM-KSK-104-KSK-106 against KSK-104 and KSK-106. Dose-response curve of different mutants (exemplary DSRM #1- DSRM #4; DSRM #9 – DSRM #12) of **(A-B)** DSRM-KSK-106-KSK-104, which uses SRM-KSK-106 #5 as a parental strain. It was incubated on agar plates containing the 8- to 10-fold MIC_{90} of KSK-104 and **(C-D)** DSRM-KSK-104-KSK-106, which uses SRM-KSK-104 #1 as a parental strain. It was incubated on agar plates containing the 8- to 10-fold MIC_{90} of KSK-106. **(A; C)** DSRM strains were tested against KSK-104 or **(B; D)** KSK-106. *M. tuberculosis* H37Rv WT, SRM-KSK-104 #1, and SRM-KSK-106 #5 are used as control. Data are shown as means of *n*=3 ±SEM.

To determine whether further resistance development also impacted other KSK derivatives, a selection of derivatives was tested against both DSRMs compared to the parental SRMs and the WT. Some KSK-104 and KSK-106 derivatives have been selected, representing different groups of derivatives. Among the KSK-104 derivatives (Figure 41), it was noticeable that ABK-275 showed little activity and was therefore excluded from further consideration. All other substances had the highest activity in the

WT, followed by SRM-KSK-106, DSRM-KSK-104-KSK-106, and SRM-KSK-104. The highest increase in resistance was seen in DSRM-KSK106-KSK-104 for each substance.

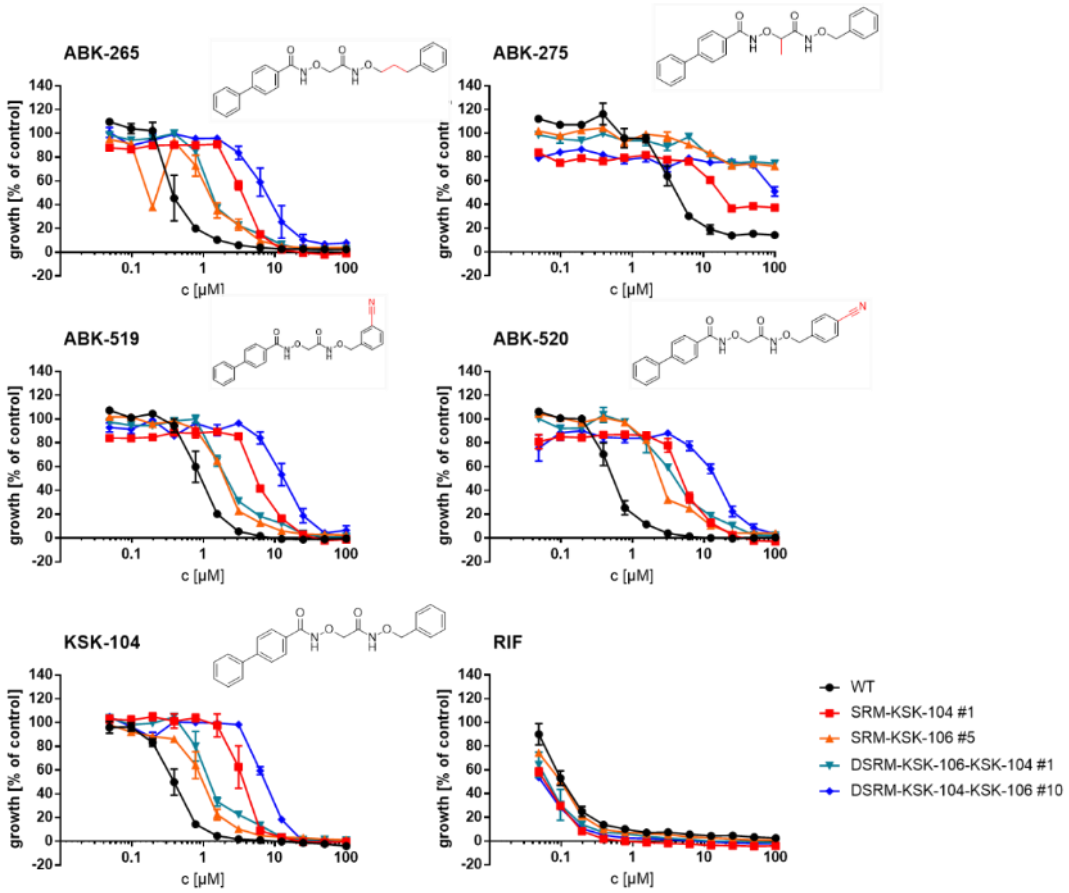

Figure 41: Resistance pattern of DSRMs and SRMs against several KSK-104 derivatives. Dose-response curve of different mutants (SRM-KSK-104 #1, SRM-KSK-106 #5, DSRM KSK-106-KSK-104 #1 and DSRM-KSK-104-KSK-106 #10 in comparison to H37Rv WT) against several KSK-104 derivatives. The red highlighted areas in the molecule represent the structural variation compared to the parental compound. Data are shown as means of *n*=3 ±SEM.

No specific resistance pattern was detectable for KSK-106-derived derivatives (Figure 40). For OMK-171, in which region A was altered, the most potent form of resistance formation was seen in SRM-KSK-104 and DSRM-KSK-106-KSK-104.

When the oxygen atom was exchanged against a carbon (ABK-257), SRM-KSK-104, SRM-KSK-106, and DSRM-KSK-104-KSK-106 behaved similarly to the WT. Only DSRM-KSK-104 has evolved more resistance. If the carbon-oxygen linker between regions B and C was omitted entirely, as in the case of OMK-170, the most prominent resistances were found in SRM-KSK-106 and DSRM-KSK-106-KSK-104. With an extended carbon chain (OMK-61), all strains except SRM-KSK-104 showed similar activity. Only SRM-KSK-104 showed better activity.

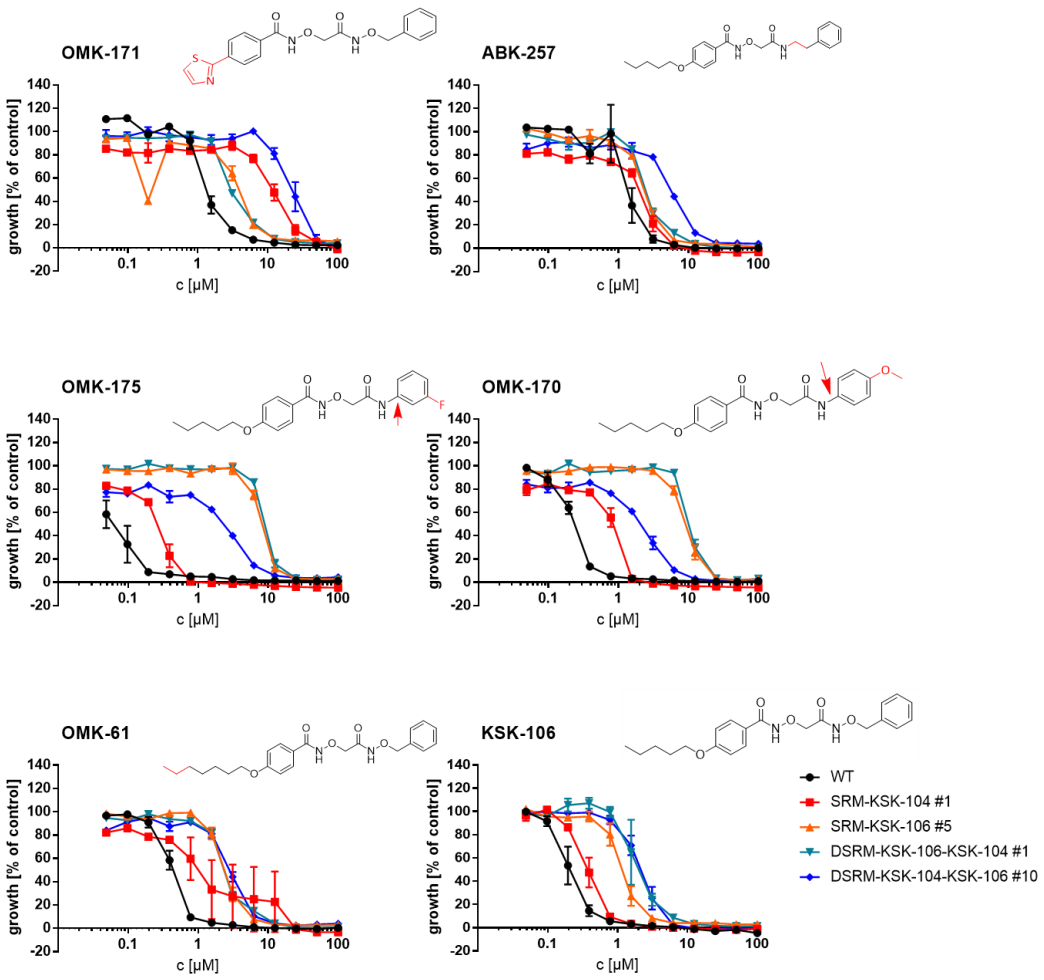

Figure 42: Resistance pattern of DSRM and SRM against several KSK-106 derivatives. Dose-response curve of different mutants (SRM-KSK-104 #1, SRM-KSK-106 #5, DSRM KSK-106-KSK-104 #1 and DSRM-KSK-104-KSK-106 #10, and H37Rv WT) against several KSK-106-derivatives. The red highlighted areas in the molecule represent the structural variation, whereas the arrow indicates the position of substituents that have been removed in comparison to the parental compound. Data are shown as means of *n*=3 ±SEM.

The result indicates that the KSKs and their derivatives are very complex structures with a complex mode of action. Minor changes can cause different activities and resistant patterns in SRMs and DSRMs. To obtain further information, the whole genome of the strains must be sequenced. One mutant (DSRM-KSK-104-KSK-106 #9) was sequenced by whole genome sequencing. It revealed mutations in *amiC*, *rv0552,* and *ppsA*, as shown in Table S2. In *amiC*, an insertion (of the bases cggc) at position 1046 has occurred, resulting in a frameshift. In *rv0552*, a base exchange has occurred, resulting in an amino acid change at position 276 from glycine to asparagine. In this double mutant, both amidohydrolases are mutated, which likely hinders one amidohydrolase from compensating for the other's activity. The protein encoded by the gene *ppsA* plays a role in cell wall biosynthesis, particularly of the PDIMs (see Chapter 3.2.4). Analyses

of further DSRMs, especially a DSRM-KSK-106-KSK-104, can lead to a conclusion about the different mutants. Which mutation leads to the different resistance patterns? This can then be analyzed in more detail concerning the different derivatives.

substance	structure	WT	SRM-104#1	SRM-106#5	DSRM-106-104	DSRM-104-106
OMK-171	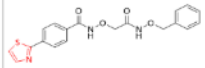	6.25	50	12.50	12.50	50
ABK-265	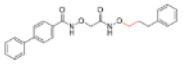	3.13	12.50	12.50	12.50	25
ABK-257	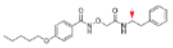	3.13	6.25	6.25	12.50	25
ABK-519	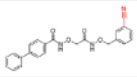	3.13	25	12.50	25	50
ABK-520	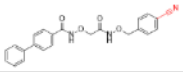	3.13	25	25	50	50
ABK-275	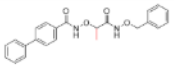	>100	>100	>100	>100	>100
OMK-175	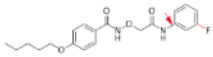	0.19	0.78	25	25	12.5
OMK-61	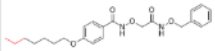	0.78	3.13	6.25	12.5	12.5
OMK-170	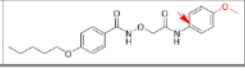	0.78	1.56	25	25	12.5

MIC_{90} [µM]
0.05 – 0.1
0.2 – 0.4
0.8 – 1.6
3.2 – 6.5
12.5 – 25
50 – >100

Figure 43: **Resistance pattern of DSRM and SRM of the KSKs against several KSK derivatives.** The table shows a heatmap of the MIC_{90} values in µM of several KSK-derivatives tested against different mutants (SRM-KSK-104 #1, SRM-KSK-106 #5, DSRM KSK-106-KSK-104 #1, DSRM-KSK-104-KSK-106 #10, and H37Rv WT). The red highlighted areas in the molecule represent the structural variation, whereas the arrow indicates the position of substituents that have been removed in comparison to the parental compound. MIC_{90}-values were determined in triplicates.

3.2.6 Affinity enrichment approach for identification of proteins putatively interacting with the KSKs

Different PEG3-biotin conjugated derivatives were designed and produced by RG Kurz to perform an affinity enrichment approach. Since the active moiety that is released by amidohydrolases from the KSKs is unknown, the biotin tag was added to different positions of KSK-104 and KSK-106, respectively. Figure 44 shows the PEG3-biotin conjugated derivatives. OMK-307 and OMK-312 are KSK-106 derivatives, whereas ABK-661 and ABK-662 are KSK-104 derivatives. ABK-661 can be derived from both molecules because region A, which distinguishes the two molecules, is missing. To better understand the structure, the PEG-3-biotin linker is highlighted in green, region C of the KSK molecule in blue, region B in black, and region A in red.

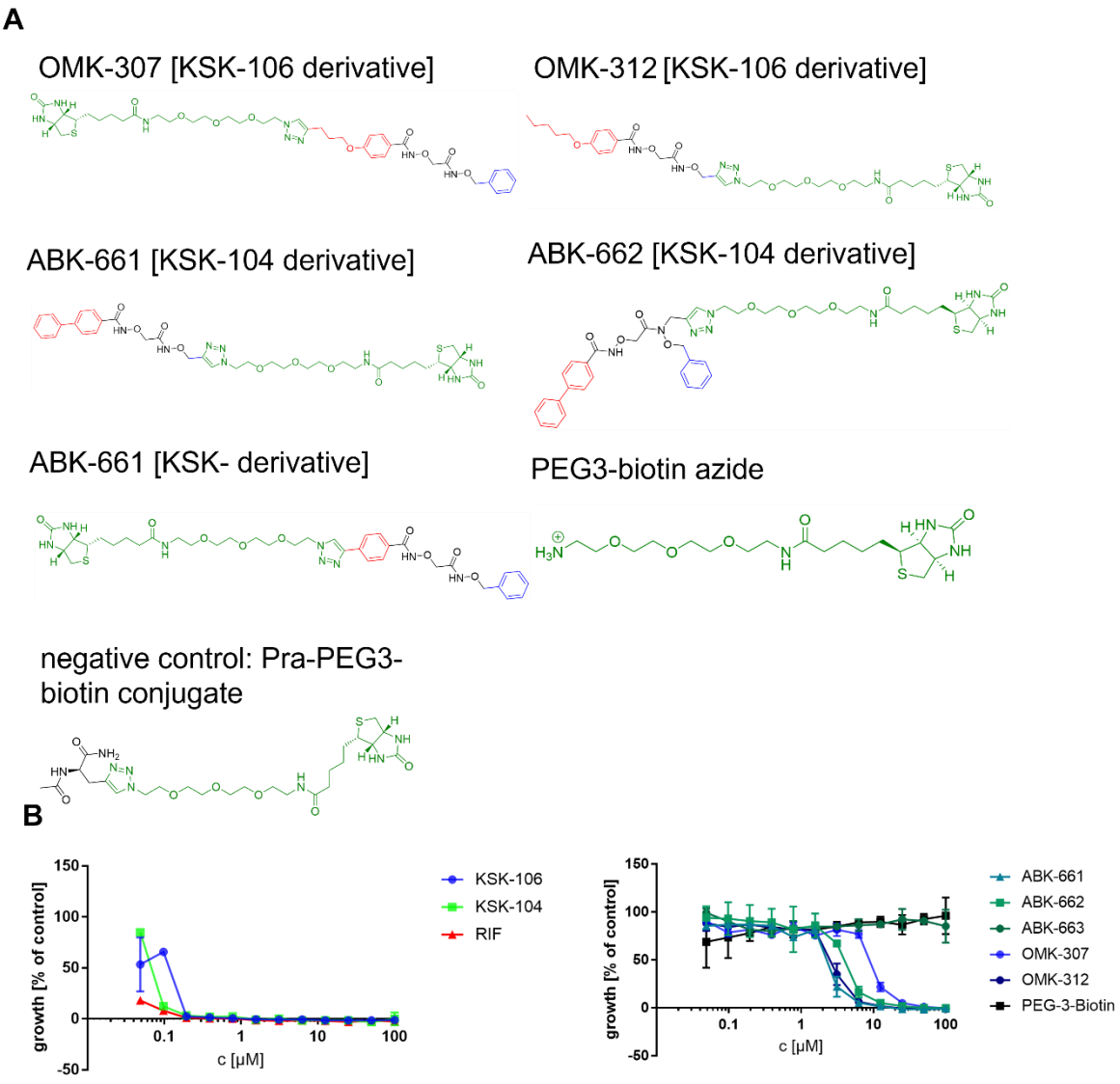

Figure 44: Growth inhibitory activity of PEG3-biotin-tagged KSK variants against *M. tuberculosis* mc²6230. PEG3-biotin azide was clicked to different KSK-104 and KSK-106 derivatives, resulting in two KSK-104 derivatives, ABK-661 and ABK-662, and two KSK-106 derivatives, OMK-307 and OMK-312, and one derivative, which cannot be assigned to either of the groups (ABK-661). The structures are shown in (**A**). Dose-response curves of these derivatives and the PEG-3-biotin azide alone against the attenuated *M. tuberculosis* strain mc²6230 are shown in (**B**). The reference compounds are KSK-104, KSK-106, and RIF. Data are shown as means of *n*=3 ±SEM.

To gain a deeper understanding of whether these PEG3-biotin-tags are influencing the activity of the KSKs and if these bigger molecules can still be internalized, *M. tuberculosis* strain mc²6230, an attenuated variant of *M. tuberculosis* H37Rv, was screened in a MIC assay against these compounds. The attenuated strain was used because the affinity enrichment approach should also be performed with this strain. The only differences between the virulent strain H37Rv and the attenuated version are the deletion of the RD1 region and the *panCD* genes. As positive controls, KSK-104 and KSK-106 were used. It is noticeable that ABK-663 and the negative control PEG-3-biotin

had no detectable anti-tuberculosis activity (MIC_{90} of >100 µM). All other derivatives exhibited a dose-dependent inhibition of growth with MIC_{90} values ranging from 25 µM for OMK-307, 12.5 µM for ABK-662 and OMK-312, to 6.25 µM for ABK-661. That means these molecules can be internalized and probably interact with their molecular target similarly like the parental KSKs to inhibit *M. tuberculosis* growth and, thus, meet a necessary requirement for this experiment. First, the KSK-106 derivatives OMK-307 and OMK-312 were used for an affinity enrichment approach with a protein lysate extracted from *M. tuberculosis* $mc^2$6230. These studies were performed in cooperation with the research group of Prof. Dr. Markus Kaiser and the Analytics Core Facility Essen (ACE, University of Duisburg-Essen, Germany). Total cytosolic protein lysate was prepared using bead-beating to disrupt the cells mechanically and induce cell lysis. The filter-sterilized lysate was incubated with OMK-307 and OMK-312, respectively, to allow the binding to putative target proteins. For competitive inhibition, KSK-106 was added to some of the approaches. These enriched proteins were bound to avidin-agarose, washed, and then on-bead digested and measured by LC-MS/MS. It is an approach for finding cytosolic targets or interaction partners. It does not give any information about targets, which are located in the membrane or lipids. Those proteins require solubilization out of membrane preparations by detergents, which are incompatible with this affinity enrichment procedure.

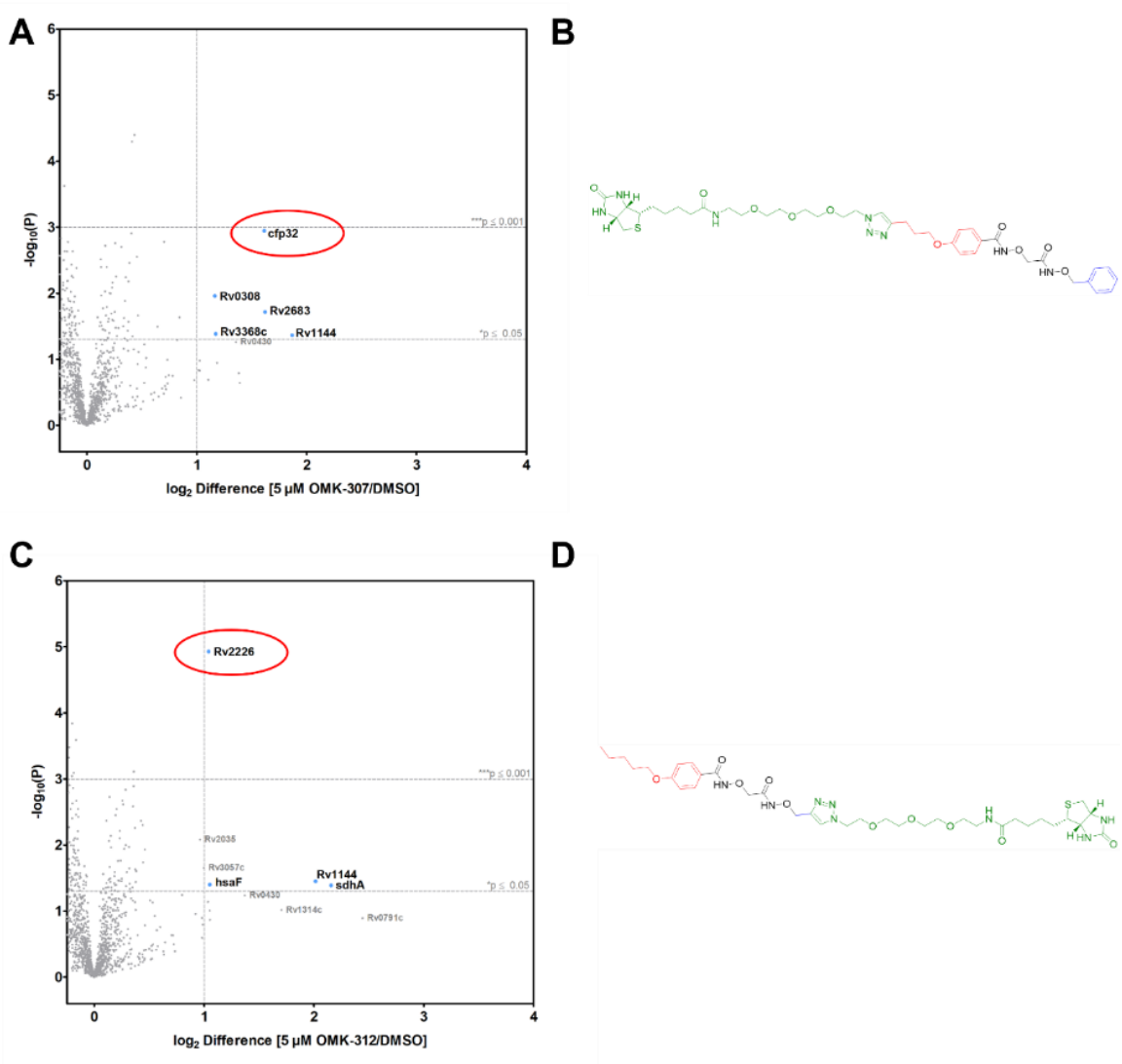

Figure 45: Affinity enrichment using PEG3-biotin-tagged KSK-106 variants and protein lysate of *M. tuberculosis* mc²6230. Biotin-tagged KSK-106 probes were used for the enrichment of putatively interacting proteins. These probes are **(A; B)** OMK-307 and **(C; D)** OMK-312, selected for identifying enriched proteins by LC-MS/MS after incubating them with the cytosolic protein lysate and the avidin agarose beads. **(A; C)** The enriched proteins were illustrated as volcano plots. The proteins circled in red are those that are considered best hits and had valid values in the analysis. It shows means of *n*=4 runs in comparison to the negative control. The experiment was performed in cooperation with the Kaiser group at the ACF (University of Duisburg-Essen, Germany).

After further analysis including subtracting background resulting from unspecific binding to PEG3-biotin, grouping of the technical replicates, and performing a t-test, only two proteins were found as probable hits in this experiment. Only weak enrichment was seen with the used probes, and most of the hits were statistical artifacts caused by the imputation of missing values. Nevertheless, Rv2226 seemed to be a potential candidate for OMK-312 binding. Additionally, Cfp32 was considered a probable hit, but the identification rate was not as confident as for Rv2226. Somehow the competition did not work in both cases, impairing the credibility of the identified hits. Alternatively, this might

also indicate a possible covalent mechanism, which would prevent bead-wash competition. The hits are shown in the volcano plot in Figure 45. For OMK-307, Cfp32 (Rv0577) was a candidate to look further at. It is a non-essential gene [265, 266] whose function is unknown, but it is a putative glyoxylase with a size of 261 amino acids [267]. Human glyoxylases, like GLO1 and GLO2, are key metalloenzymes involved in detoxifying reactive methylglyoxal into D-lactate using glutathione as a cofactor [268]. An interesting information about this is that the overexpression leads to resistance to pyrimidine-imidazole compounds [267]. It is a hint that the biotinylated KSK-derivatives could interact with the glycerol metabolization pathway. In another experiment, SRM against KSK-106 of *M. bovis* BCG Pasteur revealed a mutation in *glpK* in six of seven individual clones. They appeared twice at positions A68V, or L71F, and once at V423M and E277G. Because there are many hints that the KSKs could interact in the glycerol metabolism, the growth of *M. tuberculosis* was tested with different carbon sources in the presence of KSK-104 and KSK-106, which is described in Chapter 3.2.7.

For OMK-312, on the other hand, Rv2226 appears to be a good candidate in this context. A literature search reveals that it is a conserved protein with an unknown function. It is also a non-essential gene with a size of 513 amino acids [31, 266, 269]. Since the function is unknown in *M. tuberculosis*, the protein was blasted [256]. Orthologous proteins have an identity of 100% in *M. tuberculosis (*strain ATCC25177/H37Ra). This homolog is a CHAD and CYTH domain-containing protein [270]. Both functions are unknown yet. It is predicted that these two groups functionally interact with each other. The CHAD is predicted to be an alpha-helical domain. It contains conserved histidines, which could be crucial for its function. The CYTH domain could be an enzymatic domain, which may be involved in nucleotide or organic phosphate metabolism. It is predicted that these domains can chelate two divalent cations and have a reaction mechanism dependent on two metal ions. They furthermore could play a role in polyphosphate and nucleotide metabolism [271].

Since both proteins depend on metal ions, a zinc and iron chelating assay was performed for the KSKs to investigate whether they can chelate metal ions, like zinc or iron. This result is shown in Chapters 3.2.8 and 3.2.9.

3.2.7 The carbon source influences the activity of the KSKs

As there is some evidence that the KSKs might act on proteins involved in glycerol metabolism, the activity of KSK-104 and KSK-106 was tested in the presence of different carbon sources. To test the best concentration of cholesterol and glycerol, they were mixed in Sauton´s medium. Sauton's medium without additional glycerol consists of

limited carbon sources, with 2.0 g/l citric acid and 4.0 g/l asparagine. The growth behavior of *M. tuberculosis* was tested with different concentrations of carbon sources, and the OD_{600} was monitored at different time points. Figure 46A shows that the best growth conditions for the respective carbon source were 0.1% cholesterol and 0.5% glycerol. Previous experiments showed that Sauton´s medium supplemented with 1% glucose is optimal for cell growth. Since it is impossible to dissolve cholesterol in water or DMSO, a stock solution of cholesterol in MeOH was first prepared. To test the potential background growth resulting from the solvent, 7H9 medium containing 1% MeOH was compared to medium without MeOH. However, the influence of this amount of MeOH on the growth condition is not significant and can be disregarded.

The influence of the carbon source in the presence of KSK-104 and KSK-106 on the growth of *M. tuberculosis* determined by MIC assays is shown in Figure 46B and C. It demonstrates that KSK-104 and KSK-106 behave similarly. Both have the greatest growth inhibitory effect in the presence of glucose and glycerol. When cholesterol was added to the medium, the growth was comparable to that in the complex 7H9 medium. However, it is also noticeable that the activity of the KSKs is stronger in Sauton´s medium than in 7H9 medium. This can be explained by the fact that the 7H9-complex medium is perfectly adapted to the growth of *M. tuberculosis*. Worse conditions, as is the case in the Sauton´s medium, might cause stress to the cells, which may lead to an increased effect of the KSKs.

To make conclusions about the effect of KSKs with respect to the carbon source, a control experiment with other antibiotics should still be done. This could show that the effect is specific to the KSKs. If confirmed, this could indicate that the KSKs are involved in the carbon source metabolism, independent of cholesterol. The main carbon source used in energy metabolism is especially glycerol, but also glucose. Cholesterol is only an alternative carbon source [267, 272].

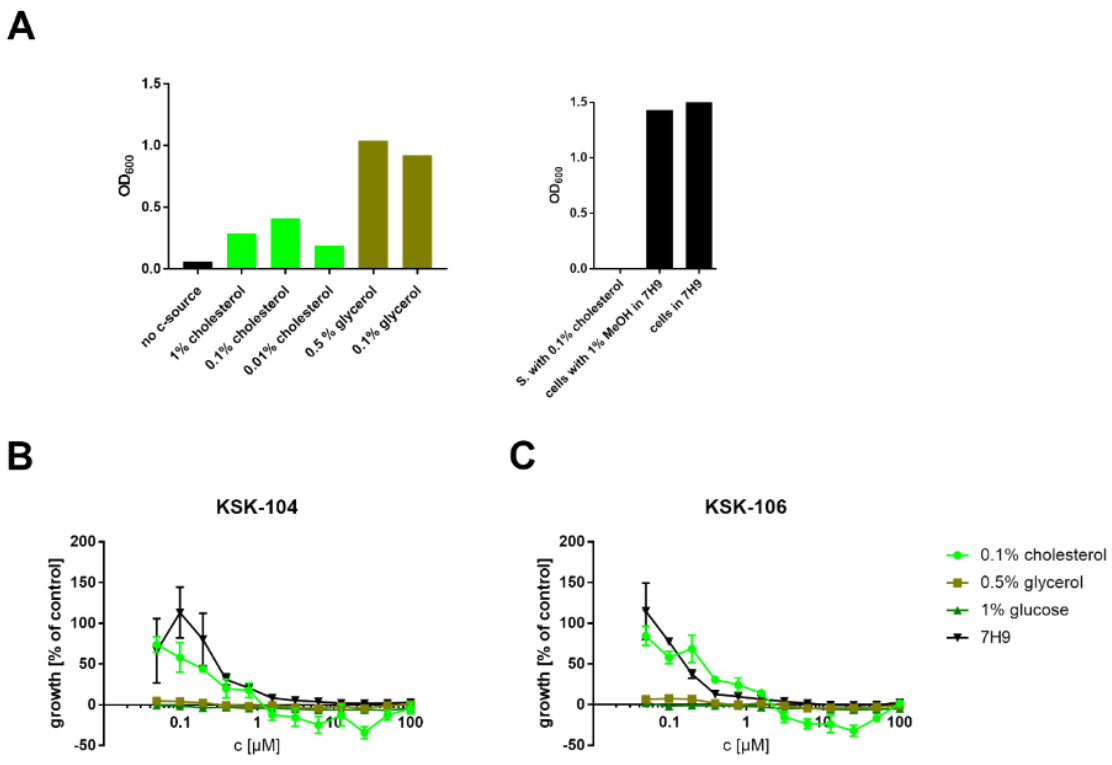

Figure 46: Influence of the carbon source on the growth of *M. tuberculosis*. **(A)** Cells were grown in Sauton´s medium supplemented with different concentrations of glycerol and cholesterol to find the best-fitting concentration of the carbon sources for the assay. Therefore, the optical density was measured after nine days. Dose-response curves of **(B)** KSK-104 and **(C)** KSK-106 are shown in the presence of the different carbon sources against *M. tuberculosis* H37Rv. Data are shown as means of *n*=3 ±SEM.

3.2.8 The KSKs are slightly chelating iron

There was evidence from the previous experiments that the KSKs might affect proteins that require metal ions for activity (see Chapter 3.2.6). An iron and zinc chelating assay was performed to investigate if the KSKs have a chelating ability. The zinc chelating assay is described in more detail in Chapter 3.2.9.

The basic procedure of the iron chelating assay is shown in Figure 47A. The substance is diluted and then mixed with Fe(II)Cl_2. After an incubation time, ferrozine is added to the mixture. Free Fe^{2+}-ions bind to ferrozine, which leads to a formation of a purple complex. In the absence of Fe^{2+}, the mixture remains colorless [273]. The result of the iron chelating assay is shown in Figure 47C for the substances shown in Figure 47B. There is a concentration-dependent effect for all tested compounds. The most effective chelating effect is detectable for the positive control EDTA. Ampicillin was also used as a positive control, and there was also a concentration-dependent chelating ability. The negative control was isoniazid. For that compound, no chelating effect was detectable in the tested range. KSK-104, KSK-106, KSK-107, and ABK-113 all showed no chelating

ability exceeding 40%. The only substance with a higher chelating effect was KSK-099. At the highest concentration of 10 mM, it had a chelating ability of about 60%. That means that all tested substances can chelate Fe^{2+}-ions to some extent. However, since the chelating effect occurred at concentrations by far exceeding the MIC_{90}, this can probably be ruled out as the mode of action.

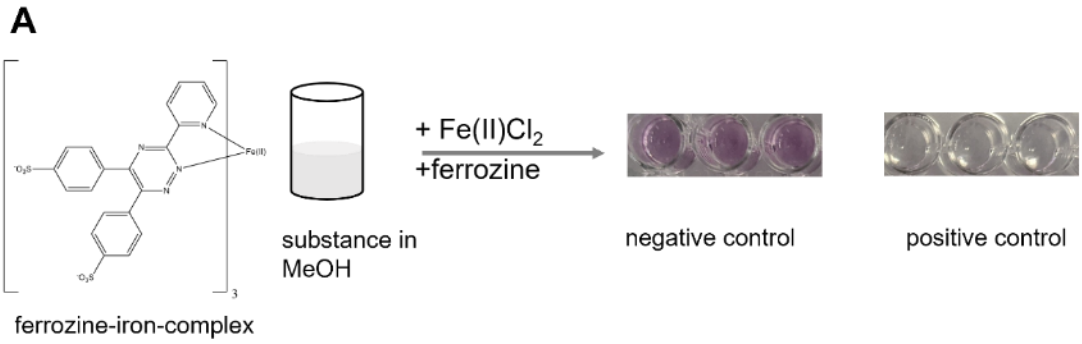

B

compound	structure	compound	structure
KSK-104		KSK-99	
KSK-106		KSK-107	
ABK-113		Isoniazid	
EDTA		Ampicillin	

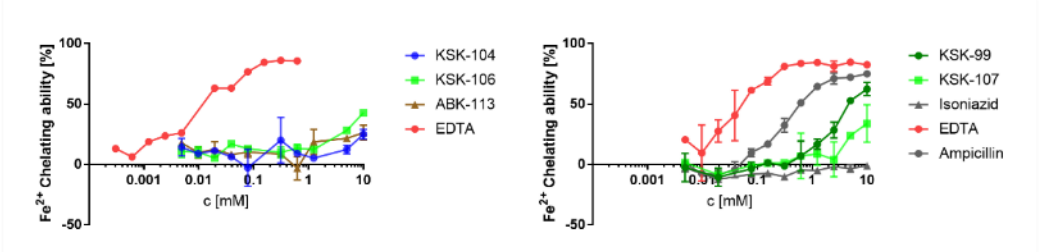

Figure 47: Iron chelating ability of the KSKs and their derivatives. **(A)** The basic mechanism of the Fe^{2+} chelating assay is shown with the relevant substances. **(B)** Structure and name of the used KSK-derivatives. **(C)** Dose-response curve of the resulting iron chelating activity in percent tested in the presence of different concentrations of the shown KSK derivatives. Data are shown as means of *n*=3 ±SEM.

3.2.9 The KSKs are not chelating zinc-ions

In the previous chapter, it has been shown that there is a very low Fe^{2+} chelating ability of the KSK derivatives. However, it is not clear whether this chelating ability is restricted to Fe^{2+} ions. To answer this question, a zinc chelating assay has been performed. The

substances shown in Figure 48B were added to dissolved zinc chloride and incubated. Dithizone was then added to the mixture. Dithizone is a substance that can form complexes. The substance alone is green and changes its color in complex with different substituents. In a complex with zinc ions, it turns pink [274]. Afterward, color development and zinc complex formation was measured (Figure 48A).

The result is shown in Figure 48C. The positive control EDTA had a potent zinc chelating ability, whereas no chelating ability was measurable for isoniazid in the tested concentration range. For ampicillin, there is only a weak chelating ability up to approx. 30%. No zinc chelation is detectable for any of the derivatives tested. It means that the mechanism of action of the KSKs should be independent of zinc chelation.

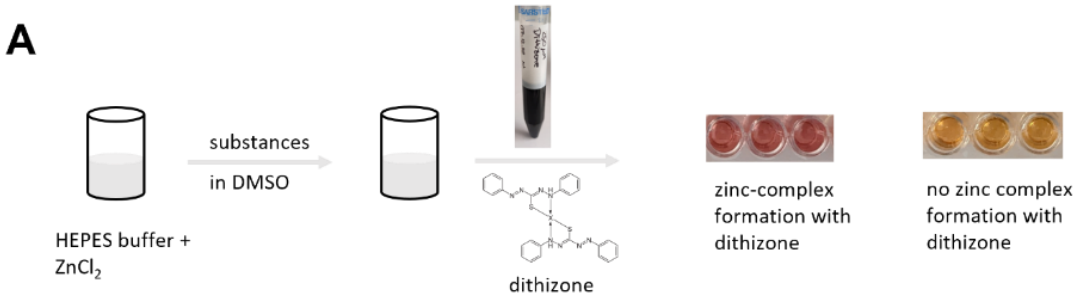

B

compound	structure
KSK-104	
KSK-106	
Isonazid	
Ampicillin	
EDTA	

compound	structure
Biphenyl-4-carboxylic acid (A104)	
4-Amyloxybenzoic acid (A106)	
Aminooxyacetic acid hemichloride (B)	1/2 HCl
O-Benzylhydroxamin hydrochlorid (C)	

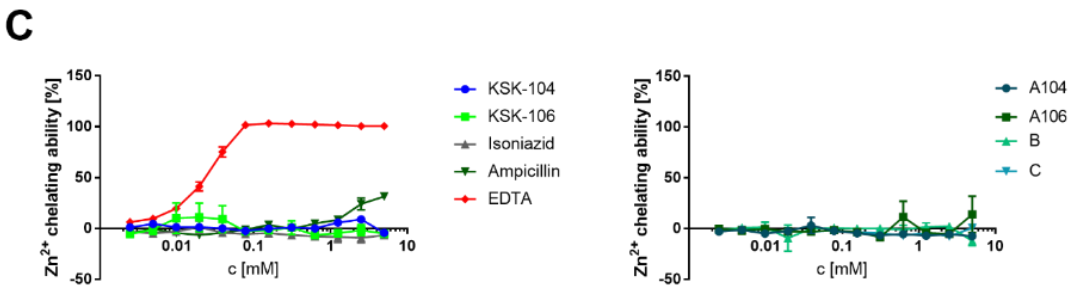

Figure 48: Zinc chelating ability of the KSKs and their cleavage products. **(A)** A schematic illustration of the basic mechanism of the Zn^{2+} chelating assay is shown with the most relevant chemicals. **(B)** The table shows the tested derivatives and control compounds with their structures and names. **(C)** Dose-response curves of the zinc chelating activity in percent tested in the presence of the compounds. Data are shown as means of *n*=3 ±SEM.

3.2.10 Characterization of fluorescent KSK-probes

As shown in previous experiments, the KSKs are likely cleaved by amidohydrolases. Nevertheless, their localization inside the bacteria and the exact mode of action following cleavage is still unknown. In the case of localization of the KSKs at the cell surface, it would indicate that the KSKs act on the cell wall. Fluorescent probes have been designed and prepared to obtain more information about their intracellular localization. One substance was tagged with a Cy5 fluorophore (OMK-399) and two with a FAM fluorophore (OMK-391 and OMK-376). In order to exclude that the attachments lead to inactivation, an MIC assay was initially performed. To get more information on whether these samples retain the same mechanism as the parental KSKs, they were also tested against SRM-KSK-106 and SRM-KSK-104. With a lower activity in one or both SRMs compared to the WT, it could be assumed that the fluorophore-tagged KSKs can still be cleaved by amidohydrolases. The fluorophore-tagged KSKs all showed a deterioration in activity compared to KSK-104 and KSK-106, but all still exhibited a concentration-dependent growth inhibitory effect. For OMK-376, only a slight resistance appeared in SRM-KSK-104 while SRM-KSK-106 behaved like the WT. OMK-391, on the other hand, was found to result in resistance in both SRMs. The reason for this could be attributed to the fact that both amidohydrolases AmiC and Rv0552 contribute to cleaving and subsequently activating this molecule. OMK-399 exhibited no detectable resistance in the tested SRMs. This indicates that the substance is equally well hydrolyzed by Rv0552 and AmiC so that inactivation of one enzyme is compensated by the other amidohydrolase. Alternatively, it can also not be ruled out that further amidohydrolases or different enzymes are mediating activation of this compound or that this compound does not rely at all on hydrolysis for activation.

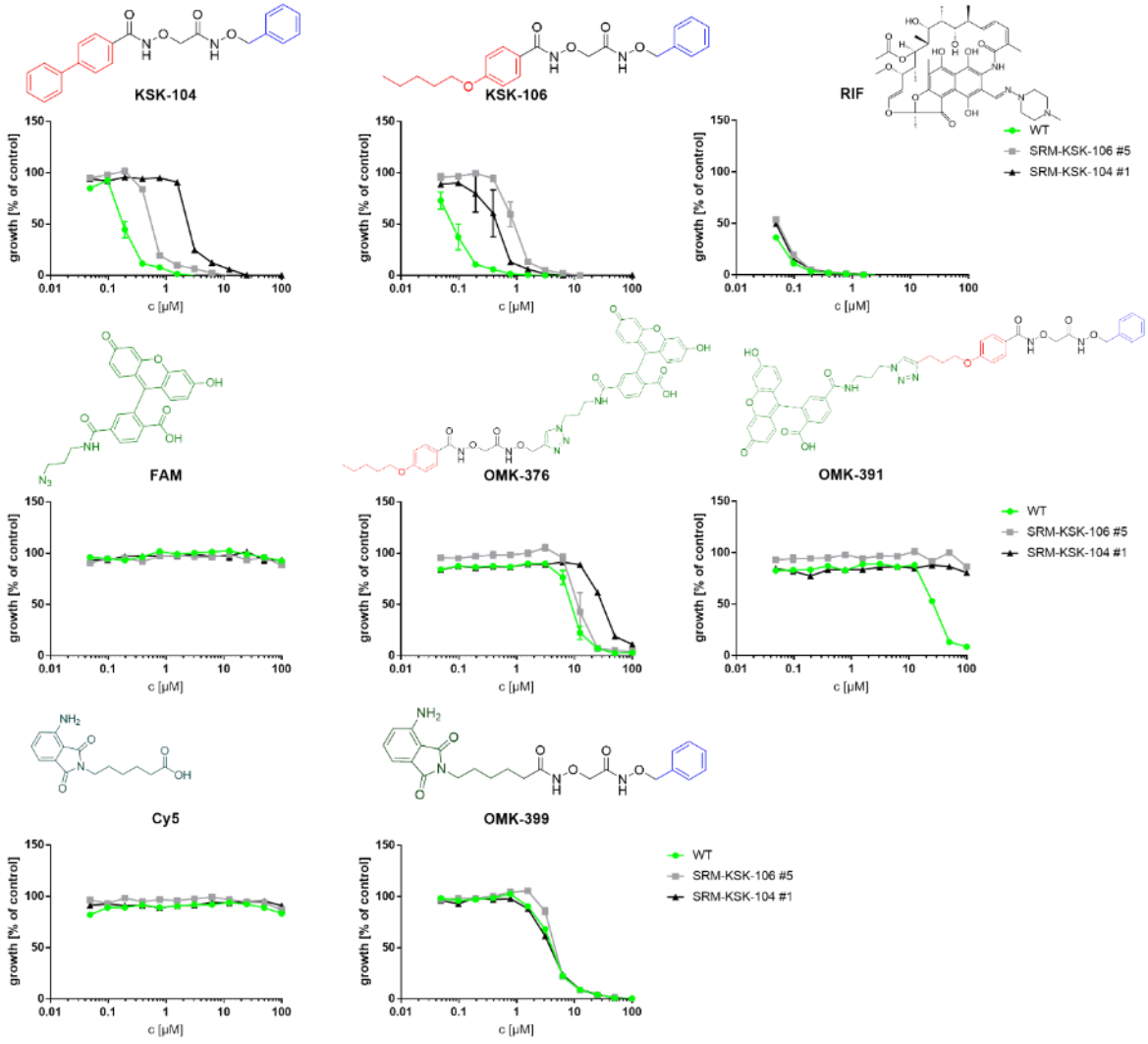

Figure 49: Characterization of fluorophore-tagged KSK-probes. Dose-response curves of different fluorophore-tagged KSK-derivatives tested against SRM-KSK-104 #1, SRM-KSK-106 #5, and H37Rv WT. The structure above the graph represents the analyzed molecule. The dark green highlighted areas in the molecule represent the fluorophore tag. Data are shown as means of *n*=3 ±SEM.

Therefore, the derivatives OMK-376 and OMK-391 are suitable for further microscopic studies as the fluorophore tag has minimal impact on their resistance mechanism and they are probably internalized because of their activity on whole cells. For this purpose, cells of the *M. tuberculosis* pBEN::mCherry (Hsp60) reporter strain, which constitutively expresses mCherry from the Hsp60 promoter, were incubated with the fluorescent KSK-derivatives, which were detectable in the green channel. Treatment with FAM was used as a reference. To rule out the possibility of detecting background fluorescence of untreated cells in the green channel, a DMSO control was used as a negative control and analyzed with the Nikon Eclipse TS100 fluorescence microscope. This control, however, showed no signals in the green channel (excitation 475 nm, emission 510 nm)

but red fluorescence in the red channel (excitation 585 nm, emission 610 nm) (Figure 50). These red spots represent cells of *M. tuberculosis*.

The cells were next incubated with the probes at 1-fold MIC_{90} for two days and subsequently washed twice to remove the non-internalized compounds from the cell surface. In the case of a signal in the green channel, this could, therefore, only originate from an internalized substance.

Green signals were visible for both tested substances. For OMK-391, however, the signal intensity is weak, but there was co-localization of the fluorophore and the cells in both cases. It shows that both substances can be taken up. Referring to the cleavage of the KSKs and the fact that FAM alone is not found inside the cell, this shows that the position of the fluorophore does not significantly influence the internalization of the KSKs, also shown by the MIC_{90} values. For more precise statements about the localization, the samples need to be imaged with a microscope with a higher resolution. Since both samples faded very quickly during microscopy, a spinning disk, in which the exposure with the laser is reduced to a minimum, would be most suitable.

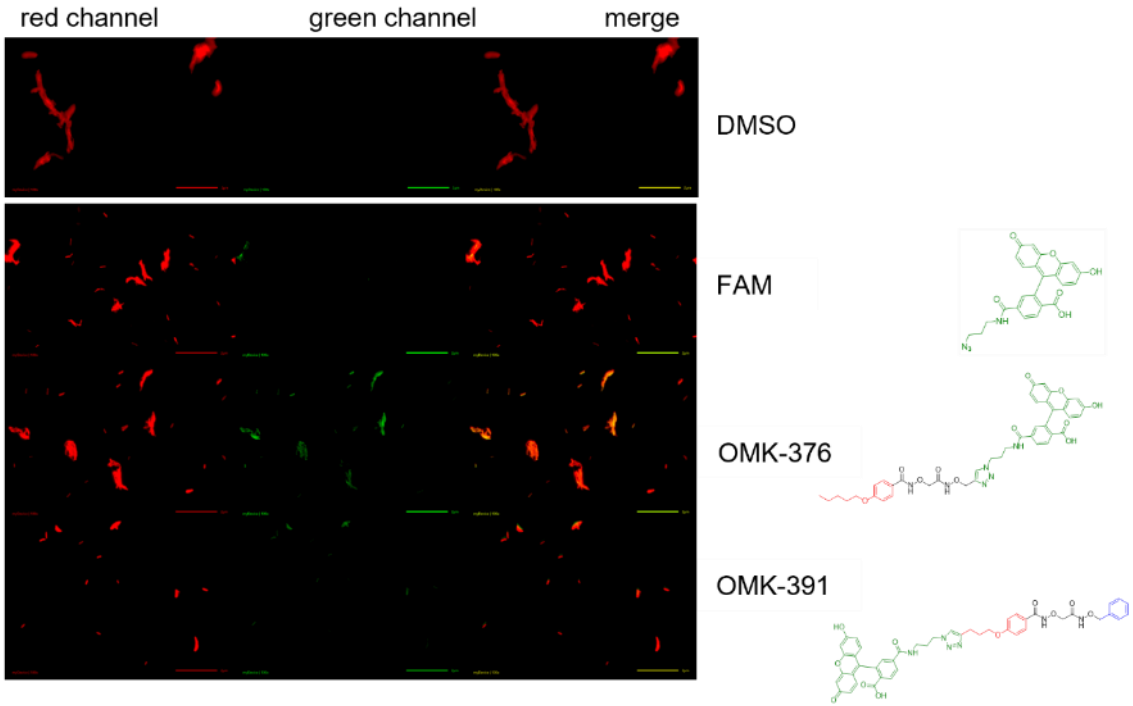

Figure 50: Microscopic analysis of fluorophore-tagged KSK probes. 1-fold MIC_{90} of the compounds on the right was incubated with the *M. tuberculosis* pBEN-mCherry reporter strain for two days. After washing, fixing, and adding to the prepared poly-D-lysine slides, they were analyzed using a Nikon Eclipse TS100 fluorescence microscope (600 ms exposure time, 100 x magnification). The scale bar represents 20 µm. Merged pictures were created using Fiji (ImageJ).

3.2.11 A pharmaceutical formulation for the KSKs

Given that the KSKs have excellent anti-tubercular activity also against pre-XDR-TB strains while exhibiting no cytotoxicity, further preclinical efficacy studies in a relevant animal infection model would be the next logical step to assess whether the observed *in vitro* effects can translate into *in vivo* conditions. Furthermore, the fact that the compounds require activation by amidohydrolases raises the questions whether certain host hydrolases might also be capable of cleaving the KSKs before internalization by mycobacterial cells, which would strongly curtail their *in vivo* efficacy.

For the pending mouse trials, however, suitable formulations were needed allowing peroral (PO) and intravenous (IV) administration to the animals, respectively. The biggest obstacle was that the KSKs were difficult to dissolve in aqueous solutions. In cooperation with RG Kurz, different mixtures were tested. Finally, a mixture of 80% propylene glycol and 20% water has been found for PO administration. For IV administration, 20% propylene glycol, 5% DMSO, 5% Tween-80, and 70% saline solution were used. To exclude that the formulation harms the activity of the substances, the KSKs were tested in these formulations for their activity. Figure 51 shows the result of this test. The KSKs behave almost the same regardless of the solvent with nearly no differences in the growth of *M. tuberculosis* visible in the presence of the different formulations for KSK-104 and KSK-106. The formulations have the same efficacy as the control in which the KSKs are dissolved in DMSO, meaning that IV and PO formulations are well-suited for the pending mouse experiments.

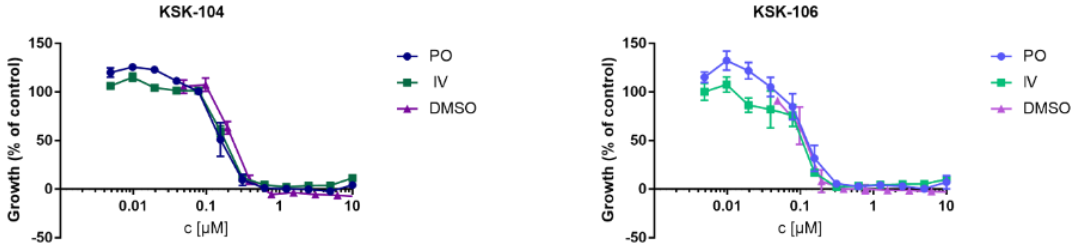

Figure 51: Activity of the KSKs in different formulations. Dose-response curve of *M. tuberculosis* H37Rv against KSK-104 (left) and KSK-106 (right). PO is the peroral formulation comprising 80% propylene glycol and 20% water. In the intravenous (IV) mixture, the KSKs are solved in 20% propylene glycol, 5% DMSO, 5% Tween-80, and 70% saline solution. Data are shown as means of *n*=3 ±SEM.

3.3 The thiazole-containing substance FFK-088

In a screening of substance library provided by the RG Kurz, multiple compounds were tested against diverse bacteria, and among them, a compound containing a thiazole group exhibited promising activity against *M. tuberculosis* H37Rv. Therefore, further tests have been carried out and are shown in the following chapters.

3.3.1 FFK-088 is a new lead structure

A library of compounds was tested to discover new active substances against *M. tuberculosis*. Here only a selection of 24 substances is shown. They are characterized by the presence of a thiazole group as a common structural element. FFK-088 (= ethyl 4-(4-((tert-butoxycarbonyl)amino)phenyl)thiazole-2-carboxylate) turned out to be the most active compound with an MIC_{90} of 0.78 µM. The substituent at the fourth position in the phenyl ring is particularly emphasized. FFK-088 can be divided into three regions. The left region, shown in pink in Figure 52A, consists of a butyloxycarbonyl (Boc) protected amino group and will be mentioned as region A in the following. The middle region consists of a phenylthiazole. This is shown in black and is defined as region B. Region C, which consists of an ethyl ester, is highlighted in green.

The comparison with the other analogues showed that small but also large changes lead to a drastic decrease in activity. Examples of changes in region A include the replacement of the carbamate moiety with a corresponding amide moiety (FFK-423). It already led to an increase in the MIC_{90} to 6.25 µM. This suggests that while the presence of the oxygen atom at this position is crucial for achieving high activity, it is not strictly mandatory. The presence of pyrrolidine instead of the entire A region also led to the same MIC_{90} value (FFK-193). The results show that substituents containing nitrogen are suitable at this position. It is supported by many derivatives that do not have nitrogen in region A, such as FFK-125, FFK-175, FFK-176, FFK-87, FFK-163, and FFK-168, exhibiting less activity compared to FFK-088. It is furthermore possible that there is a requirement for a *para*-substitution. FFK-196 is *ortho*-substituted, which led to a deterioration of the activity to an MIC_{90} of 25 µM. That indicates that *para*-substitution is much better for anti-tubercular activity than *meta*- and *ortho*-substitution. The presence of the terminal tert-butyl-group appears to be important for the activity. An indicator for this is that the trichloroethyl group at this position led to a complete loss of activity (FFK-415; also seen in: FFK-275; FFK-421). Region C appears to be essential for the activity. The complete absence of this region (FFK-497) resulted in an MIC_{90} of 25 µM, and the exchange of the ester moiety to an amide moiety led to a complete loss of activity (FFK-

498). This is an indication that FFK-088 could be a prodrug. Generally, amide moieties are more stable than an esters making cleaving difficult, while esterases can cleave esters rather easily [272].

In summary, FFK-088 is a substance with good anti-tubercular activity. Besides the thiazole group, other regions, such as region C, are responsible for the activity. Although FFK-088 has by far the best activity, five other molecules have an activity of up to 12.5 µM and many more with an activity of 25 µM, which provides many possibilities for changes within the molecule without leading to a complete loss of activity. SAR analysis with more derivatives needs to be performed for more detailed information. In the following, FFK-088 will be examined in more detail as the most active derivative.

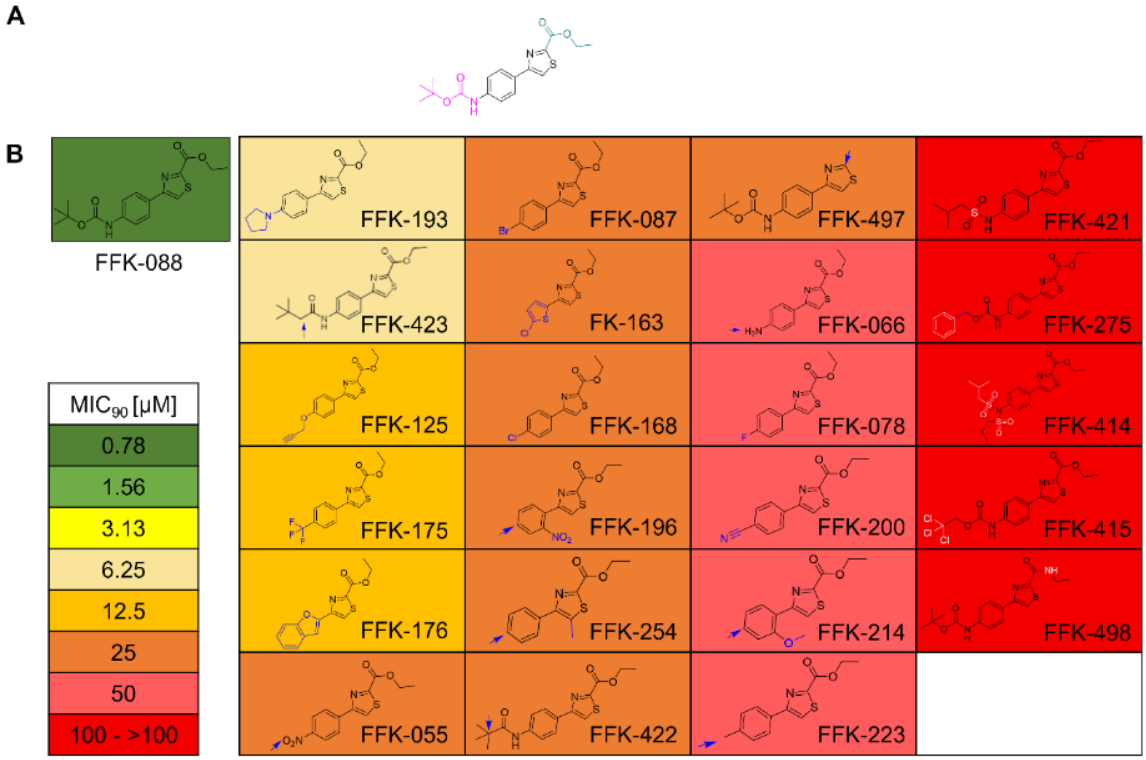

Figure 52: Heatmap representing MIC_{90} values of different FFK-088 derivatives. (A) Structure of FFK-088, the most active substance and presumed lead structure. In this, region A is pink, region B is black and region C green. **(B)** Heatmap of the substances sorted by their activity. The blue, or white highlighted areas in the molecule represent the structural variation, whereas the arrow indicates the position of substituents that have been removed in comparison to the parental compound. Fabian Fischer, University of Düsseldorf, Germany, has synthesized all derivatives. The heatmap shows a color code of the MIC_{90}, which was determined in triplicates.

3.3.2 FFK-088 has activity against *M. tuberculosis* H37Rv

To analyze the selectivity of FFK-088, it was first tested against different mycobacteria. Figure 53A shows the concentration-dependent course of growth inhibition of FFK-088 against *M. tuberculosis* H37Rv. This resulted in a MIC_{90} of 0.78 µM. The compound has been further tested against *M. bovis* BCG Danish 1331 as another slow-growing

mycobacterium (Figure 53B). FFK-088 had an activity with an MIC_{90} of 6.25 µM. With that result, it is less effective against *M. bovis* than against *M. tuberculosis*. *M. smegmatis* mc^2155 has been selected as a fast-growing mycobacterium. However, FFK-088 had no effect at all in the tested concentration range. While only a narrow spectrum of mycobacteria were tested, this already suggests a high selectivity of the substance towards *M. tuberculosis.*

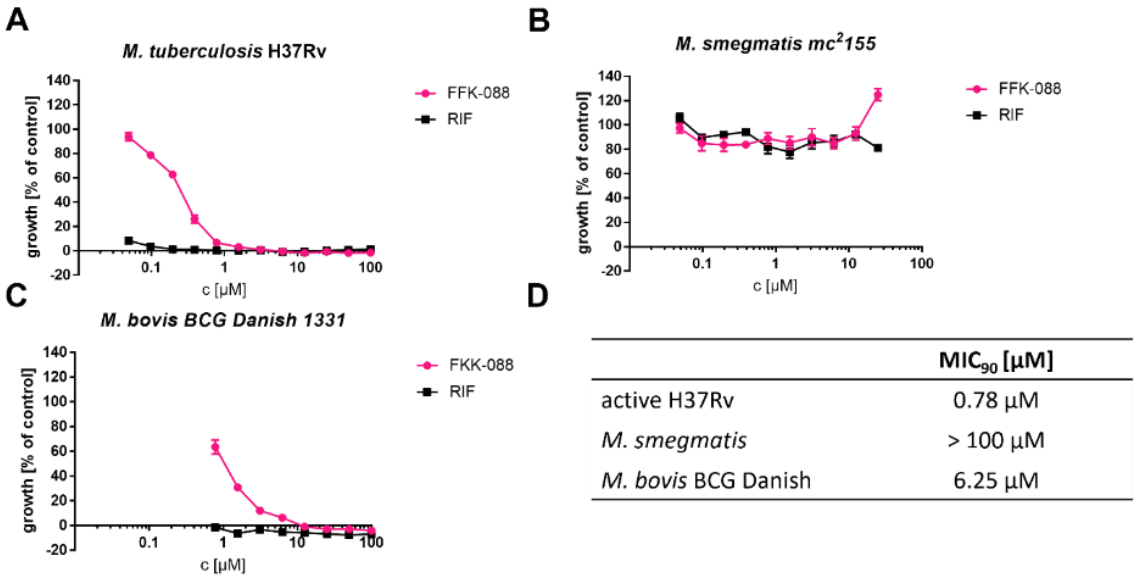

	MIC_{90} [µM]
active H37Rv	0.78 µM
M. smegmatis	> 100 µM
M. bovis BCG Danish	6.25 µM

Figure 53: Activity of FFK-088 against different mycobacteria. Dose-response curve of FFK-088 and RIF against **(A)** actively growing H37Rv WT, **(B)** *M. smegmatis,* and **(C)** *M. bovis* BCG Danish. **(D)** Table of MIC_{90} values resulting from **A**-**C**. Data are shown as means of *n*=3 ±SEM.

To get the first information about the mechanism of action, the compound has been tested against pre-XDR TB. These are clinical isolates with resistances, as described in Chapter 1.3.3. Figure 54 shows the result of this MIC screening. All isolates tested are resistant to RIF but have sensitivity towards BDQ. Regarding activity to FFK-088, the result showed that none of the tested isolates exhibited strong resistance. Compared to the WT, which has an MIC_{90} of 1.56 µM, pre-XDR clinical isolates KZN #13 and KZN #14 had a MIC_{90} of 3.13 µM, KZN #6 of 6.25 µM and only KZN #16 had a significant change to an MIC_{90} of 25 µM. Overall, this result indicates that FFK-088 likely has a novel mechanism of action, as there was no consistent resistance for the pre-XDR strains. The mutations present in the pre-XDR strains make them resistant to 10 different antibiotics as described above (see Chapter 1.3.3) [137]. If FFK-088 had a mechanism of action comparable to any of these antibiotics, significant resistance to FFK-088 would also likely have occurred.

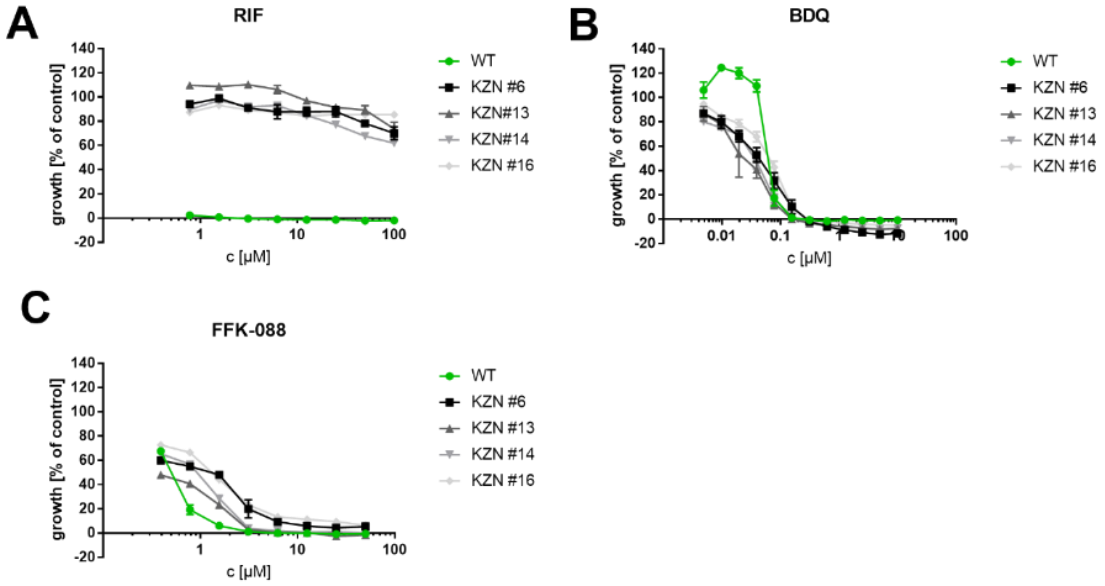

Figure 54: Activity of FFK-088 against *M. tuberculosis* pre-XDR clinical isolates. Dose-response curve of several clinical isolates (KZN #6, KZN #13, KZN #14, KZN #16) in comparison to H37Rv WT screened against **(A)** RIF, **(B)** BDQ as controls, and **(C)** FFK-088. Data are shown as means of *n*=3 ±SEM.

Next, various cell lines were used to assess the cytotoxic potential of FFK-088, namely THP-1, HEK293, and HuH7. Thus, also potential renal- and hepatotoxic side effects could be addressed. However, dose-response curves showed strong selectivity as there was no cytotoxicity in the measured concentration range. Growth inhibition of the human cell lines was detected at 100 µM (in THP-1) or >100 µM. This resulted in a selectivity index of ≥128, corresponding to a large therapeutic window.

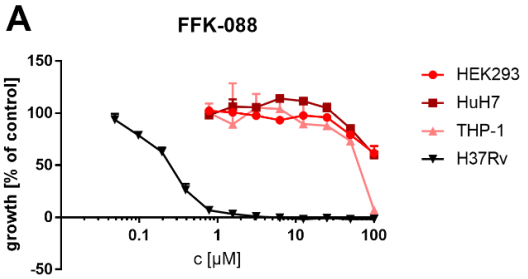

B

cell line	IC_{50} / MIC_{90}
HEK-293 (IC_{50})	>100 µM
Huh-7 (IC_{50})	>100 µM
THP-1 (IC_{50})	100 µM
H37Rv (MIC_{90})	0.78 µM
SI (IC_{50}/MIC_{90})	≥128

Figure 55: Cytotoxicity of FFK-088. (A) Dose-response curve of FFK-088 against *M. tuberculosis* H37Rv compared to its cytotoxicity against various human cell lines (HEK293, HuH7, and THP-1). Data are shown as means of *n*=3 ±SEM. **(B)** Table of MIC_{90} and IC_{50} values resulting from **A**. The selectivity index (SI) was calculated as a ratio between IC_{50} and MIC_{90} values.

3.3.3 FFK-088 is not inhibiting intracellular replication of *M. tuberculosis* in a macrophage infection assay

Since *M. tuberculosis* is a pathogen that replicates and persists intracellularly in macrophages, the growth inhibitory effect of FFK-088 against internalized bacteria is also of great interest. In this study, a macrophage infection assay was performed. For this purpose, THP-1 cells were stimulated by PMA to differentiate to macrophage-like cells. These cells were infected with a reporter strain of *M. tuberculosis*, which is constitutively expressing mCherry, allowing monitoring of intracellular growth by fluorescence microscopy. Three hours post-infection, macrophages were treated with FFK-088 or the control antibiotics RIF and STREP. The result was analyzed 5 days post-infection. The cells only treated with DMSO showed signs of high bacterial burden. They have also started to detach from the surface. The cells that were not infected (UI) had a healthy morphology and no fluorescence signals, as no bacteria were added to the cells. It is worth mentioning that the cells treated with STREP showed only a slight decrease in fluorescence intensity compared to the DMSO control. The determined integrated density of red fluorescence signals was around 50% compared to the DMSO-treated control. The addition of RIF led to healthy cell morphology and only a marginal fluorescence signal of about 9%, as illustrated in Figure 57. Surprisingly, using 5x MIC_{90} of FFK-088 had no visible effect on fluorescence signals compared to the DMSO control. Also, the detected fluorescence density decreases by only about 24% compared to the DMSO-treated cells. Even the treatment with 10-fold MIC_{90} did not have a much stronger influence. The fluorescence density decreased by only about 32% compared to the DMSO-treated cells. It means that FFK-088 had no strong intracellular killing effect.

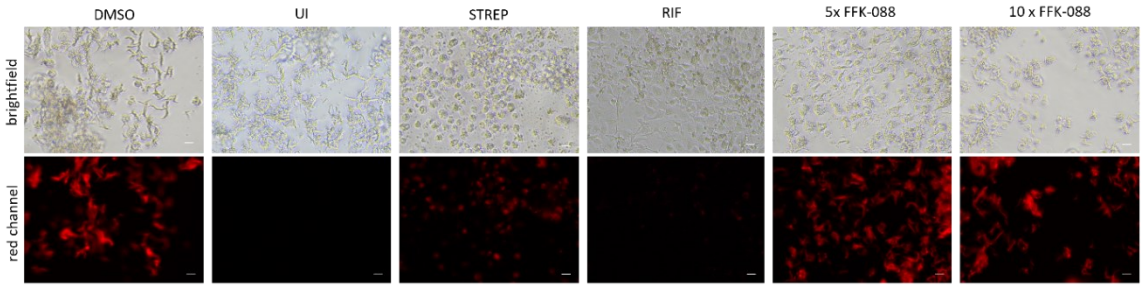

Figure 56: Intracellular activity of FFK-088 in a macrophage infection model. The THP-1 cells were differentiated into macrophage-like cells using PMA. These cells were infected with a mCherry expressing reporter strain of H37Rv for three hours and then treated with 20 µM STREP, 3 µM RIF, 3.9 µM (5x MIC_{90}) or 7.8 µM (10xMIC_{90}) FFK-088. Control cells were treated with 0.2% (v/v) DMSO, and all cells were analyzed using fluorescence microscopy (500 ms exposure time, 100 x magnification). The result is representative of two independent experiments. The scale bar represents 50 µm.

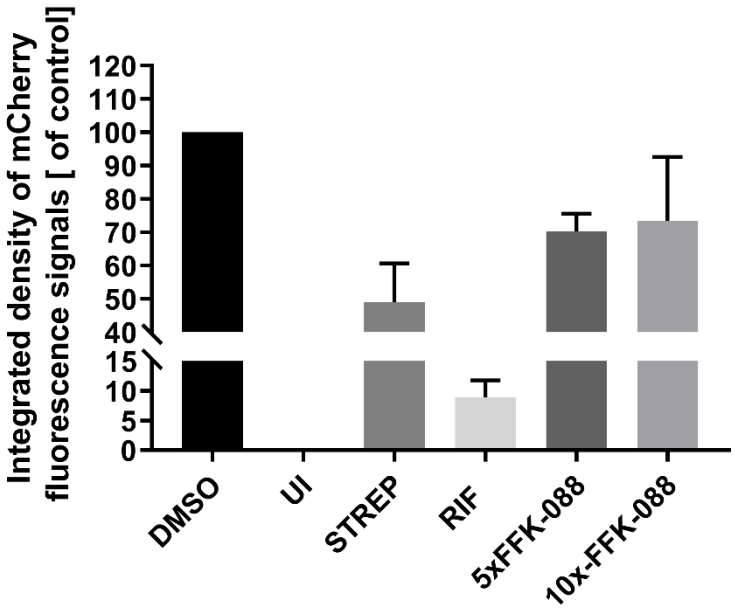

Figure 57: Integrated density of mCherry signals compared to DMSO. The THP-1-derived macrophage-like cells were infected with an mCherry expressing reporter strain of H37Rv for three hours and then treated with 20 µM STREP, 3 µM RIF, 3.9 µM FFK-088 (5x MIC_{90}) and 7.8 µM FFK-088 (10x MIC_{90})**.** Control cells were treated with 0.2% (v/v) DMSO. Cells were analyzed using fluorescence microscopy. For each approach, five fields per view were analyzed using Fiji (ImageJ), and the percentage of the integrated density was calculated compared to the DMSO control (100%) and the uninfected (UI) control (0%). Error bars represent SEM.

3.3.4 Killing kinetics of FFK-088

Since the anti-mycobacterial activity of FFK-088 was demonstrated, this raised the question of how FFK-088 acts. As tuberculosis therapy is a combination therapy and thus several antibiotics are administered simultaneously, any new antitubercular drug candidate must not have antagonistic effects with these antibiotics. Thus, the fractional inhibition concentration index (FICI) was tested for FFK-088 against RIF, and DELA. The index indicates a partial synergistic effect for RIF (FICI: 0.75) and DELA (FICI: 0.625). This result is already auspicious. Therefore, killing kinetics of various combination treatments was measured next to corroborate these findings.

Table 9: Fractional inhibitory concentration index (FICI) of FFK-088. Calculated FICI values of the analysis of FFK-088 in combination with the antibiotics RIF and DELA.

	FICI-Index	
0.1 mM RIF	0.75	partial synergistic
0.5 mM DELA	0.625	partial synergistic

For this purpose, the viability of compound-treated *M. tuberculosis* cells was analyzed for 45 days (Figure 58A). These killing kinetics showed that FFK-088 in monotreatment had a bactericidal effect for approx. 4 days. After that, the cells start to grow again. When looking at the effects of combination treatments, the combination of FFK-088 with INH, led to a synergistic effect. The viable cell count decreased for a longer time, leading to a 2-log reduction in viability. This bactericidal effect was evident for the first 11 days of treatment, after which a plateau phase was reached lasting for another ten days. Subsequently, the cell count slowly increased again. A robust synergistic effect was detectable for the combination with the three other antibiotics, ETB, RIF, and DELA. The cell count steadily decreased over 45 days, leading to a 4-log reduction in viable cell numbers expressed as CFU/mL. It should be noted that no development of resistance and, thus, no increase in cell count could be detected with the respective combinations. With the individual antibiotics used in monotreatment, regrowth of cultures could already be seen after days 11 to 20. That indicates a positive drug-drug interference for FFK-088 with DELA, INH, RIF, and ETB.

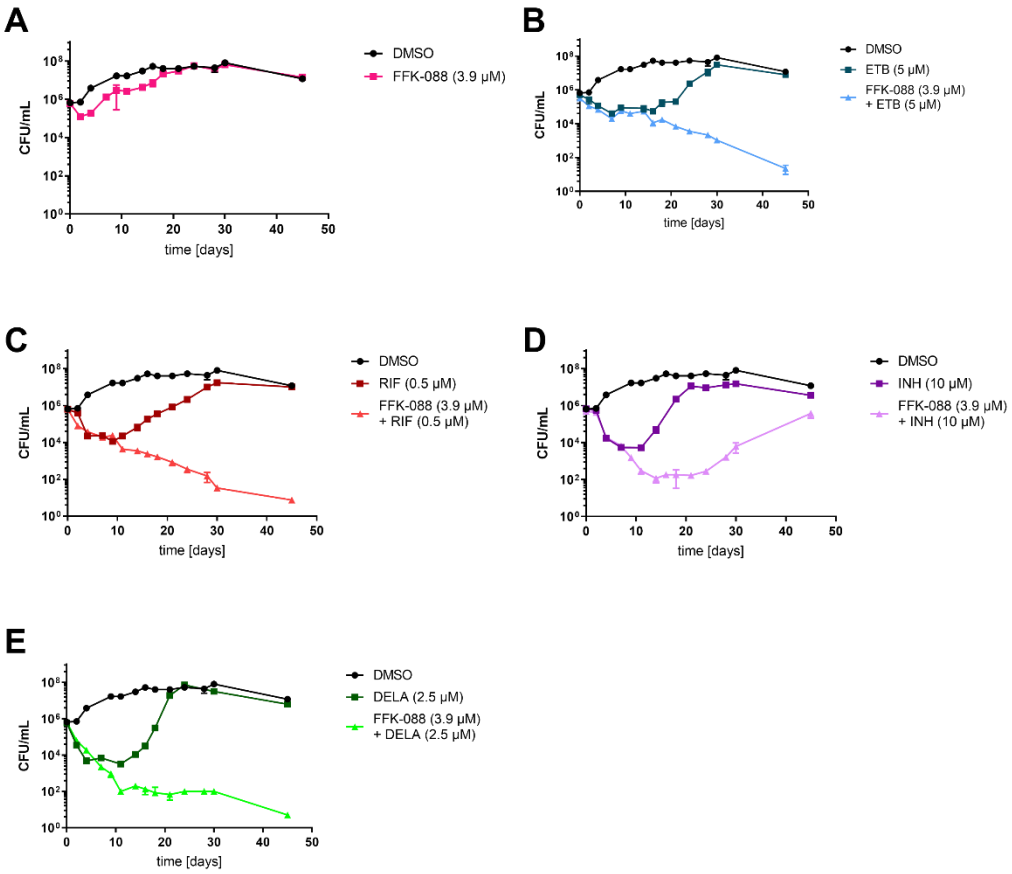

Figure 58: ***In vitro* killing kinetic of FFK-088 in *M. tuberculosis* H37Rv.** *M. tuberculosis* H37Rv was treated with the shown antibiotics alone or in combination with 3.9 µM FFK-088. **(A)** The monotreatment of FFK-088 results only in a short-lived slightly bactericidal effect, after which growth resumes quickly. In combination with different drugs **(B-E),** FFK-088 shows strong synergistic effects that potentiates the bactericidal effect of the tested antibiotics (squares) and either delays (INH) or suppresses (ETB, RIF, DELA) regrowth of the bacteria that is seen in monotherapy during the observed 45 day time frame. Experiments have been performed in triplicates. The limit of detection was 100 CFU/mL until day 24, and 10 CFU/mL for the following time points.

3.3.5 Spontaneous-resistant mutants of FFK-088 have mutations in different genes

To obtain further information on the mechanism of action of FFK-088, spontaneous resistant mutants were generated by plating and incubating *M. tuberculosis* H37Rv on medium containing 10-fold MIC_{90} of FFK-088. After five weeks of incubation, mutants appeared at a frequency of 10^{-7}. Individual clones were incubated, and resistance was analyzed by MIC assay. The result of this is shown in Figure 59A. It is noticeable that the examined mutants only had a four-fold decrease in sensitivity, whereas the susceptibility against RIF was unaltered. Since there was only low-level resistance, SRM-FFK-088 #13 was again plated on a medium with 10-fold MIC_{90} of the SRM #13 to obtain a stepwise increase in resistance. Mutants were formed with a frequency of 10^{-8}.

Some of these have been re-incubated and analyzed by MIC assay. Figure 59D shows that two independent clones exhibited a strong resistance phenotype, resulting in a MIC_{90} of >100 µM. In a second approach, the WT was plated again on a medium with a 10-fold MIC_{90} of FFK-088. Interestingly, one isolated clone (SRM 1.4) already showed high-level resistance but with a different pattern than all other tested mutants (Figure 59C). To obtain an indication of the mechanism of action, the genomic DNA of some of these clones was isolated and subjected to whole genome sequencing.

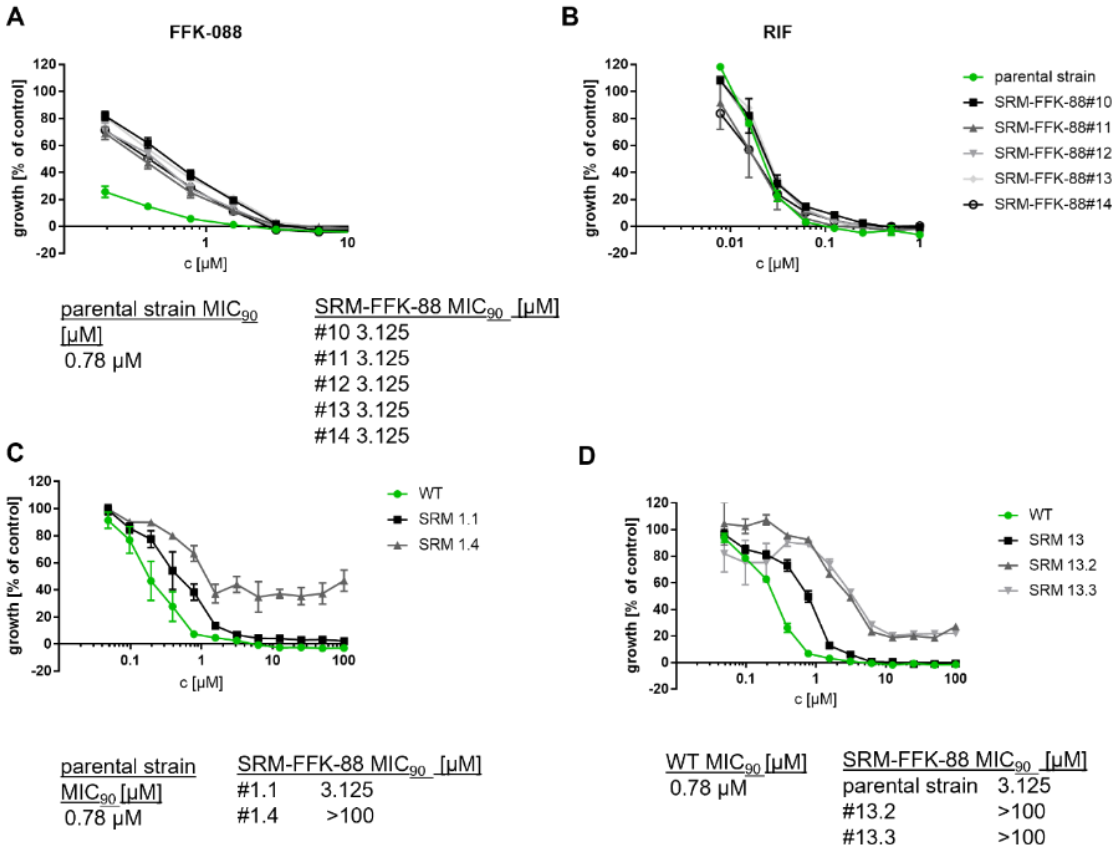

Figure 59: Resistance pattern of SRM-FFK-088 against FFK-088. Dose-response curve of different mutants (SRM #10- SRM #14) tested against **(A)** FFK-088 and **(B)** RIF. Dose-response curve of **(C)** SRM 1.1 and SRM 1.4, which were created in a second approach, **(D)** SRM 13.1-13.3 formed by replating SRM-FFK-088 #13. All SRMs were isolated by plating cells on a medium containing 10-fold MIC_{90}. M. tuberculosis H37Rv WT is shown as a control. The resulting MIC_{90} values are shown underneath the graph. Data are shown as means of n=3 ±SEM.

Interestingly, mutations have occurred in various genes whose proteins play a role in diverse processes. Many of these genes have not been characterized in *M. tuberculosis* yet. SRM 13 has a mutation in *Rv2714*, which encodes a conserved alanine and leucine-rich protein whose function is still unknown. A BLAST analysis showed 100% identity to PAC2 family proteins that act as chaperones for the 26S proteasomes, which mediate ubiquitin-dependent proteolysis [275]. Another mutation has occurred in the gene *guaB*,

which encodes a guanosine monophosphate reductase. It plays a role in the purine salvage pathway, in which guanosine monophosphate is converted to inosine monophosphate (IMP). This catalysis is dependent on NADPH [276]. It can be positively regulated by GTP and negatively regulated by ATP based on pH. Although it is not essential in *M. tuberculosis*, it may regulate purine nucleotides by recycling guanosine monophosphate to inosine monophosphate [277]. Another mutation occurred in *Rv0674*. It is a conserved hypothetical protein with an unknown function. A BLAST analysis revealed that it is a PaaX domain-containing protein. About these proteins also little is known. In *E. coli,* it could be linked to the regulation of the expression of proteins involved in the metabolism of phenylacetic acid. Some members contain a winged-helix DNA-binding domain [278, 279]. Another mutation has occurred in the gene *fadA6*. However, this is a silent mutation and therefore has not been further investigated. The same mutations occurred in mutants 13.2 and 13.3, which is plausible since both were generated from the same parental strain SRM-FFK-088 13. In 13.2, however, an additional mutation occurred in *pirG*, probably leading to stronger resistance. This gene encodes a surface-exposed protein, which is required for multiplication and intracellular growth [280]. Recent studies have classified PirG as a virulence-associated factor, and Rv2212, which is responsible for cAMP production, was found to be a direct binding partner in a yeast two-hybrid system [281]. In SRM 13.3, two further mutations were found. One mapped to *Rv2346*, but since it is a silent mutation, it probably does not influence the resistance of the bacteria and was therefore not further considered. However, there was a second mutation in *pks7*. It codes for a probable polyketide synthase potentially involved in an intermediate step of the polyketide synthesis. These polyketides could be involved in secondary metabolism [30, 282]. However, the specified function is unknown, yet.

In SRM 1.4, different mutations appeared. There was a mutation in *Rv0991c*, coding for a conserved serine-rich protein with an unknown function. There is evidence that it is a molecular chaperone activated by oxidation. It appears to function analogously to the *E. coli* redox-regulated chaperone Hsp33. It promotes refolding by an Hsp70 chaperone system and can interact with DnaK and many other proteins. With this, the authors propose that it protects the bacteria from proteotoxicity during oxidative stress [283]. Finally, there was a mutation in *fadD28.* It is involved in phthiocerol dimycocerosate (DIM) biosynthesis and has thus been linked to the cell wall biosynthetic pathway and drug resistance [284].

In summary, the analysis of SRM did not identified genes that were consistently found mutated in all resistant clones. Thus, the analysis did not directly revealed an obvious

resistance mechanism for FFK-088. Therefore, further analyses need to be done to find the target and mechanism of action of FFK-088.

Table 10: SNPs identified in FFK-088 spontaneous resistant mutants.

Mutant	Gene	Mutation	Function
SRM 13	**guaB1**	S465 A t→g	Probable inosine-5'-monophosphate dehydrogenase GuaB1(imp dehydrogenase) (IMPDH) (IMPD)→ **SNP**
	Rv0674	T146 R c→g	Conserved hypothetical protein → **SNP**
	Rv2714	Del 531-t	Conserved alanine and leucine rich protein → Deletion leading to a **frameshift**
	fadA6	G131 G c→g	Probable acetyl-CoA acetyltransferase FadA6 (acetoacetyl-CoA thiolase) → **silent mutation**
SRM 13.2 (further mutations)	**pirG**	T58R	Surface-exposed protein required for multiplication and intracellular growth. Seems to play a role in virulence. → **SNP**
SRM 13.3 (further mutations)	Rv2346c	G39G t→ c	Putative ESAT-6 like protein EsxO (ESAT-6 like protein 6) → **silent mutation**
	pks7	V1504 G t → g	Probable polyketide synthase Pks7 → **SNP**
SRM 1.4	**Rv0991c**	T55 A a → g	Conserved serine rich protein → **SNP**
	fadD28	T489 W c → g	Involved in phthiocerol dimycocerosate (dim) biosynthesis → **SNP**

4 Discussion and Outlook

Today, *M. tuberculosis* is found almost everywhere in the world. Due to the development of resistance to first-line antibiotics, a wide variety of second-line antibiotics are used for treatment. As a result, resistance to these antibiotics has also developed, leading to XDR-TB and even TDR-TB. TDR-TB are resistant to all standard antibiotics [134]. It shows the critical situation concerning antibiotic resistance. After the golden era of antibiotics, very few new agents have entered the market, and only three antituberculars have been added in the last decades (see Chapter 1.3.3.1). Resistance has been found for all but pretomanid so far [285]. Some promising compounds are still in the clinical development pipeline for anti-TB drugs [286]. However, it is crucial to find new lead structures with new modes of action to act against XDR- and TDR-TB. This work analyzed three lead structures with anti-mycobacterial activity in more detail, as discussed below.

4.1 Chlorflavonin as an antibiotic lead structure against *M. tuberculosis*

In previous studies, CF was found to be active against *M. tuberculosis* in a natural product screen. Further analysis has shown that CF inhibits the IlvB1 catalytic subunit of AHAS. It blocks the *de novo* biosynthesis of BCAA such as valine, leucine, isoleucine, as well as of pantothenic acid. Currently, no approved anti-TB drug is known to inhibit AHAS or any enzyme in BCAA biosynthesis [225, 287]. It makes CF a good lead structure for the development of new drugs. With natural substances, there is often the problem that they can only be obtained in small quantities, making further analysis very difficult. Therefore, chemical synthesis of CF has been established in RG Kurz [253]. It also enabled to synthesize derivatives of CF that allow SAR studies. In the process, another very active substance was found, BrF. BrF has comparable activity to CF with an MIC_{90} of 0.78 µM, and the synthetic CF variant has an MIC_{90} of 1.56 µM. Further analysis also showed that BrF and CF have no cytotoxicity against the tested cell lines, such as the monocyte cell line THP-1 or lung fibroblast cell line MRC-5. High anti-bacterial activity and no cytotoxicity are essential elements for discovering new drugs. To identify whether BrF and CF have similar mechanisms of action, compounds have also been tested *in vitro* in the AHAS enzyme assay [233]. It was shown that BrF also inhibits the condensation of pyruvate to acetolactate in a concentration-dependent manner. For all these reasons, it can be assumed that BrF has the identical mechanism

as CF, and therefore both have been used and analyzed as potential new lead structures. Another characteristic of an excellent new compound is the presence of activity against clinical pre-XDR isolates. Since the mechanism of action of CF and BrF are already known, activity should also be found against them. The hypothesis could also be confirmed, as both have only minor changes in activity compared to the WT. This decrease in activity is probably due to a decreased fitness caused by the mutations in XDR strains [288]. This activity against these pre-XDR clinical isolates demonstrates the relevance of CF and BrF. Interestingly, activity was found only against slow-growing mycobacteria, such as *M. tuberculosis* H37Rv, the attenuated *M. tuberculosis* $mc^2$6230, and the two vaccine strains *M. bovis* BCG Pasteur and *M. bovis* BCG Danish 1331. Almost no activity was found against the fast-growing mycobacteria *M. smegmatis* and *M. marinum*. As the name suggests, the doubling time is the most significant difference between these two groups. This results in a wide variety of differences. An important factor is an endowment with porins in the cell wall. This can lead to different cell wall permeabilities due to different pore sizes and densities, ion selectivities, and conductivities [289]. Another factor is the different metabolism, e.g., malate metabolism [290]. One explanation would then be that due to the differences in the cell wall, or porins, CF does not enter the cell and thus cannot inhibit IlvB1. However, the different activities cannot be explained by the absence of IlvB1 because, according to the BLAST analysis, this enzyme is found in all tested species. However, according to BLAST research, there are some IlvB1 homologs present in other mycobacteria, but not all of them are present in in *M. tuberculosis* [225]. Perhaps these homologs, which are not present in *M. tuberculosis,* take over the activity of the inhibited IlvB1 in the variants without inhibition of CF [291]. There are two ways to test this method: one is to examine the AHAS activity of recombinantly expressed IlvB1 homologs that are absent in *M. tuberculosis* using the AHAS assay, and the other is to clone the missing IlvB1 homologs into *M. tuberculosis* and determine if the CF activity is reduced.

The classical SAR performed as part of this dissertation could only provide a few general clues about the structural requirements responsible for the activity of CF. This is due to the fact that even very minor structural changes led to a complete loss of activity. In the course of 52 tested derivatives, only two could be found with good activity (CF and BrF), two with acceptable activity (BLK-248 and ABK-516 MIC_{90} of 6.25 µM and 25 µM) and two with detectable activity (ABK-535 and TAKK-210; MIC_{90} of 50 µM) (see Chapter 3.1.1). All others had no growth inhibitory effect on *M. tuberculosis*. The loss of activity of this high number of substances, even with minor structural changes, may result from various factors. Examples are the reduced permeability through the cell wall, further

metabolization by a wide variety of enzymes, reduced interaction with the active site of the catalytic subunit IlvB1, or solubility problems in the medium [253, 289]. An indication of inactivation or the absence of anti-mycobacterial activity should bring different methodological approaches. For some derivatives, a yellow precipitate could already be detected by eye when the dilution series of the MIC assay was prepared.

For this reason, the solubility of some substances was determined in the medium in cooperation with Talea Knak (RG Kurz). It showed that some of the inactive substances precipitated strongly, while others did not precipitate at all. It means that a solubility problem cannot be the only explanation for the inactivity [253, 292]. To investigate whether the derivatives have lost activity only in *M. tuberculosis* and may still show activity in other mycobacteria, all have been tested against slow- and fast-growing mycobacteria (Chapters 3.1.6). However, neither in *M. bovis* BCG Pasteur, *M. bovis* BCG Danish 1331 nor in *M. smegmatis* any significantly better growth inhibitory effect could be detected for the tested analogues. Since there was no antimycobacterial activity of CF and BrF in *M. smegmatis*, the inactivity of the other derivatives was expected. In contrast, in the *M. bovis* BCG strains, it was astonishing that all other derivatives had no growth inhibitory effect. It means that the individual differences between the mycobacteria, such as metabolism or different ABC transport systems or porins for uptake, also do not lead to an improved activity compared to *M. tuberculosis* [289]. Another possibility of lack of activity of a substance is metabolism by bacterial enzymes. Examples of these enzymes, which make the bacteria resistant to the drug, are hydrolases, e.g., β-lactamases, which catalyze antibiotic hydrolysis [293, 294]. This could also mean that the derivatives are inactivated by enzymes present in all tested mycobacteria. However, since there is anti-mycobacterial activity of CF and BrF against some of the tested mycobacteria, it is unlikely that the enzymes can bind and inactivate all derivatives except CF and BrF. Another example are transferases, which covalently attach various chemical groups to the antibiotics. The main groups differ in the type of modification, mechanism of action, and substrate specificity [293, 295, 296]. CF has been analyzed as an active substance to understand whether *M. tuberculosis* enzymes might modifiy the inactive substances. CF was compared to TAKK-009 as an inactive substance, and the UV-spectrum after different incubation periods with *M. tuberculosis* has been investigated using a Dionex-HPLC (Chapter 3.1.7). Here, CF behaved similarly to TAKK-009, and after 8 days of incubation, a second smaller peak could be seen eluting just before the compound in both cases. These results suggest that *M. tuberculosis* may have a slow-acting mechanism that degrades or alters CF. CF is also possible to be covalently bound to cell wall components and was not efficiently extracted by methanol

inactivation and bead beating. Due to the significant decrease in peak height for both compounds, both likely behave similarly. It is conceivable that both derivatives can be internalized. It is more complicated to isolate the internalized compounds instead substances from the supernatant. However, this allows us to rule out metabolization as inactivation mechanism for this substance. For more detailed information, more derivatives should be tested similarly or analyzed with an LC-MS/MS to exclude conversion in any way as an inactivation method.

The last and most important question was if the inactive compounds cannot bind to the active site of IlvB1, and with this, they cannot inactivate IlvB1. In order to provide an answer, all derivatives were tested in the enzyme assay employing purified IlvB1 protein (Chapter 3.1.4) [233, 235]. Based on available crystal structures of AHAS proteins (*Saccharomyces cerevisiae* and *Arabidopsis thaliana;* PDB IDs 1T9C and 1YBH*),* a homology model was generated for *M. tuberculosis* IlvB1, and molecular docking with CF was performed by Rehberg *et al.* [297, 298]. It showed that CF can bind into the putative active site of IlvB1 and forms salt bridges, hydrogen bonds, a π-π interaction, and a cation- π interaction. The chlorine atom acts as a lipophilic appendage to fill the hydrophobic subpocket, lined by leucine 65, methionine 512 and valine 513. It may lead to better binding affinities [225]. The CF derivatives were designed with this model in mind. Surprisingly, there are nevertheless many derivatives that have no inhibitory effect on IlvB1 *in vitro*. However, it turns out that, for example, the bromide atom can take over the task of the chloride atom. Also, the exchange to a fluorine atom, an iodine atom (data not shown), or a trifluoromethyl group can inhibit this enzyme although the inhibition is not as strong as for CF. The inhibition, for instance, is poorest with the trifluoromethyl group, which is likely linked to steric parameters. It is worth pointing out, however, that other halogens in this position are acceptable and provides mediocre activity toward the isolated protein *in vitro*. However, since they had no growth inhibitory effect in the MIC assay except for BrF, this suggests that these substances do not pass through the cell wall due to their physicochemical properties and, thus, do not have anti-mycobacterial activity. These halogen elements are electronegative elements with an oxidizing ability. Except for bromide, they are essential nutritional elements. Drugs with bromide atoms have a long history. They were used in the mid-1800s as anticonvulsants and sedative-hypnotics [299]. They have been almost entirely replaced by discovering better agents, such as barbiturates. It is also because many patients who took bromide-containing drugs had bromide intoxications (LD_{50} = 14 mg/kg), which include vomiting, weight loss, and nausea [300]. Therefore, it is essential for active ingredients containing bromide to have robust activity against the organism and to be well absorbed by it so that the dosing

of active ingredient is kept as low as possible. Nevertheless, some drugs containing bromides can be found again today. Examples are the anti-malarial drug quinine hydrobromide or the Parkinson's drug bromocriptine [301, 302]. On the other hand, iodine is considered to have antiseptic and antimicrobial effects. Since an adult human needs about 150 µg daily, this element is often used to develop active substances [303]. Chlorine compounds, in contrast, are also used in disinfectants [304]. An explanation for this is that halogens, particularly iodine, generally enhance membrane permeability and thus also the uptake of the substances to the desired target site [305]. In summary, halogens can be used in medicines, but it depends a lot on the used halogen, and the dosing should be kept as low as possible. In addition, the enzyme assay showed that all substances that had activity in the MIC assay also had activities in the enzyme assay. It means that the four derivatives most likely have the same mechanism of action. Furthermore, many inactive derivatives in the MIC assay also showed little to no inhibitory effect in the enzyme assay. It indicates a very narrow substrate specificity of IlvB1. However, on the other hand, some substances had no growth inhibitory effect on *M. tuberculosis* in the MIC assay but inhibited IlvB1 in the enzyme assay. Taken together with the other results that the derivatives are probably not metabolized, it suggests they have an internalization problem due to their chemical structure. It is an important path for the future of CF. So, there should be a focus on increasing drug solubility and the permeability of the substances through the mycobacterial cell wall. There are many approaches to this for other substances. According to drug solubility, the basic techniques can be divided into physical, chemical, and other groups. One example of a modification is the reduction of the particle size and an increased ratio of surface area to volume. Methods for this are comminution and spray drying, and micronization [306, 307]. These techniques were already used for different drugs, leading, e.g., to a 10-fold increase in dissolution for the drug fenofibrate [308, 309]. Another approach is nanosuspension, a biphasic system of nanosized active ingredients stabilized in surfactants [310, 311]. The last possibility to be presented here is the inclusion complex formation-based technique. It is particularly suitable for poorly water-soluble substances. Inclusion complexes are formed by inserting a nanopolar molecule (known as a guest) into the cavity of another molecule (known as a host). Mainly cyclodextrins are used as host molecules. These are water-soluble, crystalline, non-reducing, and cyclic oligosaccharides consisting of glucose monomers [312]. These methods could become important during CF development to increase solubility and, thus, uptake. In addition to water solubility, overcoming the mycobacterial cell wall as a barrier for active substances also plays an important role. Nanotechnologies are also applied here as pharmaceutical technologies. As with water solubility, examples include the nanosuspension due to

nanonization [313]. This would be a perfect combination of increasing water solubility, as required for many derivatives, and uptake into *M. tuberculosis* cells. Another option is nanoemulsions. These are thermodynamically stable oil-in-water dispersions that have a droplet size between 10 and 100 nm [314]. The enhanced uptake of nanoemulsions by cells of the phagocytic system makes these nanocarriers passive targeting properties [315]. In addition, there are ninosomes. These are thermodynamically stable liposome-like vesicles produced by the hydration of cholesterol, non-ionic surfactants, or charge-inducing components [316]. The advantage of this is the inclusion of both hydrophilic drugs in the core and lipophilic in the hydrophobic domains. There are many more possibilities, such as packaging into polymeric and non-polymeric nanoparticles, or polymeric micelles [317]. These should be considered in the course of further preclinical optimization studies of CF, particularly in view of the moderate metabolic stability in human liver microsomes [253]. These methods are also already used in tuberculosis research to lead to better bioavailability or activity. One example is INH incorporated into a poly (DL-lactide-co-glycolide) microparticle carrier. This showed better bioavailability *in vivo*, as well as *in vitro* [318]. Another example is a linezolid nanoemulsion, which is effective against lymph node TB. In this study, the antibacterial potential was demonstrated and *in vivo* studies showed high bioavailability in the targeted organs [319]. This once again highlights the importance of formulation discovery in addition to substance discovery.

Strategies to reveal further information in the mode of action of CF

Thus, with CF and BrF, two excellent substances have been found that still require slight medicinal chemical improvements to become relevant for clinical trials. With the novel mechanism of action of inhibiting AHAS, this compound can potentially be used against XDR- and TDR-TB. It is also supported by the previously described mild antimycobacterial activity of a plant AHAS inhibitor sulfometuron in mouse experiments [320]. However, this could only be induced by a very high daily dose of this substance. In mouse experiments, other monosubstituted sulfonylurea derivatives were already more active and had activity against XDR-TB [321]. It shows the relevance of research on CF and BrF to get a more potent drug against *M. tuberculosis*. To get closer to this goal, it is crucial to analyze the homologs of *ilvB1*. It is especially evident since *M. tuberculosis ilvB1* gene deletion mutants show little attenuation for virulence during infection in mouse and in bone marrow-derived macrophages [322], indicating that isolated inhibition of IlvB1 will not result in a strong phenotype *in vivo*. *In vitro*, *ilvB1* is

essential, although, in *M. tuberculosis,* there are three other homologs encoding IlvB2, IlvX, and IlvG [291, 322]. These will need to be further investigated in terms of their AHAS activity and possible inhibition, as they may be able to take over some or all of the activity of IlvB1 in macrophage infection or mouse experiments [291]. This would then explain the results of the AHAS assay that some derivatives inhibited IlvB1 in this assay but had no growth inhibitory effect on *M. tuberculosis* in the MIC assay. Further starting points are the better uptake of CF derivatives and the analysis of inactive substances regarding their metabolization.

4.2 KSKs are new, highly active lead structures against *M. tuberculosis*

Previous studies found the KSKs in a synthetic library screening as highly active compounds against *M. tuberculosis* [240]. Both have excellent activities with an MIC_{90} of 0.78 µM (KSK-104) and 0.39 µM (KSK-106), requiring further analysis to obtain their mechanism of action and target. They show a large therapeutic window with great activity and no cytotoxicity in various human cell lines [240]. An advantage of these substances over many natural products is the relatively simple synthesis and, thus, the availability of larger quantities of the KSKs for further experiments. This synthesis has been established by Dr. Alexander Berger and Dr. Oliver Michel and allows the preparation of various derivatives [323]. It has been shown by SAR analysis of over 200 derivatives that regions A and C are highly variable, and region B cannot be structurally altered to maintain activity. The two alkoxyamide groups in region B are important for their strong activity. Many changes have been made for regions A and C, which have consistent or worse activity. An explanation for this will be given later. SAR analyses focus on two important points. On the one hand, the analysis of the basic structural components that are responsible for their activity. And on the other hand, the identification of potentially more active and less cytotoxic molecules. It can involve different points: In particular, the anti-mycobacterial activity, but also, e.g., the improvement in cytotoxicity, stability, or chemical and pharmacological properties [324]. Here, four substances with improved antimycobacterial activity have been found. These are, e.g., OMK-175 and OMK-366, indicating that the KSKs are novel parental compounds that could yield various other active compounds through further SAR analysis. Although previous SAR studies have shown that region B is important for activity, it was possible to introduce certain modifications in this region. In the case of OMK-366, there is a huge structural change, indicating that this analog may be an agent with a different mechanism of action.

However, the pentylester in the region leads to enhanced activity in *M. tuberculosis*. To figure out whether this substance is also suitable as a new lead structure, OMK-175 was analyzed in more detail. This analysis highlights that the substance has excellent properties. These include high activity and lack of cytotoxicity against the monocyte cell line THP-1. Furthermore, in parallel with the KSKs, OMK-175 is active against slow-growing mycobacteria and inactive against fast-growing ones. It may be due to changes in the metabolism, structure, or components of the cell wall so that the KSKs and also OMK-175 are unable to enter the cell, or the target is not present in the fast-growing species. An outstanding result is the activity against pre-XDR clinical isolates. The biggest problem in the treatment of TB is currently the antibiotic resistance that has developed in many cases. OMK-175 also has activity against the pre-XDR clinical isolates, which is not as strong as against the WT. However, this is not surprising since the isolates lose fitness due to their mutations and the associated development of resistance [288]. However, since the shift in MIC_{90} is not huge, it is unlikely that OMK-175 has the same molecular target as any currently used antibiotics the isolates are resistant against. Analysis of OMK-175 spontaneous resistant mutants showed resistance with different patterns. A fraction was tested against KSK-106. One of the SRMs also had resistance to KSK-106, whereas the other was susceptible to KSK-106. It could mean that there are different ways to gain resistance to OMK-175, which are probably similar mechanisms. Also, in the other direction, SRM-KSK-106 was resistant, and SRM-KSK-104 was not resistant to OMK-175, suggesting that all three compounds have a similar resistance mechanism. SRM-KSK-104 has a mutation in the gene *Rv0552* coding for the predicted amidohydrolase Rv0552. In contrast, SRM-KSK-106 has a mutation in the gene *amiC* coding for the amidohydrolase AmiC, suggesting the hypothesis that KSKs are prodrugs that first have to be cleaved by amidohydrolases and thus be activated (see Figure 60) [240]. Activation of OMK-175 by another enzyme that has hydrolase activity would be conceivable. To answer this hypothesis, some SRMs should be sequenced. These data should provide clues to the mechanism of resistance for OMK-175. In summary, OMK-175 was thus found to be a promising new lead structure that can also be used for the further analysis of KSKs. One example of this further analysis is that this compound could be used to prove that region B of KSKs tolerates certain structural alterations. For this purpose, further OMK-175 derivatives should be analyzed. However, it is important to find the mechanism of action of the KSKs in order to then be able to make a statement as to whether OMK-175 is a substance with the same mechanism of action or whether the change in structure leads to an active substance with a different mechanism of action. If there are different mechanisms of action, the two substances should be considered separately. In order to figure this out,

a wide variety of analyses still has to be made, also concerning the KSKs. In this work, a strong focus was placed on the cleavage products of the KSKs. As described above, it has already been shown that the amidohydrolases AmiC and Rv0552 are mutated in SRMs of KSK-104 and KSK-106, respectively, which has led to the hypothesis that the KSKs are prodrugs that are first cleaved by the amidohydrolases [240]. Amidohydrolases are known to hydrolyze linear and cyclic amides [325]. In the KSKs, there are two amides and, thus, two sites of attack for the amidohydrolases. In cooperation with RG Kurz, these putative cleavage products have been synthesized. However, they showed little to no activity against *M. tuberculosis* in the MIC assay. It suggests that the structure of the original KSKs is important for internalization. Another explanation would be that only the combination of the different cleavage products leads to the activity against *M. tuberculosis*, as the individual cleavage products have different targets. However, this hypothesis could not be proven because the cleavage products had little anti-tubercular activity even when combined. This could again be explained by poor uptake of at least some of the cleavage products. Thus, the hypothesis of KSKs as "dirty drugs" could not be proven by this experiment. The definition of a "dirty drug" is that these compounds target multiple structurally unrelated proteins, a cell complex consisting of multiple proteins, and/or molecules that control multiple downstream metabolic pathways [326]. The single cleavage products could target different molecules. Previous proteomic analyses or RNA-Seq of stressed *M. tuberculosis* cells did not provide hints toward a specific target. By adding a sublethal colistin concentration, the *M. tuberculosis* cell wall was attacked, allowing the putative cleavage products to diffuse into the cell. This is because colistin has been associated with increased permeability of the mycobacterial cell wall [327]. But even this approach could not render the cleavage products more active, and they also could not kill the bacteria in combination. This may further indicate that the active substance cannot enter the cell, even with increased permeability.

To further classify the mode of resistance, all derivatives have been tested against SRMs and some against DSRMs. It could, as described in Chapter 3.2.5, establish different correlations. First, it can be assumed that AmiC and Rv0552 are substrate specific, as there is weak cross-resistance among the KSK-SRMs. Thus, even the minor structural differences, such as those in KSK-104 and KSK-106, result in substantial discremination of the other KSK. Concerning the amidohydrolases, this experiment could show that the mutation in Rv0552 in SRM-KSK-104 results in the specific inability to cleave only the KSK-104 derivatives. In contrast, the mutation has very little or no effect on the activity of KSK-106 derivatives. It likely means that Rv0552 can cleave KSK-104 derivatives but not KSK-106 derivatives.

In contrast, the mutation in *amiC* in SRM-KSK-106 results in the inability to cleave both KSK-104 and KSK-106 derivatives. It suggests that Rv0552 has a narrower substrate specificity, assuming that apart from Rv0552 and AmiC, no other amidohydrolase are involved in the cleavage of the KSKs. Some other amidohydrolases are available in mycobacteria, which are linked to different processes. An example is urease, which specifically hydrolyzes urea and is likely a virulence factor by alkalinizing the microenvironment and preventing phagosome-lysosome fusion [328]. In *M. tuberculosis*, several uncharacterized proteins are likely to possess an amidohydrolase function. Among these examples is AmiA1, which based on gene ontology is likely to function as an N-acyl-L-amino acid amidohydrolase. [279]. Additionally, AmiB1 is another protein that could play a role in cellular metabolism and exhibit activity towards carbon aliphatic amides as well as numerous aromatic amides [279, 329]. Another example of an amidohydrolase is lactonase, which is characterized in *M. avium*. It hydrolyzes *N*-acyl-homoserine lactones, which are involved in the quorum-sensing pathway [330]. Lactonases are also found in *M. tuberculosis,* like members of the phosphotriesterase-like lactonase family, which use phosphotriesters as a substrate, but have also lactonase activity [331]. Thus, there is a possibility that another amidohydrolase may take over the amidohydrolase function of AmiC and Rv0552 for certain KSK derivatives.

Antibiotics need to have as few side effects as possible in the human body. BLAST analyses have shown that these amidohydrolases are not found in mammals and other nosocomial bacteria [332]. As a result, the KSKs cannot be cleaved, and thus the active moiety cannot be formed. On human cell lines, the KSKs themselves have no cytotoxic effect. The homolog of *amiC* in *M. smegmatis* (*msmeg_2521*) is also coding for AmiC. It is 65% identical to the enzyme in *M. tuberculosis*. This homolog has already been shown to have the function of inducer of acetamidase expression. Thus, amides can be the sole carbon source [333]. It could explain the inactivity of the KSKs towards *M. smegmatis*, as Msmeg_2521 could have different substrate specificity, and thus the KSKs cannot be cleaved into the active form in *M. smegmatis*. In the year 2021, a research paper discussing the enzyme activity of AmiC in *M. tuberculosis* was published. It describes the hydrolysis of indole-4-carboxamide as an activation of this substance; thus, this substance also represents a prodrug [242]. There is no empirical data on Rv0552 yet. Therefore, obtaining more detailed information on this enzyme is essential. For this purpose, Rv0552 should be recombinantly expressed, and the amidohydrolase activity should be analyzed by an *in vitro* assay [334]. Another possibility is the examination of KSKs and cleavage products after incubation with *M. tuberculosis*. Initially, it was shown (Chapters 3.2.2 – 3.2.2.1) that the cleavage product of regions A and B were formed in

the WT. In the first experiment, the focus was only on that cleavage product. It was the first time that the cleavage of KSKs could be shown. Since no complete substance recovery was available, which is also unlikely, further hydrolyses should be investigated by metabolite screening. The results performed with Dionex HPLC show the fast cleavage of KSKs in the WT. After only one day, a considerable amount of the KSKs has been cleaved into region A, whereas in the SRMs, mainly the AB region is found. It clearly shows that AmiC and Rv0552 play a role in the hydrolysis of the KSKs. The samples were also measured using a more accurate analytical procedure by LC-MS to support these results. This method also demonstrated the cleavage of the KSKs. Again, hydrolysis can be shown and also the slow-acting mechanism in the SRMs. After two days of incubation with KSK-104, only AB-KSK-104 could be detected in the treated SRM-KSK-104 sample. In contrast, mainly A-KSK-106 could be found in the batch with SRM-KSK-106 during incubation with KSK-106. It means that the mutation in SRM-KSK-104 has a more decisive influence on the degradation of the KSKs. However, both SRMs have a strong resistance to the respective substance [240]. Because region AB is found, also region C must have been released somehow. The same applies to the degradation of region AB to A and B. In that case, only region A was measured. However, it remains elusive what happens to region B or region C after hydrolytic release. Region B alone is too small to be detected since this LC-MS method only measures substances weighing 100 g/mol or more. In contrast, there is no methodological or technical explanation for the non-detection of region C. It could be because this part binds covalently to another substance or cell component, which may be the target, and remain further bound after the extraction procedures and thus is not measured. Another explanation could be further metabolization. Examples of metabolization would be further degradation of the substance by other enzymes so that the substance is smaller and no longer recognized by LC-MS. Another possibility is that substituents are attached to this region, thus changing the molecular weight and making them less easy to identify. In summary, the KSKs' core structure and chemical properties are likely required for internalization. Intracellularly, the amidohydrolases AmiC and/or Rv0552 attack the amide bonds, forming all three regions [242]. However, region A is predominantly found in the cell suspension. To confirm the prodrug hypothesis, a conceivable approach would be to first elucidate the mode of action. If it is determined that an enzyme is inhibited by the KSKs for instance, conducting an *in vitro* assay could assess the activity of the individual cleavage products to identify which ones contribute the antimycobacterial activity. Alternatively, more targeted pre-tests could be done to investigate the active molecule.

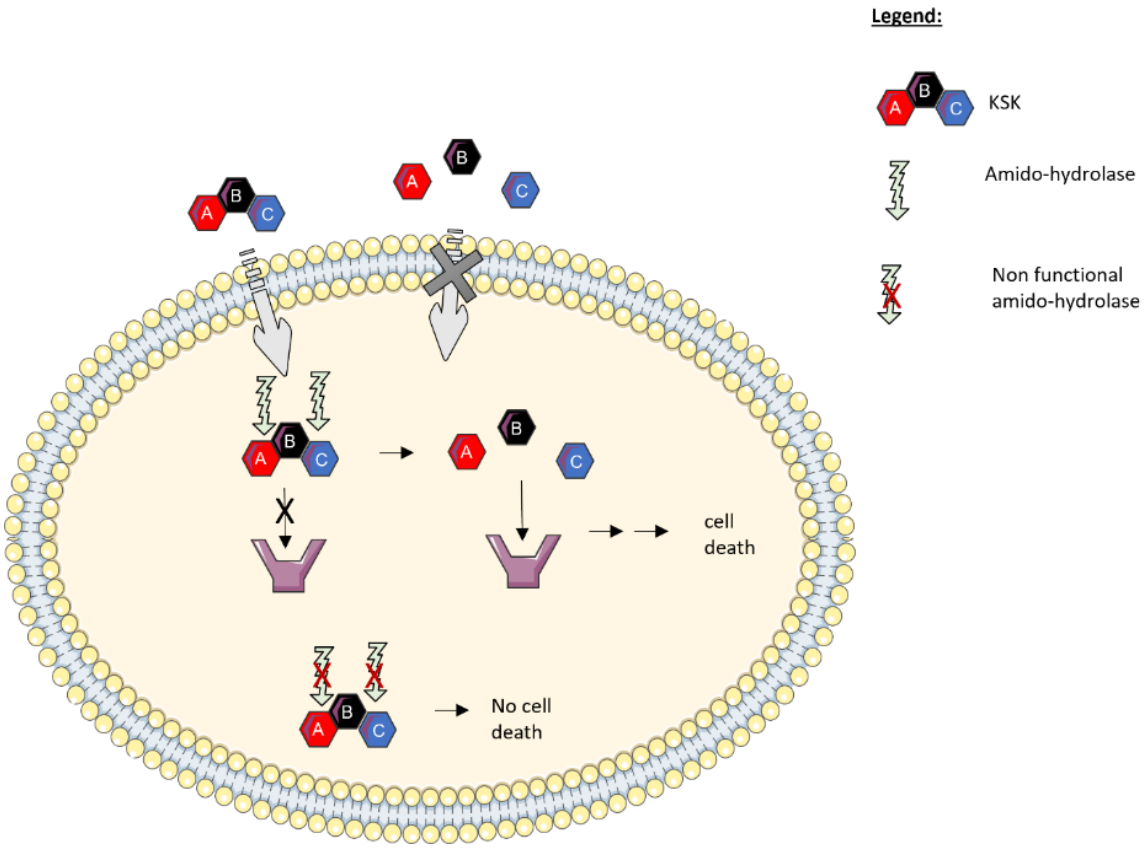

Figure 60: The interaction of KSKs with mycobacteria. Schematic illustration of KSKs entering the cell only as an uncleaved molecule, while the individual cleavage products cannot be internalized. The amidohydrolases cleave the internalized KSKs, yielding the degradation products A, B, and C. One of these products can then bind to a receptor or enzyme and lead to the death of *M. tuberculosis*. In the case of nonfunctional amidohydrolases, the KSKs cannot be cleaved and thus fail to bind efficiently. Therefore, the KSKs are not activated.

Even though the analysis of the KSKs is very advanced, the present work could not uncover the mechanism of action, but many targets have already been excluded. It has previously been shown by ATP assay that KSKs induce mild ATP depletion, suggesting indirect inhibition of ATP production [240]. Taken together with the fact that the KSKs only have no synergistic effect with BDQ, this brings the energy metabolism as a target for the KSKs into the closer selection [240]. BDQ inhibits F_1F_0- ATP synthase, resulting in decreased ATP generation [335-337]. With this inhibition of the ATP synthase, no energy gets produced by ATP synthesis [338, 339]. A similar mechanism of action in KSKs would explain the absence of the synergistic effect. Since it has been shown that the KSKs are prodrugs, the individual cleavage products must be considered in more detail in this context. One known way of inhibiting ATP synthesis is the chelation of metal ions. These metal ions are, for example, essential in cytochromes in the electron transport chain. They can no longer work appropriately by binding the KSK cleavage products to them, and the PMF cannot be built up. This hypothesis has also been further

strengthened by the finding of Rv2226 in an affinity-enrichment approach. It is a protein that has not yet been described but is predicted to carry a CHAD and a CYTH domain [270]. However, the CYTH domain is predicted to chelate divalent cations and have a reaction mechanism dependent on metal ions [271]. The metal ions bound to Rv2226 could then bind to the KSK cleavage products through the metal ion, explaining the binding and finding of Rv2226 in the affinity-enrichment approach. A zinc and iron chelating assay was performed to verify this chelating property of the KSKs. However, no iron chelating effect could be detected, but a low zinc chelating effect. Therefore, zinc chelation could play a role in the mode of action of the KSKs, but this is subordinate because the effect was not comparable to the positive control EDTA. In this assay, the putative cleavage products were not used because they were unavailable then. To confirm the zinc chelation, the assay should be repeated with the available prodrugs.

In addition, in mycobacteria, the F_1F_0- ATP synthase is encoded by only one operon *Rv1303-atpBEFHAGDC-Rv1312)* [340]. A transcriptional regulator, BlaI (Rv1846c), is found for this operon, and it is suggested to have a role in stress and antibiotic response [341, 342]. Further analysis indicated that BlaR (Rv1845c) plays a role in cleaving BlaI and itself during the depression of the operon. It is a zinc-dependent metalloprotease [341, 343]. One explanation could be that the KSKs chelate the zinc ions and are thus no longer available for BlaR and thus for the regulation of the operon. Compared to actively growing mycobacteria, the ATP level in the dormant forms is reduced 5-10-fold [344, 345]. Drug-induced reduction of the already low energy level in dormant mycobacteria can lead to the death of the bacilli.

Moreover, the carbon source is also crucial for energy metabolism. It is due to the fact that *M. tuberculosis* uses host-derived fatty acids and cholesterol as energy supplies in human macrophages instead of fermentable energy sources [346]. With fermentable energy sources such as glycerol or glucose, ATP can be synthesized by glycolysis or oxidative phosphorylation. In contrast, only oxidative phosphorylation and not the glycolytic pathway can be used for ATP production during growth on fatty acids. By finding Cfp32 (Rv0577), a putative glyoxylase in the native pull-down assay, a link between KSKs and the glycerol pathway has been established for the first time. Glyoxylases, in general (such as GLO1 and GLO2 in humans), are involved in detoxifying reactive methyl glyoxylate into D-Lactate using glutathione as a cofactor (see Chapter 3.2.6). In another study, SRM-KSK-106 was produced in *M. bovis,* and whole genome sequencing showed a mutation in *glpK* in 6 of the 7 individual clones. It is a glycerol kinase that plays a role in regulating glycerol uptake and metabolism [347]. Combined with the KSKs acting differently in the presence of different carbon sources, this indicates

inhibition of a process involving the carbon source. Maybe this is also linked to a lower ATP level.

In addition, identifying only two hits in the pull-down assay could have several causes. It is possible that KSK-106 does not have a target in the cytosol. As a result, these targets are not present in the cell-free lysate. Thus, there is no binding with the target possible. With that method, these types of targets cannot be found. Another explanation could be that, as shown earlier, the KSKs are cleaved by amidohydrolases, which could also happen in the cell lysate. In that case, it is conceivable that the biotin linker is no longer connected to the substance at the correct position to “fish” for the targets. It would require the production of probes consisting of the active, cleaved KSK molecule.

In summary, these results show that the KSKs are more likely to have their mode of action up in one metabolic pathway, influencing many other routes. Another explanation is that the individual hydrolysis products of the KSKs have different targets and thus act similarly to a "dirty drug". Finding more information about the mode of action is still essential. For that purpose, generating further biotin-tagged probes of the prodrugs is critical for identifying the targets in a pull-down assay. Further analysis should be performed to identify if there is a synergism with other energy metabolism-targeting compounds, such as pyrazinamide.

Since the KSKs are very promising in their effects, the following way forward is further preclinical testing. In these experiments, detailed information on the toxicity and the dose for the clinical tests, i.e., the first in-human studies, will be obtained *in vivo* and *in vitro* [348]. It includes an active pharmaceutical ingredient preparation, such as chemical properties (solubility, stability, and counter ion salt or polymorphic form), but also formulation studies [349]. This section was taken over by the chemists at RG Kurz and is described in more detail in their doctoral thesis. With the formulations described in Chapter 3.2.11, two solutions have been found that are suitable for different applications (PO and IV). Both kept a potent inhibition of activity compared to DMSO, although the KSKs are poorly soluble in aqueous solutions. Another large section of the preclinical tests deals with bioanalytical and analytical methods [349]. *In vitro* studies on absorption, distribution, metabolism, and excretion have been performed in collaboration (data not shown) and found to be promising, so the first pharmacokinetic studies in mice were performed (data not shown). Mouse infection models are essential for the final confirmation of the activity of KSKs. These have already been initiated and will provide results concerning efficacy against *M. tuberculosis*, side effects, and detection of KSKs or their degradation products in organs or blood.

4.3 The thiazole-containing molecule FFK-088 is a new lead structure

As described in Chapter 1.3.3.1, finding new lead structures as an active agent against TB is significant. For this purpose, various thiazole-containing substances have been investigated in a substance screening concerning their activity against *M. tuberculosis*. A broad spectrum of biological activities has been previously recognized for thiazole-containing substances [350]. It includes activity against *M. tuberculosis*. Examples comprise 2-amino-4-methylthiazole-5-carboxylic acid ethyl ester and derivatives and 2-aminothiazoles in general [351, 352]. In the substance screening, FFK-088 was the most active substance with high activity. It was promising and therefore chosen for further analysis. There was activity against slow-growing *M. bovis* BCG Danish 1331, but no activity against fast-growing *M. smegmatis,* meaning that its effect is probably selective for slow-growing mycobacteria. However, the slow-growing mycobacteria usually represent higher pathogenicity [353]. Therefore, this activity is of greater importance. In addition, the activity of FFK-088 against clinical pre-XDR isolates was an excellent result. The current effort was to find new drugs with a new mechanism of action to combat XDR-TB. Thus, with FFK-088, a substance was found that probably has a different mechanism of action than the antibiotics against which the KZN-pre-XDR strains are resistant (see Chapter 1.3.3) [288]. These results, combined with the finding that FFK-088 shows no cytotoxicity in the tested range against the analyzed cell lines THP-1, Huh-7, and HEK-293, indicate a big therapeutic window. It does not reveal any cell-damaging effects in liver, kidney, and monocytic cells. Since *M. tuberculosis* is internalized by macrophages, it is essential that the compounds also act within macrophages. A macrophage infection assay has been performed for this purpose. It shows no growth inhibitory effect on the *M. tuberculosis* cells in the macrophages, which could have several reasons. On the one hand, this could mean that the substance with its chemical properties cannot be internalized into macrophages in this way. It would then have to be improved by further SAR analysis. On the other hand, there is the possibility of the chemical degradation of the substance by the macrophages' enzymes. FFK-088 comprises an ethyl ester structure. Substances containing this group are often prodrugs for carboxylic acids. An example of this is oseltamivir, which is an inhibitor of the influenza virus [354]. Esters, in general, are relatively labile functional groups. Replacing the ester with a more stable tert-butyl ester can have a stabilizing effect, as these are more hydrolytically stable and presumably are no suitable substrates for esterases. Alternatively, the ester can be exchanged against an amide moiety. However, in that case, the problem is known that amides serve as substrates for proteases. The exchange

to an amide has also been investigated. This derivative had no activity in the MIC assay. Further analyses are necessary to find a substance that can be used as an active agent against *M. tuberculosis*. However, there are also examples of antibiotics that have an anti-tubercular effect in humans but not in the macrophage infection assay like STREP [355]. This could also be investigated for FFK-088. Killing kinetics should be used to investigate the general response and the behavior in combination with different anti-tuberculosis drugs. It is an important information because the TB therapy is a combination therapy consisting of the four antibiotics INH, RIF, ETB, and PZA in the intensive phase [99]. The activity of FFK-088 alone is very weak, with a short bacteriostatic phase. The bacterial count increased after a short time in the viewed cultures. However, the substance in combination shows an excellent effect. FFK-088 initially has no significant synergistic effect in the first seven days because the combinations of antibiotics always behave like the individually studied first-line or second-line antibiotic. However, a synergistic effect and inhibited resistance formation in INH can be seen in the following period. For ETB, RIF, and DELA, a synergistic effect and inhibition of resistance formation can be seen even after 45 days. All these results show that FFK-088 can be used in combination therapy as an adjuvant that increases the activity of the other antibiotics and prevents the development of resistance, which displays a significant problem in tuberculosis therapy [356].

An ideal antibiotic combines no toxic properties against the host and its microbiome, a substantial growth inhibitory property against the pathogen causing the disease, and meager resistance [357]. While the first two points have already been shown, the frequency of resistance generation by SRM has been analyzed. Resistance formation has occurred with a frequency of 10^{-7}. It is a great result compared to previous antibiotics, INH and DELA, which occur with a frequency between 10^{-5} and 10^{-6} [154]. The resistance pattern is also relatively low, so further anti-mycobacterial activity can be maintained by increasing the active ingredient. Analysis of SRM mutations does not directly reveal a gene match nor different genes encoding proteins that work together in a biosynthetic pathway or other cellular processes. Since some of these proteins' functions are not thoroughly investigated, only guesses can be made about how resistance to FFK-088 evolved. For the analysis, looking at the mutants with high resistance is essential. Here, in SRM 1.4 with a mutation in *fadD28*, cell wall biosynthesis is affected by PDIM biosynthesis. An intact cell wall is a vital permeability barrier in mycobacteria. Some lipids incorporated in the cell wall are responsible for virulence in this context. PDIM is one of these and is only found in pathogenic mycobacteria [358-361]. FadD28, an adjoining acyl-coenzyme A synthase, catalyzes the activation of long-chain fatty acids, like acyl-

adenylates. These molecules are transferred to the polyketide synthase Mas for further chain extension [361]. An upregulation of *fadD28* was suggested to be a regulator for changes in the cell-wall-associated lipids [362]. It is also associated with host phagosome maturation arrest [363].

For SRM 13.2, *pirG*, also known as *erp,* is mutated. The protein Erp (exported repetitive protein) is a cell surface component with three domains. N-terminal, there is a canonical Sec-dependent signal sequence. In the middle, there is a repetitive sequence, and C-terminal, there is a conserved hydrophobic domain, which could be involved in the loose anchoring of Erp to the cell surface [364, 365]. Its presence is needed for bacterial resistance against detergents [365]. For SRM 13.3, a mutation appears to be in *pks7*, linked to the polyketide synthase, which has a role in polyketide and fatty acid biosynthesis. Members of these polyketide synthases, like *pks10, pks7, pks8,* and *pks9,* generate unreduced polyketides*,* typically associated with anthocyanin pigments and flavonoids. The function of these synthases is unknown [30]. Some publications link their biological significance to intracellular growth. Due to the adjacent ORFs, which play a role in the biosynthesis and localization of PDIMs, they also could have activities associated with acyltransferases and transporters [366]. Deleting *pks7* leads to *M. tuberculosis* deficiency to produce PDIMs [367]. The infection of *pks7* deletion strains in BALB/c mice was also affected, which supports the role of Pks7 in PDIM biosynthesis and links it with virulence through infection. Therefore, Pks7 and FadD28 can both be linked to PDIM biosynthesis. Thus, there is evidence that the resistance mechanism is associated with PDIM biosynthesis. There are many different ways in which resistance develops. One possibility is the prodrug hypothesis. That means that FFK-088 first needs to be structurally modified by enzymes to acquire its activity. If these enzymes are mutated, the activation can no longer take place. It is doubtful to explain this with the mutations here because the enzyme Pks7 is a polyketide synthase, and FadD28 catalyzes the activation of long-chain fatty acids. Since *M. tuberculosis* also develops resistance mechanisms impairing PDIM formation during PZA treatment, the cross-resistance of FFK-SRMs towards PZA should be tested, thus having closer information about the resistance mechanism. Another possibility is that the mutations in the SRMs result in altered PDIM levels and, thus, cell wall assembly, making FFK-088 uptake more difficult. Fluorescent FFK-088 derivatives could help to address this possibility. If internalization can be detected only in the WT and not in the SRM strains, this would be an indicator for this hypothesis. More SRMs need to be sequenced to analyze the resistance mechanism further and possibly the mode of action of FFK-088. It will hopefully result in consistent mutations in a specific gene. A second possibility would be

that the resistance mechanism can be narrowed down to a cellular process or pathway through the mutated genes.

4.4 Conclusion and final remarks

The three projects presented here deal with three anti-mycobacterial substances at different research stages. With CF, a substance has been found whose mechanism of action is known to be involved in inhibiting the catalytic subunit of AHAS IlvB1 [225]. It is a compound with high anti-mycobacterial activity, also acting within infected macrophages, with no cytotoxicity and high selectivity [225]. Further research should go deeper into preclinical research. Mouse experiments concerning the metabolization of CF and BrF are essential but also efficacy studies in mouse infection models. It will help to figure out whether these substances, similar to the plant AHAS inhibitors, inhibit the growth of mycobacteria in mice and thus have a chance as potential active substances for treating TB in humans [320, 321]. For this purpose, knowing the complete mechanism of action with all involved and subordinate systems is advantageous. There should be a closer look at IlvB1 homologs concerning their AHAS activity. The question should be answered whether CF can also inhibit the potentially existing AHAS activity of IlvB2, IlvG, and IlvX [291]. Finally, a closer look at the inactive CF derivatives should be made to understand their inactivity in more detail. For this purpose, the methods presented here (Chapter 3.1.4) should be repeated with more derivatives.

With the KSKs, two compounds were found to have excellent antibacterial potency, no cytotoxicity, high selectivity, and intracellular activity in infected macrophages. With the hypothesis that KSKs are prodrugs cleaved by AmiC and/or Rv0552, further analyses are available [240]. A closer look at amidohydrolases was done in parallel by Kristin Schwechel, including the generation of *M. tuberculosis* knockouts. Furthermore, recombinant expression and analysis of both enzymes in an *in vitro* assay are underway. Further research should be done to find the active form of the KSKs as described above and the mechanism of action. Although the mechanism of action is not yet precisely investigated, this is still an excellent result since there are some established drugs in TB therapy whose mechanism is not yet fully known (Chapter 1.3.3.1). Nevertheless, KSKs should continue to be evaluated in preclinical studies. The KSK derivatives represent many structural variances but many still have excellent activity. Examples of analogues with superior activity are OMK-175 and OMK-366. However, to move forward in comparative studies, it would be important that the mechanism of action gets clarified. It will allow further analysis of whether these and many other active KSK derivatives have

the same mechanism of action or if they are defined as a new compound with a new mechanism of action.

Lastly, FFK-088 was found to be a new compound, with antibacterial activity, even against clinical pre-XDR-isolates, and no cytotoxicity. The activity within infected macrophages should be improved by further SAR analysis. Furthermore, the resistance mechanism and the mode of action must be ruled out.

Along with several other substances, these three can be used to work on the antibiotic shortage that has arisen due to the AMR. Besides the approach of finding new antibiotics, the development of resistance should also be tried to reduce. It can only be done through better diagnosis and treatment, so antibiotics are only administered for known pathogens. It will decrease the number of broad-spectrum antibiotics. One idea is the use of FFK-088 as an adjunct antibiotic in TB to reduce the development of resistance. Another significant issue is the usage of antibiotics in farming to control infections, prevent diseases and promote animal growth. However, the misuse and overuse of antibiotics in this context have also contributed to the dissemination and selection of resistant bacteria. It should be significantly minimized, as multi-resistance is often transferred between animals and humans [1]. Consequently, these antibiotic-resistant bacteria limit the effectiveness of antibiotic treatments, including those used for TB. In this context, education is very important, that antibiotics are not always used in animal breeding, and thus the development of resistance is reduced. However, research is also very important, as further antibiotics must be found against which resistance has not yet formed. It is equally crucial to gain a precise understanding of the mode of action exhibited by antibiotics to enable their targeted and specific utilization. FK-088, CF, and the KSKs with its most potent derivatives OMK-175, OMK-355, and OMK-366 can therefore be an important step in the development of antibiotics due to their specific effect against TB, as these cannot be used as broad-spectrum antibiotics in farming and therefore resistance cannot develop rapidly in this regard. It is therefore important that research continues on the three lead structures in order to introduce them to the market after the hopefully positive preclinical and clinical studies.

5 Supplement

Table S1: Orthologous proteins of IlvB1 in different mycobacteria. Using the BLAST tool, sequences were blasted to identify corresponding proteins in other mycobacteria [256]. All tested mycobacteria have an orthologue with an identity of 100%.

Strain	IlvB1
M. smegmatis mc^{2}155	100%
M. bovis BCG Pasteur	100%
M. bovis BCG Danish 1331	100%
M. marinum ATCC927	100%

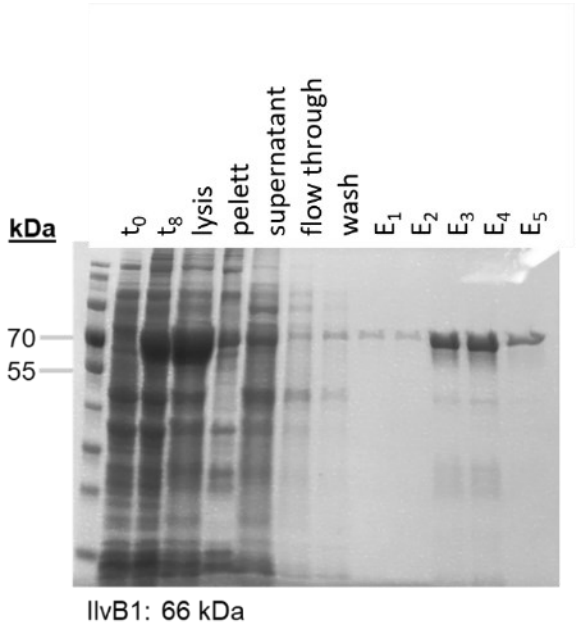

Figure S1: Coomassie-stained SDS-PAGE analysis of recombinant expressed and purified IlvB1. Samples of uninduced (t_0) and induced (t_8) cells, lysate, pellet fraction and supernatant, flow through, a washing step and elution steps (E_1-E_5) were applied on the gel. On the left side, there is the marker in kDa. Directly before the application of the samples to a PROTEAN® TGX™ gel, they were mixed with loading dye and denaturized at 99 °C for 5 min.

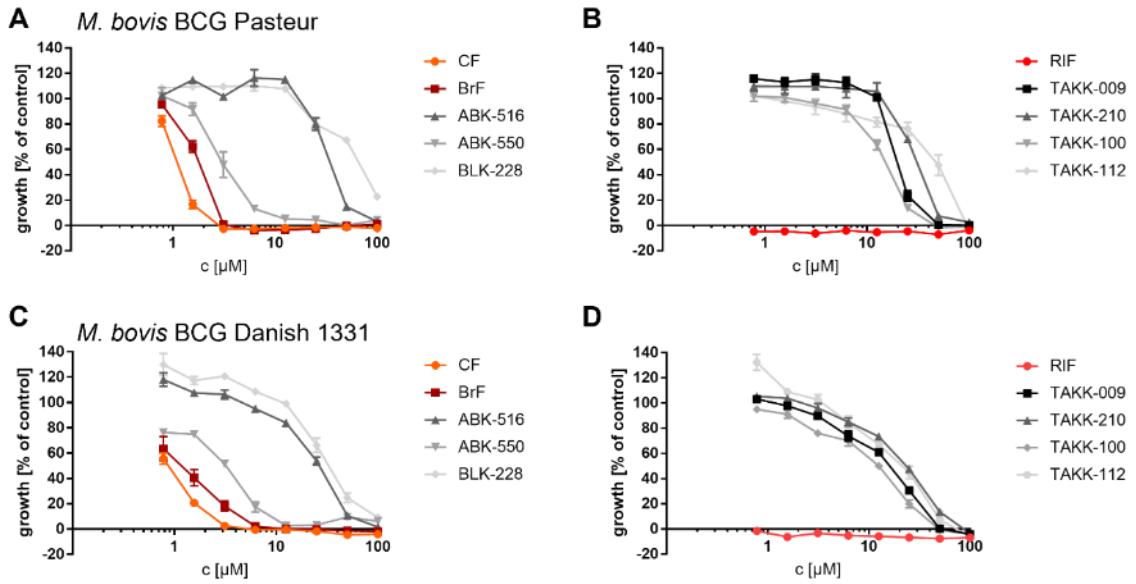

Figure S2: Activity of different CF derivatives against *M. bovis*. Dose-response curve of various CF derivatives against **(A; B)** *M. bovis* BCG Pasteur, and **(C; D)** *M. bovis* BCG Danish 1331. Data are shown as means of n=3 ±SEM.

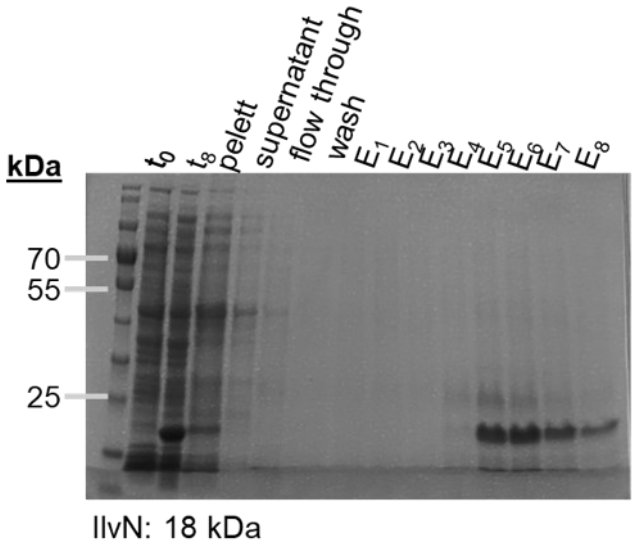

Figure S3: Coomassie-stained SDS-PAGE analysis of recombinant expressed and purified IlvN. Samples of uninduced (t_0) and induced (t_8) cells, pellet fraction and supernatant, flow through, washing step, and elution steps (E_1-E_8) were applied on the gel. The marker in kDa is on the left side of the gel. Before applying the samples to a PROTEAN® TGX™ gel, they were mixed with loading dye and denaturized at 99 °C for 5 min.

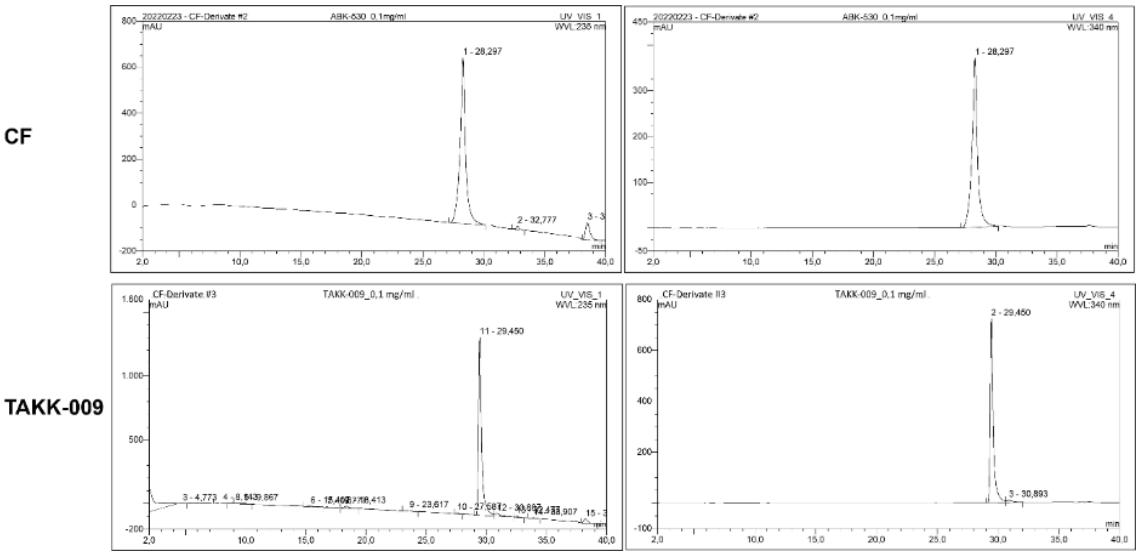

Figure S4: CF stability assay. Result of the measurement of CF and TAKK-009 dissolved in MeOH. The samples have been measured with a HPLC with DAD (Dionex).

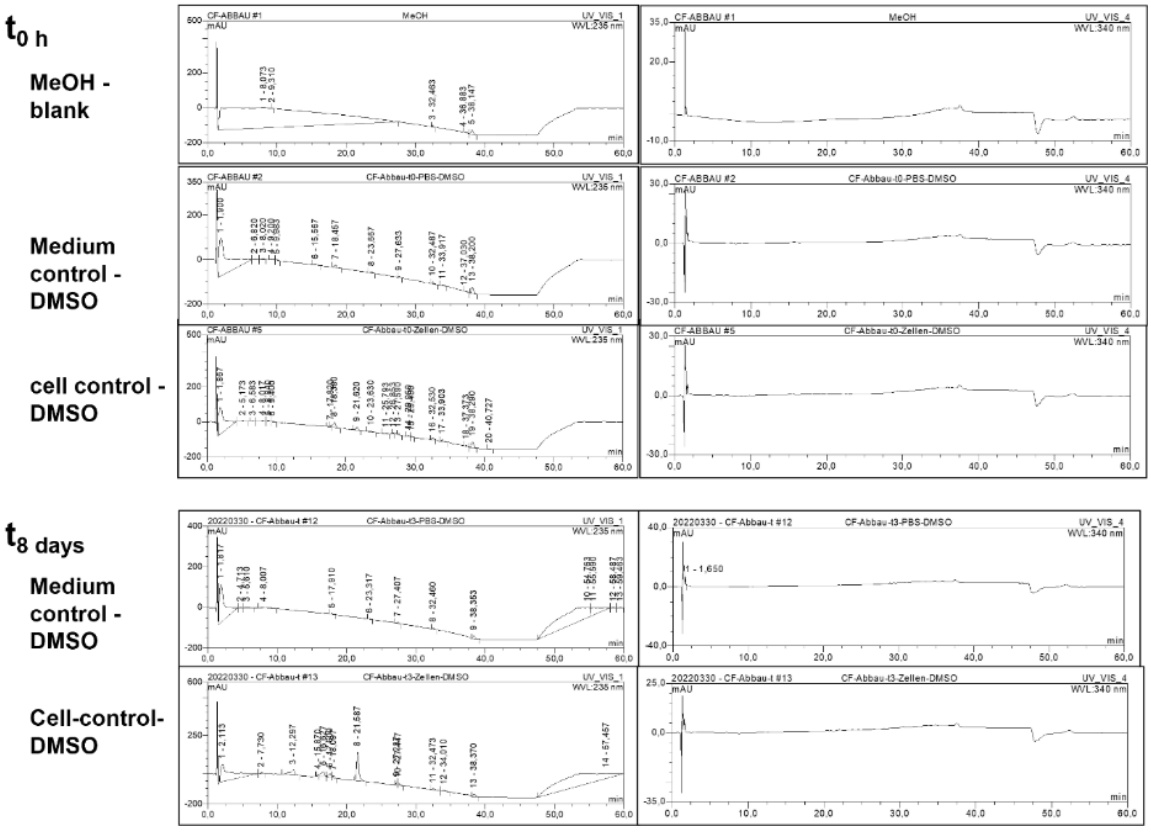

Figure S5: CF stability assay. Result of the CF stability screening. CF and TAKK-009 were incubated with *M. tuberculosis* H37Rv WT or medium for several periods. Samples were taken, prepared, and measured with a HPLC with DAD (Dionex). It shows the control samples: the methanol blank, the medium control, and the cell control, which all were incubated with DMSO directly and 8 days after the addition of DMSO.

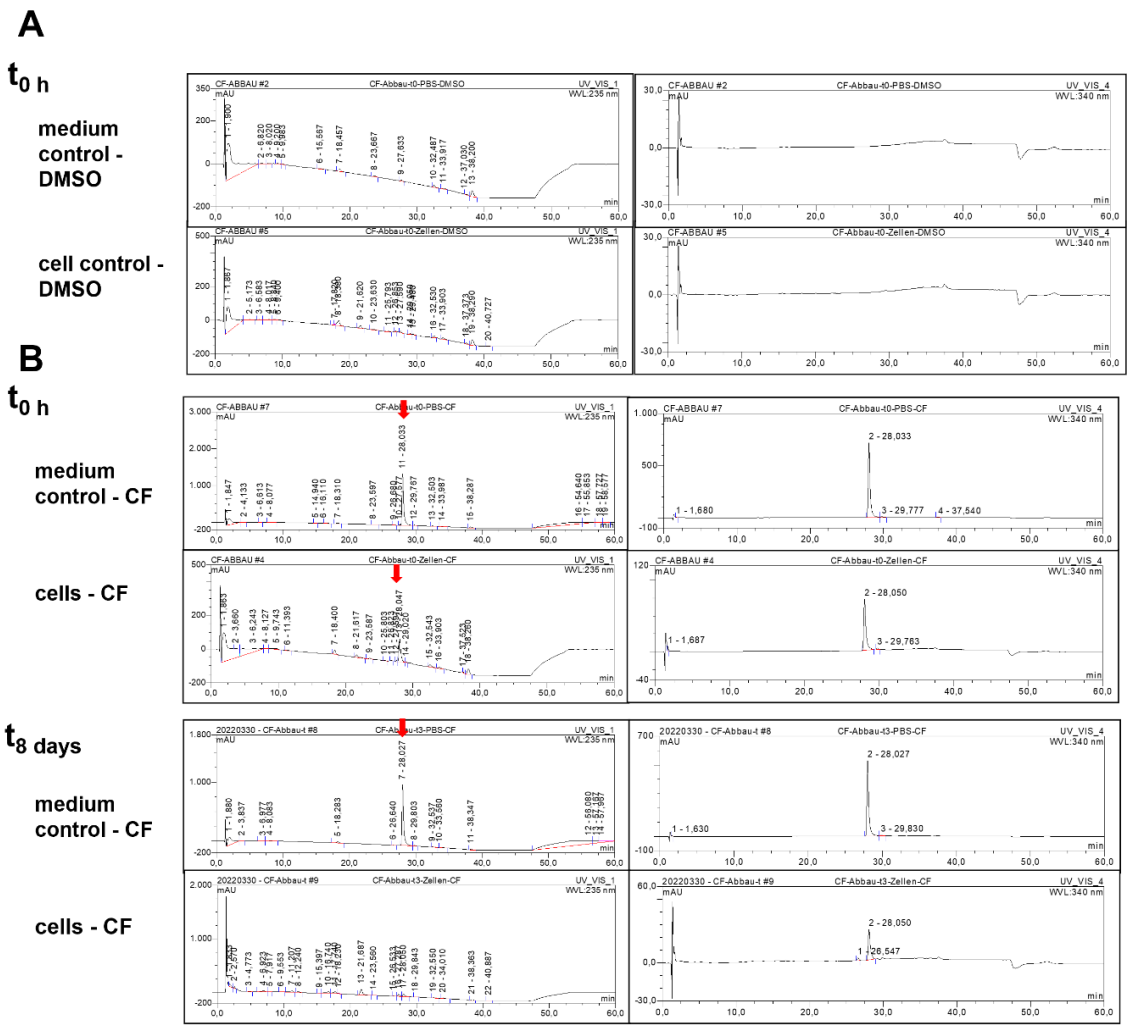

Figure S6: CF stability assay. (A-B) Result of the screening, which was measured with a HPLC with DAD (Dionex) at 235 nm (left) and 340 nm (right). In **(A)** are the control samples, the medium control, and the cell control, which were incubated with DMSO. **(B)** demonstrates the result of the CF-treated medium and cell suspension directly and 8 days after adding the compounds. The signal intensity is displayed as mAU on the Y axis towards the retention time on the X axis. The red arrow shows the expected CF peak.

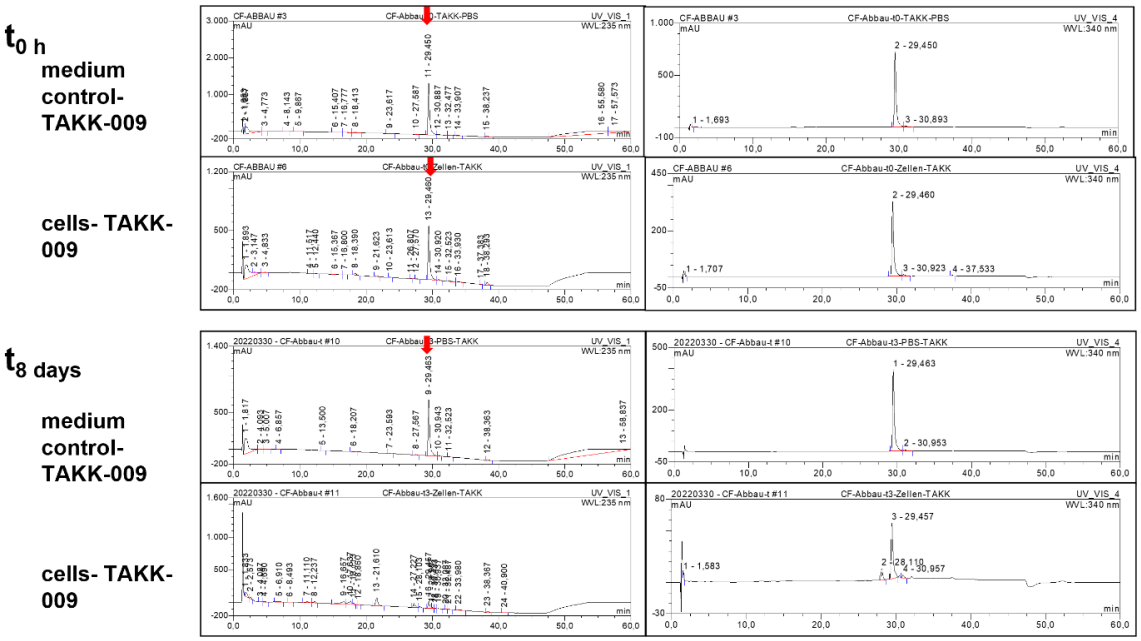

Figure S7: TAKK-009 stability assay. The result of the screening was measured with a HPLC with DAD (Dionex) at 235 nm (left) and 340 nm (right). It shows the result of the TAKK-009-treated cell suspension and medium control at t_0 and 8 days after the addition of the compound. The signal intensity is displayed as mAU on the Y axis towards the retention time on the X axis. The red arrow shows the expected TAKK-009 peak.

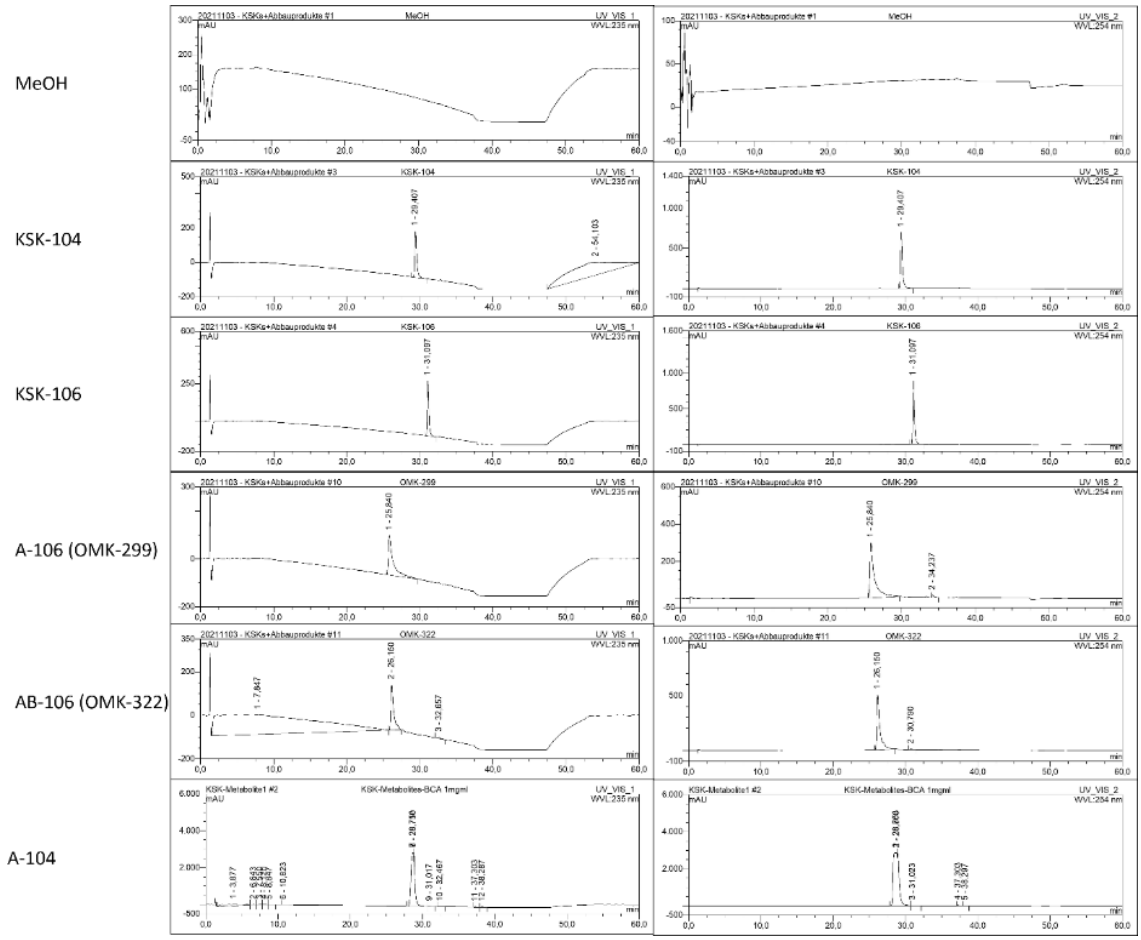

Figure S8: KSK metabolization assay. Result of the measurement of the reference substances required for the degradation screening. These are dissolved in MeOH (1mg/mL) and measured with a HPLC with DAD (Dionex) at a wavelength of 235 nm (left) and 254 nm (right).

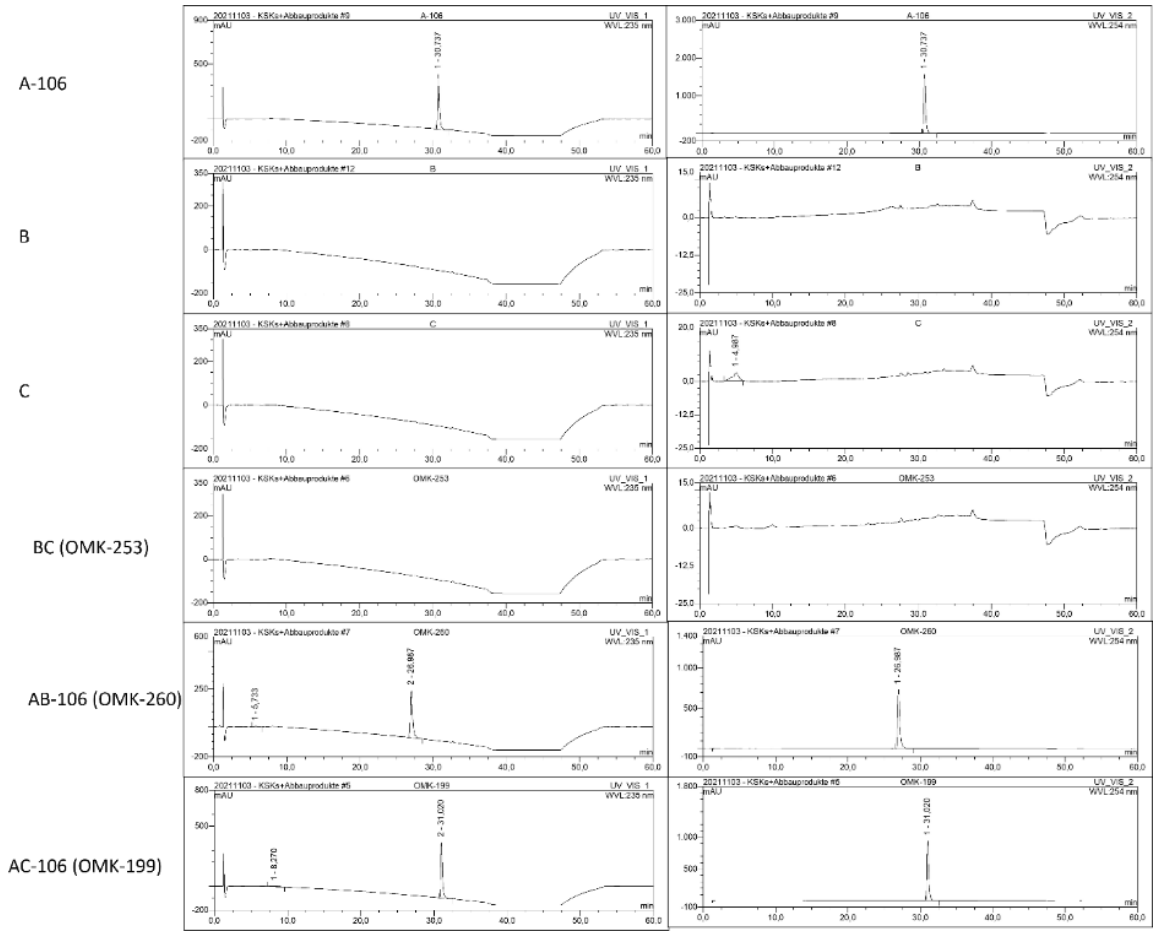

Figure S9: KSK metabolization assay. Result of the measurement of the reference substances required for the degradation screening. These are dissolved in MeOH (1mg/mL) and measured with a HPLC with DAD (Dionex) at a wavelength of 235 nm (left) and 254 nm (right).

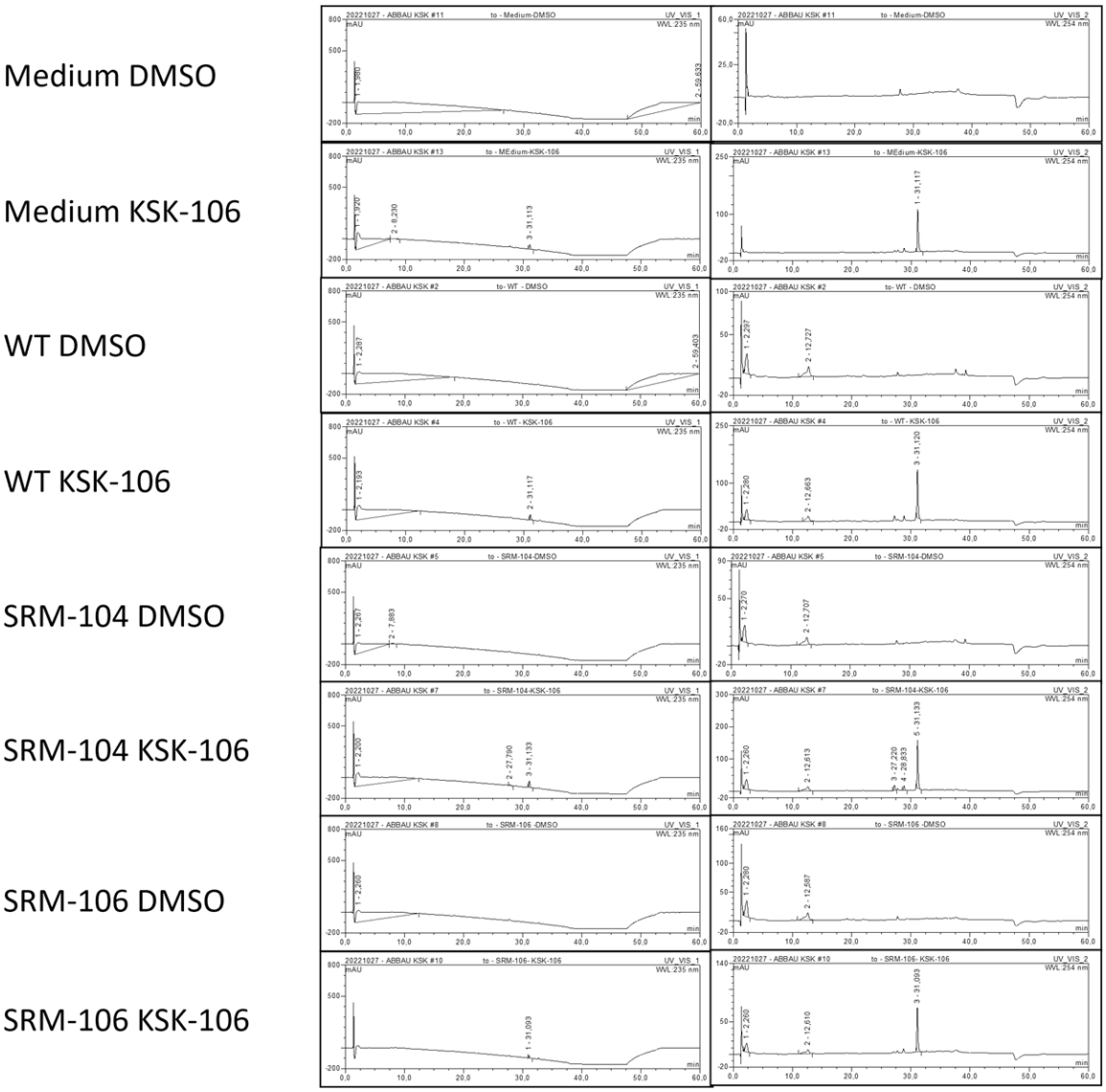

Figure S10: KSK-106 metabolization assay. Result of the screening, which was measured with a HPLC with DAD (Dionex). The graphs show the result of the measurement for the wavelength of 235 nm (left) and 254 nm (right) and the resulting UV-spectrum for the detected KSK molecules and their cleavage products (next page), which was found by comparison with a molecule library. Shown are the results for the incubation with 100 µM KSK-106 or DMSO, which were incubated with the wildtype strain (WT), SRM-KSK-104#1 (*rv0552*: H67R), and SRM KSK-106#5 (*amiC* E129*) *) for 0 h (t_0).

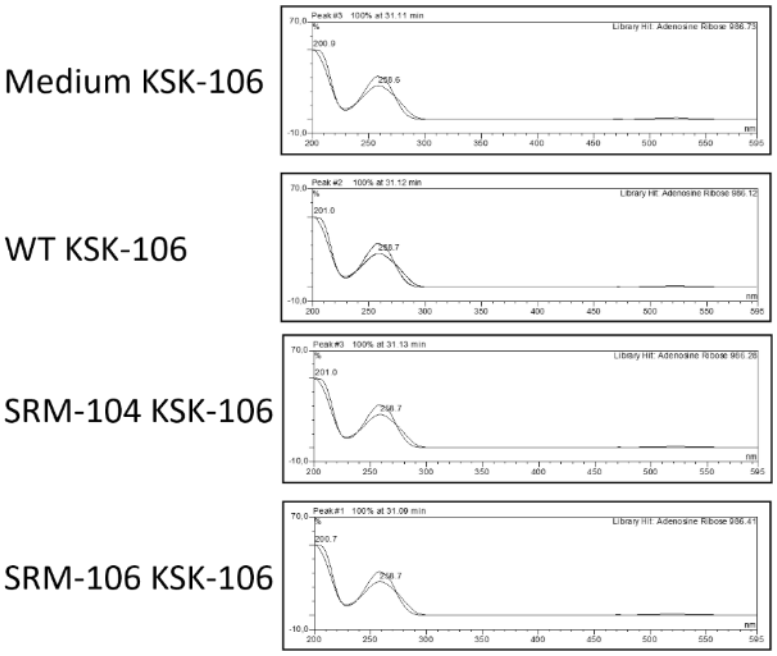

Figure S8a: KSK-106 metabolization assay t_0.

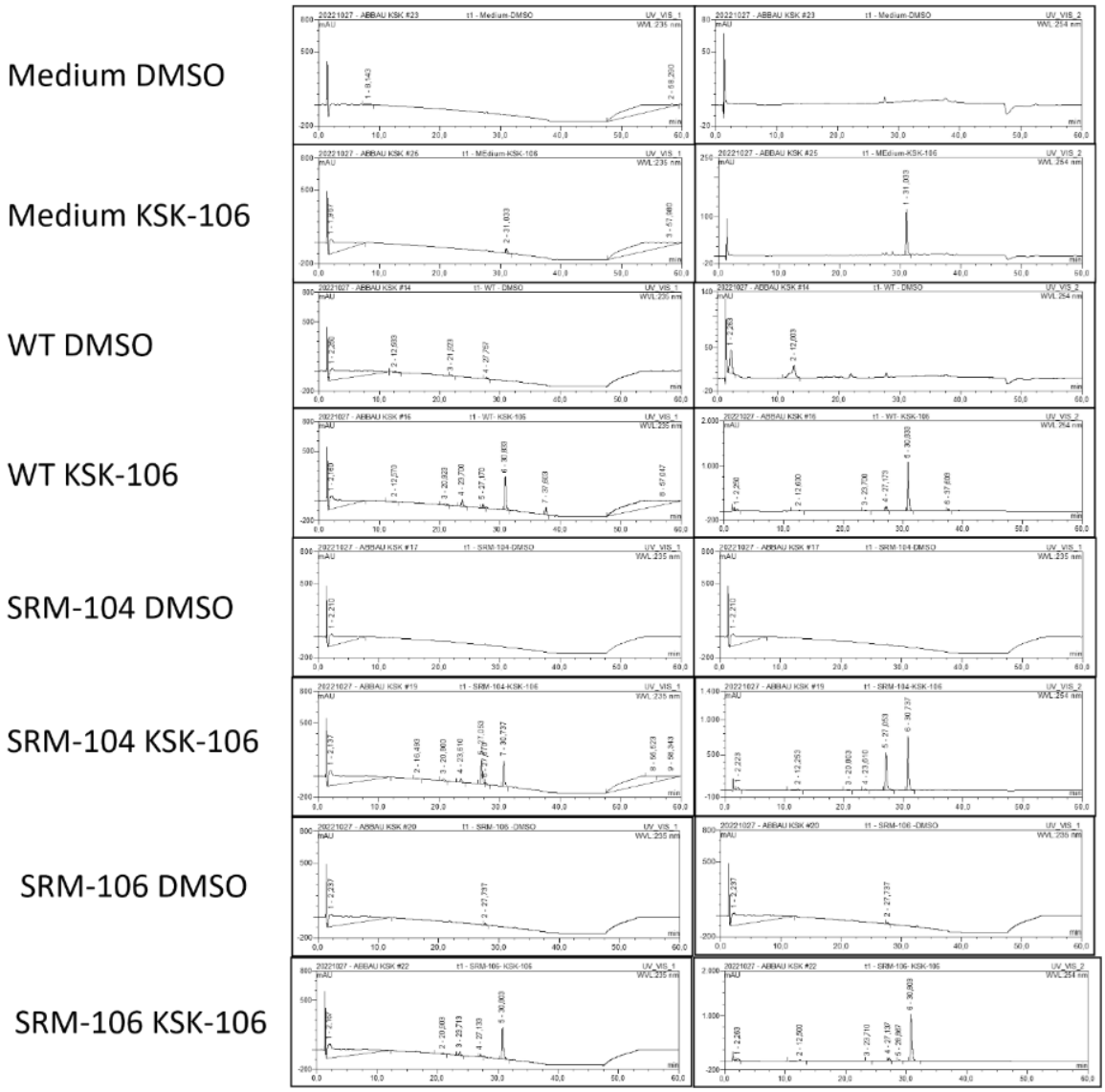

Figure S11: KSK-106 metabolization assay. Result of the screening, which was measured with a HPLC with DAD (Dionex). The graphs show the result of the measurement for the wavelength of 235 nm (left) and 254 nm (right) and the resulting UV-spectrum for the detected KSK molecules and their cleavage products (next page), which was found by comparison with a molecule library. Shown are the results for the incubation with 100 µM KSK-106 or DMSO, which were incubated with the wildtype strain (WT), SRM-KSK-104#1 (*rv0552*: H67R), and SRM KSK-106#5 (*amiC* E129*) for 24 h (t_1).

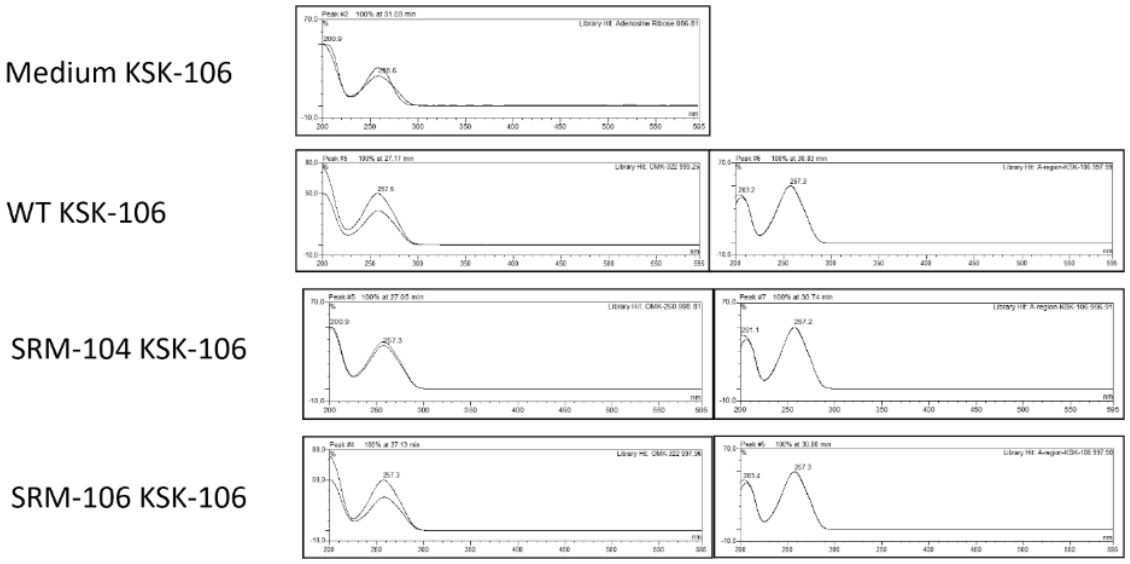

Figure S11a: KSK-106 metabolization assay t_1.

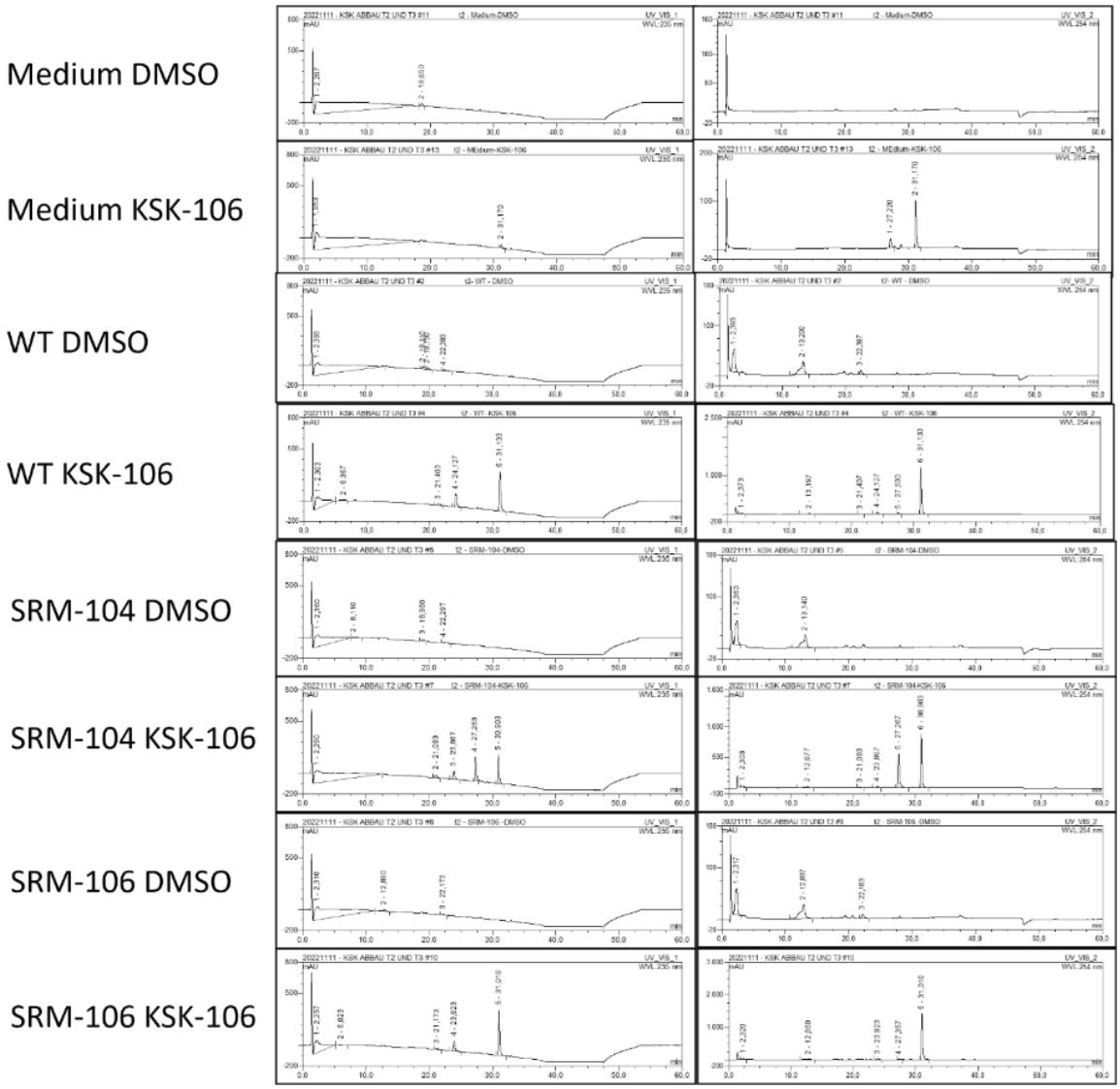

Figure S12: KSK-106 metabolization assay. Result of the screening, which was measured with a HPLC with DAD (Dionex). The graphs show the result of the measurement for the wavelength of 235 nm (left) and 254 nm (right) and the resulting UV-spectrum for the detected KSK molecules and their cleavage products (next page), which was found by comparison with a molecule library. Shown are the results for the incubation with 100 µM KSK-106 or DMSO, which were incubated with the wildtype strain (WT), SRM-KSK-104#1 (*rv0552*: H67R), and SRM KSK-106#5 (*amiC* E129*) for 48 h (t_2).

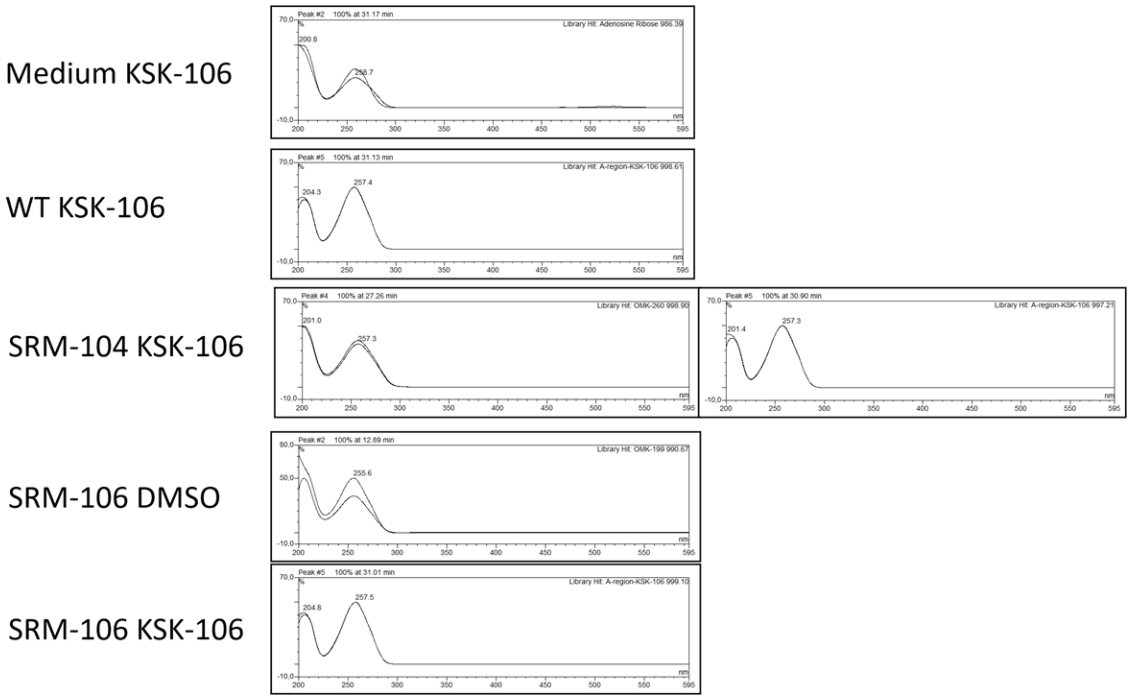

Figure S12a: KSK-106 metabolization assay t_2.

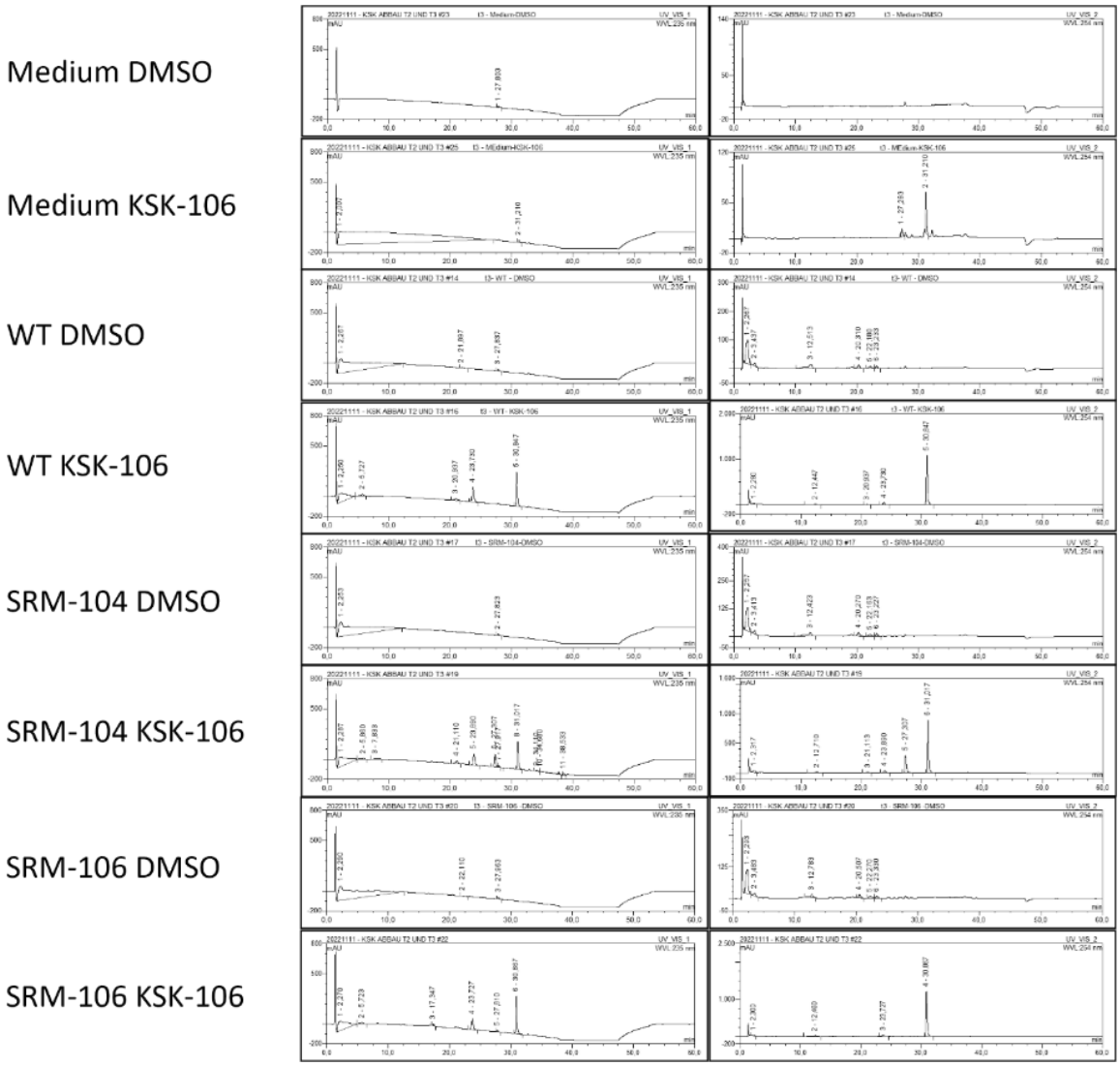

Figure S13: KSK-106 metabolization assay. Result of the screening, which was measured with a HPLC with DAD (Dionex). The graphs show the result of the measurement for the wavelength of 235 nm (left) and 254 nm (right) and the resulting UV-spectrum for the detected KSK molecules and their cleavage products (next page), which was found by comparison with a molecule library. Shown are the results for the incubation with 100 µM KSK-106 or DMSO, which were incubated with the wildtype strain (WT), SRM-KSK-104#1 (*rv0552*: H67R), and SRM KSK-106#5 (*amiC* E129*) for 7 days h (t_3).

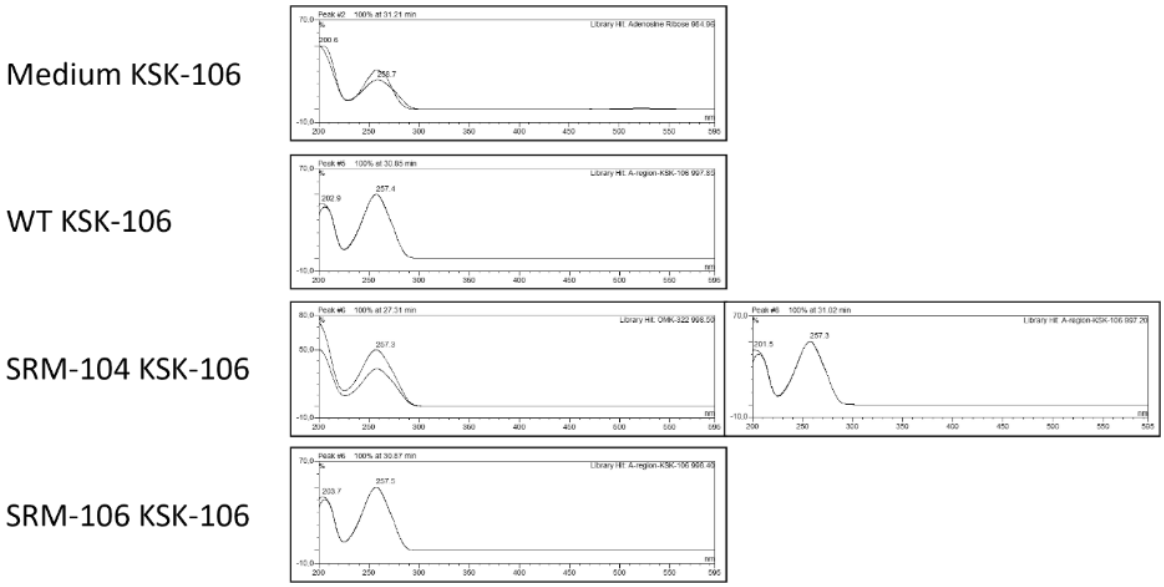

Figure S13a: KSK-106 metabolization assay t_3.

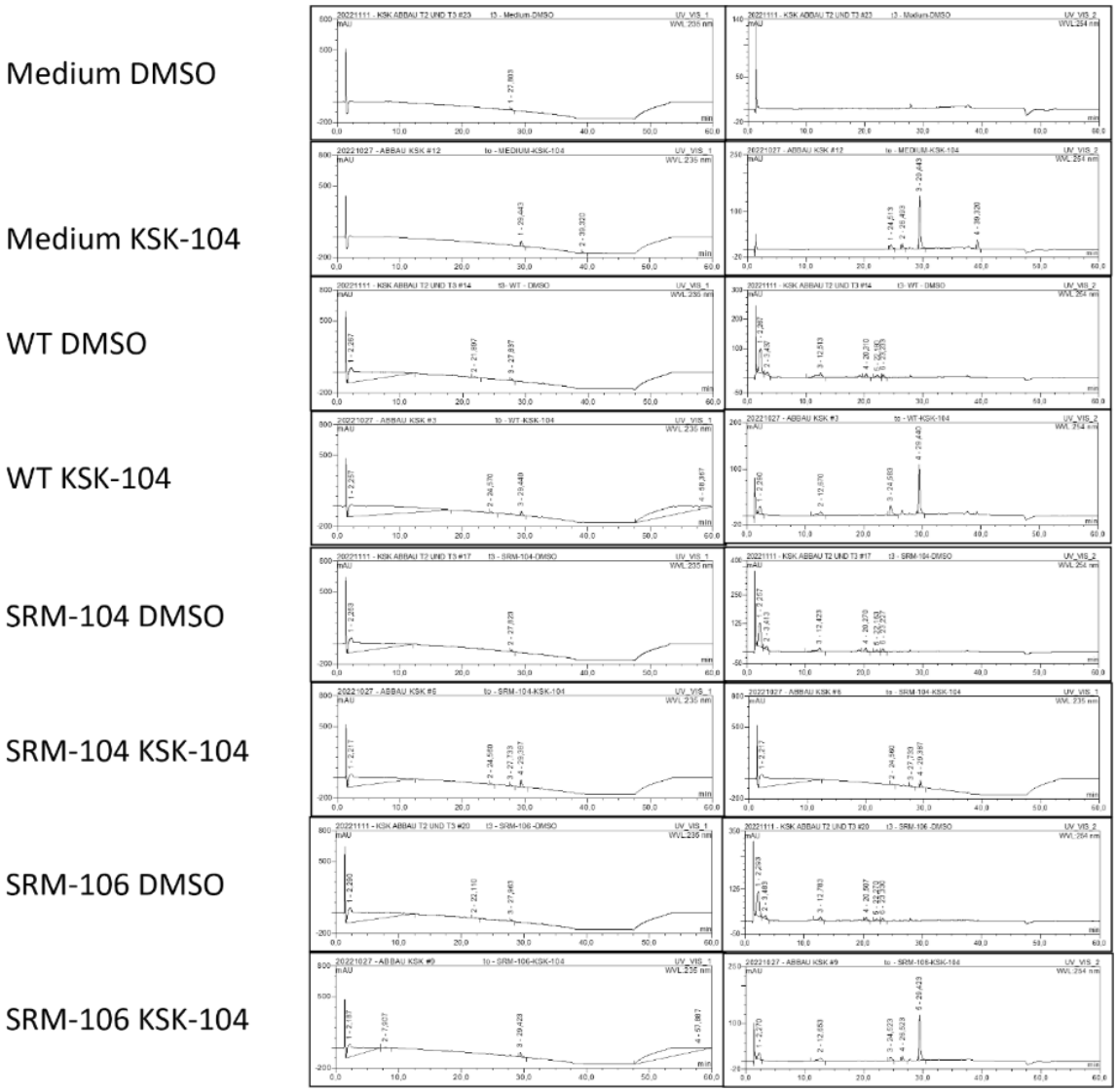

Figure S14: KSK-104 metabolization assay. Result of the screening, which was measured with a HPLC with DAD (Dionex)The graphs show the result of the measurement for the wavelength of 235 nm (left) and 254 nm (right) and the resulting UV-spectrum for the detected KSK molecules and their cleavage products (next page), which was found by comparison with a molecule library. Shown are the results for the incubation with 100 µM KSK-104 or DMSO, which were incubated with the wildtype strain (WT), SRM-KSK-104#1 (*rv0552*: H67R), and SRM KSK-106#5 (*amiC* E129*) for 0 h (t_0).

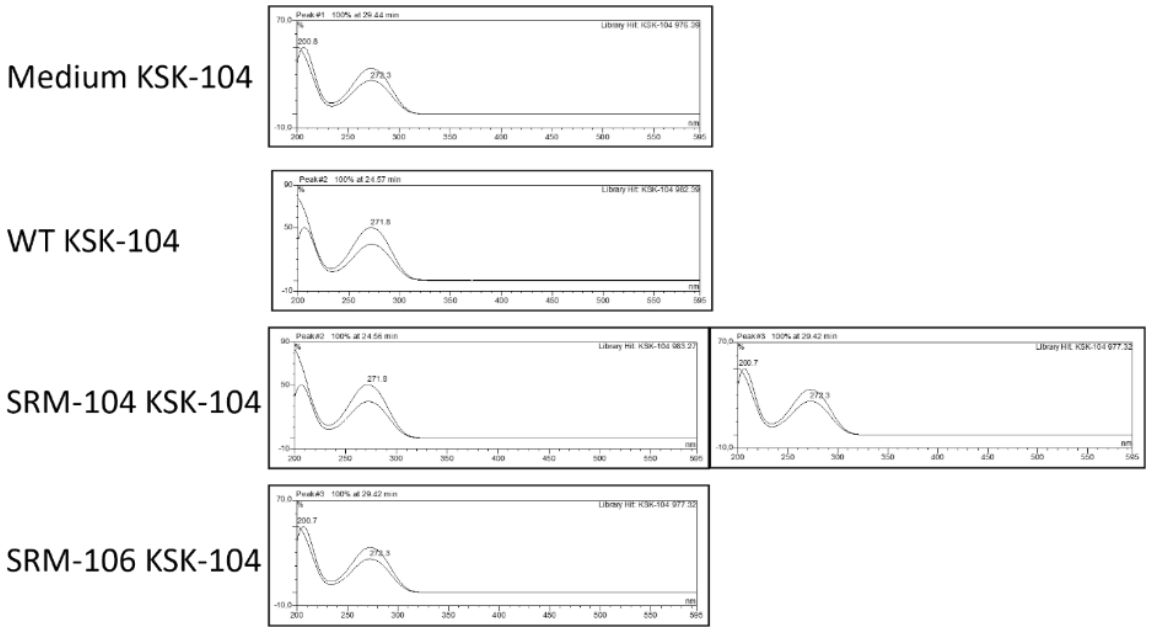

Figure S14: KSK-104 metabolization assay t_0.

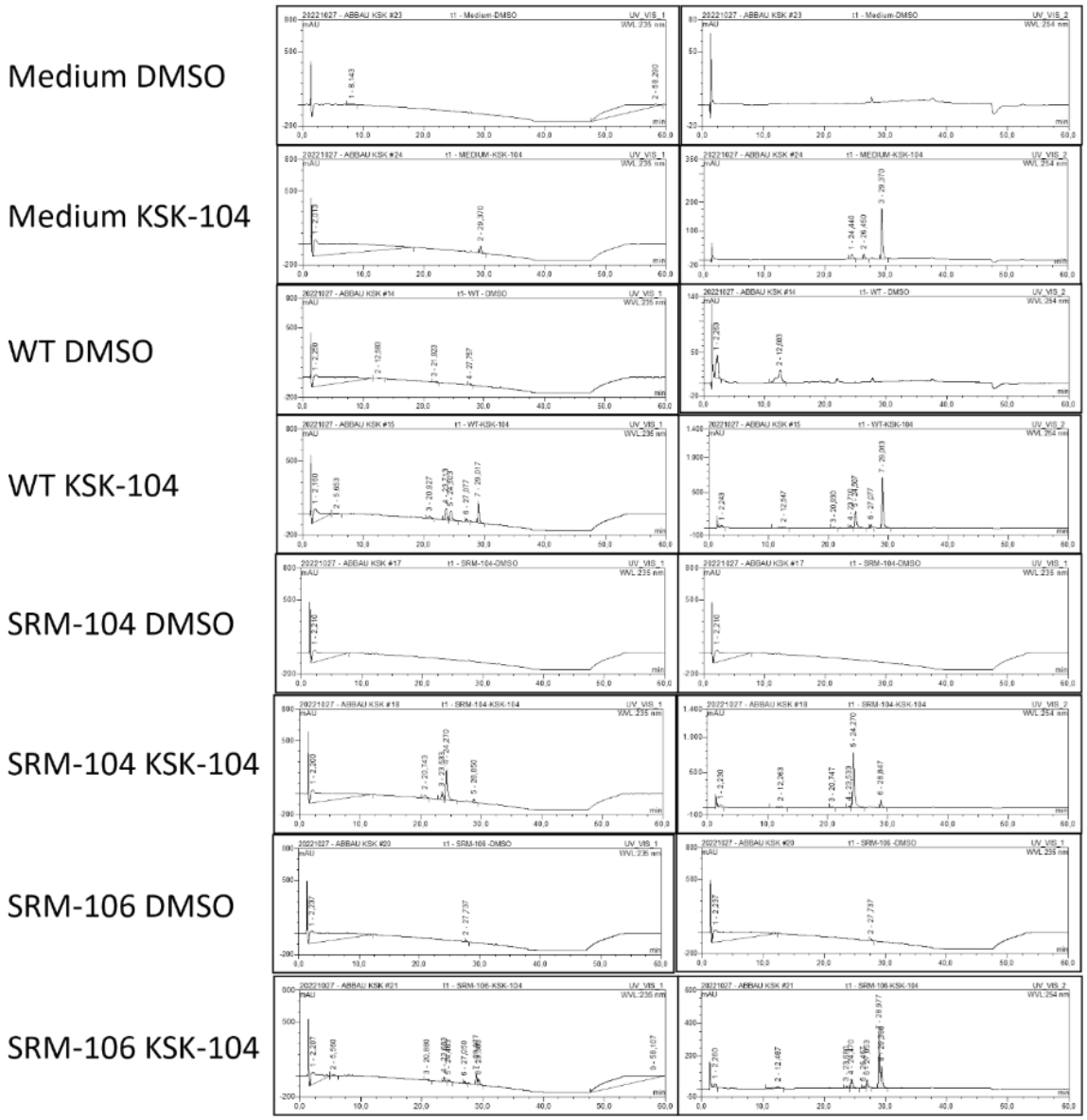

Figure S15: KSK-104 metabolization assay. Result of the screening, which was measured with a HPLC with DAD (Dionex). The graphs show the result of the measurement for the wavelength of 235 nm (left) and 254 nm (right) and the resulting UV-spectrum for the detected KSK molecules and their cleavage products (next page), which was found by comparison with a molecule library. Shown are the results for the incubation with 100 µM KSK-104 or DMSO, which were incubated with the wildtype strain (WT), SRM-KSK-104#1 (*rv0552*: H67R), and SRM KSK-106#5 (*amiC* E129*) for 24 h (t_1).

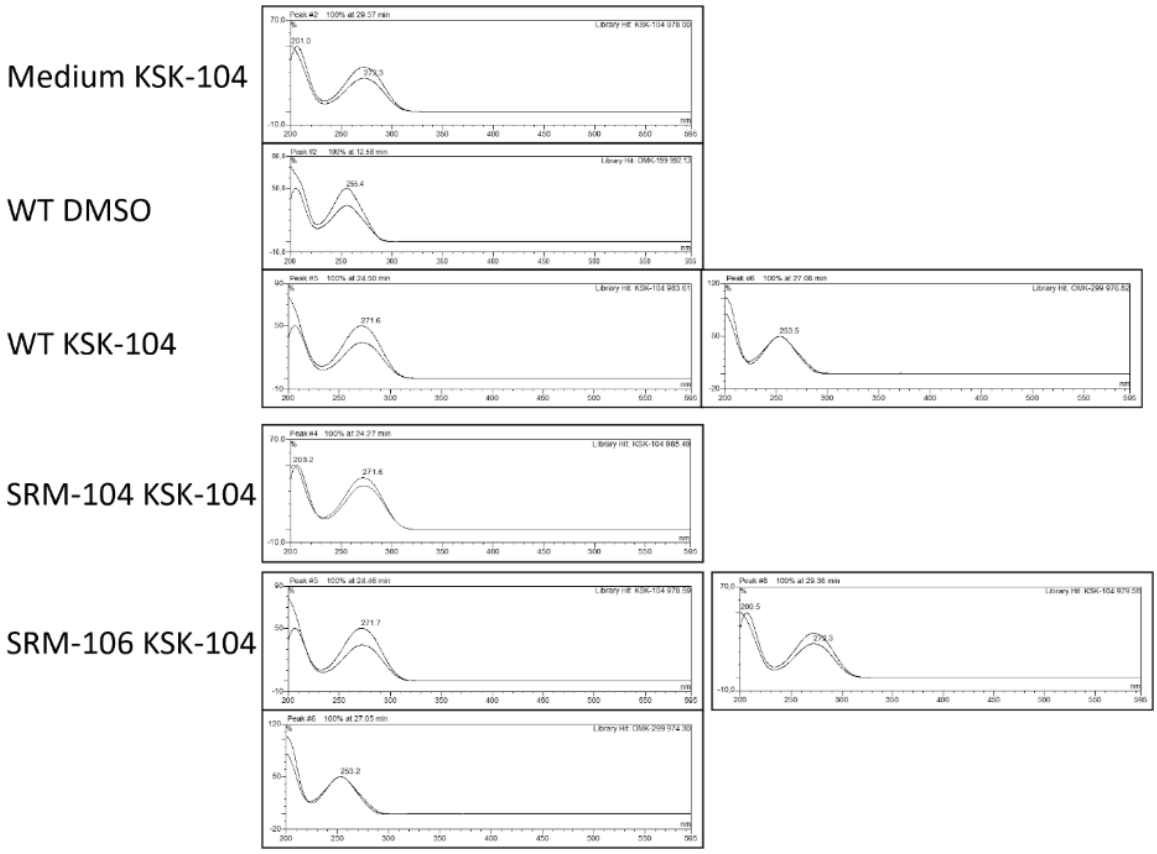

Figure S15a: KSK-104 metabolization assay t_1.

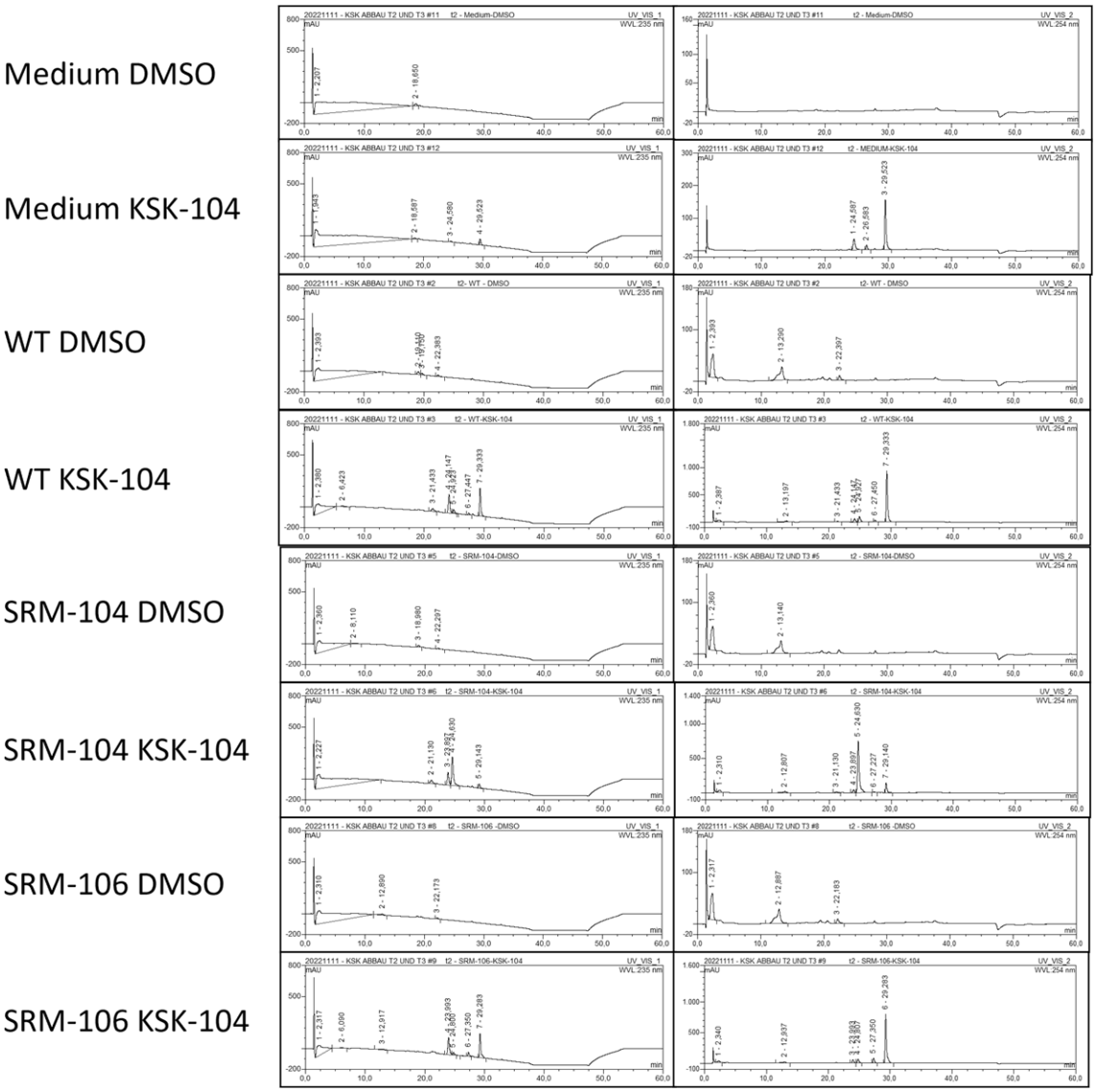

Figure S16: KSK-104 metabolization assay. Result of the screening, which was measured with a HPLC with DAD (Dionex). The graphs show the result of the measurement for the wavelength of 235 nm (left) and 254 nm (right) and the resulting UV-spectrum for the detected KSK molecules and their cleavage products (next page), which was found by comparison with a molecule library. Shown are the results for the incubation with 100 µM KSK-104 or DMSO, which were incubated with the wildtype strain (WT), SRM-KSK-104#1 (*rv0552*: H67R), and SRM KSK-106#5 (*amiC* E129*) for 48 h (t_2).

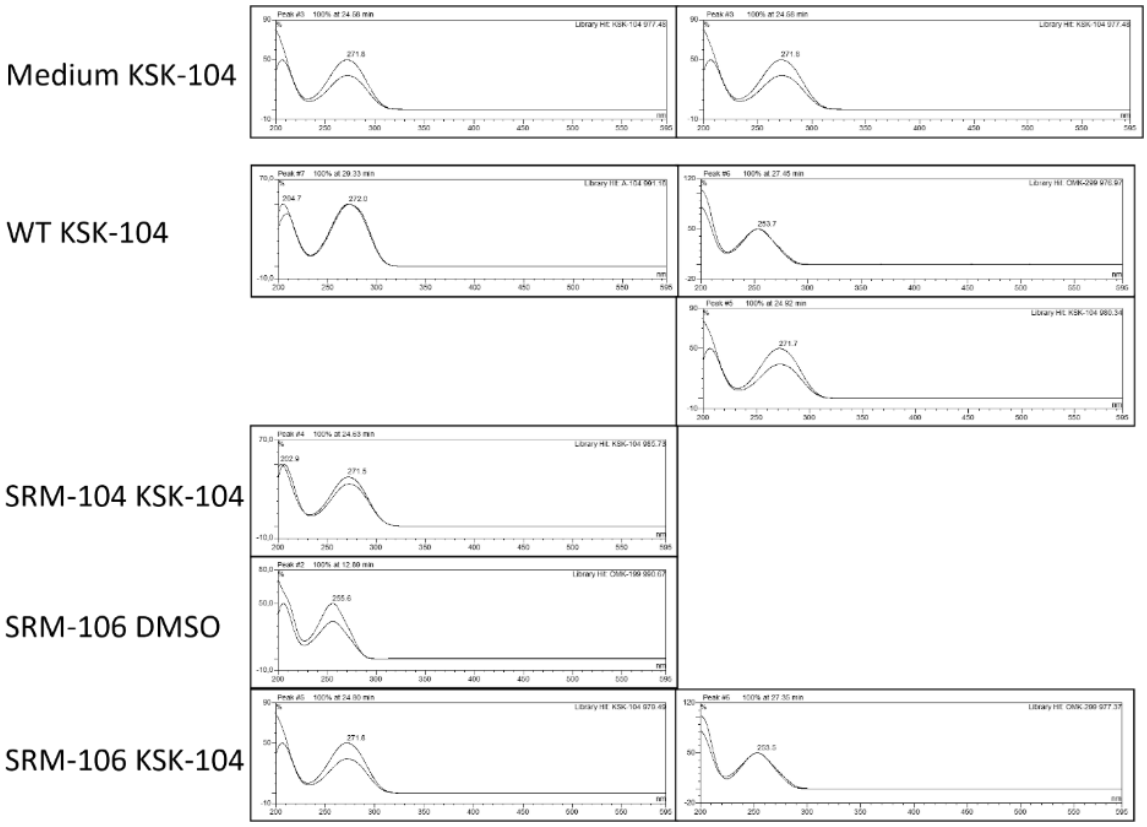

Figure S16a: KSK-104 metabolization assay t_2.

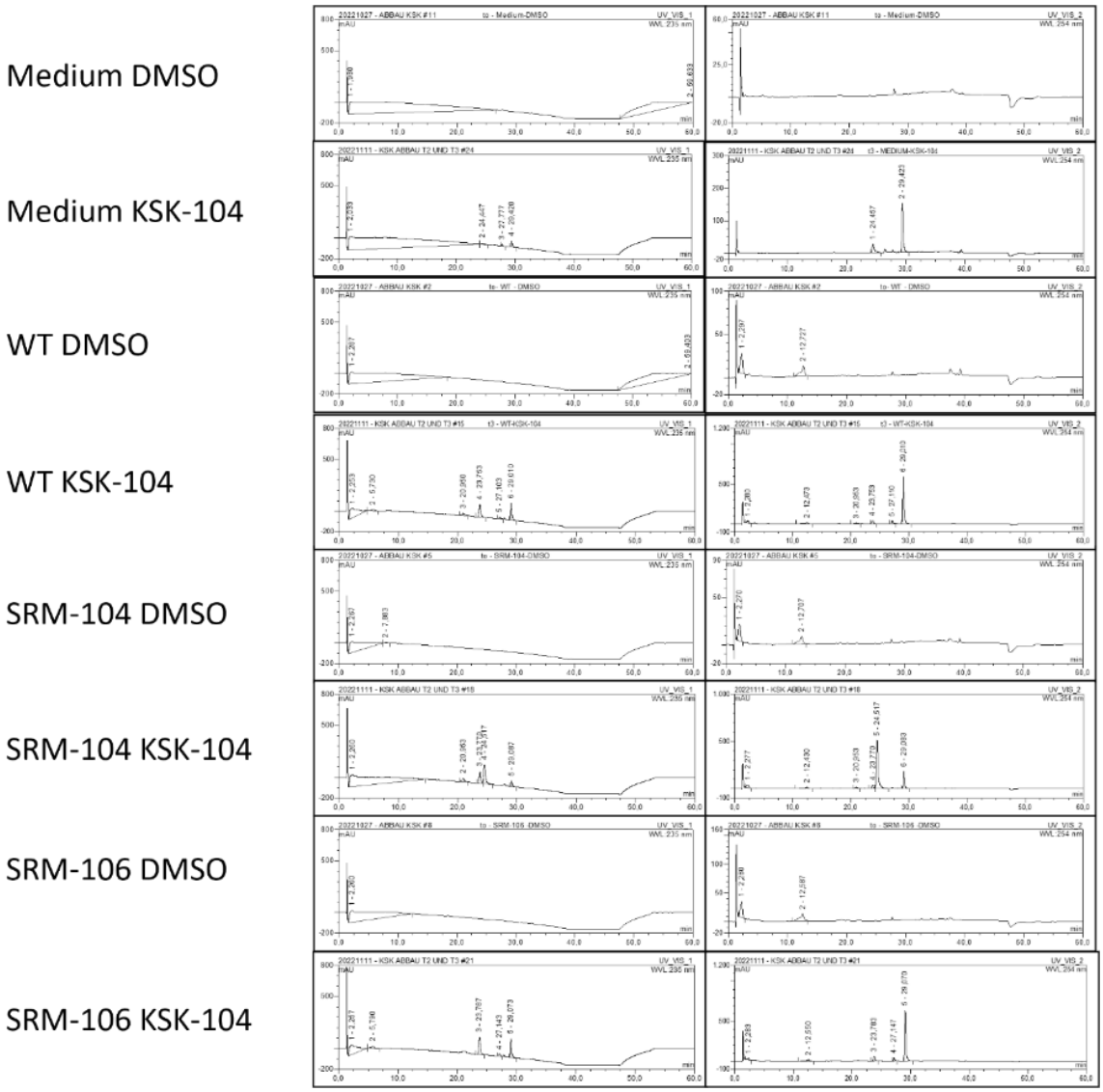

Figure S17: KSK-104 metabolization assay. Result of the screening, which was measured with a HPLC with DAD (Dionex). The graphs show the result of the measurement for the wavelength of 235 nm (left) and 254 nm (right) and the resulting UV-spectrum for the detected KSK-106 molecules and their cleavage products (next page), which was found by comparison with a molecule library. Shown are the results for the incubation with 100 µM KSK-104 or DMSO, which were incubated with the wildtype strain (WT), SRM-KSK-104#1 (*rv0552*: H67R), and SRM KSK-106#5 (*amiC* E129*) for 7 days (t_3).

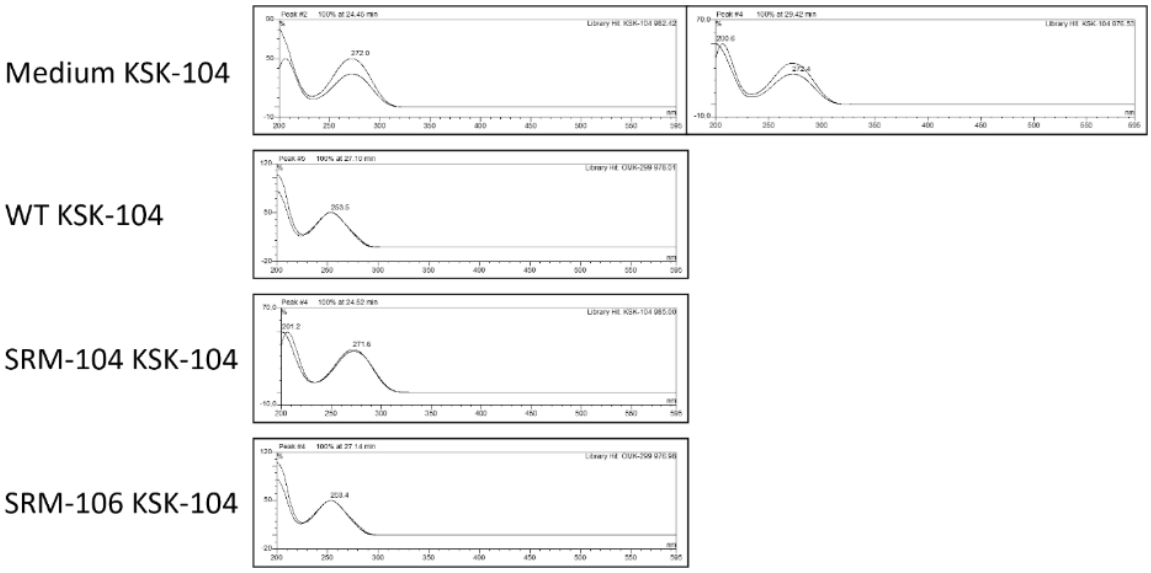

Figure S17a: KSK-104 metabolization assay t_3.

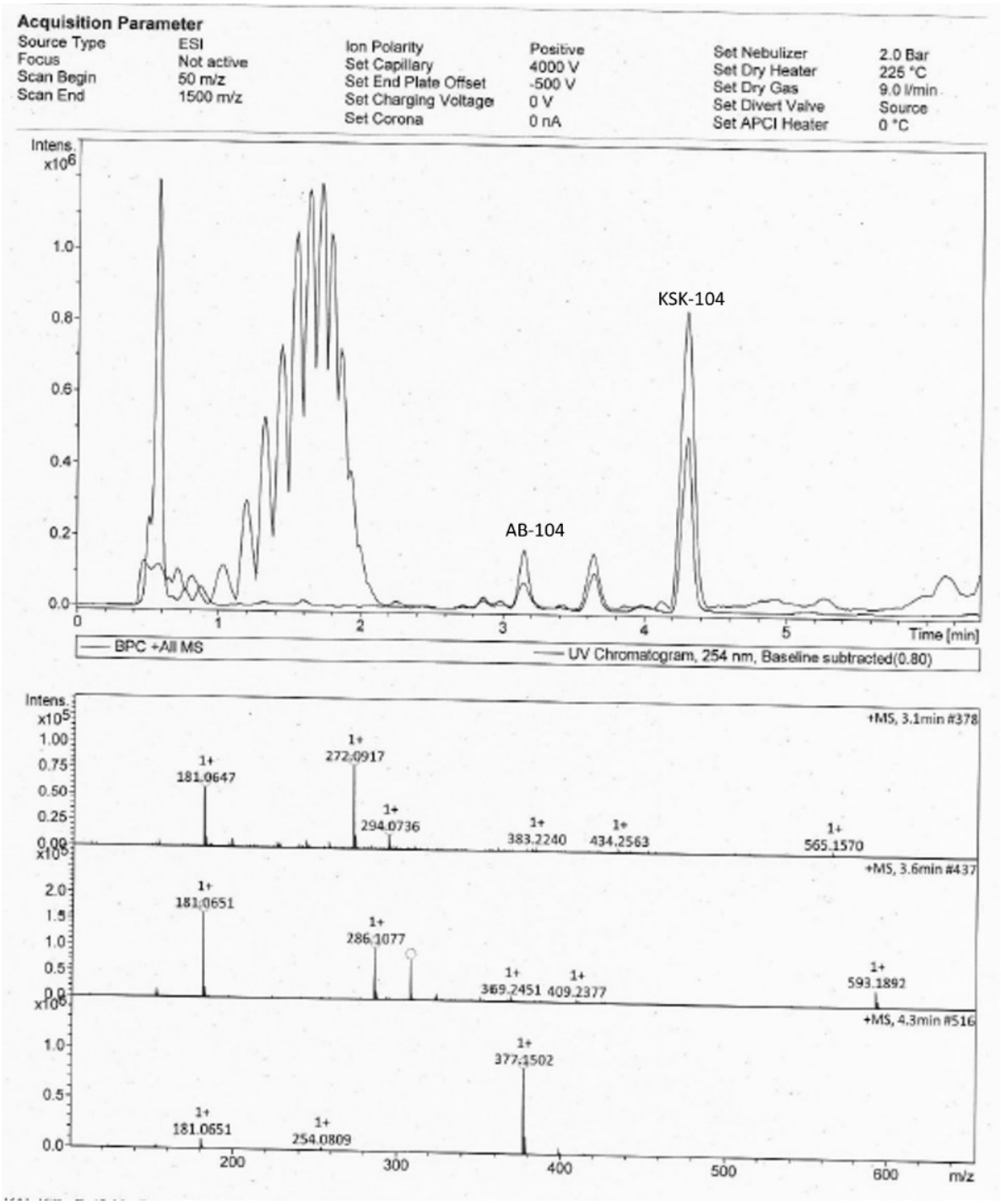

Figure S18: KSK-104 metabolization assay. Result of the screening, which was measured with the LC-MS. The results for the incubation with 100 µM KSK-104 are shown, which was incubated in a medium only for 48 h (t_2). The KSK derivative matching the molecular weight is written above the peak.

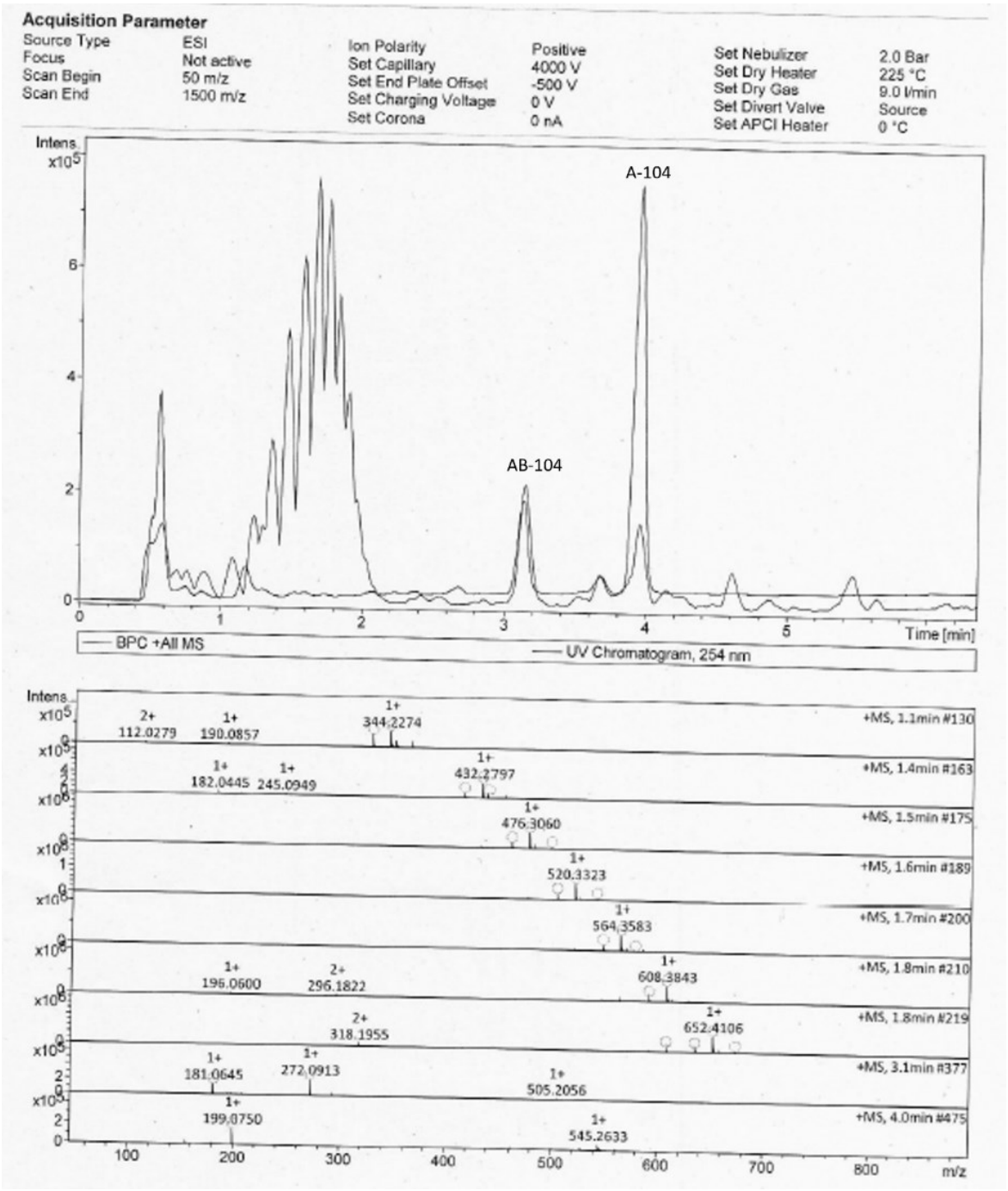

Figure S19: **KSK-104 metabolization assay.** Result of the screening, which was measured with the LC-MS. The results for the incubation with 100 µM KSK-104 are shown, which was incubated with H37Rv WT for 48 h (t_2). The KSK derivative matching the molecular weight is written above the peak.

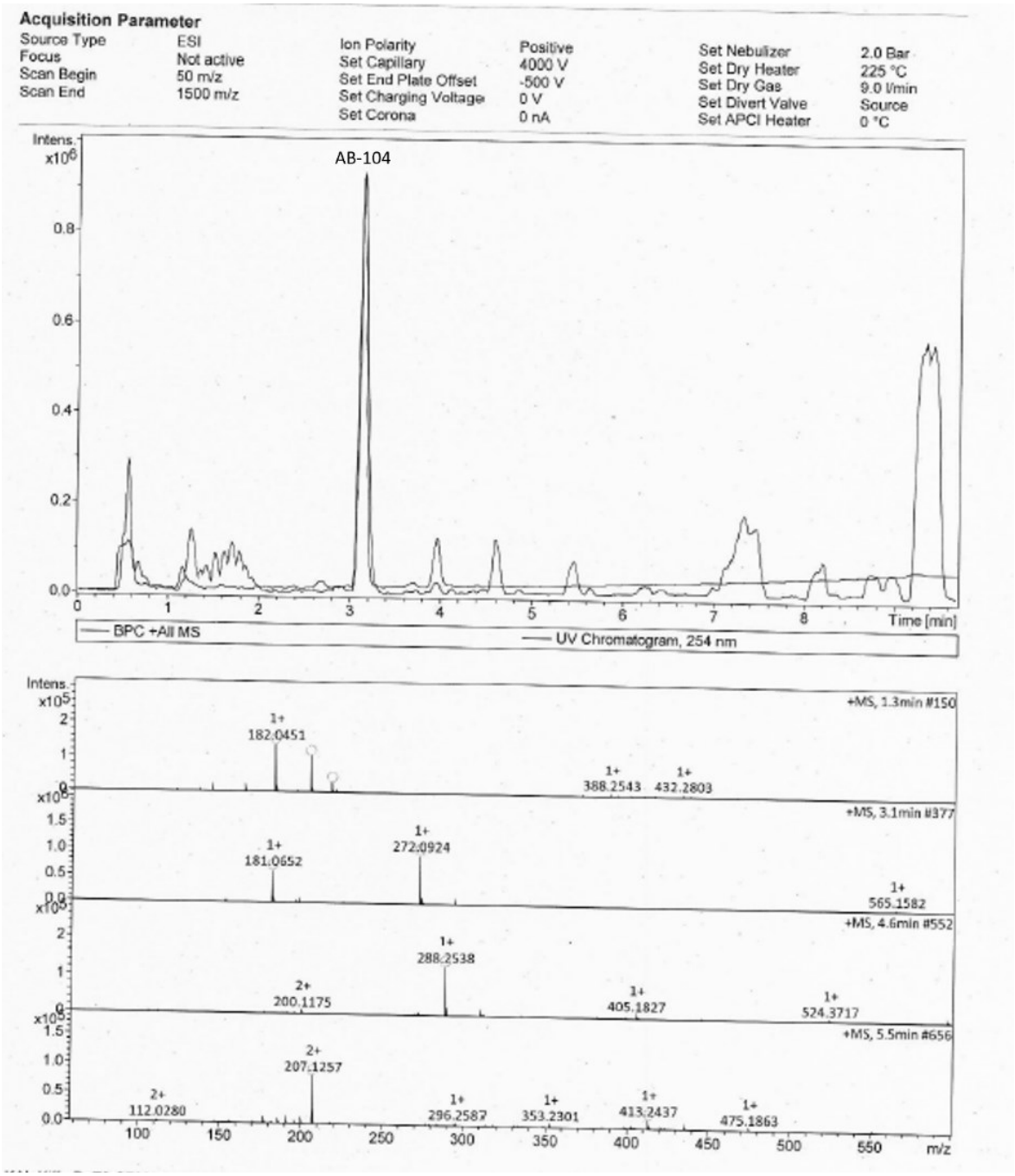

Figure S20: KSK-104 metabolization assay. Result of the screening, which was measured with the LC-MS. The results for the incubation with 100 µM KSK-104 are shown, which was incubated with SRM-KSK-104#1 (*rv0552*: H67R) for 48 h (t_2). The KSK derivative matching the molecular weight is written above the peak.

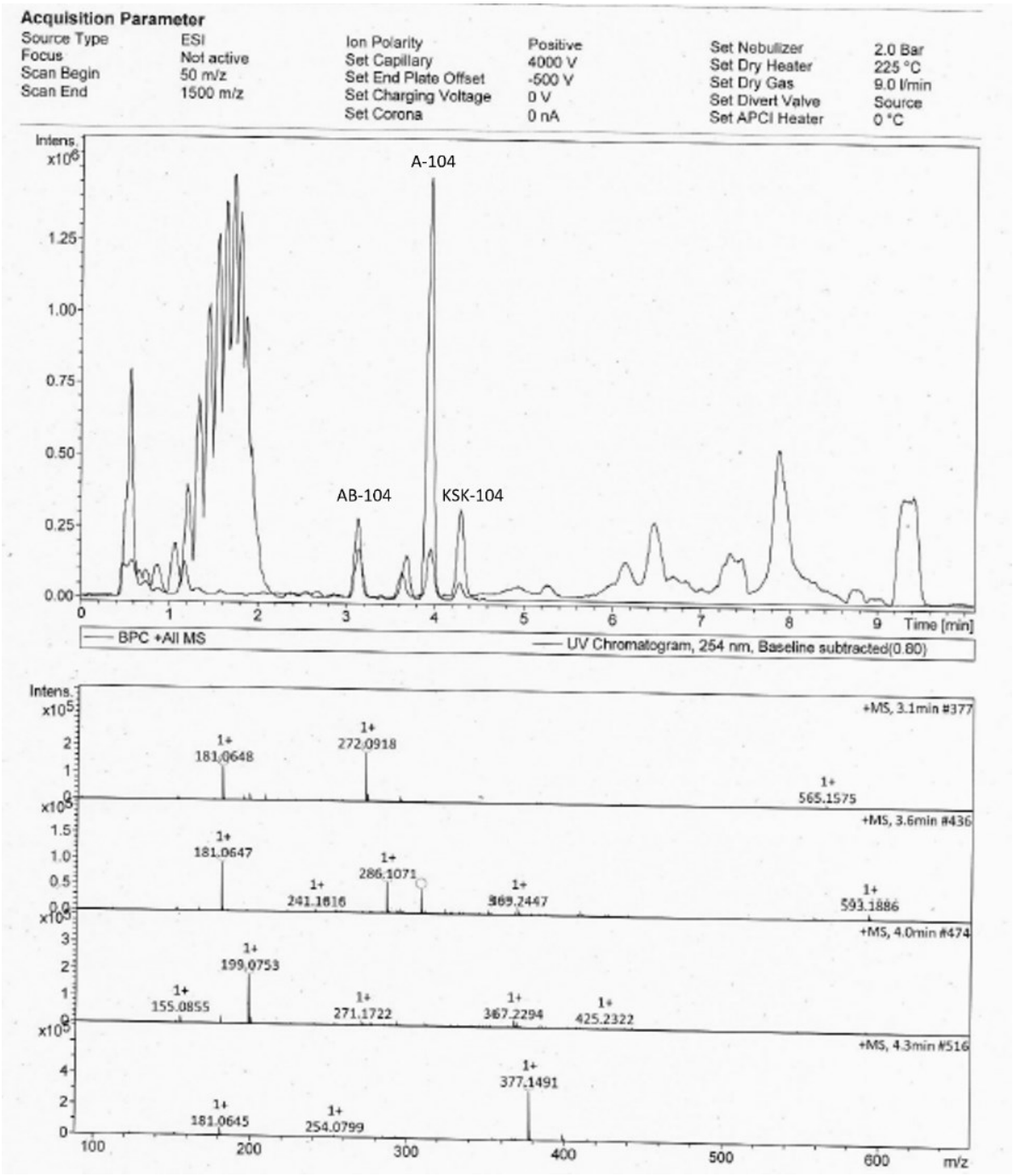

Figure S21: KSK-104 metabolization assay. Result of the screening, which was measured with the LC-MS. The results for the incubation with 100 µM KSK-104 are shown, which was incubated with SRM KSK-106#5 (*amiC* E129*) for 48 h (t_2). The KSK derivative matching the molecular weight is written above the peak.

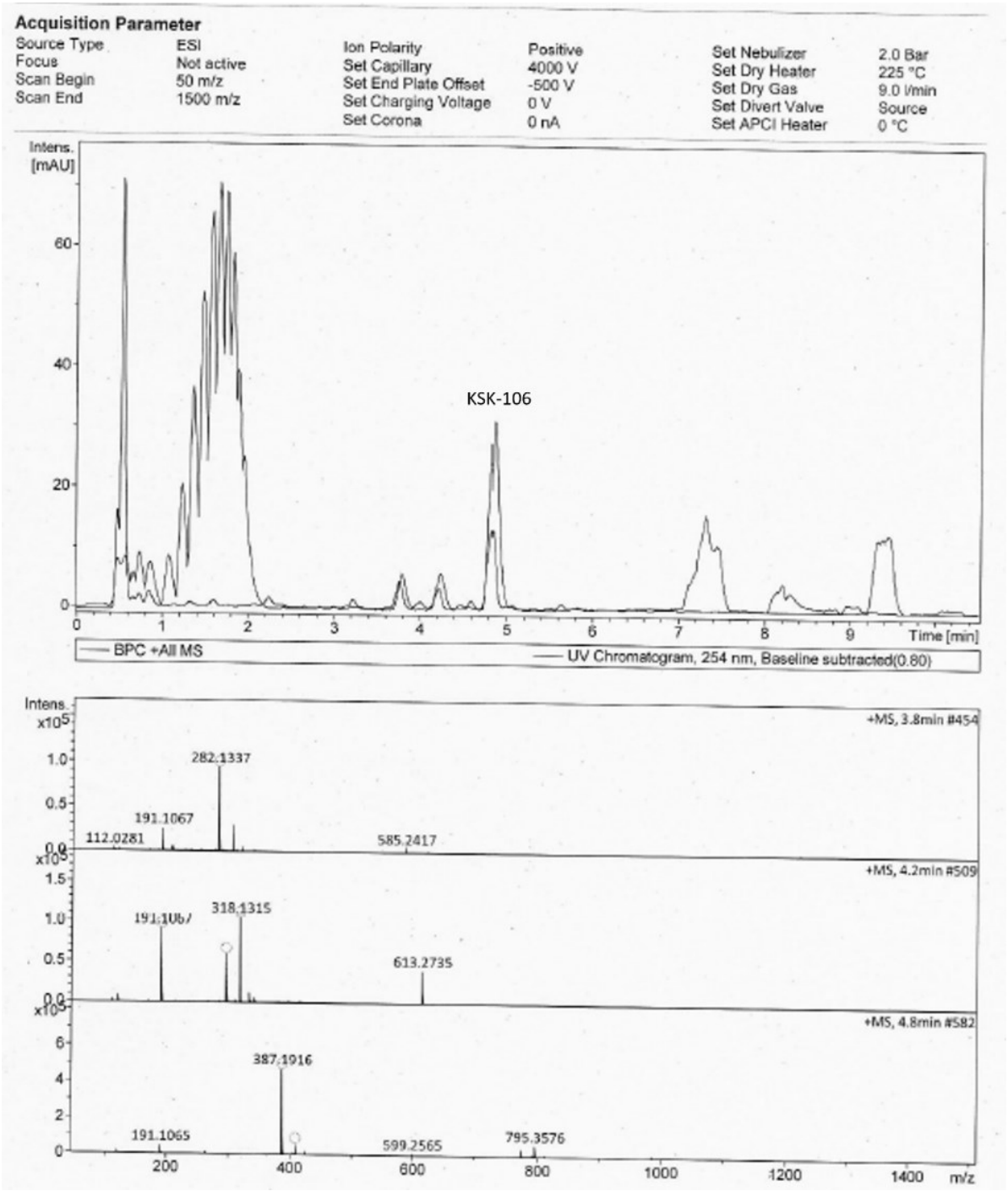

Figure S22: KSK-106 metabolization assay. Result of the screening, which was measured with the LC-MS. The results for the incubation with 100 µM KSK-106 are shown, which was incubated in a medium only for 48 h (t_2). The KSK derivative matching the molecular weight is written above the peak.

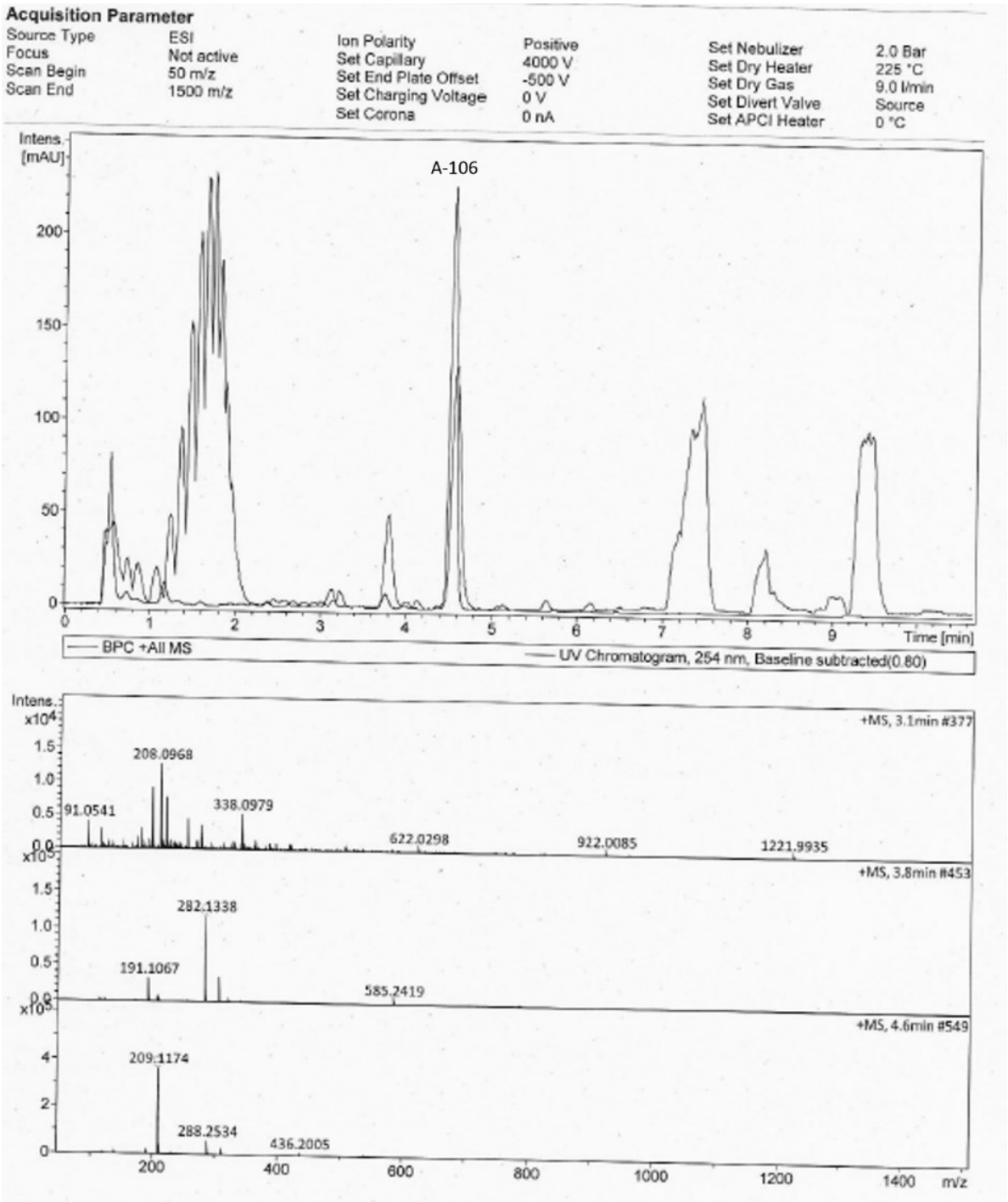

Figure S23: KSK-106 metabolization assay. Result of the screening, which was measured with the LC-MS. The results for the incubation with 100 µM KSK-106 are shown, which was incubated with H37Rv WT for 48 h (t_2). The KSK derivative matching the molecular weight is written above the peak.

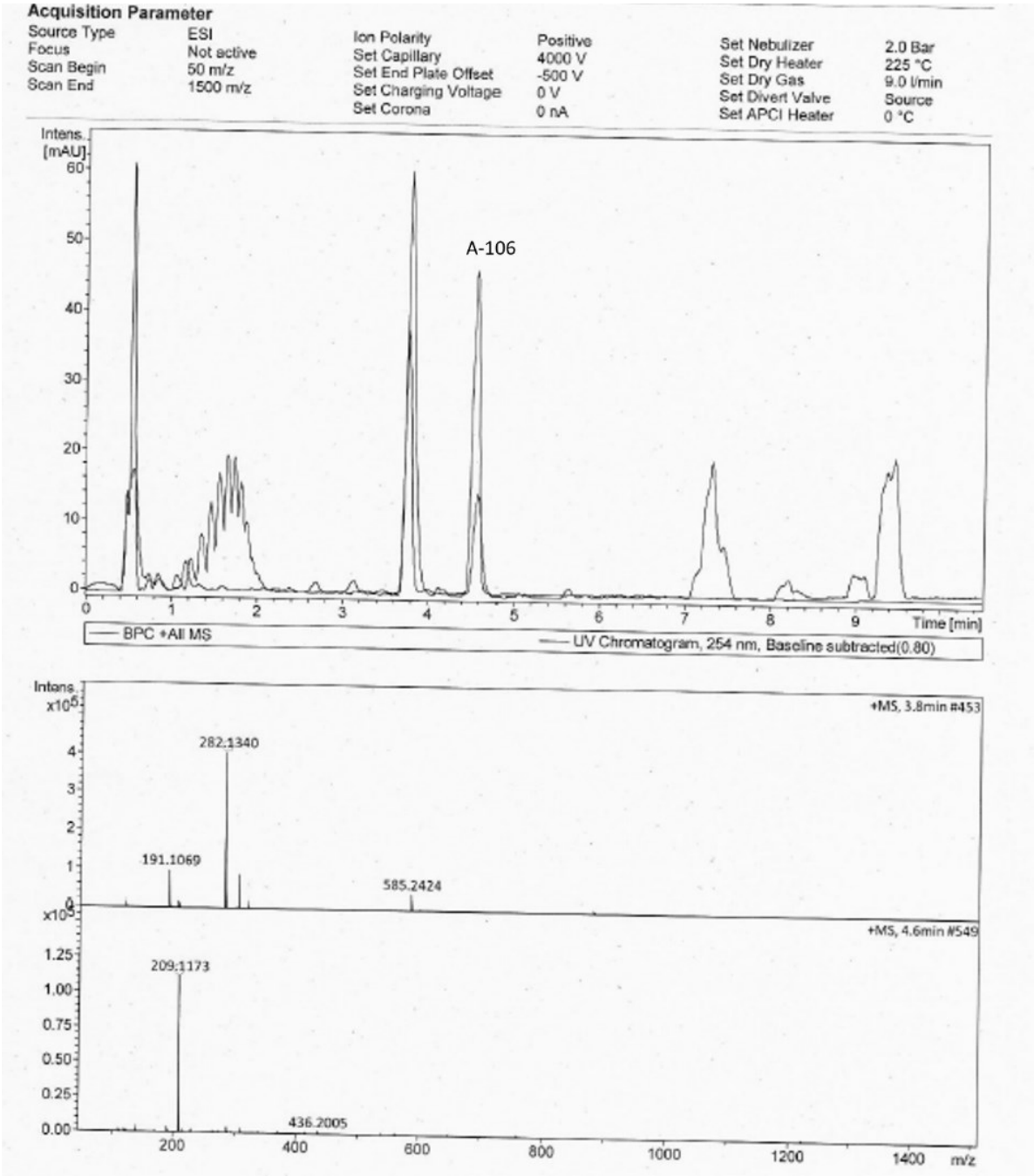

Figure S24: KSK-106 metabolization assay. Result of the screening, which was measured with the LC-MS. The results for the incubation with 100 µM KSK-106 are shown, which was incubated with SRM-KSK-104#1 (*rv0552*: H67R) for 48 h (t_2). The KSK derivative matching the molecular weight is written above the peak.

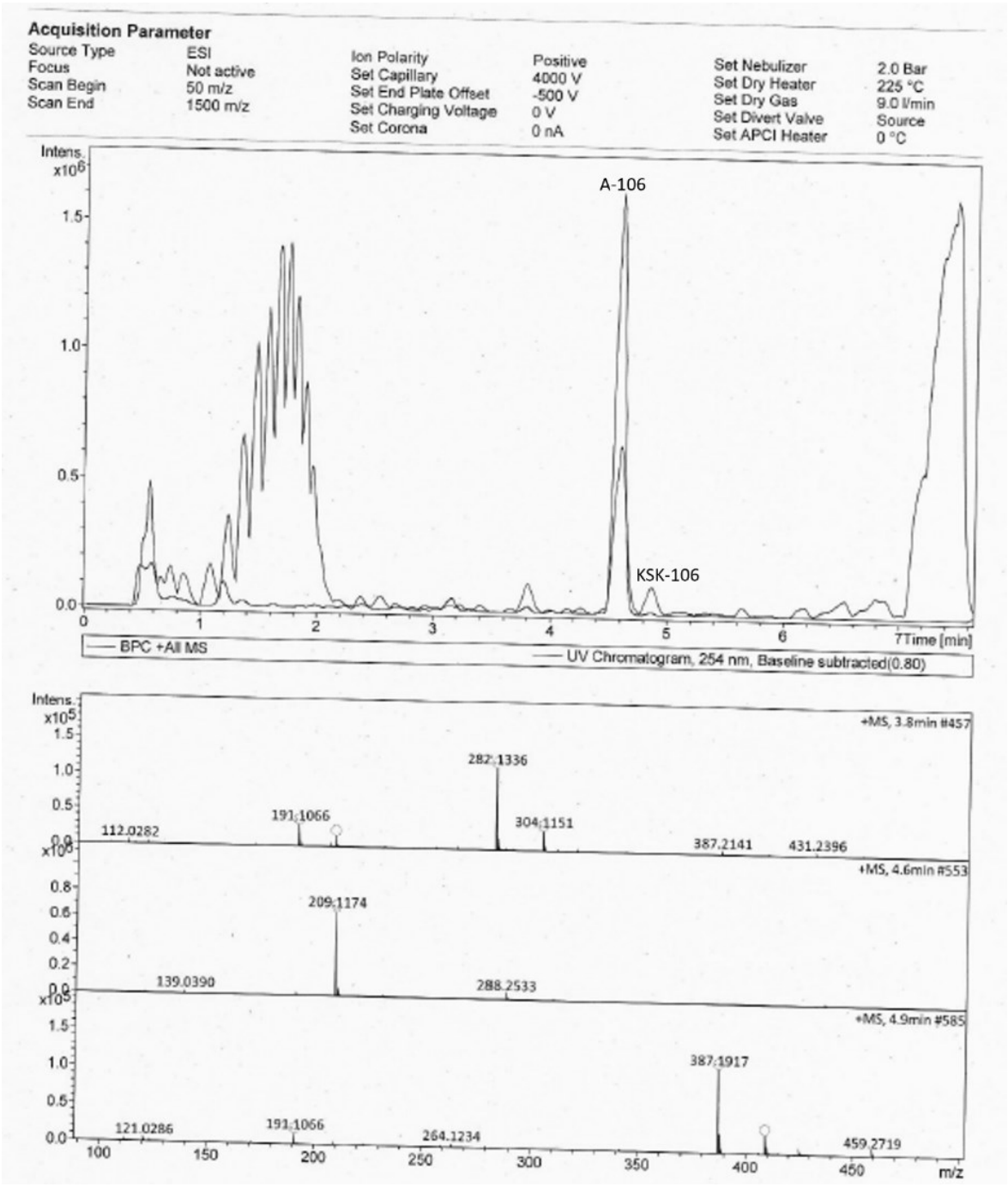

Figure S25: KSK-106 metabolization assay. Result of the screening, which was measured with the LC-MS. The results for the incubation with 100 µM KSK-106 are shown, which was incubated with SRM KSK-106#5 (*amiC* E129*) for 48 h (t_2). The KSK derivative matching the molecular weight is written above the peak.

Table S2: SNPs of spontaneous resistant mutants. SNPs of DSRM incubated on KSK-104 and KSK-106 (upper row) and two SRM incubated on a KSK-derivative, ABK-334.

Mutant	Gene	Region	Mutation
DSRM-KSK-104-106#9	ppsA	3248722	W1294 *
	Rv0552	643717	G276 R
	amiC	3196635^3196636	Ins1046 +cggc
ABK-334#1	ppsA	3248722	W1294 *
	amiC	3197318	Del 363 –g (121/474)
ABK-334#2	ppsA	3248722	W1294 *
	amiC	3197318	Del 363 –g (121/474)

6 References

1. *Global tuberculosis report 2022*, ed. W.H. Organization. 2022.
2. Fleming, A., *On the Antibacterial Action of Cultures of a Penicillium, with Special Reference to their Use in the Isolation of B. influenzæ.* Br J Exp Pathol, 1929. **10**(3): p. 226-36.
3. *2 - General Principles in the Diagnosis of Infection*, in *Diagnostic Pathology of Infectious Disease (Second Edition)*, L.K. Richard, Editor. 2018, Elsevier. p. 3-15.
4. O'NEILL, J., *TACKLING DRUG-RESISTANT INFECTIONS GLOBALLY: FINAL REPORT AND RECOMMENDATIONS. THE REVIEW ON ANTIMICROBIAL RESISTANCE*. 2016.
5. Steven, L.P. and W.W. David, *Chapter Nine - Mycobacterium*, in *Microbiology of Waterborne Diseases (Second Edition)*, L.P. Steven, et al., Editors. 2014, Academic Press: London. p. 177-207.
6. Iivanainen, E., *Mycobacteria in boreal soil and water environments.* 1999.
7. Falkinham, J.O., 3rd, *Epidemiology of infection by nontuberculous mycobacteria.* Clin Microbiol Rev, 1996. **9**(2): p. 177-215.
8. *Taxonomy of Mycobacteria , bookTitle= Mycobacteria: I Basic Aspects*. 1998, Boston, MA: Springer US. 1--71.
9. Vogelsang, T.M., *Discovery of Leprosy Bacillus.* JAMA, 1963. **184**(11): p. 901-902.
10. Koch, R., *Die aetiologie der tuberkulose.* 2010.
11. Crothers, J.W., A.C. Laga, and I.H. Solomon, *Clinical Performance of Mycobacterial Immunohistochemistry in Anatomic Pathology Specimens.* Am J Clin Pathol, 2021. **155**(1): p. 97-105.
12. Chung-Jong, K., et al., *Differentiating rapid- and slow-growing mycobacteria by difference in time to growth detection in liquid media.* Diagnostic Microbiology and Infectious Disease, 2013. **75**(1): p. 73-76.
13. T, J.A.S., et al., *Features of the biochemistry of Mycobacterium smegmatis, as a possible model for Mycobacterium tuberculosis.* Journal of Infection and Public Health, 2020. **13**(9): p. 1255-1264.
14. Wallace, R.J., Jr., et al., *Human Disease Due to Mycobacterium smegmatis.* The Journal of Infectious Diseases, 1988. **158**(1): p. 52-59.
15. Newton, G.L. and R.C. Fahey, *Mycothiol biochemistry.* Archives of microbiology, 2002. **178**: p. 388-394.
16. Brown-Elliott, B.A. and R.J. Wallace, Jr., *Clinical and taxonomic status of pathogenic nonpigmented or late-pigmenting rapidly growing mycobacteria.* Clin Microbiol Rev, 2002. **15**(4): p. 716-46.
17. Brown-Elliott, B.A. and J.V. Philley, *Rapidly Growing Mycobacteria.* Microbiol Spectr, 2017. **5**(1).
18. Sparks, I.L., et al., *Mycobacterium smegmatis: The Vanguard of Mycobacterial Research.* J Bacteriol, 2023. **205**(1): p. e0033722.
19. Andries, K., et al., *A diarylquinoline drug active on the ATP synthase of Mycobacterium tuberculosis.* Science, 2005. **307**(5707): p. 223-7.
20. Kanipe, C. and M.V. Palmer, *Mycobacterium bovis and you: A comprehensive look at the bacteria, its similarities to Mycobacterium tuberculosis, and its relationship with human disease.* Tuberculosis (Edinb), 2020. **125**: p. 102006.
21. Ramakrishnan, L., *Revisiting the role of the granuloma in tuberculosis.* Nat Rev Immunol, 2012. **12**(5): p. 352-66.
22. Devi, K.R., et al., *Occupational exposure and challenges in tackling M. bovis at human-animal interface: a narrative review.* Int Arch Occup Environ Health, 2021. **94**(6): p. 1147-1171.

23. Mahairas, G.G., et al., *Molecular analysis of genetic differences between Mycobacterium bovis BCG and virulent M. bovis.* J Bacteriol, 1996. **178**(5): p. 1274-82.
24. *The Bacillus Calmette-Guérin (B.C.G.).* British Journal of Tuberculosis, 1931. **25**(1): p. 24-30.
25. Lange, C., et al., *100 years of Mycobacterium bovis bacille Calmette-Guérin.* Lancet Infect Dis, 2022. **22**(1): p. e2-e12.
26. Fedrizzi, T., et al., *Genomic characterization of Nontuberculous Mycobacteria.* Sci Rep, 2017. **7**: p. 45258.
27. Gordon, S.V. and T. Parish, *Microbe Profile: Mycobacterium tuberculosis: Humanity's deadly microbial foe.* Microbiology (Reading), 2018. **164**(4): p. 437-439.
28. Hayman, J., *Mycobacterium ulcerans: an infection from Jurassic time?* The Lancet, 1984. **324**(8410): p. 1015-1016.
29. Sakula, A., *Robert koch: centenary of the discovery of the tubercle bacillus, 1882.* Can Vet J, 1983. **24**(4): p. 127-31.
30. Cole, S.T., et al., *Deciphering the biology of Mycobacterium tuberculosis from the complete genome sequence.* Nature, 1998. **393**(6685): p. 537-44.
31. Sassetti, C.M., D.H. Boyd, and E.J. Rubin, *Genes required for mycobacterial growth defined by high density mutagenesis.* Mol Microbiol, 2003. **48**(1): p. 77-84.
32. Kalscheuer, R., et al., *The Mycobacterium tuberculosis capsule: a cell structure with key implications in pathogenesis.* Biochem J, 2019. **476**(14): p. 1995-2016.
33. Zuber, B., et al., *Direct visualization of the outer membrane of mycobacteria and corynebacteria in their native state.* J Bacteriol, 2008. **190**(16): p. 5672-80.
34. Hoffmann, C., et al., *Disclosure of the mycobacterial outer membrane: cryo-electron tomography and vitreous sections reveal the lipid bilayer structure.* Proc Natl Acad Sci U S A, 2008. **105**(10): p. 3963-7.
35. Jackson, M., *The mycobacterial cell envelope-lipids.* Cold Spring Harb Perspect Med, 2014. **4**(10).
36. Liu, J., et al., *Mycolic acid structure determines the fluidity of the mycobacterial cell wall.* J Biol Chem, 1996. **271**(47): p. 29545-51.
37. Jankute, M., et al., *Assembly of the Mycobacterial Cell Wall.* Annu Rev Microbiol, 2015. **69**: p. 405-23.
38. Vincent, A.T., et al., *The Mycobacterial Cell Envelope: A Relict From the Past or the Result of Recent Evolution?* Frontiers in Microbiology, 2018. **9**.
39. Khan, A., et al., *Macrophage heterogeneity and plasticity in tuberculosis.* J Leukoc Biol, 2019. **106**(2): p. 275-282.
40. Russell, D.G., *Mycobacterium tuberculosis: here today, and here tomorrow.* Nature Reviews Molecular Cell Biology, 2001. **2**(8): p. 569-578.
41. Bloom, B.R., et al., *Tuberculosis*, in *Major Infectious Diseases*, K.K. Holmes, et al., Editors. 2017, The International Bank for Reconstruction and Development / The World Bank© 2017 International Bank for Reconstruction and Development / The World Bank.: Washington (DC).
42. Furin, J., H. Cox, and M. Pai, *Tuberculosis.* Lancet, 2019. **393**(10181): p. 1642-1656.
43. Natarajan, A., et al., *A systemic review on tuberculosis.* Indian J Tuberc, 2020. **67**(3): p. 295-311.
44. Law, S., et al., *Emergence of drug resistance in patients with tuberculosis cared for by the Indian health-care system: a dynamic modelling study.* The Lancet Public Health, 2017. **2**(1): p. e47-e55.
45. Trauer, J.M., J.T. Denholm, and E.S. McBryde, *Construction of a mathematical model for tuberculosis transmission in highly endemic regions of the Asia-pacific.* Journal of Theoretical Biology, 2014. **358**: p. 74-84.
46. Mehra, M., et al., *Assessment of tuberculosis burden in China using a dynamic disease simulation model.* Int J Tuberc Lung Dis, 2013. **17**(9): p. 1186-94.
47. Comas, I., et al., *Out-of-Africa migration and Neolithic coexpansion of Mycobacterium tuberculosis with modern humans.* Nature Genetics, 2013. **45**(10): p. 1176-1182.

48. Pai, M., et al., *Tuberculosis.* Nature Reviews Disease Primers, 2016. **2**(1): p. 16076.
49. Houben, R.M. and P.J. Dodd, *The Global Burden of Latent Tuberculosis Infection: A Re-estimation Using Mathematical Modelling.* PLoS Med, 2016. **13**(10): p. e1002152.
50. Migliori, G.B., et al., *Worldwide Effects of Coronavirus Disease Pandemic on Tuberculosis Services, January–April 2020.* Emerging Infectious Disease journal, 2020. **26**(11): p. 2709.
51. Modlin, R.L. and B.R. Bloom, *TB or Not TB: That Is No Longer the Question.* Science Translational Medicine, 2013. **5**(213): p. 213sr6-213sr6.
52. Drain, P.K., et al., *Incipient and Subclinical Tuberculosis: a Clinical Review of Early Stages and Progression of Infection.* Clin Microbiol Rev, 2018. **31**(4).
53. Barry, C.E., 3rd, et al., *The spectrum of latent tuberculosis: rethinking the biology and intervention strategies.* Nat Rev Microbiol, 2009. **7**(12): p. 845-55.
54. Esmail, H., et al., *The ongoing challenge of latent tuberculosis.* Philos Trans R Soc Lond B Biol Sci, 2014. **369**(1645): p. 20130437.
55. Dorhoi, A. and S.H.E. Kaufmann, *Perspectives on host adaptation in response to Mycobacterium tuberculosis: Modulation of inflammation.* Seminars in Immunology, 2014. **26**(6): p. 533-542.
56. Queval, C.J., R. Brosch, and R. Simeone, *The Macrophage: A Disputed Fortress in the Battle against Mycobacterium tuberculosis.* Front Microbiol, 2017. **8**: p. 2284.
57. Manzanillo, P.S., et al., *Mycobacterium tuberculosis activates the DNA-dependent cytosolic surveillance pathway within macrophages.* Cell Host Microbe, 2012. **11**(5): p. 469-80.
58. Pieters, J., *Mycobacterium tuberculosis and the macrophage: maintaining a balance.* Cell Host Microbe, 2008. **3**(6): p. 399-407.
59. Adams, D.O., *The granulomatous inflammatory response. A review.* Am J Pathol, 1976. **84**(1): p. 164-92.
60. Spector, W.G., *The granulomatous inflammatory exudate.* Int Rev Exp Pathol, 1969. **8**: p. 1-55.
61. Williams, G.T. and W.J. Williams, *Granulomatous inflammation--a review.* J Clin Pathol, 1983. **36**(7): p. 723-33.
62. Lin, P.L. and J.L. Flynn, *Understanding Latent Tuberculosis: A Moving Target.* The Journal of Immunology, 2010. **185**(1): p. 15-22.
63. Colditz, G.A., et al., *The efficacy of bacillus Calmette-Guérin vaccination of newborns and infants in the prevention of tuberculosis: meta-analyses of the published literature.* Pediatrics, 1995. **96**(1 Pt 1): p. 29-35.
64. Gengenbacher, M. and S.H. Kaufmann, *Mycobacterium tuberculosis: success through dormancy.* FEMS Microbiol Rev, 2012. **36**(3): p. 514-32.
65. Reyrat, J.M., F.X. Berthet, and B. Gicquel, *The urease locus of Mycobacterium tuberculosis and its utilization for the demonstration of allelic exchange in Mycobacterium bovis bacillus Calmette-Guérin.* Proc Natl Acad Sci U S A, 1995. **92**(19): p. 8768-72.
66. Selvaraj, S., et al., *In silico analysis of DosR regulon proteins of Mycobacterium tuberculosis.* Gene, 2012. **506**(1): p. 233-41.
67. Dutta, N.K. and P.C. Karakousis, *Latent tuberculosis infection: myths, models, and molecular mechanisms.* Microbiol Mol Biol Rev, 2014. **78**(3): p. 343-71.
68. Park, H.D., et al., *Rv3133c/dosR is a transcription factor that mediates the hypoxic response of Mycobacterium tuberculosis.* Mol Microbiol, 2003. **48**(3): p. 833-43.
69. Gerasimova, A., et al., *Comparative genomics of the dormancy regulons in mycobacteria.* J Bacteriol, 2011. **193**(14): p. 3446-52.
70. Bartek, I.L., et al., *The DosR regulon of M. tuberculosis and antibacterial tolerance.* Tuberculosis (Edinb), 2009. **89**(4): p. 310-6.
71. Mukamolova, G.V., et al., *The rpf gene of Micrococcus luteus encodes an essential secreted growth factor.* Mol Microbiol, 2002. **46**(3): p. 611-21.

72. Leistikow, R.L., et al., *The Mycobacterium tuberculosis DosR regulon assists in metabolic homeostasis and enables rapid recovery from nonrespiring dormancy.* J Bacteriol, 2010. **192**(6): p. 1662-70.
73. Mc, D.W., *Microbial persistence.* Yale J Biol Med, 1958. **30**(4): p. 257-91.
74. Organization, W.H., *WHO Director-General's opening remarks at the media briefing on COVID-19-11 March 2020*. 2020, Geneva, Switzerland.
75. Wu, Z. and J.M. McGoogan, *Characteristics of and Important Lessons From the Coronavirus Disease 2019 (COVID-19) Outbreak in China: Summary of a Report of 72 314 Cases From the Chinese Center for Disease Control and Prevention.* JAMA, 2020. **323**(13): p. 1239-1242.
76. Ong, C.W.M., et al., *Epidemic and pandemic viral infections: impact on tuberculosis and the lung.* A consensus by the World Association for Infectious Diseases and Immunological Disorders (WAidid), Global Tuberculosis Network (GTN), and members of the European Society of Clinical Microbiology and Infectious Diseases Study Group for Mycobacterial Infections (ESGMYC), 2020. **56**(4): p. 2001727.
77. Waksman, S.A., *Definition of antibiotic.* Int Rec Med Gen Pract Clin, 1956. **169**(2): p. 87-8.
78. Fleming, A., *On the antibacterial action of cultures of a penicillium, with special reference to their use in the isolation of B. influenzae. 1929.* Bull World Health Organ, 2001. **79**(8): p. 780-90.
79. Hutchings, M.I., A.W. Truman, and B. Wilkinson, *Antibiotics: past, present and future.* Curr Opin Microbiol, 2019. **51**: p. 72-80.
80. Christensen, S.B., *Drugs That Changed Society: History and Current Status of the Early Antibiotics: Salvarsan, Sulfonamides, and β-Lactams.* Molecules, 2021. **26**(19).
81. Kardos, N. and A.L. Demain, *Penicillin: the medicine with the greatest impact on therapeutic outcomes.* Appl Microbiol Biotechnol, 2011. **92**(4): p. 677-87.
82. Wohlleben, W., et al., *Antibiotic drug discovery.* Microb Biotechnol, 2016. **9**(5): p. 541-8.
83. Waksman, S.A., A. Schatz, and D.M. Reynolds, *PRODUCTION OF ANTIBIOTIC SUBSTANCES BY ACTINOMYCETES*†.* Annals of the New York Academy of Sciences, 2010. **1213**(1): p. 112-124.
84. Waksman, S.A. and H.B. Woodruff, *Actinomyces antibioticus, a New Soil Organism Antagonistic to Pathogenic and Non-pathogenic Bacteria.* J Bacteriol, 1941. **42**(2): p. 231-49.
85. Newman, D.J. and G.M. Cragg, *Natural Products as Sources of New Drugs from 1981 to 2014.* Journal of Natural Products, 2016. **79**(3): p. 629-661.
86. Katz, L. and R.H. Baltz, *Natural product discovery: past, present, and future.* Journal of Industrial Microbiology and Biotechnology, 2016. **43**(2-3): p. 155-176.
87. Organization, W.H., *Global action plan on antimicrobial resistance.* 2015.
88. Murray, C.J.L., et al., *Global burden of bacterial antimicrobial resistance in 2019: a systematic analysis.* The Lancet, 2022. **399**(10325): p. 629-655.
89. Tenover, F.C. and J.E. McGowan, *Reasons for the Emergence of Antibiotic Resistance.* The American Journal of the Medical Sciences, 1996. **311**(1): p. 9-16.
90. Fernandes, P., *Antibacterial discovery and development--the failure of success?* Nat Biotechnol, 2006. **24**(12): p. 1497-503.
91. WHO *Antibiotic resistance-key facts*. 2020.
92. Ventola, C.L., *The antibiotic resistance crisis: part 1: causes and threats.* P t, 2015. **40**(4): p. 277-83.
93. Blair, J.M., et al., *Molecular mechanisms of antibiotic resistance.* Nat Rev Microbiol, 2015. **13**(1): p. 42-51.
94. Pannek, S., et al., *Multidrug efflux inhibition in Acinetobacter baumannii: comparison between 1-(1-naphthylmethyl)-piperazine and phenyl-arginine-beta-naphthylamide.* J Antimicrob Chemother, 2006. **57**(5): p. 970-4.

95. Tacconelli, E., et al., *Discovery, research, and development of new antibiotics: the WHO priority list of antibiotic-resistant bacteria and tuberculosis.* Lancet Infect Dis, 2018. **18**(3): p. 318-327.
96. *THE END TB STRATEGY*, ed. W.H. Organization. 2015.
97. Richter, M.F., et al., *Predictive compound accumulation rules yield a broad-spectrum antibiotic.* Nature, 2017. **545**(7654): p. 299-304.
98. Nathan, C. and F.M. Goldberg, *Outlook: the profit problem in antibiotic R&D.* Nat Rev Drug Discov, 2005. **4**(11): p. 887-91.
99. Gilpin, C., et al., *The World Health Organization standards for tuberculosis care and management.* Eur Respir J, 2018. **51**(3).
100. Connolly, L.E., P.H. Edelstein, and L. Ramakrishnan, *Why is long-term therapy required to cure tuberculosis?* PLoS Med, 2007. **4**(3): p. e120.
101. Eldholm, V. and F. Balloux, *Antimicrobial Resistance in Mycobacterium tuberculosis: The Odd One Out.* Trends Microbiol, 2016. **24**(8): p. 637-648.
102. Dye, C. and B.G. Williams, *Eliminating human tuberculosis in the twenty-first century.* J R Soc Interface, 2008. **5**(23): p. 653-62.
103. Crofton, J. and D.A. Mitchison, *Streptomycin resistance in pulmonary tuberculosis.* Br Med J, 1948. **2**(4588): p. 1009-15.
104. Spickler, C., M.-N. Brunelle, and L. Brakier-Gingras, *Streptomycin binds to the decoding center of 16 S ribosomal RNA11Edited by M. Gottesman.* Journal of Molecular Biology, 1997. **273**(3): p. 586-599.
105. Ruiz, P., et al., *Investigation of the in vitro activity of streptomycin against Mycobacterium tuberculosis.* Microb Drug Resist, 2002. **8**(2): p. 147-9.
106. Springer, B., et al., *Mechanisms of streptomycin resistance: selection of mutations in the 16S rRNA gene conferring resistance.* Antimicrob Agents Chemother, 2001. **45**(10): p. 2877-84.
107. Sreevatsan, S., et al., *Characterization of rpsL and rrs mutations in streptomycin-resistant Mycobacterium tuberculosis isolates from diverse geographic localities.* Antimicrob Agents Chemother, 1996. **40**(4): p. 1024-6.
108. Timmins, G.S. and V. Deretic, *Mechanisms of action of isoniazid.* Mol Microbiol, 2006. **62**(5): p. 1220-7.
109. Zhang, Y., S. Dhandayuthapani, and V. Deretic, *Molecular basis for the exquisite sensitivity of Mycobacterium tuberculosis to isoniazid.* Proc Natl Acad Sci U S A, 1996. **93**(23): p. 13212-6.
110. Rozwarski, D.A., et al., *Modification of the NADH of the isoniazid target (InhA) from Mycobacterium tuberculosis.* Science, 1998. **279**(5347): p. 98-102.
111. Rawat, R., A. Whitty, and P.J. Tonge, *The isoniazid-NAD adduct is a slow, tight-binding inhibitor of InhA, the Mycobacterium tuberculosis enoyl reductase: adduct affinity and drug resistance.* Proc Natl Acad Sci U S A, 2003. **100**(24): p. 13881-6.
112. Sensi, P., *History of the development of rifampin.* Rev Infect Dis, 1983. **5 Suppl 3**: p. S402-6.
113. Vall-Spinosa, A., et al., *Rifampin in the treatment of drug-resistant mycobacterium tuberculosis infections.* N Engl J Med, 1970. **283**(12): p. 616-21.
114. Wehrli, W. and M. Staehelin, *Actions of the rifamycins.* Bacteriol Rev, 1971. **35**(3): p. 290-309.
115. Telenti, A., et al., *Detection of rifampicin-resistance mutations in Mycobacterium tuberculosis.* Lancet, 1993. **341**(8846): p. 647-50.
116. Goldstein, B.P., *Resistance to rifampicin: a review.* J Antibiot (Tokyo), 2014. **67**(9): p. 625-30.
117. Taniguchi, H., et al., *Rifampicin resistance and mutation of the rpoB gene in Mycobacterium tuberculosis.* FEMS Microbiol Lett, 1996. **144**(1): p. 103-8.
118. Thomas, J.P., et al., *A new synthetic compound with antituberculous activity in mice: ethambutol (dextro-2,2'-(ethylenediimino)-di-l-butanol).* Am Rev Respir Dis, 1961. **83**: p. 891-3.

119. Belanger, A.E., et al., *The embAB genes of Mycobacterium avium encode an arabinosyl transferase involved in cell wall arabinan biosynthesis that is the target for the antimycobacterial drug ethambutol.* Proc Natl Acad Sci U S A, 1996. **93**(21): p. 11919-24.
120. Amin, A.G., et al., *EmbA is an essential arabinosyltransferase in Mycobacterium tuberculosis.* Microbiology (Reading), 2008. **154**(Pt 1): p. 240-248.
121. Goude, R., et al., *The arabinosyltransferase EmbC is inhibited by ethambutol in Mycobacterium tuberculosis.* Antimicrob Agents Chemother, 2009. **53**(10): p. 4138-46.
122. Pawar, A., et al., *Ethambutol targets the glutamate racemase of Mycobacterium tuberculosis-an enzyme involved in peptidoglycan biosynthesis.* Appl Microbiol Biotechnol, 2019. **103**(2): p. 843-851.
123. Ghiraldi-Lopes, L.D., et al., *New insights on Ethambutol Targets in Mycobacterium tuberculosis.* Infect Disord Drug Targets, 2019. **19**(1): p. 73-80.
124. Mitchison, D.A., *The action of antituberculosis drugs in short-course chemotherapy.* Tubercle, 1985. **66**(3): p. 219-25.
125. Heifets, L. and P. Lindholm-Levy, *Pyrazinamide sterilizing activity in vitro against semidormant Mycobacterium tuberculosis bacterial populations.* Am Rev Respir Dis, 1992. **145**(5): p. 1223-5.
126. Scorpio, A. and Y. Zhang, *Mutations in pncA, a gene encoding pyrazinamidase/nicotinamidase, cause resistance to the antituberculous drug pyrazinamide in tubercle bacillus.* Nat Med, 1996. **2**(6): p. 662-7.
127. Shi, W., et al., *Pyrazinamide inhibits trans-translation in Mycobacterium tuberculosis.* Science, 2011. **333**(6049): p. 1630-2.
128. Sayahi, H., et al., *Pyrazinamide, but not pyrazinoic acid, is a competitive inhibitor of NADPH binding to Mycobacterium tuberculosis fatty acid synthase I.* Bioorg Med Chem Lett, 2011. **21**(16): p. 4804-7.
129. Gopal, P., et al., *Pharmacological and Molecular Mechanisms Behind the Sterilizing Activity of Pyrazinamide.* Trends Pharmacol Sci, 2019. **40**(12): p. 930-940.
130. Boshoff, H.I., V. Mizrahi, and C.E. Barry, 3rd, *Effects of pyrazinamide on fatty acid synthesis by whole mycobacterial cells and purified fatty acid synthase I.* J Bacteriol, 2002. **184**(8): p. 2167-72.
131. Elad, N., et al., *Structure of Type-I Mycobacterium tuberculosis fatty acid synthase at 3.3 Å resolution.* Nature Communications, 2018. **9**(1): p. 3886.
132. Grotz, E., et al., *Nanotechnology in Tuberculosis: State of the Art and the Challenges Ahead.* Pharmaceutical Research, 2018. **35**.
133. Shenoi, S. and G. Friedland, *Extensively drug-resistant tuberculosis: a new face to an old pathogen.* Annu Rev Med, 2009. **60**: p. 307-20.
134. Velayati, A.A., et al., *Emergence of new forms of totally drug-resistant tuberculosis bacilli: super extensively drug-resistant tuberculosis or totally drug-resistant strains in iran.* Chest, 2009. **136**(2): p. 420-425.
135. CDC, *Notice to readers: revised definition of extensively drug-resistant tuberculosis.* MMWR Morb Mortal Wkly Rep, 2006.
136. Gandhi, N.R., et al., *Extensively drug-resistant tuberculosis as a cause of death in patients co-infected with tuberculosis and HIV in a rural area of South Africa.* Lancet, 2006. **368**(9547): p. 1575-80.
137. Ioerger, T.R., et al., *Genome Analysis of Multi- and Extensively-Drug-Resistant Tuberculosis from KwaZulu-Natal, South Africa.* PLOS ONE, 2009. **4**(11): p. e7778.
138. Hards, K., et al., *Bactericidal mode of action of bedaquiline.* Journal of Antimicrobial Chemotherapy, 2015. **70**(7): p. 2028-2037.
139. Lohrasbi, V., et al., *Trends in the discovery of new drugs for Mycobacterium tuberculosis therapy with a glance at resistance.* Tuberculosis, 2018. **109**: p. 17-27.
140. Chahine, E.B., L.R. Karaoui, and H. Mansour, *Bedaquiline: a novel diarylquinoline for multidrug-resistant tuberculosis.* Annals of Pharmacotherapy, 2014. **48**(1): p. 107-115.

141. de Jonge, M.R., et al., *A computational model of the inhibition of Mycobacterium tuberculosis ATPase by a new drug candidate R207910.* Proteins: Structure, Function, and Bioinformatics, 2007. **67**(4): p. 971-980.
142. Kundu, S., et al., *Bedaquiline targets the ε subunit of mycobacterial F-ATP synthase.* Antimicrobial agents and chemotherapy, 2016. **60**(11): p. 6977-6979.
143. Lakshmanan, M. and A.S. Xavier, *Bedaquiline–The first ATP synthase inhibitor against multi drug resistant tuberculosis.* Journal of Young Pharmacists, 2013. **5**(4): p. 112-115.
144. Kim, C.T., et al., *Bedaquiline and delamanid for the treatment of multidrug-resistant tuberculosis: a multicentre cohort study in Korea.* European Respiratory Journal, 2018. **51**(3).
145. Achar, J., et al., *Off-label use of bedaquiline in children and adolescents with multidrug-resistant tuberculosis.* Emerging Infectious Diseases, 2017. **23**(10): p. 1711.
146. Hartkoorn, R.C., S. Uplekar, and S.T. Cole, *Cross-resistance between clofazimine and bedaquiline through upregulation of MmpL5 in Mycobacterium tuberculosis.* Antimicrob Agents Chemother, 2014. **58**(5): p. 2979-81.
147. Cholo, M.C., et al., *Mechanisms of action and therapeutic efficacies of the lipophilic antimycobacterial agents clofazimine and bedaquiline.* Journal of Antimicrobial Chemotherapy, 2016. **72**(2): p. 338-353.
148. Huitric, E., et al., *Rates and mechanisms of resistance development in Mycobacterium tuberculosis to a novel diarylquinoline ATP synthase inhibitor.* Antimicrob Agents Chemother, 2010. **54**(3): p. 1022-8.
149. Kadura, S., et al., *Systematic review of mutations associated with resistance to the new and repurposed Mycobacterium tuberculosis drugs bedaquiline, clofazimine, linezolid, delamanid and pretomanid.* Journal of Antimicrobial Chemotherapy, 2020. **75**(8): p. 2031-2043.
150. Liu, Y., et al., *Delamanid: From discovery to its use for pulmonary multidrug-resistant tuberculosis (MDR-TB).* Tuberculosis, 2018. **111**: p. 20-30.
151. Singh, R., et al., *PA-824 kills nonreplicating Mycobacterium tuberculosis by intracellular NO release.* Science, 2008. **322**(5906): p. 1392-5.
152. Vilchèze, C., *Mycobacterial cell wall: a source of successful targets for old and new drugs.* Applied Sciences, 2020. **10**(7): p. 2278.
153. *WHO Guidelines Approved by the Guidelines Review Committee*, in *The Use of Delamanid in the Treatment of Multidrug-Resistant Tuberculosis in Children and Adolescents: Interim Policy Guidance*. 2016, World Health Organization Copyright © World Health Organization 2016.: Geneva.
154. Fujiwara, M., et al., *Mechanisms of resistance to delamanid, a drug for Mycobacterium tuberculosis.* Tuberculosis (Edinb), 2018. **108**: p. 186-194.
155. Khoshnood, S., et al., *Mechanism of Action, Resistance, Synergism, and Clinical Implications of Delamanid Against Multidrug-Resistant Mycobacterium tuberculosis.* Front Microbiol, 2021. **12**: p. 717045.
156. Stover, C.K., et al., *A small-molecule nitroimidazopyran drug candidate for the treatment of tuberculosis.* Nature, 2000. **405**(6789): p. 962-6.
157. Administration, U.S.F.a.D., *FDA Approves New Treatment for Highly Drug-Resistant Forms of Tuberculosis*. 2019.
158. Shobo, A., et al., *Tissue distribution of pretomanid in rat brain via mass spectrometry imaging.* Xenobiotica, 2016. **46**(3): p. 247-52.
159. Manjunatha, U., H.I. Boshoff, and C.E. Barry, *The mechanism of action of PA-824: Novel insights from transcriptional profiling.* Commun Integr Biol, 2009. **2**(3): p. 215-8.
160. Boshoff, H.I., et al., *The transcriptional responses of Mycobacterium tuberculosis to inhibitors of metabolism: novel insights into drug mechanisms of action.* J Biol Chem, 2004. **279**(38): p. 40174-84.

161. Wilson, M., et al., *Exploring drug-induced alterations in gene expression in Mycobacterium tuberculosis by microarray hybridization.* Proc Natl Acad Sci U S A, 1999. **96**(22): p. 12833-8.
162. Jünemann, S., *Cytochrome bd terminal oxidase.* Biochimica et Biophysica Acta (BBA)-Bioenergetics, 1997. **1321**(2): p. 107-127.
163. Rifat, D., et al., *Mutations in fbiD (Rv2983) as a Novel Determinant of Resistance to Pretomanid and Delamanid in Mycobacterium tuberculosis.* Antimicrob Agents Chemother, 2020. **65**(1).
164. Venugopala, K.N., et al., *Anti-tubercular activity and molecular docking studies of indolizine derivatives targeting mycobacterial InhA enzyme.* Journal of Enzyme Inhibition and Medicinal Chemistry, 2021. **36**(1): p. 1471-1486.
165. Berning, S.E., *The role of fluoroquinolones in tuberculosis today.* Drugs, 2001. **61**(1): p. 9-18.
166. Khisimuzi, M. and M. Zhenkun, *Mycobacterium tuberculosis DNA Gyrase as a Target for Drug Discovery.* Infectious Disorders - Drug Targets, 2007. **7**(2): p. 159-168.
167. Hooper, D.C., *Clinical applications of quinolones.* Biochim Biophys Acta, 1998. **1400**(1-3): p. 45-61.
168. Hooper, D.C., *Mechanisms of action of antimicrobials: focus on fluoroquinolones.* Clinical infectious diseases, 2001. **32**(Supplement_1): p. S9-S15.
169. Andriole, V.T., *The quinolones: past, present, and future.* Clinical infectious diseases, 2005. **41**(Supplement_2): p. S113-S119.
170. Pommier, Y., et al., *DNA topoisomerases and their poisoning by anticancer and antibacterial drugs.* Chemistry & biology, 2010. **17**(5): p. 421-433.
171. Levine, C., H. Hiasa, and K.J. Marians, *DNA gyrase and topoisomerase IV: biochemical activities, physiological roles during chromosome replication, and drug sensitivities.* Biochimica et Biophysica Acta (BBA)-Gene Structure and Expression, 1998. **1400**(1-3): p. 29-43.
172. Champoux, J.J., *DNA topoisomerases: structure, function, and mechanism.* Annual review of biochemistry, 2001. **70**(1): p. 369-413.
173. Aldred, K.J., et al., *Fluoroquinolone interactions with Mycobacterium tuberculosis gyrase: Enhancing drug activity against wild-type and resistant gyrase.* Proc Natl Acad Sci U S A, 2016. **113**(7): p. E839-46.
174. Falzon, D., et al., *World Health Organization treatment guidelines for drug-resistant tuberculosis, 2016 update.* European Respiratory Journal, 2017. **49**(3).
175. Avalos, E., et al., *Frequency and Geographic Distribution of gyrA and gyrB Mutations Associated with Fluoroquinolone Resistance in Clinical Mycobacterium Tuberculosis Isolates: A Systematic Review.* PLOS ONE, 2015. **10**(3): p. e0120470.
176. Jnawali, H.N., et al., *Characterization of mutations in multi- and extensive drug resistance among strains of Mycobacterium tuberculosis clinical isolates in Republic of Korea.* Diagnostic Microbiology and Infectious Disease, 2013. **76**(2): p. 187-196.
177. Maus, C.E., B.B. Plikaytis, and T.M. Shinnick, *Mutation of tlyA confers capreomycin resistance in Mycobacterium tuberculosis.* Antimicrob Agents Chemother, 2005. **49**(2): p. 571-7.
178. Yamada, T. and K.H. Bierhaus, *Viomycin favours the formation of 70S ribosome couples.* Mol Gen Genet, 1978. **161**(3): p. 261-5.
179. Sreevatsan, S., et al., *Characterization of rpsL and rrs mutations in streptomycin-resistant Mycobacterium tuberculosis isolates from diverse geographic localities.* Antimicrobial Agents and Chemotherapy, 1996. **40**(4): p. 1024-1026.
180. Crofton, S.J., et al., *Guidelines for the management of drug-resistant tuberculosis*. 1997, World Health Organization.
181. Hong, W., L. Chen, and J. Xie, *Molecular basis underlying Mycobacterium tuberculosis D-cycloserine resistance. Is there a role for ubiquinone and menaquinone metabolic pathways?* Expert Opin Ther Targets, 2014. **18**(6): p. 691-701.

182. Bruning, J.B., et al., *Structure of the Mycobacterium tuberculosis D-alanine:D-alanine ligase, a target of the antituberculosis drug D-cycloserine.* Antimicrob Agents Chemother, 2011. **55**(1): p. 291-301.
183. Chen, J., et al., *Identification of novel mutations associated with cycloserine resistance in Mycobacterium tuberculosis.* Journal of Antimicrobial Chemotherapy, 2017. **72**(12): p. 3272-3276.
184. Wolff, K.A. and L. Nguyen, *Strategies for potentiation of ethionamide and folate antagonists against Mycobacterium tuberculosis.* Expert Rev Anti Infect Ther, 2012. **10**(9): p. 971-81.
185. Baulard, A.R., et al., *Activation of the pro-drug ethionamide is regulated in mycobacteria.* J Biol Chem, 2000. **275**(36): p. 28326-31.
186. DeBarber, A.E., et al., *Ethionamide activation and sensitivity in multidrug-resistant Mycobacterium tuberculosis.* Proceedings of the National Academy of Sciences, 2000. **97**(17): p. 9677-9682.
187. Machado, D., et al., *High-level resistance to isoniazid and ethionamide in multidrug-resistant Mycobacterium tuberculosis of the Lisboa family is associated with inhA double mutations.* Journal of Antimicrobial Chemotherapy, 2013. **68**(8): p. 1728-1732.
188. Hashemian, S.M.R., T. Farhadi, and M. Ganjparvar, *Linezolid: a review of its properties, function, and use in critical care.* Drug Des Devel Ther, 2018. **12**: p. 1759-1767.
189. Alcalá, L., et al., *In vitro activities of linezolid against clinical isolates of Mycobacterium tuberculosis that are susceptible or resistant to first-line antituberculous drugs.* Antimicrobial agents and chemotherapy, 2003. **47**(1): p. 416-417.
190. Dietze, R., et al., *Early and extended early bactericidal activity of linezolid in pulmonary tuberculosis.* American journal of respiratory and critical care medicine, 2008. **178**(11): p. 1180-1185.
191. Cynamon, M., et al., *Activities of several novel oxazolidinones against Mycobacterium tuberculosis in a murine model.* Antimicrobial agents and chemotherapy, 1999. **43**(5): p. 1189-1191.
192. Hillemann, D., S. Rüsch-Gerdes, and E. Richter, *In vitro-selected linezolid-resistant Mycobacterium tuberculosis mutants.* Antimicrob Agents Chemother, 2008. **52**(2): p. 800-1.
193. Wasserman, S., et al., *Linezolid resistance in patients with drug-resistant TB and treatment failure in South Africa.* J Antimicrob Chemother, 2019. **74**(8): p. 2377-2384.
194. Nixon, M.R., et al., *Folate pathway disruption leads to critical disruption of methionine derivatives in Mycobacterium tuberculosis.* Chemistry & biology, 2014. **21**(7): p. 819-830.
195. Chakraborty, S., et al., *Para-aminosalicylic acid acts as an alternative substrate of folate metabolism in Mycobacterium tuberculosis.* Science, 2013. **339**(6115): p. 88-91.
196. Minato, Y., et al., *Mycobacterium tuberculosis folate metabolism and the mechanistic basis for para-aminosalicylic acid susceptibility and resistance.* Antimicrobial agents and chemotherapy, 2015. **59**(9): p. 5097-5106.
197. Zheng, J., et al., *Para-Aminosalicylic Acid Is a Prodrug Targeting Dihydrofolate Reductase in Mycobacterium Tuberculosis♦.* Journal of Biological Chemistry, 2013. **288**(32): p. 23447-23456.
198. Zhang, T., et al., *Para-aminosalicylic acid increases the susceptibility to isoniazid in clinical isolates of Mycobacterium tuberculosis.* Infect Drug Resist, 2019. **12**: p. 825-829.
199. Minato, Y., et al., *Mycobacterium tuberculosis folate metabolism and the mechanistic basis for para-aminosalicylic acid susceptibility and resistance.* Antimicrob Agents Chemother, 2015. **59**(9): p. 5097-106.
200. Rengarajan, J., et al., *The folate pathway is a target for resistance to the drug para-aminosalicylic acid (PAS) in mycobacteria.* Molecular microbiology, 2004. **53**(1): p. 275-282.
201. Bax, R. and N. Mullan, *Response of the pharmaceutical industry to antimicrobial resistance.* BAILLIERES CLINICAL INFECTIOUS DISEASES, 1999. **5**(2): p. 289-304.

202. Coates, A.R. and Y. Hu, *Novel approaches to developing new antibiotics for bacterial infections.* Br J Pharmacol, 2007. **152**(8): p. 1147-54.
203. Freiberg, C. and H. Brötz-Oesterhelt, *Functional genomics in antibacterial drug discovery.* Drug discovery today, 2005. **10**(13): p. 927-935.
204. Mills, S.D., *When will the genomics investment pay off for antibacterial discovery?* Biochemical pharmacology, 2006. **71**(7): p. 1096-1102.
205. Schmid, M.B., *Do targets limit antibiotic discovery?* Nature biotechnology, 2006. **24**(4): p. 419-420.
206. Weng, J.K., R.N. Philippe, and J.P. Noel, *The rise of chemodiversity in plants.* Science, 2012. **336**(6089): p. 1667-70.
207. Wang, H., et al., *Simultaneous determination and qualitative analysis of six types of components in Naoxintong capsule by miniaturized matrix solid-phase dispersion extraction coupled with ultra high-performance liquid chromatography with photodiode array detection and quadrupole time-of-flight mass spectrometry.* Journal of Separation Science, 2018. **41**(9): p. 2064-2084.
208. Lam, K.S., *New aspects of natural products in drug discovery.* Trends Microbiol, 2007. **15**(6): p. 279-89.
209. Singh, S.B. and J.F. Barrett, *Empirical antibacterial drug discovery—Foundation in natural products.* Biochemical Pharmacology, 2006. **71**(7): p. 1006-1015.
210. Rishton, G.M., *Natural products as a robust source of new drugs and drug leads: past successes and present day issues.* Am J Cardiol, 2008. **101**(10a): p. 43d-49d.
211. Nichols, D., et al., *Use of ichip for high-throughput in situ cultivation of "uncultivable" microbial species.* Appl Environ Microbiol, 2010. **76**(8): p. 2445-50.
212. Pushpakom, S., et al., *Drug repurposing: progress, challenges and recommendations.* Nature Reviews Drug Discovery, 2019. **18**(1): p. 41-58.
213. Sindhu, S. and S. Murugan, *Challenges and Opportunities in Repurposing of Drugs: Mini Review.* Bangladesh Journal of Medical Science, 2020. **19**(3): p. 365-371.
214. Borysowski, J., B. Weber-Dąbrowska, and A. Górski, *Bacteriophage endolysins as a novel class of antibacterial agents.* Experimental biology and medicine, 2006. **231**(4): p. 366-377.
215. Sulakvelidze, A., Z. Alavidze, and J.G. Morris Jr, *Bacteriophage therapy.* Antimicrobial agents and chemotherapy, 2001. **45**(3): p. 649-659.
216. Dabrowska, K., et al., *Bacteriophage penetration in vertebrates.* Journal of applied microbiology, 2005. **98**(1): p. 7-13.
217. Matsuda, T., et al., *Lysis-deficient bacteriophage therapy decreases endotoxin and inflammatory mediator release and improves survival in a murine peritonitis model.* Surgery, 2005. **137**(6): p. 639-646.
218. Yacoby, I., et al., *Targeting antibacterial agents by using drug-carrying filamentous bacteriophages.* Antimicrobial agents and chemotherapy, 2006. **50**(6): p. 2087-2097.
219. Fischetti, V.A., D. Nelson, and R. Schuch, *Reinventing phage therapy: are the parts greater than the sum?* Nat Biotechnol, 2006. **24**(12): p. 1508-11.
220. Diaz-Torres, M.L., et al., *Determining the antibiotic resistance potential of the indigenous oral microbiota of humans using a metagenomic approach.* FEMS microbiology letters, 2006. **258**(2): p. 257-262.
221. Martin, H.G., et al., *Metagenomic analysis of two enhanced biological phosphorus removal (EBPR) sludge communities.* Nature biotechnology, 2006. **24**(10): p. 1263-1269.
222. Turnbaugh, P.J., et al., *An obesity-associated gut microbiome with increased capacity for energy harvest.* nature, 2006. **444**(7122): p. 1027-1031.
223. Jones, B.V. and J.R. Marchesi, *Transposon-aided capture (TRACA) of plasmids resident in the human gut mobile metagenome.* Nature methods, 2007. **4**(1): p. 55-61.
224. Rondon, M.R., et al., *Cloning the soil metagenome: a strategy for accessing the genetic and functional diversity of uncultured microorganisms.* Applied and environmental microbiology, 2000. **66**(6): p. 2541-2547.

225. Rehberg, N., et al., *Chlorflavonin Targets Acetohydroxyacid Synthase Catalytic Subunit IlvB1 for Synergistic Killing of Mycobacterium tuberculosis.* ACS Infect Dis, 2018. **4**(2): p. 123-134.
226. Bird, A. and A. Marshall, *Structure of chlorflavonin.* Journal of the Chemical Society C: Organic, 1969(19): p. 2418-2420.
227. Richards, M., A. Bird, and J. Munden, *GHLORFLAVONIN, A NEW ANTIFUNGAL ANTIBIOTIC.* The Journal of Antibiotics, 1969. **22**(8): p. 388-389.
228. Sampson, S.L., et al., *Protection elicited by a double leucine and pantothenate auxotroph of Mycobacterium tuberculosis in guinea pigs.* Infection and immunity, 2004. **72**(5): p. 3031-3037.
229. Hondalus, M.K., et al., *Attenuation of and protection induced by a leucine auxotroph of Mycobacterium tuberculosis.* Infection and immunity, 2000. **68**(5): p. 2888-2898.
230. Radhakrishnan, A., R. Wagner, and E.E. Snell, *Biosynthesis of valine and isoleucine. III. α-keto-β-hydroxy acid reductase and α-hydroxy-β-keto acid reductoisomerase.* Journal of Biological Chemistry, 1960. **235**(8): p. 2322-2331.
231. Leaviti, R.I., *ISOLEUCINE AND VALINE METABOLISM IN ESCHERICHIA COLI XII: Characterization of a Factor Involved in Acetolactate Formation.* Journal of Bacteriology, 1964. **88**(1): p. 172-178.
232. Steinmetz, A., et al., *Valine 375 and phenylalanine 109 confer affinity and specificity for pyruvate as donor substrate in acetohydroxy acid synthase isozyme II from Escherichia coli.* Biochemistry, 2010. **49**(25): p. 5188-5199.
233. Choi, K.-J., et al., *Characterization of acetohydroxyacid synthase from Mycobacterium tuberculosis and the identification of its new inhibitor from the screening of a chemical library.* FEBS letters, 2005. **579**(21): p. 4903-4910.
234. *Isoleucine and Valine Metabolism in Escherichia coli: VIII. THE FORMATION OF ACETOLACTATE.* Journal of Biological Chemistry, 1958. **233**(5): p. 1156-1160.
235. Liu, Y., Y. Li, and X. Wang, *Acetohydroxyacid synthases: evolution, structure, and function.* Appl Microbiol Biotechnol, 2016. **100**(20): p. 8633-49.
236. Gokhale, K. and B. Tilak, *Mechanisms of bacterial acetohydroxyacid synthase (AHAS) and specific inhibitors of Mycobacterium tuberculosis AHAS as potential drug candidates against tuberculosis.* Current Drug Targets, 2015. **16**(7): p. 689-699.
237. Gokhale, K.M. and B.D. Tilak, *Mechanisms of bacterial acetohydroxyacid synthase (AHAS) and specific inhibitors of Mycobacterium tuberculosis AHAS as potential drug candidates against tuberculosis.* Current drug targets, 2015. **16 7**: p. 689-99.
238. Pang, S.S., R.G. Duggleby, and L.W. Guddat, *Crystal structure of yeast acetohydroxyacid synthase: a target for herbicidal inhibitors.* J Mol Biol, 2002. **317**(2): p. 249-62.
239. Kisfaludy, L., et al., *α-aminooxy-acid derivatives with potent antituberculotic effect.* Experientia, 1971. **27**(9): p. 1055-1056.
240. van Geelen, L., *Functional characterisation of new antimicrobial substances*. 2020.
241. *UniProt: a worldwide hub of protein knowledge.* Nucleic Acids Res, 2019. **47**(D1): p. D506-d515.
242. Libardo, M.D.J., et al., *Resistance of Mycobacterium tuberculosis to indole 4-carboxamides occurs through alterations in drug metabolism and tryptophan biosynthesis.* Cell Chemical Biology, 2021. **28**(8): p. 1180-1191.e20.
243. Cascioferro, S., et al., *Thiazoles, Their Benzofused Systems, and Thiazolidinone Derivatives: Versatile and Promising Tools to Combat Antibiotic Resistance.* J Med Chem, 2020. **63**(15): p. 7923-7956.
244. Kumar, S., et al., *11. Thiazole: A privileged scaffold in drug discovery*. 2016.
245. Kashyap, S.J., et al., *Thiazoles: having diverse biological activities.* Medicinal Chemistry Research, 2012. **21**(8): p. 2123-2132.
246. Harner, M.J., et al., *Fragment-based screening of the bromodomain of ATAD2.* J Med Chem, 2014. **57**(22): p. 9687-92.
247. Tam, B., et al., *Discovery of small-molecule inhibitors targeting the ribosomal peptidyl transferase center (PTC) of M. tuberculosis.* Chem Sci, 2019. **10**(38): p. 8764-8767.

248. Shirude, P.S., et al., *Methyl-Thiazoles: A Novel Mode of Inhibition with the Potential to Develop Novel Inhibitors Targeting InhA in Mycobacterium tuberculosis.* Journal of Medicinal Chemistry, 2013. **56**(21): p. 8533-8542.
249. Larsen, M.H., et al., *Genetic Manipulation of Mycobacterium tuberculosis.* Curr Protoc Microbiol, 2007. **Chapter 10**: p. Unit 10A.2.
250. Laemmli, U.K., *Cleavage of structural proteins during the assembly of the head of bacteriophage T4.* Nature, 1970. **227**(5259): p. 680-5.
251. Cox, J. and M. Mann, *MaxQuant enables high peptide identification rates, individualized p.p.b.-range mass accuracies and proteome-wide protein quantification.* Nat Biotechnol, 2008. **26**(12): p. 1367-72.
252. Tyanova, S., T. Temu, and J. Cox, *The MaxQuant computational platform for mass spectrometry-based shotgun proteomics.* Nature Protocols, 2016. **11**(12): p. 2301-2319.
253. Berger, A., et al., *Total Synthesis of the Antimycobacterial Natural Product Chlorflavonin and Analogs via a Late-Stage Ruthenium(II)-Catalyzed ortho-C(sp(2))-H-Hydroxylation.* Pharmaceuticals (Basel), 2022. **15**(8).
254. Nie, J., et al., *Asymmetric Construction of Stereogenic Carbon Centers Featuring a Trifluoromethyl Group from Prochiral Trifluoromethylated Substrates.* Chemical Reviews, 2011. **111**(2): p. 455-529.
255. Buratto, R., et al., *Ligand–Protein Affinity Studies Using Long-Lived States of Fluorine-19 Nuclei.* Journal of Medicinal Chemistry, 2016. **59**(5): p. 1960-1966.
256. Altschul, S.F., et al., *Basic local alignment search tool.* J Mol Biol, 1990. **215**(3): p. 403-10.
257. Westerfeld, W.W., *A colorimetric determination of blood acetoin.* J. Biol. Chem., 1945. **161**: p. 195-502.
258. Asadian, M., et al., *Genomic characteristics of two most widely used BCG vaccine strains: Danish 1331 and Pasteur 1173P2.* BMC Genomics, 2022. **23**(1): p. 609.
259. Samaritoni, J.G., et al., *Unexpected Hydrolytic Instability of N-Acylated Amino Acid Amides and Peptides.* The Journal of Organic Chemistry, 2014. **79**(7): p. 3140-3151.
260. Consortium, T.U., *UniProt: a worldwide hub of protein knowledge.* Nucleic Acids Research, 2018. **47**(D1): p. D506-D515.
261. Bax, H.I., et al., *Colistin as a potentiator of anti-TB drug activity against Mycobacterium tuberculosis.* Journal of Antimicrobial Chemotherapy, 2015. **70**(10): p. 2828-2837.
262. Nadia, K., V. Shane, and L. Du Toit, *Elucidating the antimicrobial mechanisms of colistin sulfate on Mycobacterium tuberculosis using metabolomics.* Tuberculosis, 2018. **111**: p. 14-19.
263. Bisson, G.P., et al., *Upregulation of the phthiocerol dimycocerosate biosynthetic pathway by rifampin-resistant, rpoB mutant Mycobacterium tuberculosis.* J Bacteriol, 2012. **194**(23): p. 6441-52.
264. Camacho, L.R., et al., *Analysis of the phthiocerol dimycocerosate locus of Mycobacterium tuberculosis. Evidence that this lipid is involved in the cell wall permeability barrier.* J Biol Chem, 2001. **276**(23): p. 19845-54.
265. Minato, Y., et al., *Genomewide Assessment of Mycobacterium tuberculosis Conditionally Essential Metabolic Pathways.* mSystems, 2019. **4**(4).
266. DeJesus, M.A., et al., *Comprehensive Essentiality Analysis of the Mycobacterium tuberculosis Genome via Saturating Transposon Mutagenesis.* mBio, 2017. **8**(1).
267. Pethe, K., et al., *A chemical genetic screen in Mycobacterium tuberculosis identifies carbon-source-dependent growth inhibitors devoid of in vivo efficacy.* Nat Commun, 2010. **1**(5): p. 57.
268. Adeeb, S., S. Raheem, and L. Young Sup, *Chapter Eight - Curcumin: A Potent Modulator of Multiple Enzymes in Multiple Cancers*, in *Natural Products and Cancer Signaling: Isoprenoids, Polyphenols and Flavonoids*, S.Z. Bathaie and T. Fuyuhiko, Editors. 2014, Academic Press. p. 149-174.

269. Griffin, J.E., et al., *High-resolution phenotypic profiling defines genes essential for mycobacterial growth and cholesterol catabolism.* PLoS Pathog, 2011. **7**(9): p. e1002251.
270. Zheng, H., et al., *Genetic basis of virulence attenuation revealed by comparative genomic analysis of Mycobacterium tuberculosis strain H37Ra versus H37Rv.* PLoS One, 2008. **3**(6): p. e2375.
271. Iyer, L.M. and L. Aravind, *The catalytic domains of thiamine triphosphatase and CyaB-like adenylyl cyclase define a novel superfamily of domains that bind organic phosphates.* BMC Genomics, 2002. **3**(1): p. 33.
272. Kalia, N.P., et al., *Carbon metabolism modulates the efficacy of drugs targeting the cytochrome bc(1):aa(3) in Mycobacterium tuberculosis.* Sci Rep, 2019. **9**(1): p. 8608.
273. Monika, S., P. Sukanya, and S. Rajesh Kumar, *15 - Common techniques and methods for screening of natural products for developing of anticancer drugs*, in *Evolutionary Diversity as a Source for Anticancer Molecules*, S. Akhileshwar Kumar, et al., Editors. 2021, Academic Press. p. 323-353.
274. Ntoi, L.L.A., B.E. Buitendach, and K.G. von Eschwege, *Seven Chromisms Associated with Dithizone.* The Journal of Physical Chemistry A, 2017. **121**(48): p. 9243-9251.
275. Ramos, P.C. and R.J. Dohmen, *PACemakers of proteasome core particle assembly.* Structure, 2008. **16**(9): p. 1296-304.
276. Usha, V., et al., *Identification of novel diphenyl urea inhibitors of Mt-GuaB2 active against Mycobacterium tuberculosis.* Microbiology (Reading), 2011. **157**(Pt 1): p. 290-299.
277. Knejzlík, Z., et al., *The mycobacterial guaB1 gene encodes a guanosine 5'-monophosphate reductase with a cystathionine-β-synthase domain.* The FEBS Journal, 2022. **289**(18): p. 5571-5598.
278. Ferrández, A., J.L. García, and E. Díaz, *Transcriptional regulation of the divergent paa catabolic operons for phenylacetic acid degradation in Escherichia coli.* J Biol Chem, 2000. **275**(16): p. 12214-22.
279. Gaudet, P., et al., *Phylogenetic-based propagation of functional annotations within the Gene Ontology consortium.* Brief Bioinform, 2011. **12**(5): p. 449-62.
280. Berthet, F.X., et al., *Characterization of the Mycobacterium tuberculosis erp gene encoding a potential cell surface protein with repetitive structures.* Microbiology (Reading), 1995. **141 (Pt 9)**: p. 2123-30.
281. Ganaie, A.A., et al., *Interaction of Erp Protein of Mycobacterium tuberculosis with Rv2212 Enhances Intracellular Survival of Mycobacterium smegmatis.* J Bacteriol, 2016. **198**(20): p. 2841-52.
282. Kelkar, D.S., et al., *Proteogenomic analysis of Mycobacterium tuberculosis by high resolution mass spectrometry.* Mol Cell Proteomics, 2011. **10**(12): p. M111.011627.
283. Becker, S.H., et al., *Mycobacterium tuberculosis Rv0991c Is a Redox-Regulated Molecular Chaperone.* mBio, 2020. **11**(4).
284. Kuan, C.S., et al., *Genome Analysis of the First Extensively Drug-Resistant (XDR) Mycobacterium tuberculosis in Malaysia Provides Insights into the Genetic Basis of Its Biology and Drug Resistance.* PLOS ONE, 2015. **10**(6): p. e0131694.
285. Gils, T., et al., *Pretomanid for tuberculosis: a systematic review.* Clinical Microbiology and Infection, 2022. **28**(1): p. 31-42.
286. He, Y., et al., *New perspectives on the treatment of mycobacterial infections using antibiotics.* Applied Microbiology and Biotechnology, 2020. **104**.
287. Webb, M.E., A.G. Smith, and C. Abell, *Biosynthesis of pantothenate.* Nat Prod Rep, 2004. **21**(6): p. 695-721.
288. Gagneux, S., et al., *The competitive cost of antibiotic resistance in Mycobacterium tuberculosis.* Science, 2006. **312**(5782): p. 1944-6.
289. Lewin, A. and S. Sharbati-Tehrani, *[Slow growth rate of mycobacteria. Possible reasons and significance for their pathogenicity].* Bundesgesundheitsblatt Gesundheitsforschung Gesundheitsschutz, 2005. **48**(12): p. 1390-9.

290. Tyagi, A., *Sources of energy production in Mycobacterium tuberculosis BCG.* The Indian Journal of Chest Diseases & Allied Sciences, 1976. **18**(4): p. 251-258.
291. Singh, V., et al., *Biochemical and transcription analysis of acetohydroxyacid synthase isoforms in Mycobacterium tuberculosis identifies these enzymes as potential targets for drug development.* Microbiology (Reading), 2011. **157**(Pt 1): p. 29-37.
292. Savjani, K.T., A.K. Gajjar, and J.K. Savjani, *Drug solubility: importance and enhancement techniques.* ISRN Pharm, 2012. **2012**: p. 195727.
293. Wright, G.D., *Bacterial resistance to antibiotics: enzymatic degradation and modification.* Advanced drug delivery reviews, 2005. **57**(10): p. 1451-1470.
294. Bonomo, R.A., *β-Lactamases: a focus on current challenges.* Cold Spring Harbor perspectives in medicine, 2017. **7**(1): p. a025239.
295. Morar, M. and G.D. Wright, *The genomic enzymology of antibiotic resistance.* Annual review of genetics, 2010. **44**: p. 25-51.
296. Schwarz, S., et al., *Lincosamides, streptogramins, phenicols, and pleuromutilins: mode of action and mechanisms of resistance.* Cold Spring Harbor perspectives in medicine, 2016. **6**(11): p. a027037.
297. Wang, J.G., et al., *Crystal structures of two novel sulfonylurea herbicides in complex with Arabidopsis thaliana acetohydroxyacid synthase.* Febs j, 2009. **276**(5): p. 1282-90.
298. Lonhienne, T., et al., *High Resolution Crystal Structures of the Acetohydroxyacid Synthase-Pyruvate Complex Provide New Insights into Its Catalytic Mechanism.* ChemistrySelect, 2017. **2**(36): p. 11981-11988.
299. Bowers Jr, G.N. and M. Onoroski, *lyperchloremia and the Incidence of Bromism in 1990.* Clinical Chemistry, 1990. **36**(8): p. 1399-1403.
300. Trump, D. and M. Hochberg, *Bromide intoxication.* The Johns Hopkins Medical Journal, 1976. **138**(4): p. 119-123.
301. Rogers, L.I.M.S., *Pernicious Malignant Tertian Malaria Successfully Treated by Quinine Acid Hydrobromide Intravenously and the Failure of "Splenox" in Benign Tertian Malaria.* Ind Med Gaz, 1917. **52**(11): p. 385-386.
302. Lieberman, A.N. and M. Goldstein, *Bromocriptine in Parkinson disease.* Pharmacol Rev, 1985. **37**(2): p. 217-27.
303. *Chapter 96 - Halogens (Bromine, Iodine, and Chlorine Compounds)*, in *Haddad and Winchester's Clinical Management of Poisoning and Drug Overdose (Fourth Edition)*, S. Michael W, B. Stephen W, and B. Michael J, Editors. 2007, W.B. Saunders: Philadelphia. p. 1385-1397.
304. Watson, W.A., et al., *2003 annual report of the American association of poison control centers toxic exposure surveillance system.* The American journal of emergency medicine, 2004. **22**(5): p. 335-404.
305. Govindaraj, V., et al., *Directing Traffic: Halogen-Bond-Mediated Membrane Transport.* Chemistry – A European Journal, 2019. **25**(48): p. 11180-11192.
306. Blagden, N., et al., *Crystal engineering of active pharmaceutical ingredients to improve solubility and dissolution rates.* Advanced drug delivery reviews, 2007. **59**(7): p. 617-630.
307. Savjani, K.T., A.K. Gajjar, and J.K. Savjani, *Drug Solubility: Importance and Enhancement Techniques.* ISRN Pharmaceutics, 2012. **2012**: p. 195727.
308. Vogt, M., K. Kunath, and J.B. Dressman, *Dissolution enhancement of fenofibrate by micronization, cogrinding and spray-drying: comparison with commercial preparations.* European Journal of Pharmaceutics and Biopharmaceutics, 2008. **68**(2): p. 283-288.
309. Chaumeil, J., *Micronization: a method of improving the bioavailability of poorly soluble drugs.* Methods and findings in experimental and clinical pharmacology, 1998. **20**(3): p. 211-216.
310. Muller, R., *Nanosuspension for the formulation of poorly soluble drugs, in pharmaceutical emulsion and suspension. Neilloud. F. ed. and Marti-Mestres. G. ed.* 2000, New York: Marcel Dekker Inc.

311. NASH, D.T. and M. Davies, *Some aspects of growth and metabolism of Paul's Scarlet rose cell suspensions.* Journal of Experimental Botany, 1972. **23**(1): p. 75-91.
312. Uekama, K., F. Hirayama, and T. Irie, *Cyclodextrin drug carrier systems.* Chemical reviews, 1998. **98**(5): p. 2045-2076.
313. Rabinow, B.E., *Nanosuspensions in drug delivery.* Nature Reviews Drug Discovery, 2004. **3**(9): p. 785-796.
314. Constantinides, P.P., M.V. Chaubal, and R. Shorr, *Advances in lipid nanodispersions for parenteral drug delivery and targeting.* Adv Drug Deliv Rev, 2008. **60**(6): p. 757-67.
315. Seki, J., et al., *A nanometer lipid emulsion, lipid nano-sphere (LNS), as a parenteral drug carrier for passive drug targeting.* Int J Pharm, 2004. **273**(1-2): p. 75-83.
316. Sahin, N.O., *Niosomes as Nanocarrier Systems*, in *Nanomaterials and Nanosystems for Biomedical Applications*, M.R. Mozafari, Editor. 2007, Springer Netherlands: Dordrecht. p. 67-81.
317. Sosnik, A., et al., *New old challenges in tuberculosis: potentially effective nanotechnologies in drug delivery.* Adv Drug Deliv Rev, 2010. **62**(4-5): p. 547-59.
318. Dutt, M. and G.K. Khuller, *Sustained release of isoniazid from a single injectable dose of poly (dl-lactide-co-glycolide) microparticles as a therapeutic approach towards tuberculosis.* International Journal of Antimicrobial Agents, 2001. **17**(2): p. 115-122.
319. Choudhary, A., et al., *A Novel Approach of Targeting Linezolid Nanoemulsion for the Management of Lymph Node Tuberculosis.* ACS Omega, 2022. **7**(18): p. 15688-15694.
320. Grandoni, J.A., P.T. Marta, and J.V. Schloss, *Inhibitors of branched-chain amino acid biosynthesis as potential antituberculosis agents.* J Antimicrob Chemother, 1998. **42**(4): p. 475-82.
321. Liu, Y., et al., *Evaluation of the in vivo efficacy of novel monosubstituted sulfonylureas against H37Rv and extensively drug-resistant tuberculosis.* Jpn J Infect Dis, 2014. **67**(6): p. 485-7.
322. Awasthy, D., et al., *Inactivation of the ilvB1 gene in Mycobacterium tuberculosis leads to branched-chain amino acid auxotrophy and attenuation of virulence in mice.* Microbiology (Reading), 2009. **155**(Pt 9): p. 2978-2987.
323. Berger, A., *Synthese und Strukturoptimierung der antimykobakteriellen Leitstrukturen Chlorflavonin und KSK104*. 2021.
324. Selassie, C. and R.P. Verma, *History of Quantitative Structure–Activity Relationships*, in *Burger's Medicinal Chemistry and Drug Discovery*. p. 1-96.
325. Statkevičiūtė, R., et al., *Comparative Analysis of Mesophilic YqfB-Type Amidohydrolases.* Biomolecules, 2022. **12**(10).
326. Pleyer, L. and R. Greil, *Digging deep into "dirty" drugs – modulation of the methylation machinery.* Drug Metabolism Reviews, 2015. **47**(2): p. 252-279.
327. Bax, H.I., et al., *Colistin as a potentiator of anti-TB drug activity against Mycobacterium tuberculosis.* J Antimicrob Chemother, 2015. **70**(10): p. 2828-37.
328. Clemens, D.L., B.Y. Lee, and M.A. Horwitz, *Purification, characterization, and genetic analysis of Mycobacterium tuberculosis urease, a potentially critical determinant of host-pathogen interaction.* Journal of Bacteriology, 1995. **177**(19): p. 5644-5652.
329. Ding, W., et al., *Proteomic and Morphologic Evidence for Taurine-5-Bromosalicylaldehyde Schiff Base as an Efficient Anti-Mycobacterial Drug.* J Microbiol Biotechnol, 2019. **29**(8): p. 1221-1229.
330. Chow, J.Y., L. Wu, and W.S. Yew, *Directed Evolution of a Quorum-Quenching Lactonase from Mycobacterium avium subsp. paratuberculosis K-10 in the Amidohydrolase Superfamily.* Biochemistry, 2009. **48**(20): p. 4344-4353.
331. Zhang, L., et al., *The crystal structure of the phosphotriesterase from M. tuberculosis, another member of phosphotriesterase-like lactonase family.* Biochem Biophys Res Commun, 2019. **510**(2): p. 224-229.
332. Stephen, F.A., et al., *Basic local alignment search tool.* Journal of Molecular Biology, 1990. **215**(3): p. 403-410.

333. Roberts, G., D.N. Muttucumaru, and T. Parish, *Control of the acetamidase gene of Mycobacterium smegmatis by multiple regulators.* FEMS microbiology letters, 2003. **221**(1): p. 131-136.
334. Henke, E. and U.T. Bornscheuer, *Fluorophoric assay for the high-throughput determination of amidase activity.* Anal Chem, 2003. **75**(2): p. 255-60.
335. Koul, A., et al., *Diarylquinolines target subunit c of mycobacterial ATP synthase.* Nat Chem Biol, 2007. **3**(6): p. 323-4.
336. Koul, A., et al., *Diarylquinolines target subunit c of mycobacterial ATP synthase.* Nature chemical biology, 2007. **3**(6): p. 323-324.
337. Diacon, A.H., et al., *Multidrug-resistant tuberculosis and culture conversion with bedaquiline.* New England Journal of Medicine, 2014. **371**(8): p. 723-732.
338. Bald, D., et al., *Targeting Energy Metabolism in Mycobacterium tuberculosis, a New Paradigm in Antimycobacterial Drug Discovery.* mBio, 2017. **8**(2).
339. Gengenbacher, M., et al., *Nutrient-starved, non-replicating Mycobacterium tuberculosis requires respiration, ATP synthase and isocitrate lyase for maintenance of ATP homeostasis and viability.* Microbiology (Reading), 2010. **156**(Pt 1): p. 81-87.
340. Cole, S., et al., *Barry 3rd.* CE, Tekaia, F., Badcock, K., Basham, D., Brown, D., Chillingworth, T., Connor, R., Davies, R., Devlin, K., Feltwell, T., Gentles, S., Hamlin, N., Holroyd, S., Hornsby, T., Jagels, K., Krogh, A., McLean, J., Moule, S., Murphy, L., Oliver, K., Osborne, J., Quail, MA, Rajandream, MA, Rogers, J., Rutter, S., Seeger, K., Skelton, J., Squares, R., Squares, S., Sulston, JE, Taylor, K., Whitehead, S., Barrell, BG, 1998: p. 537-544.
341. Sala, C., et al., *Genome-wide regulon and crystal structure of BlaI (Rv1846c) from Mycobacterium tuberculosis.* Molecular microbiology, 2009. **71**(5): p. 1102-1116.
342. Boshoff, H.I., et al., *The transcriptional responses of Mycobacterium tuberculosis to inhibitors of metabolism: novel insights into drug mechanisms of action.* Journal of Biological Chemistry, 2004. **279**(38): p. 40174-40184.
343. Wilke, M.S., et al., *Crystal structures of the Apo and penicillin-acylated forms of the BlaR1 β-lactam sensor of Staphylococcus aureus.* Journal of Biological Chemistry, 2004. **279**(45): p. 47278-47287.
344. Rao, S.P., et al., *The protonmotive force is required for maintaining ATP homeostasis and viability of hypoxic, nonreplicating Mycobacterium tuberculosis.* Proceedings of the National Academy of Sciences, 2008. **105**(33): p. 11945-11950.
345. Koul, A., et al., *Diarylquinolines are bactericidal for dormant mycobacteria as a result of disturbed ATP homeostasis.* Journal of Biological Chemistry, 2008. **283**(37): p. 25273-25280.
346. Wayne, L., *Dormancy of Mycobacterium tuberculosis and latency of disease.* European Journal of Clinical Microbiology and Infectious Diseases, 1994. **13**: p. 908-914.
347. Safi, H., et al., *Phase variation in Mycobacterium tuberculosis glpK produces transiently heritable drug tolerance.* Proc Natl Acad Sci U S A, 2019. **116**(39): p. 19665-19674.
348. Administration, U.S.F.a.D. *The Drug Development Process*. 2018 09.02.2023].
349. Steinmetz, K.L. and E.G. Spack, *The basics of preclinical drug development for neurodegenerative disease indications.* BMC Neurology, 2009. **9**(1): p. S2.
350. Proj, M., et al., *Fragment-Sized Thiazoles in Fragment-Based Drug Discovery Campaigns: Friend or Foe?* ACS Med Chem Lett, 2022. **13**(12): p. 1905-1910.
351. Dighe, R., et al., *Evaluation of Thiazole Derivatives for M. tuberculosis and dTDP-rhamnose Inhibitors.* 2018.
352. Devine, S.M., et al., *Promiscuous 2-aminothiazoles (PrATs): a frequent hitting scaffold.* J Med Chem, 2015. **58**(3): p. 1205-14.
353. Bachmann, N.L., et al., *Key Transitions in the Evolution of Rapid and Slow Growing Mycobacteria Identified by Comparative Genomics.* Frontiers in Microbiology, 2020. **10**.
354. He, G., J. Massarella, and P. Ward, *Clinical pharmacokinetics of the prodrug oseltamivir and its active metabolite Ro 64-0802.* Clin Pharmacokinet, 1999. **37**(6): p. 471-84.

355. Stokes, R.W. and D. Doxsee, *The Receptor-Mediated Uptake, Survival, Replication, and Drug Sensitivity of Mycobacterium tuberculosis within the Macrophage-like Cell Line THP-1: A Comparison with Human Monocyte-Derived Macrophages.* Cellular Immunology, 1999. **197**(1): p. 1-9.
356. Gill, C.M., et al., *New developments in tuberculosis diagnosis and treatment.* Breathe (Sheff), 2022. **18**(1): p. 210149.
357. Singh, S.B., K. Young, and L.L. Silver, *What is an "ideal" antibiotic? Discovery challenges and path forward.* Biochem Pharmacol, 2017. **133**: p. 63-73.
358. Camacho, L.R., et al., *Identification of a virulence gene cluster of Mycobacterium tuberculosis by signature-tagged transposon mutagenesis.* Molecular microbiology, 1999. **34**(2): p. 257-267.
359. Cox, J.S., et al., *Complex lipid determines tissue-specific replication of Mycobacterium tuberculosis in mice.* Nature, 1999. **402**(6757): p. 79-83.
360. Kolattukudy, P., et al., *Biochemistry and molecular genetics of cell-wall lipid biosynthesis in mycobacteria.* Molecular microbiology, 1997. **24**(2): p. 263-270.
361. Menendez-Bravo, S., et al., *Expanding the chemical diversity of natural esters by engineering a polyketide-derived pathway into Escherichia coli.* Metab Eng, 2014. **24**: p. 97-106.
362. Li, M.-S., et al., *cDNA–RNA subtractive hybridization reveals increased expression of mycocerosic acid synthase in intracellular Mycobacterium bovis BCG.* Microbiology, 2001. **147**(8): p. 2293-2305.
363. Brodin, P., et al., *High content phenotypic cell-based visual screen identifies Mycobacterium tuberculosis acyltrehalose-containing glycolipids involved in phagosome remodeling.* PLoS Pathog, 2010. **6**(9): p. e1001100.
364. de Mendonça-Lima, L., et al., *Erp, an extracellular protein family specific to mycobacteria.* Microbiology (Reading), 2001. **147**(Pt 8): p. 2315-2320.
365. Kocíncová, D., et al., *The Erp protein is anchored at the surface by a carboxy-terminal hydrophobic domain and is important for cell-wall structure in Mycobacterium smegmatis.* FEMS Microbiology Letters, 2004. **231**(2): p. 191-196.
366. David, E.M., et al., *The Methyl-Branched Fortifications of Mycobacterium tuberculosis.* Chemistry & Biology, 2002. **9**(5): p. 545-553.
367. Rousseau, C., et al., *Virulence attenuation of two Mas-like polyketide synthase mutants of Mycobacterium tuberculosis.* Microbiology, 2003. **149**(7): p. 1837-1847.

7 List of Figures

8 List of Tables

9 Contribution to other studies

Contributions have been made to the following publications:

Berger A, Knak T, Kiffe-Delf AL, Mudrovcic K, Singh V, Njoroge M, Burckhardt BB, Gopalswamy M, Lungerich B, Ackermann L, Gohlke H, Chibale K, Kalscheuer R, Kurz T. Total Synthesis of the Antimycobacterial Natural Product Chlorflavonin and Analogs via a Late-Stage Ruthenium(II)-Catalyzed ortho-C(sp2)-H-Hydroxylation. Pharmaceuticals (Basel). 2022 Aug 10;15(8):984.

Eze PM, Simons V, Seidemann T, Wang L, Kiffe-Delf AL, Frank M, van Geelen L, Abba CC, Esimone CO, Okoye FBC, Kalscheuer R. Serratiochelins A and B from Serratia marcescens show xenosiderophoric characteristics towards Acinetobacter baumannii and Mycobacterium tuberculosis. Trop J Pharm Res 20, 2551-2658 (2021).

Ariantari N, Frank M, Gao Y, Stuhldreier F, Kiffe-Delf AL, Hartmann R, Höfert SP, Janiak C, Wesselborg S, Müller WEG, Kalscheuer R, Liu Z, Proksch. Fusaristatins D–F and (7S,8R)-(−)-chlamydospordiol from Fusarium sp. BZCB-CA, an endophyte of Bothriospermum chinense. Tetrahedron 85, 132065 (2021).

Wang L, Kiffe-Delf AL, Ostermann PN, Simons VE, He D, Gao Y, van Geelen L, Dai HF, Zhao YX, Schaal H, Mándi A, Király SB, Kurtán T, Liu Z, Kalscheuer R. Asperphenalenones Isolated from the Biocontrol Agent *Clonostachys rosea* and Their Antimicrobial Activities. J Agric Food Chem. 2023 Jul 12. Doi: 10.1021/acs.jafc.3c00447. Epub ahead of print. PMID: 37436951.

10 Eidesstattliche Erklärung

Ich, Frau Anna-Lene Ilse Rosemarie Kiffe-Delf versichere an Eides Statt, dass die Dissertation von mir selbständig und ohne unzulässige fremde Hilfe unter Beachtung der „Grundsätze zur Sicherung guter wissenschaftlicher Praxis an der Heinrich-Heine-Universität Düsseldorf“ erstellt worden ist.

Düsseldorf, den _____

Anna-Lene Kiffe-Delf

11 Acknowledgment

First of all, I would like to thank my supervisor Prof. Dr. Rainer Kalscheuer not only for the opportunity to work on such an interesting and highly relevant topic in his institute, but also for his supervision and helpful discussions during the whole time.

I would also like to thank Prof. Dr. Thomas Kurz for his work as co-supervisor and the good collaboration during the whole time.

Next, I would like to thank the entire institute and all the people I met during my time. My special thanks go to Dr. Lasse van Geelen, Steffen Schindler, Dr. Yvonne Gröner, Dr. Dieter Meier, Kristin Schwechel, Dr. Lin Wang, Emmanuel Tola Adeniyi, and Dr. Viktor Simons. They all created a good working atmosphere and always had time to discuss in stressful moments. We really had a great time. I enjoyed the practical courses, the music-rich time in the BSL-3 lab, but also the free time, especially the bike tour to Zons.

A special thanks goes to Heike Goldbach-Gecke for her support not only with technical questions, but also for her help with any question.

I would also like to thank Prof. Dr. Thomas Kurz, Dr. Alexander Berger, Dr. Oliver Michel, Talea Knak and Fabian Fischer for providing substances for my experiments. Besides providing the substances, we were also able to have good discussions to move the work forward.

Thanks to Prof. Dr. Björn Burckhardt and the CeMSA@HHU (**Ce**nter for **M**olecular and **S**tructural **A**nalytics @ **H**einrich **H**eine **U**niversity) for recording the mass-spectrometric data.

Next, I would like to thank Prof. Dr. Hainer Schaal for the opportunity to work in the BSL-3 facility and of course Björn Wevers and Yvonne Dickschen for the technical support. Without you the BSL-3 facility would not work.

Last but not least, I would like to thank my family and friends. A special thanks goes to my parents and my brothers who helped me a lot. I had many long phone conversations during this time and they helped me to get new ideas and to stay happy.

Thank you all!